CELLULAR THALAMIC CORRELATES OF THE SLOW (<1Hz) SLEEP RHYTHM

A thesis submitted to the University of Wales for
the degree of Doctor of Philosophy

by

Kate L. Blethyn BSc (Hons)

School of Biosciences,
Cardiff University.

ProQuest LLC
789 East Eisenhower Parkway
P.O. Box 1346
Ann Arbor, MI 48106-1346

SUMMARY

Sleep and wakefulness form an inherent, biological rhythm that defines our daily lives. Despite the fact that sleep is a constant interruption to the waking state, its purpose and the neural processes occurring during this behavioural state are not fully understood. However, it is now well established that sleep is not a period of the brain 'silence'. During the transition form light to deep sleep, the activity of the corticothalamic network becomes globally synchronised into consistent, characteristic rhythmic activities at <1Hz, quite in contrast to the so-called cortical 'desynchronisation' characterising states of brain alertness. The mechanism by which global synchronisation in the corticothalamic network arises is not fully defined and previous investigation has focused principally on the role of the cortex. However a clear understanding of the activities of thalamic, as well as cortical, neurones during sleep will aid our understanding into how, and why, global synchronisation occurs, and perhaps why sleep is so fundamental to life.

In this thesis, I demonstrate a number of novel activities in two types of thalamic neurones recorded *in vitro*. Firstly, in thalamocortical neurones, the principal cell type and thalamic output neurones, I demonstrate the presence of an mGluR1a dependent slow (<1Hz) oscillation with identical properties to that seen in the intact brain during sleep. Thalamocortical neurones in relay nuclei subserving visual, somatosensory, auditory and motor systems displayed the slow (<1Hz) oscillation suggesting it could be the substrate for global thalamic synchronization at <1Hz. In addition, I provide a full characterisation of the cellular mechanism of this <1Hz oscillatory activity and demonstrate that during mGluR1a activation, the window component of the low-voltage activated Ca^{2+} current is unmasked, due to a reduction in the constitutive K^{+} leak current, inducing bistability-mediated activities that underlies the generation of the slow (<1Hz) oscillation. In neurones of the nucleus reticularis thalami, overlying the thalamus and providing an inhibitory drive to thalamocortical neurones, I also demonstrate a slow (<1Hz) oscillation, again with identical properties as seen in this cell type in the intact brain during sleep. I demonstrate that this slow (<1Hz) oscillation is dependent on mGluR1a activation and provide evidence suggesting that it is generated by a bistability-mediated mechanism as occurs in thalamocortical neurones. In light of these findings, I suggests that the thalamus,

has a significant role in aiding, as well as maintaining, the global synchronisation of the corticothalamic network at <1Hz during the transition to, and during sleep. The ability of thalamic neurones to generate rhythmic activities at <1Hz due to cortical mGluR1a activation, that results simply in a reduction of the K^+ leak current, will provide a strong excitatory drive to organise cortical activity at <1Hz.

A further novel observation was the presence of spikelets and burstlets (compounds of spikelets) in thalamocortical neurones. Investigations into the origin of these events indicated that they were electrophysiological manifestations of interneuronal electrotonic coupling. Furthermore, spikelets and burstlets had the ability to entrain the output of the neurones in which they were observed. Therefore, the presence of electrotonic coupling in thalamic neurones may have a hitherto unrealised role in the synchronization of thalamic activity during both sleep and awake states.

COLLABORATION

Sections of this thesis were performed in collaboration with the following members of Professor Crunelli's laboratory:

Electrophysiological recordings in Chapter 4 were performed in collaboration with Dr Stuart W. Hughes and Dr. David W. Cope.

Additional data from Dr Stuart W. Hughes was used to support the results described in Chapters 3 and 6.

Simulations in Chapter 4 were performed by Dr Stuart W. Hughes.

ACKNOWLEDGEMENTS

I am very grateful to everyone who I have worked with over the past three years, particularly Dr S. W. Hughes, Dr H.R. Parri and Mr T.G Gould. I also wish to thank Professor Vincenzo Crunelli for his supervision.

LIST OF CONTENTS

CHAPTER 2

MATERIALS AND METHODS

CHAPTERS 3 – 6

RESULTS

CHAPTER 3

INDUCTION AND NUCLEUS-SPECIFIC PROPERTIES OF THE SLOW (<1Hz) OSCILLATION IN THALAMOCORTICAL NEURONES *IN VITRO*

LIST OF FIGURES AND TABLES

LIST OF ABBREVIATIONS

AHP	Afterhyperpolarising potential
APV	DL-2-amino-5-phosphonovaleric acid
Ba^{2+}	Barium
BMI	Bicuculline methiodide
CBX	Carbenoxolone
CGP 56999A	P-(3-aminopropyl)-P-diethoxymethyl-phosphinic acid
CGP 54626	[S-(R*,R*)]-[3-[[1-(3,4-dichlorophenyl)ethyl]amino]-2-hydroxypropyl](cyclohexylmethyl)phosphinic acid
CNQX	6-cyano-7-nitroquinoxaline-2,3-dione
Cs^{+}	Caesium
Cx	Connexin
DHPG	(S)-3,5-dihydroxyphenylglycine
EEG	Electroencephalogram
GABA	γ-amino-butaric acid
GJ	Gap junction
HT bursting	High-threshold bursting
HVA	High voltage activated (Ca^{2+} currents)
I_T	LVA Ca^{2+} current or transient Ca^{2+} current
I_h	Hyperpolarisation-activated mixed cation current
$I_{Twindow}$	window component of I_T
I_{Kca}	$Ca2^{+}$-activated K^{+} current
I_{KLeak}	constitutive K^{+} leak current
I_{KNa}	Na^{+}-activated K^{+} current
I_{CAN}	Ca^{2+}-activated non-selective cation current
I_{Nap}	Persistent Na+ current
LGN	Lateral geniculate nucleus
LHP	Large hyperpolarising potential
LTCP	Low threshold Ca^{2+} potential
LVA	Low voltage activated (Ca^{2+} currents)
LY 367385	(+)-2-methyl-4-carboxyphenylglycine
MGN	Medial geniculate nucleus
mGluR(s)	Metabotropic glutamate receptor(s)
NRT	Nucleus reticularis thalami

NMDA	N-methyl-D-glutamic acid
PGN	Perigeniculate nucleus
REM	Rapid-eye-movement sleep
SR 95531	2-(3-carboxypropyl)-3-amino-6(4-methoxyphenyl) pyridazinium bromide
SWS	Slow-wave sleep
TC	Thalamocortical
Trans-ACPD	(+/-)-1-aminocyclopentane-*trans*-1,3-dicarboxylic acid
TTX	Tetrodotoxin
VA	Ventral anterior nucleus
VL	Ventral lateral nucleus
VP	Ventral posterior nucleus
VPL	Lateral ventral posterior nucleus
VPM	Medial ventral posterior nucleus
ZD 7288	4-(N-ethyl- N-phenylamino)-1,2-dimethyl-6-(methylamino)-pyrimidinium chloride

CHAPTER 1

GENERAL INTRODUCTION

1.1 FOREWORD

Sleep and wakefulness form an inherent biological rhythm that effectively determines the basis of our day-to-day lives. Because sleep is such a consistent interruption to the waking state and abnormal sleep patterns not only impair human performance but are associated with affective and other psychological syndromes/disorders (Gokcebay et al. 1994; Roth et al. 1999), it is clearly a fundamental part of our existence. Sleep, as a behavioural state, is formed by complex neurophysiological and behavioural patterns that follow a more or less predicable rhythmicity. Many theories have been developed regarding the role of sleep and range from theories about physical repair of the body to sleep as a time for selective consolidation or reactivation of memories (Gokcebay et al. 1994; Maquet 2001). Understanding the physiological mechanisms of sleep and the chemical and neural processes occurring during this time will presumably aid the understanding of why sleep is so important to us. In addition, a full understanding of sleep processes could have a significant medical application. Given that altered sleep patterns can be very disruptive to our lives, the ability to restore natural sleep patterns would be a beneficial therapeutic tool.

It is now well accepted that although brain activity is reduced during sleep in comparison to the awake state, sleep is by no means a time of brain silence (Steriade et al. 1993d; Steriade et al. 2001). Electrically recorded brain activity during a period of sleeping forms a cyclical pattern through a variety of sleep stages, that are defined according to electrophysiological and behavioural characteristics, and representing transitions from light to deep sleep, deep to light sleep and light to rapid eye movement (REM) sleep (see section 1.8.1). Decreases in arousal and the deepening of sleep are characterised by increasing synchronisation and global coherence. For example, electroencephalograph (EEG) recorded cortical activity decreases in frequency and develops into large amplitude slow waves at <1Hz as sleep deepens (Steriade et al. 1993d). Increasing synchronisation and the presence of large-amplitude slow-waves are also recorded in the thalamus in phase with the cortical EEG (Timofeev and Steriade 1996). The global coherence of rhythmic activity at <1Hz in the cortex and thalamus is not surprising given the dense interconnections between the two brain areas (Sherman and Guillery 1996) and suggests that the corticothalamic loop is operating as a coherent neural structure

under these conditions. The role of such global synchronisation has yet to be fully understood.

This thesis is predominantly concerned with the activity of thalamic neurones during sleep and considered in the context of the activity of the corticothalamic loop. In addition, during the course of electrophysiological recordings of thalamic neurones, a novel electrophysiological feature was observed in TC neurones: the presence of small depolarising potentials independent of synaptic activation. These observations and associated experiments are described as a separate chapter of results (Chapter 6). Therefore this introductory chapter comprises a number of sections. The first part (sections 1.2 –1.7) provides a description of the structure of the thalamus, the connectivity of thalamic neurones, both intrathalamically and with the cortex, and the electrophysiological properties of thalamic neurones. The next part (section 1.8) describes thalamic activity in the context of the corticothalamic loop during sleep. The final part (section 1.9) provides a context for the experimental observations as described in results Chapter 6.

1.2 GROSS ANATOMY OF THE THALAMUS

The diencephalon is effectively split into two halves either side of the midline, with each half comprising a thalamus, hypothalamus, subthalamus and epithalamus. The two thalami make up the greatest part of the diencephalon and form the walls of the third ventricle extending anteroposteriorly from the interventricular foramen to the posterior commissure and transversely to the internal capsule (Wilkinson 1992). Each thalamus comprises an ovoid mass of grey matter that is made of up numerous nuclei (Fig. 1.1) that fall into two broad types: 1) relay nuclei that receive modality-specific inputs from certain ascending tracts and project to the related modality specific primary cortical areas, and 2) association nuclei that do not receive inputs from ascending tracts, but extensively interconnect with other thalamic nuclei and project predominantly to cortical association areas (Wilkinson 1992). The internal medullary lamina compartmentalises the thalamus into broad groups: enclosing the anterior group and dividing the medial and lateral groups (Kandel et al. 1991) (Fig. 1.1). The lateral group is further divided into the dorsal and ventral tiers and contains specific relay nuclei that receive restricted sensory and motor inputs. The

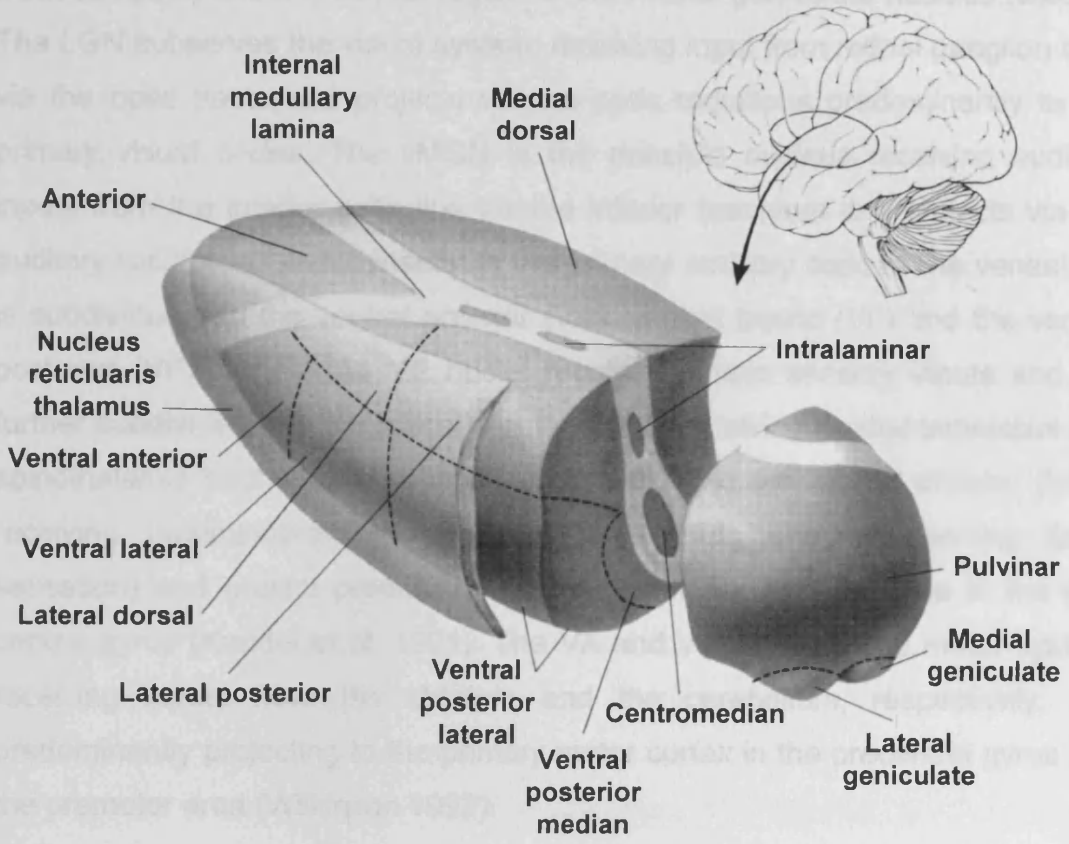

Figure 1.1 Gross anatomy of the thalamus.

The major nuclei of the thalamus as seen on the left side of the brain. The internal medullary lamina divides the anterior, lateral and medial nuclei. The lateral group is divided into dorsal and ventral tiers. The ventral tier is composed of the ventral anterior, ventral lateral and ventral posterior nuclei. The dorsal tier includes the lateral dorsal, lateral posterior and the pulvinar. The medial and lateral geniculate nuclei are clearly seen on the posterior aspect of the thalamus. Each nucleus in the ventral tier along with the medial and lateral geniculate nuclei receives specific sensory or motor information. The nucleus reticularis thalami caps the lateral aspect of the thalamus. (from Kandel et al. 1991).

specific relay nuclei of the dorsal tier comprise the dorsal lateral geniculate nucleus (LGN) and the ventral region of the medial geniculate nucleus (vMGN). The LGN subserves the visual system, receiving input from retinal ganglion cells via the optic tracts and projects via the optic radiations predominantly to the primary visual cortex. The vMGN is the principle nucleus receiving auditory inputs from the inferior colliculus via the inferior brachium and projects via the auditory radiations predominantly to the primary auditory cortex. The ventral tier is subdivided into the ventral anterior (VA), ventral lateral (VL) and the ventral posterior (VP) nuclei. The VP nuclei receive somatic sensory inputs and are further subdivided into the lateral division (VPL: receiving medial lemniscus and spinothalamic tract and representing the body) and the medial division (VPM: receiving trigeminothalamic and gustatory inputs and representing facial sensation) and project predominantly to the primary sensory area in the post central gyrus (Kandel et al. 1991). The VA and VL subserve the motor system, receiving inputs from the striatum and the cerebellum, respectively, and predominantly projecting to the primary motor cortex in the precentral gyrus and the premotor area (Wilkinson 1992).

Surrounding the lateral aspect of each thalamus and separated from the main thalamic mass by the external medullary lamina is the nucleus reticularis thalami (NRT) (Fig. 1.1) (Kandel et al. 1991). The NRT forms thin sheet-like nuclei containing an essentially homogenous population of inhibitory GABAergic neurones (Houser et al. 1980) that are strongly interconnected both between themselves and with the underlying thalamic nuclei. Despite no obvious anatomical divisions, but through the specificity of projections from the underlying thalamic regions, the NRT does appear to share a degree of modality specific compartmentalisation (Steriade et al. 1997; Crabtree et al. 1998). In particular, the portion of the NRT overlying the LGN in mammals such as cats is termed the perigeniculate nucleus (PGN). There appear to be no overt electrophysiological differences between neurones in this and other NRT regions (Steriade et al. 1997), although a degree of variation in the electrophysiological properties is reported (Llinas and Geijo-Barrientos 1988; Contreras et al. 1992).

1.3 THALAMIC RELAY NUCLEI AND THEIR CONNECTIVITY

Thalamic relay nuclei are broadly organised in the same way and contain many common elements (Fig. 1.2). In particular, each thalamic nucleus is comprised predominantly of cortically projecting, excitatory glutamatergic thalamocortical (TC) neurones with a variable complement of locally projecting, GABAergic inhibitory interneurones depending on the species and nucleus examined. For example, 25-30% of neurones in thalamic relay nuclei of primates and cats are GABAergic (Penny et al. 1983; Spreafico et al. 1983; Fitzpatrick et al. 1984), whereas in rats, around 20% of neurones are GABAergic in the LGN (Gabbott et al. 1986), but are almost completely absent in other thalamic relay nuclei (Barbaresi et al. 1986; De Biasi et al. 1988). These interneurones are completely contained within a given nucleus and therefore provide very localised inhibitory influences. GABAergic NRT neurones provide a second inhibitory influence to thalamic relay nuclei and through their exclusively intrathalamic projections they are also involved in many aspects of thalamic and thus corticothalamic activity. The connectivity of these three neuronal elements follows broadly the same principles regardless of the thalamic relay nucleus examined and are described in the following sections in order to fully appreciate their interacting influences.

1.3.1 Thalamocortical neurones.

TC neurones are the predominant cell type in all thalamic relay nuclei. Morphologically, TC neurones are broadly described as "bushy" cells, where dendrites extend radially from the soma. Variations in somal size, orientation and morphology of the dendritic arbour and complement of dendritic appendages have all been observed and lead to the description of morphologically distinct classes of TC neurones within different relay nuclei. The greatest variation has been described in the LGN in cats: comprising X, Y and W TC neurones that are correlated with the distinct functional pathways carrying visual information form X, Y and W retinal ganglion neurones. (Friedlander et al. 1981; Stanford et al. 1981; Stanford et al. 1983). It is also apparent that morphological differences can confer variations in passive cable properties: X cells having higher membrane input resistances and longer time constants than Y cells, but both having similar electrotonic lengths and dendritic-to-somatic conductances (Bloomfield et al. 1987; Crunelli et al. 1987b). Other thalamic relay nuclei do not show such distinctive morphological subtypes of TC neurones and appear to be variations that can be likened to LGN TC neurone subtypes. In the VP nucleus,

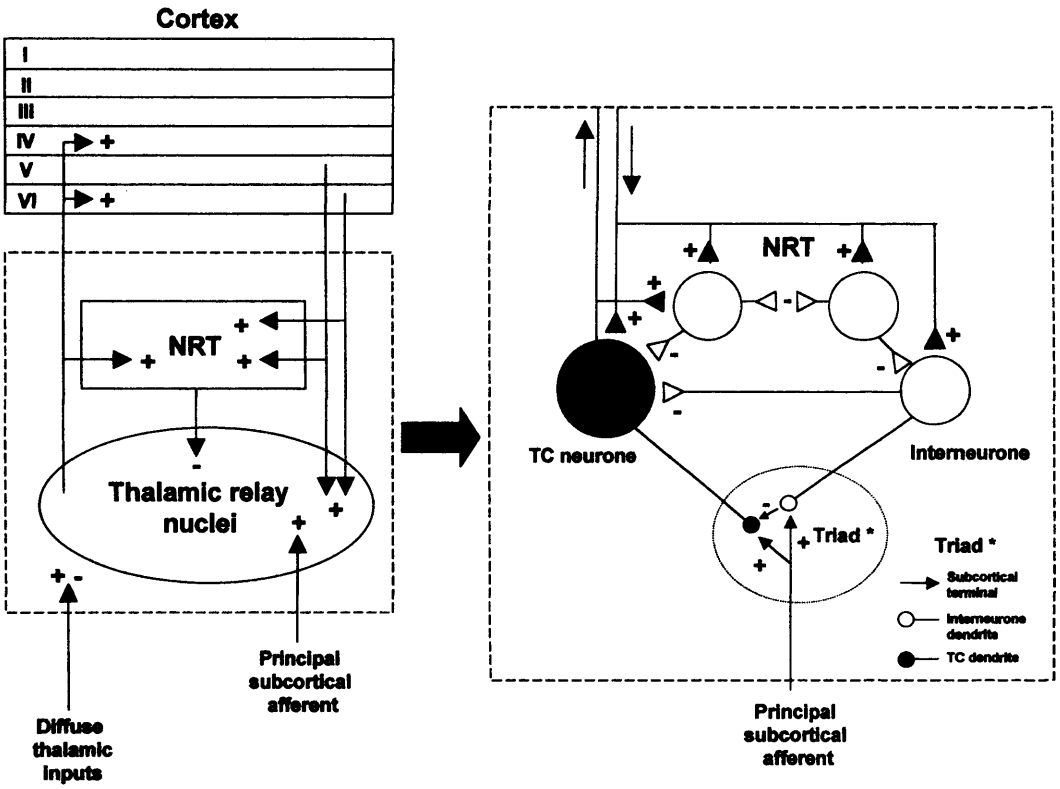

Figure 1.2 Schematic representation of the principle circuitry and cortical connections of thalamic relay nuclei.

The principle connections to and from thalamic relay nuclei are shown on the left. The expanded diagram on the right shows the intrathalamic circuitry. Excitatory (glutamatergic) neurones are black and inhibitory (GABAergic) neurones are white. Excitatory and inhibitory synapses are denoted by + or -, respectively.

morphological differences amongst TC neurones have distinguished 2 types of TC neurones (Spreafico et al. 1983; Yen et al. 1985b; Turner et al. 1997) and with some distinction between their response properties to peripheral stimuli (Yen et al. 1985b), but little difference between their electrophysiological membrane properties (Turner et al. 1997). TC neurones of the VA-VL complex have been described as having the typical radial dendritic arbour surrounding a centrally located soma seen in other TC neurones, but no morphological subdivisions have been described although it is apparent that some variation, including the dendritic arbour and complement of dendritic appendages, are possible (Sawyer et al. 1994; Sato et al. 1997). The vMGN is conspicuous for the rigid, laminar organisation of the large principle TC neurones (Morest 1965) with very little morphological variation (Winer 1985). vMGN TC neurones are described as having medium-sized, elongated soma with dendrites emerging from either end giving the dendritic arbour a polarised appearance with the long-axis of the arbour running parallel to the dorsoventral plane and is shortest lateromedially (Winer 1985)

The predominant projection site of TC neurones in modality-specific thalamic relay nuclei is the superficial and deep regions of layer 4, but also to layer 6, in the corresponding primary cortical areas (Steriade et al. 1997) (Fig. 1.2), where they evoke excitatory monosynaptic responses in the recipient cortical neurones (Agmon and Connors 1991; Salt et al. 1995). In addition, axon collaterals from these cortically projecting neurone also terminate in the NRT (Jones 1975) where they also have excitatory monosynaptic influences (Kim and McCormick 1998b).

Thalamic relay nuclei are functionally defined by the topographic modality-specific subcortical input. These inputs constitute around 10-20% of synapses onto LGN TC neurones (Hamos et al. 1987; Montero 1991). This principle subcortical input to TC neurones is glutamatergic (De Biasi and Rustioni 1990; Montero 1990; De Biasi et al. 1994) and predominantly terminate on the most proximal dendrites of TC neurones (Hamos et al. 1987; Sherman and Guillery 1996) evoking excitatory post-synaptic responses (Bloomfield and Sherman 1988). Although this is a significant synaptic input, TC neurones only receive inputs from a few subcortical neurones. For example, in the cat LGN, each TC

neurone only receives input from a few retinal ganglion cells (Hamos et al. 1987; Usrey et al. 1999) so the receptive field of the retinal ganglion cells is reliably transferred to the LGN maintaining the retinotopic distribution. By far the greatest synaptic input to TC neurones is derived from the cortex (Montero 1991; Erisir et al. 1998). Cortical areas receiving TC axonal projections, send reciprocal axonal projections back to the same thalamic nucleus (Jones 1985). Cortical neurones involved in this reciprocal circuit arise in layer 5 (motor circuitry) or 6 (sensory circuitry) (Steriade et al. 1997). Corticothalamic terminals synapse principally on the distal dendrites of TC neurones (Liu et al. 1995a), are glutamatergic (De Biasi and Rustioni 1990) and evoke excitatory monosynaptic responses (Ahlsen et al. 1982). Inhibitory terminals form a substantial part of the synaptic input to TC neurones, both derived from local interneurones and NRT neurones constituting 24-40% of the total synaptic input (Montero and Scott 1981; Wilson et al. 1984; Erisir et al. 1998).

1.3.2 Interneurones.

Interneurones, where present and regardless of the species or nucleus examined, have a characteristic morphology. Typically, they are characterised by a small soma (10-20 μm) (Majorossy and Kiss 1976; Spreafico et al. 1983; Montero and Singer 1985) and a compact dendritic field made up of long, thin, sinuous processes (Sherman and Friedlander 1988). Interneurones give rise to axons that terminate locally (Guillery 1966; Hamos et al. 1985) and to presynaptic dendrites that terminate on TC neurones and other interneurones (Jones and Powell 1969; Famiglietti and Peters 1972; Lieberman 1973; Spacek and Lieberman 1974). The specialised presynaptic dendrites are vesicle containing presynaptic specialisations that form symmetrical synapses (Lieberman 1973) and are implicated in the fine-tuning of incoming signals through their particular aggregation with terminals arising from sensory afferents at the proximal TC dendrites. Presynaptic dendrites arising from interneurones can be interposed between the subcortical terminal and the TC dendrites in an arrangement described as a triad (Fig. 1.2). In some nuclei, these aggregations are ensheathed by glial cells and have been called glomeruli (Jones and Powell 1969; Famiglietti and Peters 1972; Wilson 1989). This arrangement strongly suggests that modality-specific signals may modulated through a feed-forward inhibitory mechanism (Famiglietti and Peters 1972; Hamos et al. 1985).

Other sources of synaptic inputs arise from cortical afferents and terminate on the presynaptic dendrites (Friedlander et al. 1981; Kultas-Ilinsky and Ilinsky 1988; Ralston et al. 1988) or dendritic shafts (Friedlander et al. 1981; Weber et al. 1989). Although the density of corticothalamic terminals on interneurones is less than on TC neurones (Winfield 1980; Friedlander et al. 1981; Ralston et al. 1988; Erisir et al. 1998), the observation that corticothalamic stimulation evokes disynaptic inhibitory postsynaptic response in TC neurones mediated by interneurones implies effective functional innervation (Soltesz et al. 1989b; Deschenes and Hu 1990). The greatest source of inhibitory terminals to interneurones presumably derives from within the thalamic relay nuclei, that is from interneurones themselves as NRT neurones project predominantly to TC neurones and make few contacts to interneurones (Ohara et al. 1980; Montero and Scott 1981; Ohara et al. 1989; Wang et al. 2001).

1.3.3 Neurones of the nucleus reticularis thalami.

GABAergic NRT neurones constitute a fairly morphologically homogeneous population of neurones (Lubke 1993), although some variation in size has been reported, with smaller neurones present in anterior regions of the nucleus (Jones 1975). Somas are typically oval in shape, with a maximal diameter of 25-50 μm (Yen et al. 1985a; Llinas and Geijo-Barrientos 1988) and with dendritic processes arising from both ends giving a bipolar appearance (Houser et al. 1980; Yen et al. 1985b; Llinas and Geijo-Barrientos 1988). The dendritic arborisation is discoidal in shape and flattened parallel to the borders of the nucleus (Yen et al. 1985b; Lubke 1993). Dendrites tend to be long, branching irregularly and with occasional dendritic appendages that in some species give rise to presynaptic dendrites that primarily terminate on other NRT dendrites (Deschenes et al. 1985; Yen et al. 1985a; Mulle et al. 1986; Pinault et al. 1997). It has been shown that further specialisation can occur at these dendrodendritic appositions, through the formation of small, intercellular junctions called "puncta adherentia" (Ohara and Lieberman 1985; Pinault et al. 1997). These junctions have been speculatively introduced as a potential site of electrotonic communication that has now been demonstrated among subsets of NRT neurones (Landisman et al. 2002). However, these junctions remain as yet morphologically described without any determination of functionality.

NRT axons project to the underlying thalamic area, but give rise to 2-3 short axon collaterals that terminate locally within the NRT, close to the originating neurone (Yen et al. 1985a; Mulle et al. 1986; Uhlrich et al. 1991; Liu et al. 1995b). GABAergic terminals have been shown to terminate on both proximal and distal dendrites and specialised dendritic appendages of NRT neurones (Liu and Jones 1999), but contribute fewer terminals (10-25%) in comparision to TC and cortical inputs (Liu and Jones 1999). Nonetheless, this is presumably enough to provide a mechanism for mutual inhibition (von Krosigk et al. 1993; Huguenard and Prince 1994; Bal et al. 1995b; Shu and McCormick 2002). Axons that pass to the underlying thalamic territory ramify mainly in the nucleus related to that sector of the NRT where the originating soma arises. Terminals are concentrated in one part of the thalamic nucleus apparently giving rise to a crude topographic relationship between related thalamic and NRT nuclei (Liu et al. 1995b; Pinault et al. 1995b; Pinault et al. 1995a). Axons terminate predominantly on the soma, and dendrites of TC neurones (Ohara et al. 1989; Cucchiaro et al. 1991; Bal et al. 1995a; Liu et al. 1995b; Wang et al. 2001).

NRT neurones receive synaptic inputs from axon collaterals of TC and cortical neurones (Jones 1975; Montero 1989; Williamson et al. 1993), with the corticothalamic terminals providing the greatest density of inputs particularly at distal dendritic sites and TC inputs predominantly aggregated on proximal dendrites (Liu and Jones 1999). The TC input has functionally been demonstrated through the stimulation of principal subcortical inputs to thalamic relay nuclei resulting in disynaptically evoked EPSPs in NRT neurones (Ide 1982; Montero 1989). Additionally, powerful activation leading to prolonged spike barrages is observed in NRT neurones after cortical or corticothalamic tract stimulation (Frigyesi 1972; Steriade and Wyzinski 1972; Waszak 1974). There is also evidence indicating that the cortex has a more powerful excitatory effect on NRT neurones than TC neurones (Golshani et al. 2001).

1.3.4 Diffusely projecting inputs to the thalamus.

In addition, the thalamus also receives many other diffusely projecting inputs from the brainstem and a variety of other structures that utilise a number of different neurotransmitters. These include the 5-hydroxytryptamine (5-HT)

containing neurones arising in raphe nuclei, noradrenaline (NA) containing neurones arising in the locus coeruleus and acetylcholine (Ach) containing neurones arising from the pedunculopontine tegmental and lateral dorsal tegmental nuclei of the brainstem (Leger et al. 1975; Morrison and Foote 1986; Hallanger et al. 1987; Pare et al. 1988; Smith et al. 1988; Steriade et al. 1988). Additionally, Ach containing fibres arise from the basal forebrain (Hallanger et al. 1987; Parent et al. 1988; Semba 2000), whilst histamine (HA) containing neurones arise from the tuberomammillary nucleus of the hypothalamus (Panula et al. 1989; Uhlrich et al. 1993). Furthermore, a variety of other neuroactive peptides have been shown to be co-localised in thalamic afferents or thalamic neurones, and to have a role in modulating thalamic activity, including: adenosine (Pape 1992), nitric oxide (NO) (Pape and Mager 1992; Bickford et al. 1993), cholecystokinin (CCK) (Cox et al. 1995; Lee and McCormick 1997), Neuropeptide Y (Morris 1989; Qian-Quan et al. 2001; Qian-Quan et al. 2003), opioids (Brunton and Charpak 1998) and somatostatin (Leresche et al. 2000; Qian-Quan et al. 2002). Rostrally projecting brainstem projections are implicated in cortical arousal and maintaining states of consciousness, acting in part via the thalamus (Steriade et al. 1982; Steriade et al. 1990; Steriade 1993).

1.3.5 Synaptic physiology of thalamic circuitry.

Within the thalamus, two neurotransmitters dominate: glutamate as the predominant excitatory neurotransmitter and GABA as the predominant inhibitory transmitter, in a system that is based simplistically on a system of excitatory input and outputs driving intrathalamic inhibitory neurones that sculpt and modulate the output. However, utilisation of different neurotransmitter receptors within thalamic circuitry adds to the complexity of the system (Fig. 1.3).

Glutamatergic activity within the thalamocortical loop arises through both fast responses mediated by ionotropic receptors and slower responses mediated through G-protein coupled metabotropic glutamate (mGluR) receptors. mGluR receptors fall into 3 groups: Group I (mGluR 1 and 5), Group II (mGluR 2 and 3) and Group III (mGluR 4,6 and 7) (Pin and Duvoisin 1995). Glutamatergic inputs arising from the principal subcortical afferents to TC neurones are mediated via non-N-methyl-D-aspartate (NMDA) and NMDA receptors (Salt 1986; Salt 1987; Scharfman et al. 1990; Sillito et al. 1990a; Sillito et al. 1990b; Turner et al. 1994).

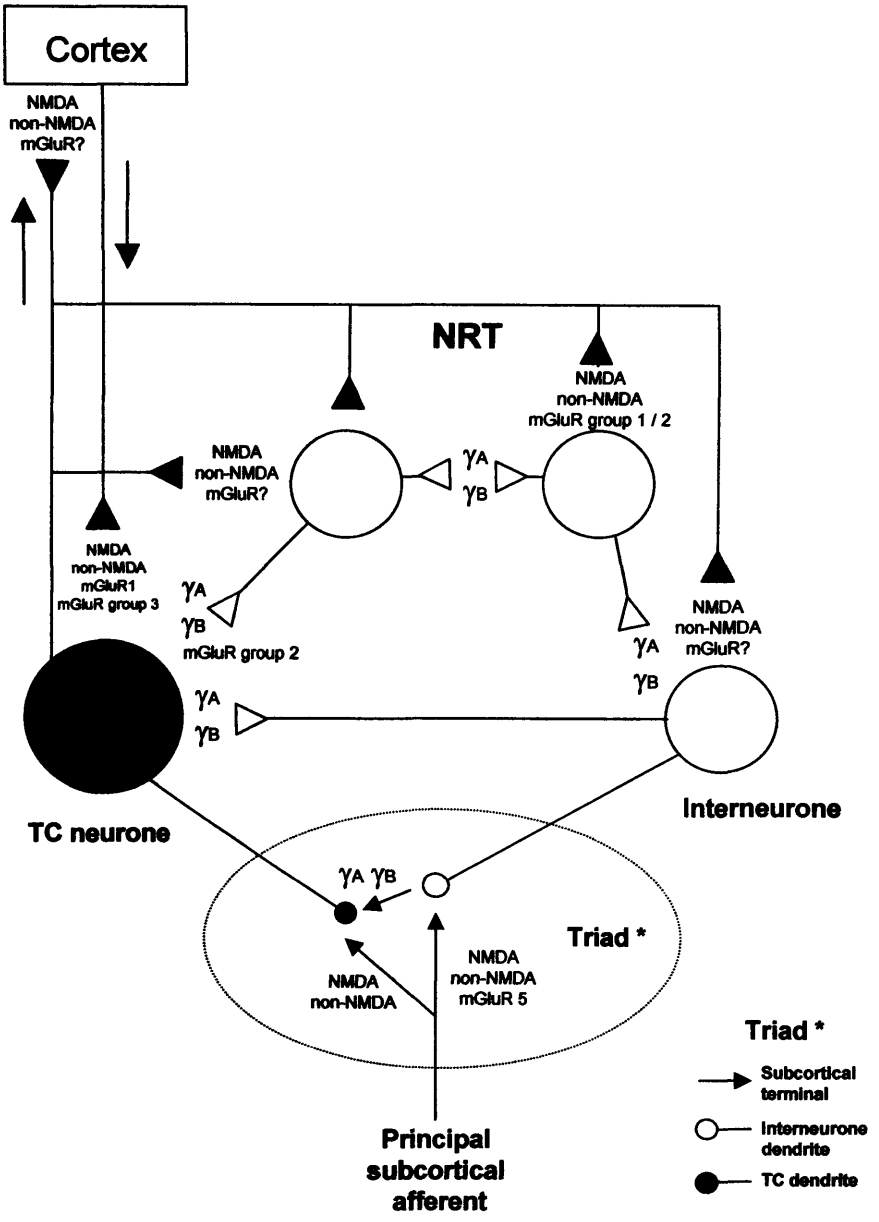

Figure 1.3 Postsynaptic receptors of thalamic circuitry.

Schematic representation of the excitatory and inhibitory synaptic connectivity of the thalamocorticothalamic and intrathalamic loops. The presence of postsynaptic glutamatergic receptors are denoted by NMDA (N-methyl-D-aspartate), non-NMDA and mGluR (metabotropic gluatamate receptors). GABAergic receptors are denoted by γA and γB corresponding to $GABA_A$ and $GABA_B$ receptor subtypes, respectively. Black shading indicates excitatory neurones and terminals, and unshaded (white) indicates inhibitory neurones and terminals as in Fig. 1.2. Presynaptic receptors have been excluded for clarity.

Stimulation of the optic tract can also evoke non-NMDA and NMDA responses in interneurones (Pape and McCormick 1995; Williams et al. 1996). Identification of mGluR 5 receptors on the dendrites of interneurones associated with the retinal inputs to LGN TC neurones (Godwin et al. 1996) suggests that mGluRs may have a role in modulating the subcortical afferent input. In keeping with this, mGluR receptor activation can activate the relatively electrically isolated dendrites of interneurones thereby inhibiting TC neurones and suggesting a role for mGluR modulation of subcortical inputs within the triadic arrangement (Cox et al. 1998). TC glutamatergic inputs to the cortex and NRT also evoke both non-NMDA and NMDA receptor-mediated responses (Salt et al. 1995; Gil and Amitai 1996).

Activation of corticothalamic pathways elicits responses mediated through non-NMDA and NMDA receptors and also through mGluR receptors (Deschenes and Hu 1990; McCormick and von Krosigk 1992; Eaton and Salt 1996), leading to an initial fast response and a slower long-lasting depolarisation (McCormick and von Krosigk 1992) in TC neurones. This long-lasting response occurs primarily through mGluR 1 receptors (Salt et al. 1999; Turner and Salt 2000) and in accordance with this an mGluR1α splice-variant of the mGluR1a receptor subtype has been localised to TC dendrites and predominantly postsynaptic to corticogeniculate inputs in the LGN (Godwin et al. 1996). Repetitive corticogeniculate stimulation can also enhance response in TC neurones that is thought to be in part brought about by a reduction in inhibition (McCormick and von Krosigk 1992). A reduction of cortically evoked EPSPs in TC neurones was observed after activation of Group III mGluRs in the rat VB, that might have a functional role following prolonged cortical barrages (Turner and Salt 1999). Excitatory corticothalamic responses in the NRT are also mediated via non-NMDA, NMDA and mGluR receptors (De Curtis et al. 1989; Salt and Eaton 1996; Lee and McCormick 1997). In accordance with this, depolarisation of NRT neurones via Group I mGluRs (Lee and McCormick 1997; Cox and Sherman 1999) has been observed, although hyperpolarisation also occurs via Group II mGluRs (Cox and Sherman 1999) in NRT neurones.

GABAergic inhibition is also mediated through fast ionotropic ($GABA_A$) and slower G-protein coupled metabotropic ($GABA_B$) receptors in the thalamus (Fig.

1.3). Inputs to TC neurones following subcortical afferent stimulation results in a 2-component fast $GABA_A$ and slow $GABA_B$ response through activation of local interneurones (Crunelli et al. 1988; Soltesz et al. 1989a). Likewise, activation of NRT neurones evokes fast and slow IPSPs in TC neurones (Bal et al. 1995b; Sanchez-Vives and McCormick 1997; von Krosigk et al. 1999). In rat VB neurones (where the inhibitory input derives from the NRT) a reduction of inhibition in response to sensory stimulation was observed following Group III mGluR activation (Salt and Turner 1998). Inhibitory input to the NRT is mainly mediated by $GABA_A$ receptors although functional $GABA_B$ receptors are present (Ulrich and Huguenard 1996; Sanchez-Vives et al. 1997). Inhibitory input to interneurones have been shown, as stimulation of the optic tract can evoke $GABA_A$, but not $GABA_B$ response in LGN interneurones (Williams et al. 1996).

1.4 MEMBRANE CURRENTS OF THALAMOCORTICAL NEURONES

The predominant description given here applies to TC neurones. However, some references are made to interneurones in order to highlight functional similarities or differences.

1.4.1 Na^+ currents.

TC neurones, posses the ability to fire tonic trains of Na^+ dependent action potentials either in response to injection of depolarising d.c. current or in response to depolarising current steps (Fig. $1.4A_1$) (Jahnsen and Llinas 1984b; Jahnsen and Llinas 1984a). In addition, a persistent Na^+ current with a lower activation threshold than action potential generation has also been demonstrated in TC neurones (Jahnsen and Llinas 1984b; Jahnsen and Llinas 1984a; Parri and Crunelli 1998). Both fast and persistent components of the Na^+ current are sensitive to TTX and the same functional channels in TC neurones is strongly suggested to underlie both components (Parri and Crunelli 1998). Interneurones also fire tonic trains of Na^+ dependent action potentials and typically within a higher frequency range than TC neurones (Pape and McCormick 1995; Williams et al. 1996).

1.4.2 Ca^{2+} currents.

Ca^{2+} currents in TC neurones comprise 2-types, low-voltage activated (LVA, or T-type) Ca^{2+} currents activated from hyperpolarised membrane potentials

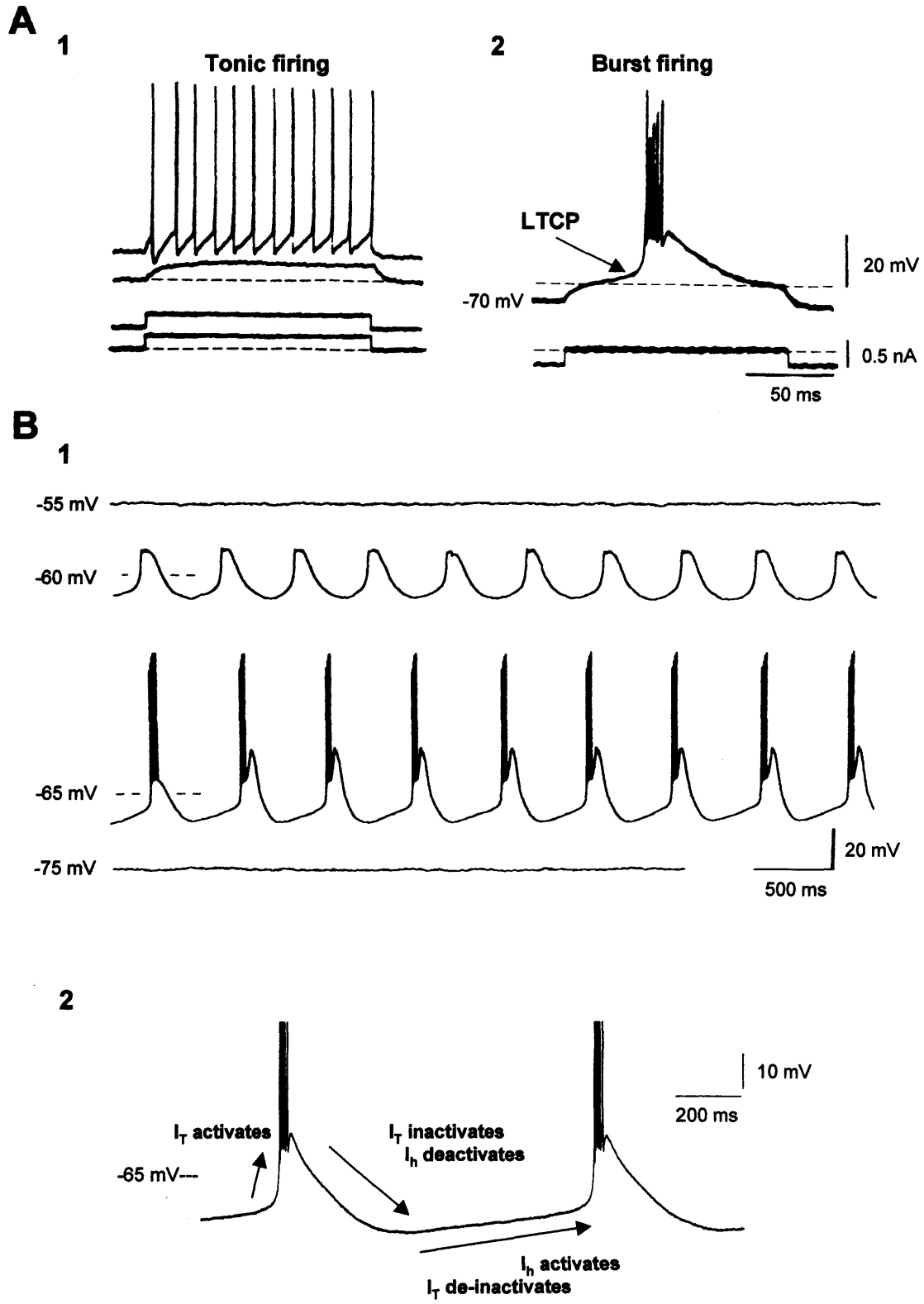

Figure 1.4 Intrinsic electrophysiological properties of TC neurones.

Figure 1.4 Intrinsic electrophysiological properties of TC neurones.

(A) The burst and tonic firing modes in a TC neurone. Injection of a constant amplitude depolarising current step at three different levels of membrane potential. From a depolarised membrane potential a positive depolarising voltage response is evoked and from the most depolarised membrane potential, the current pulse evokes a train of action potentials (1). From the most hyperpolarised membrane potential the current pulse evokes a burst of action potentials (2). Broken horizontal lines in the upper traces of 1 and 2 indicate the same membrane potential. Broken lines in the lower traces of 1 and 2 indicate the same level of injected d.c. current. (from Jahnsen and Llinas 1984b).

(B) Voltage dependence of the δ oscillation. Intracellular voltage recording from a TC neurone in the cat dLGN maintained *in vitro*. The δ oscillation was observed within the membrane potential range of –57 to –73 mV. Note that in the trace marked –60mV, the large depolarisations have a higher frequency and smaller amplitude than those observed in the trace marked –65 mV and do not evoke action potential bursts (1). (from Leresche et al. 1991). Schematic figure showing the interaction of I_T and I_h in the generation of the δ oscillation. Action potentials have been truncated (2).

(<-60mV) and high-voltage activated (HVA) Ca^{2+} currents activated at more depolarised membrane potentials. The HVA currents are dissociated into L, N, P, Q and R-types using various pharmacological tools: the L-type current is dihydropyridine sensitive, the N-type current is ω-conotoxin GVIA sensitive. N, the P and Q-type currents are ω-conotoxin MVIIC sensitive. In addition, the P-type current is potently ω-agatoxin IVA sensitive where as the Q-type current is weakly sensitive to ω-agatoxin IVA and the residual R-type current is insensitive to dihydropyridines and toxins (Nowycky et al. 1985; Hillyard et al. 1992; Ellinor et al. 1993; Zhang et al. 1993; Randall and Tsien 1995)

The presence of Ca^{2+} conductances has been known for some time in TC neurones, most prominently in the expression of the low-threshold calcium potential (LTCP) (Fig. 1.4A_2) that is dependent on the T-type current (I_T) (Coulter et al. 1989; Crunelli et al. 1989; Hernandez-Cruz and Pape 1989). I_T is activated following depolarisation from fairly hyperpolarised membrane potentials (<-60mV) and has relatively fast activation and inactivation properties (Crunelli et al. 1989). Activation of I_T by depolarising current steps or at the offset of hyperpolarising current steps applied at membrane potentials around -60mV leads to the generation of a LTCP that may evoke a burst of Na^+ dependent action potentials (Jahnsen and Llinas 1984a; Jahnsen and Llinas 1984c; Crunelli et al. 1989). Removal of inactivation of I_T is both time- and voltage-dependent. I_T can be de-inactivated following membrane potential shifts to below around -65mV for around 500-600ms under physiological conditions (Crunelli et al. 1989). The particular kinetics of I_T and required refractory period can thus lead to intrinsic, repetitive burst firing, typically at 1-2 Hz, in TC neurones (Fig. 1.4B) (δ-oscillation, see section 1.5.3) seen at fairly hyperpolarised membrane potentials (Leresche et al. 1991). The distribution of T-type Ca^{2+} channels in TC neurones has been shown to be non-uniform and is greatest around the proximal dendrites (Williams and Stuart 2000). Additionally, the region of overlap observed between the activation and inactivation curves of I_T in TC neurones (Coulter et al. 1989; Crunelli et al. 1989) results to the manifestation of a steady-state component $I_{Twindow}$ (Williams et al. 1997a). Thus in a small region of membrane potentials centred around –60mV I_T is always active and underlies bistability-mediated activities in TC neurones (see section 1.5.4) (Williams et al. 1997a; Toth et al. 1998; Hughes et al. 1999).

Interneurones can evoke single action potentials or bursts of action potentials at the offset of a hyperpolarising pulse, but do not display a LTCP (Pape and McCormick 1995; Williams et al. 1996). The lack of the LTCP in interneurones has been attributed its suppression due to the presence of opposing K^+ channels, in particular I_A (Pape and McCormick 1995). In TC neurones, the activation threshold of I_T (~ -80mV) was ~ -20mV more negative compared to the activation threshold of I_A. In interneurones the activation curve of I_T was more positive compared to TC neurones (V_{half} = -54.9mV and -64.5mV, respectively) whilst the activation curve of I_A was more negative (-25mV and -14.5mV, respectively) (Pape et al. 1994).

The existence of HVA Ca^{2+} currents in TC neurones is well established (Jahnsen and Llinas 1984b; Hernandez-Cruz and Pape 1989; Guyon and Leresche 1995; Kammermeier and Jones 1997; Budde et al. 1998) and have been identified as L-type, N-type, two ω-conotoxin MVIIC sensitive currents differing in their sensitivity to ω-agatoxin IVA (thus presumably representing P and Q-type currents) with a small insensitive component remaining (Guyon and Leresche 1995; Kammermeier and Jones 1997). Functionally, HVA Ca^{2+} channels are thought to underlie subthreshold Ca^{2+} spikes and high frequency oscillatory activity predominantly at 25-50 Hz when neurones were depolarised beyond -45mV (Pedroarena and Llinas 1997). Simulations of TC activity indicate that HVA Ca^{2+} currents are involved in controlling firing patterns and the formation of individual action potentials (McCormick and Huguenard 1992; Toth and Crunelli 1992). The high density of active K^+ channels at depolarised membrane potentials and the proposed dendritic location of subtypes of HVA Ca^{2+} channels (Pedroarena and Llinas 1997) presumably effectively dampen voltage responses recorded somatically and may underestimate the role of HVA Ca^{2+} currents in relatively electrically isolated dendritic regions.

1.4.3 K^+ currents.

TC neurones possess a variety of K^+ currents that primarily serve to provide outward rectification and repolarise the membrane potential following depolarising events.

The delayed rectifier current is involved in the repolarising phase of action potentials. However various other K^+ channels are also implicated in this function. Action potentials in TC neurones are followed by a pronounced afterhyperpolarisation (AHP) that is markedly Ca^{2+} sensitive (Jahnsen and Llinas 1984b). Both fast-activating and more slowly activating Ca^{2+} dependent K^+ conductances have been identified in TC neurones (Huguenard and Prince 1991; Budde et al. 1992). Both show voltage-dependence and are activated after depolarisation, thus given their differential activation kinetics they could contribute both to the AHP and to spike repolarisation itself. Additional voltage-dependent transient K^+ currents are also present in TC neurones that have differential activation and inactivation kinetics. One such current is I_A. I_A is rapidly activated above –60mV and than more slowly inactivated, and is thus active in the same membrane potential region as I_T (Huguenard et al. 1991). As such I_A is implicated in mediating the delay before the onset of tonic firing activity in response to a depolarising current step from membrane potential above -60mV, in shaping the LTCP evoked from more depolarised membrane potentials and also in the action potential repolarisation and shaping the AHP (Jahnsen and Llinas 1984b; Huguenard et al. 1991; Budde et al. 1992; Huguenard and McCormick 1992). Other identified voltage dependent transient K^+ channels have slower inactivation kinetics (Huguenard et al. 1991; Huguenard and Prince 1991; McCormick 1991b; Budde et al. 1992). In striking contrast, another K^+ channel has been identified in VB TC neurones (I_{KIR}). I_{KIR} is an outward rectifying (hyperpolarising) Ba^{2+}-sensitive current that is activated by membrane hyperpolarisation. Functionally I_{KIR} in VB TC neurones is fast activating and is hypothesised to amplify incoming IPSPs and aid de-inactivation of I_T to promote LTCP production (Williams et al. 1997b). Finally, TC neurones have a constitutive K^+ leak current (I_{KLeak}). The functional implication of reduction of this current have been investigated both through pharmacological manipulation (Lee and McCormick 1997; Salt et al. 1999; Turner and Salt 2000) and use of the dynamic clamp technique (Hughes et al. 1999). Such studies demonstrate that a reduction of I_{KLeak} results in neuronal depolarisation (Lee and McCormick 1997; Salt et al. 1999; Turner and Salt 2000) and can allow the expression of $I_{Twindow}$ and bistability-mediated activities in TC neurones (see section 1.5.4) (Williams et al. 1997a; Hughes et al. 1999).

1.4.4 Hyperpolarisation-activated mixed cation current.

A depolarising "sag" potential in response to hyperpolarising current steps is well documented in TC neurones and indicative of the presence of a hyperpolarisation activated mixed cation current (I_h) (Deschenes et al. 1984; Pape and McCormick 1989; McCormick and Pape 1990; Soltesz et al. 1991). I_h in TC neurones has been extensively investigated and is defined by 1) Voltage-dependence: I_h is active in the voltage range between about –60 to – 90mV; 2) kinetics: has slow activation and is non-inactivating; 3) is carried by Na^+ and K^+ ions; 4) is blocked by extracellular application of Cs^+ and the bradycardic agent ZD 7288 (McCormick and Pape 1990; Soltesz et al. 1991; Williams et al. 1997b). The interaction of I_h and I_T in TC neurones gives rise to rhythmic bursting (δ-oscillation, see section 1.5.3). The presence of the pronounced depolarising "sag" potential is regarded as one of the defining electrophysiological features of TC neurones amongst thalamic neurones (McCormick and Pape 1988; Bal and McCormick 1993).

1.5 ELECTROPHYSIOLOGY OF THALAMOCORTICAL NEURONES

Two "classical" distinctive modes of firing are observed in TC neurones, the "tonic" and the "burst" mode (Fig. 1.4A) (Jahnsen and Llinas 1984a) that predominate during different behavioural states (Glenn and Steriade 1982; McCarley et al. 1983). At depolarised membrane potentials (-50mV or above), the activity of TC neurones is dominated by sustained tonic action potential firing that is well correlated with the high-frequency, low-amplitude EEG activity that characterises wakefulness and REM sleep (Steriade et al. 1997). In contrast, hyperpolarisation of TC neurones (of up to 20mV) results in the de-inactivation of I_T and induction of LTCP-mediated bursts of action potentials that dominate TC activity during decreased arousal and sleep states where the EEG is characterised by large-amplitude slow waves (Cooper 1994). However, although this "classical" distinction in the functional mode of TC neurones under the respective behavioural state may predominate, burst firing has also been observed during the waking state (Guido and Weyand 1995; Ramcharan et al. 2000; Swadlow and Gusev 2001; Weyand et al. 2001). In the LGN, bursts are predominantly associated with stimulus presentation and are thought to have a role in stimulus detection (Guido et al. 1992; Guido and Weyand 1995; Guido and Sherman 1998; Reinagel et al. 1999). As thalamic bursting occurs during

states of drowsiness, inattention or under anaesthesia, thalamic bursting has also been suggested to be involved in attentional mechanisms (Sherman and Guillery 1996; Swadlow and Gusev 2001).

1.5.1 Tonic firing.

Sustained tonic firing of action potentials in TC neurones, typically observed during states of increased arousal and REM sleep, can be induced in TC neurones during neuronal depolarisation at membrane potentials above around -50mV (Fig. 1.4A_1). These repetitive events are classical Na^+/K^+ mediated regenerative action potentials, each followed by an afterhyperpolarising potential (AHP) and with the frequency increasing with the level of depolarisation (Jahnsen and Llinas 1984b; Jahnsen and Llinas 1984a). The ability of TC neurones to fire sustained, repetitive action potentials allows a more linear TC output in response to incoming stimuli and thus faithful transfer of information to the cortex presumably for stimulus analysis and perception.

1.5.2 Burst firing.

Burst firing in TC neurones is mediated by activation of I_T following its de-inactivation at hyperpolarised membrane potentials. When TC neurones are depolarised from a hyperpolarised membrane potential or can be readily hyperpolarised by incoming IPSPs, then the response elicited will comprise, after a variable delay, a LTCP resulting from activation of I_T (Fig. 1.4A_2) (see section 1.4.2). Generally, activation of I_T is large enough to produce a LTCP that will reach the threshold for action potential generation and thus will elicit a high frequency burst of 2-8 action potentials at 200-400 Hz (Steriade et al. 1997). The rapid inactivation of I_T and the refractory period required for de-inactivation before subsequent activation would suggest that the ability of burst firing to reliably transmit information is limited. Thus during states of decreased arousal and sleep when the brain is essentially cut off from external stimuli at least, rhythmic burst firing in TC neurones acts as a gating mechanism to prevent reliable signal transfer to the cortex. A variety of rhythmic bursting activities which involve LTCPs are seen in TC neurones in different sleep stages: namely the slow <1Hz oscillation, spindle oscillations and δ-oscillations. The δ-oscillation is an intrinsic TC activity (Leresche et al. 1990; Leresche et al. 1991; Soltesz and Crunelli 1992) and will be described here although its role within the

thalamocortical circuitry and relation to other sleep oscillations are described in sections 1.8.

1.5.3 δ-oscillation.

The δ-oscillation in TC neurones arises through the interaction of I_T and I_h and given the overlapping activation ranges of both currents (see sections 1.4.2 and 1.4.4) is distinctly voltage-dependent, existing at hyperpolarised membrane potentials (around -60mV to -80mV) (Fig. 1.4B) (McCormick and Pape 1990; Leresche et al. 1991; Soltesz et al. 1991). The δ oscillation arises through the following sequence of events: neuronal hyperpolarisation results in activation of I_h that subsequently causes a slow depolarisation of the TC neurone. The slow depolarisation provides sufficient time for de-inactivation of I_T and brings the membrane potential to the threshold for I_T activation. Thus when the threshold of I_T activation is reached a LTCP is evoked often giving rise to a burst of action potentials. The hyperpolarisation following the peak of the LTCP results from the rapid de-inactivation of I_T and is accentuated by deactivation of I_h during the depolarisation of the LTCP. Hyperpolarisation serves to reactivate I_h so that the cycle is regenerative and oscillatory activity is maintained (Fig. 1.4C) (McCormick and Pape 1990; Soltesz et al. 1991). In this way I_h serves as a "pacemaker" current and in combination with the time-dependent de-inactivation of I_T the δ-oscillation can occur within the frequency range of 0.5-4 Hz (Leresche et al. 1991). Within the range of membrane potential where the δ-oscillation exists a voltage dependent transformation of the waveform occurs. At more hyperpolarised levels, the δ-oscillation is slightly slower, LTCPs are larger in amplitude and duration and are more likely to support high frequency bursts of action potentials (Fig. 1.4B) (Leresche et al. 1991).

1.5.4 Membrane bistability and bistability-mediated activities.

In TC neurones, $I_{Twindow}$ has been shown to have a role in determining the neuronal output. The interaction of $I_{Twindow}$ and I_{KLeak}, underlies bistability-mediated activities in TC neurones. $I_{Twindow}$ arises due to the overlapping region of the steady-state activation and inactivation curves of I_T (Fig. 1.5A). This means that in a small region of membrane potentials centred around -60 mV, a small proportion of T-type Ca^{2+} channels remain open thus providing a steady influx of Ca^{2+} into the neurone and steady depolarisation. When the absolute

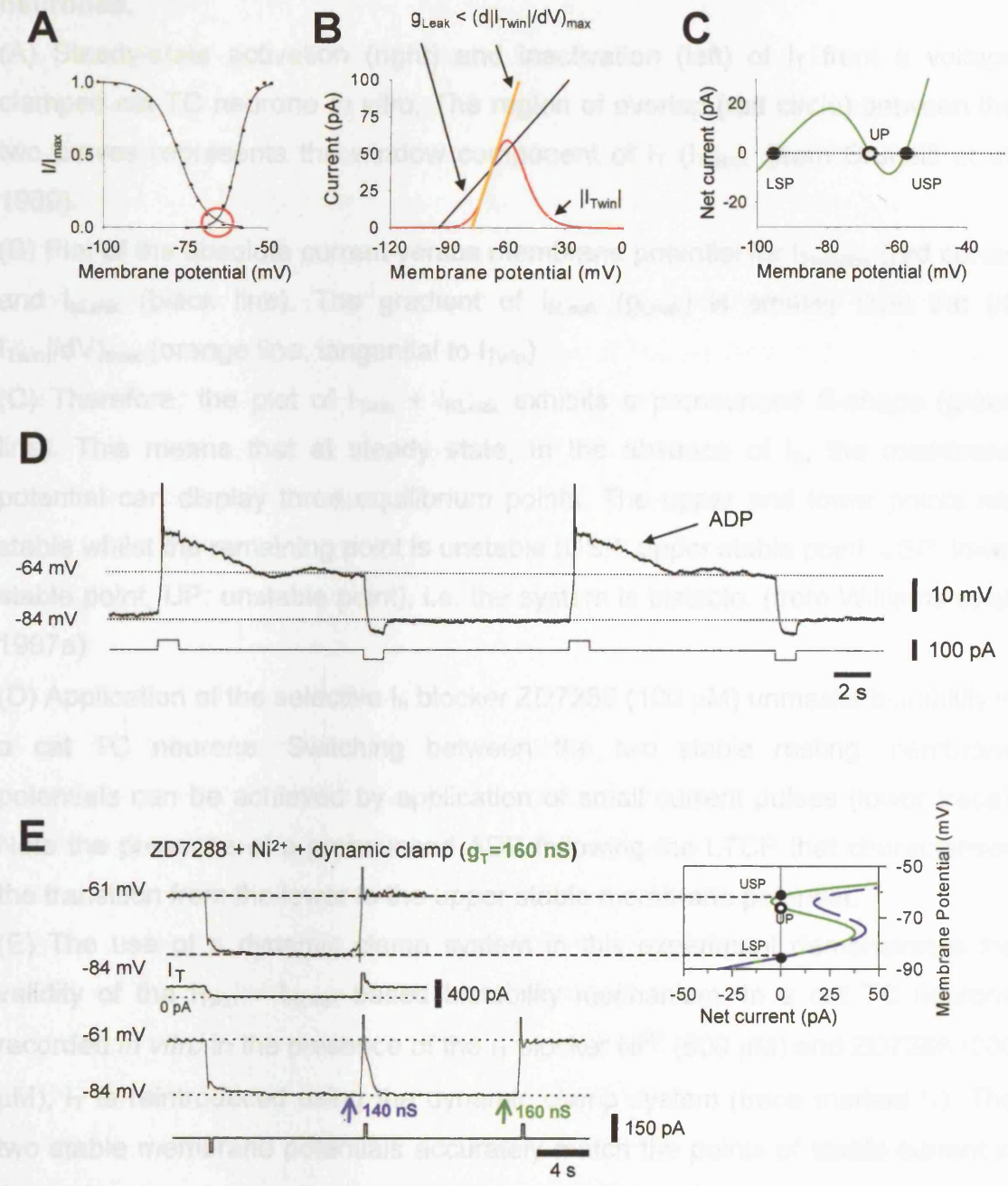

Figure 1.5 Biophysical mechanisms of $I_{Twindow}$ based bistability in TC neurones.

Figure 1.5 Biophysical mechanism of $I_{Twindow}$ based bistability in TC neurones.

(A) Steady-state activation (right) and inactivation (left) of I_T from a voltage clamped cat TC neurone *in vitro*. The region of overlap (red circle) between the two curves represents the window component of I_T (I_{Twin}). (from Crunelli et al. 1989).

(B) Plot of the absolute current versus membrane potential for $I_{Twindow}$ (red curve) and I_{kLeak} (black line). The gradient of I_{kLeak} (g_{Leak}) is smaller than the $(d|I_{Twin}|/dV)_{max}$ (orange line, tangential to I_{Twin}).

(C) Therefore, the plot of I_{Twin} + I_{KLeak} exhibits a pronounced S-shape (green line). This means that at steady state, in the absence of I_h, the membrane potential can display three equilibrium points. The upper and lower points are stable whilst the remaining point is unstable (USP: upper stable point, LSP: lower stable point, UP: unstable point), i.e. the system is bistable. (from Williams et al. 1997a).

(D) Application of the selective I_h blocker ZD7288 (100 μM) unmasks bistability in a cat TC neurone. Switching between the two stable resting membrane potentials can be achieved by application of small current pulses (lower trace). Note the presence of a pronounced ADP following the LTCP that characterises the transition from the lower to the upper stable membrane potential.

(E) The use of a dynamic clamp system in this experiment demonstrates the validity of the I_{Twin} – I_{KLeak} based bistability mechanism. In a cat TC neurone recorded *in vitro* in the presence of the I_T blocker Ni^{2+} (500 μM) and ZD7288 (300 μM), I_T is reintroduced using the dynamic clamp system (trace marked I_T). The two stable membrane potentials accurately match the points of stable current in the voltage vurses net current plot constructed using this neurone's g_{Leak} (calculated as $1/R_N$) and the indicated artificial I_T (continuous green line in plot).

A decrease in the conductance of artificial I_T from 160nS to 140nS fails to elicit bistability as only one equilibrium point is present for this combination of g_{Leak} and I_T (broken blue line in plot). However, bistability is reinstated when the conductance of artificial I_T is increased back to 160nS.

(D, E and F from Hughes et al. 1999).

value of $I_{Twindow}$ is plotted against the conductance of I_{KLeak} (g_{Leak}), if g_{Leak} is smaller than $(d|_{Ttwindow}|/dV)_{max}$, then the plot of g_{Leak} crosses the plot of $I_{Twindow}$ at three points (Fig. 1.5B). Given that $I_{Twindow}$ is an inward current and I_{KLeak} is an outward current, these three points correspond to three membrane potentials where the net current is 0pA (Fig. 1.5C). Therefore at steady state and in the absence of other substantial currents in the same membrane potential region, predominantly I_h, the membrane potential displays three equilibrium points corresponding to 0pA net current and have been described as the upper stable point (USP), lower stable point (LSP) and the unstable point (UP) (Fig. 1.5C). Thus under these conditions, the interaction of $I_{Twindow}$ and I_{KLeak} gives rise to bistability, with TC neurones displaying two stable resting membrane potentials (USP and LSP), separated by about 30mV, at the same value of injected d.c. current and that can be "flipped" between through appropriate small d.c. current perturbations (Fig. 1.5D and E) (Hughes et al. 1998; Toth et al. 1998; Hughes et al. 1999).

The outcome of the interaction of $I_{Twindow}$ and I_{KLeak} under physiological conditions is the induction of bistability-mediated activities. These include: 1) low (<1Hz) frequency oscillatory activity due to a "shoulder" following the LTCP (Fig. 1.6A), 2) temporal and voltage amplification, that is where small d.c. current steps or postsynaptic potentials applied at membrane potentials around -60mV are amplified both in time (Fig. 1.6B) and voltage (Fig. 1.6C). A small percentage (15%) of TC neurones have been shown to display these bistability-mediated activities in control conditions (Williams et al. 1997a). Subsequently, the use of a dynamic clamp system has shown that by effectively reducing endogenous I_{KLeak} 95% of TC neurones can express bistability-mediated activities (Hughes et al. 1999). Physiologically, the presence of bistability mediated activities may allow subthreshold postsynaptic potentials to be amplified in voltage and thus generate an output, perhaps providing a mechanism ensuring even small subthalamic inputs reach the cortex (Williams et al. 1997a). Given that I_{KLeak} is modulated by a number of neurotransmitters and neuroactive agents in TC neurones (McCormick 1991a; Lee and McCormick 1997), the possibility of unmasking bistability-mediated activities in TC neurones with endogenous agents seems very likely.

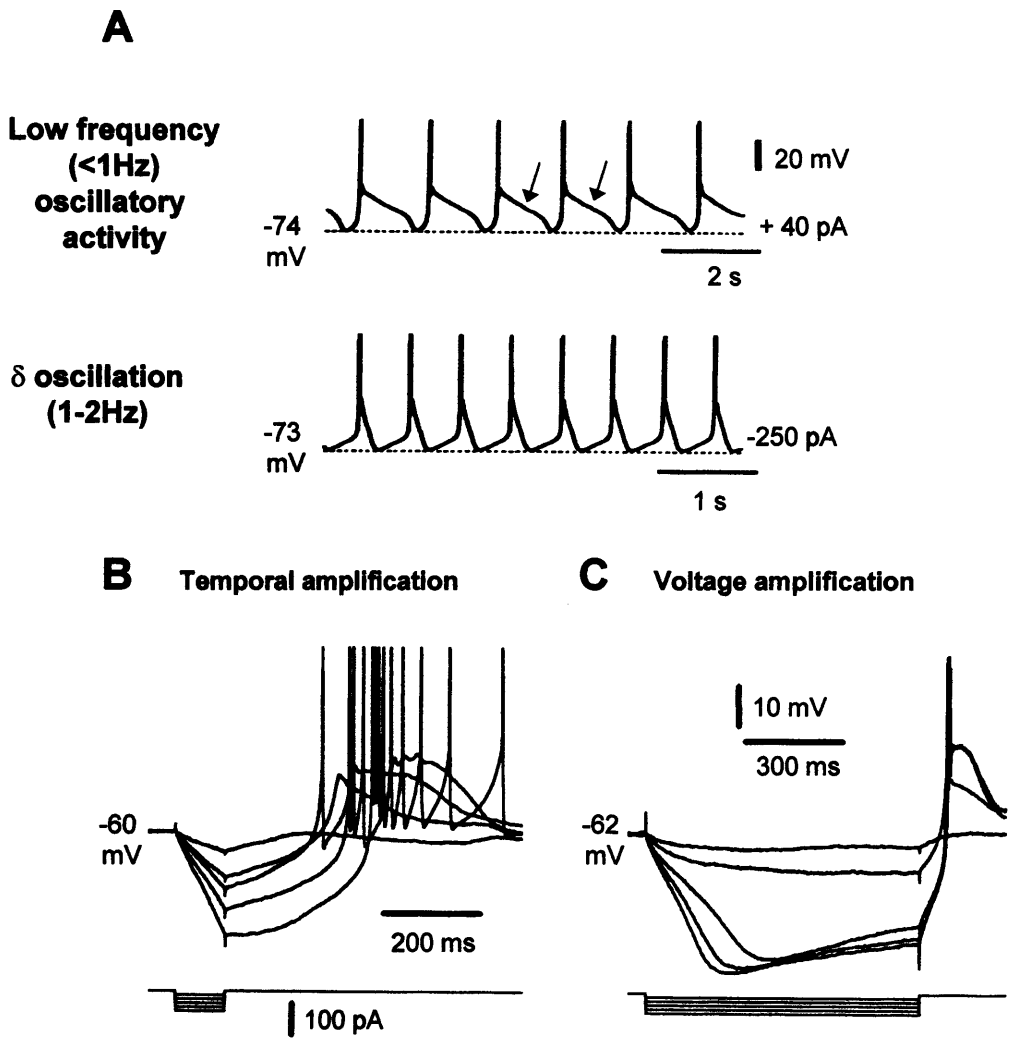

Figure 1.6 Bistability-mediated activities in TC neurones.

(A) Bistability-mediated low frequency oscillatory activity in a TC neurone (upper trace) is characterised by a "shoulder" following the burst of action potentials. This oscillatory activity is abolished and a typical δ oscillation instated (lower trace) through injection of hyperpolroising d.c. current. (from Hughes et al. 1999).

(B) Temporal amplification of voltage responses evoked by small, hyperpolarising current steps in a TC neurone. The duration of the voltage response outlasts the current step by ~3 times. (from William et al. 1997).

(C) Voltage amplification of responses to longer hyperpolarizing current steps in a TC neurone. The 3 largest current steps evoke a greater voltage response than would be predicted if the injected current steps evoked linear voltage responses. (from Hughes et al. 1999).

1.6 MEMBRANE CURRENTS IN NEURONES OF THE NUCLEUS RETICULARIS THALAMI

1.6.1 Na^+ currents.

NRT neurones, possess the ability to fire tonic trains of Na^+ dependent action potential either in response to injection of depolarising d.c. current or in response to depolarising current steps (Fig. 1.7A_1) (Llinas and Geijo-Barrientos 1988; Spreafico et al. 1988; Avanzini et al. 1989; McCormick and Wang 1991; Bal and McCormick 1993). In addition, a persistent Na^+ current (I_{Nap}) with a lower activation threshold than action potential generation is also suggested to be present in NRT neurones (Llinas and Geijo-Barrientos 1988; Bal and McCormick 1993).

1.6.2 Ca^{2+} currents.

NRT neurones, like TC neurones, also posses the ability to generate LTCP-mediated bursts of action potentials (Fig. 1.7A_2 and B), however with a distinctive manifestation from that observed in TC neurones (Domich et al. 1986; Llinas and Geijo-Barrientos 1988). LTCPs in NRT neurones are also mediated by I_T but substantial differences in kinetic properties are observed: in particular I_T is activated at more positive membrane potentials than in TC neurones, inactivates more slowly and is activated from more depolarised levels than in TC neurones (Huguenard and Prince 1992; Bal and McCormick 1993) and has been proposed to be predominantly dendritic in location (Destexhe et al. 1996). These properties presumably give rise to the difference in burst structure that characterises NRT LTCP-mediated burst firing. While bursts in TC neurones are short (5-20ms) and comprise a decelerating pattern, in NRT neurones bursts are characterised by an accelerating-decelerating pattern that typically lasts longer than 50ms (Domich et al. 1986).

Furthermore differences in the characteristics of I_T in TC and NRT neurones are also derived from differences in subunit composition of I_T channels. Three genes encoding putative membrane spanning and pore forming sequences of T-type Ca^{2+} channels have been identified: α1G, α1H and α1I (Perez-Reyes 2003). mRNA transcripts corresponding to these genes have differential distributions in the brain with α1G heavily expressed in thalamic relay nuclei and α1H detected

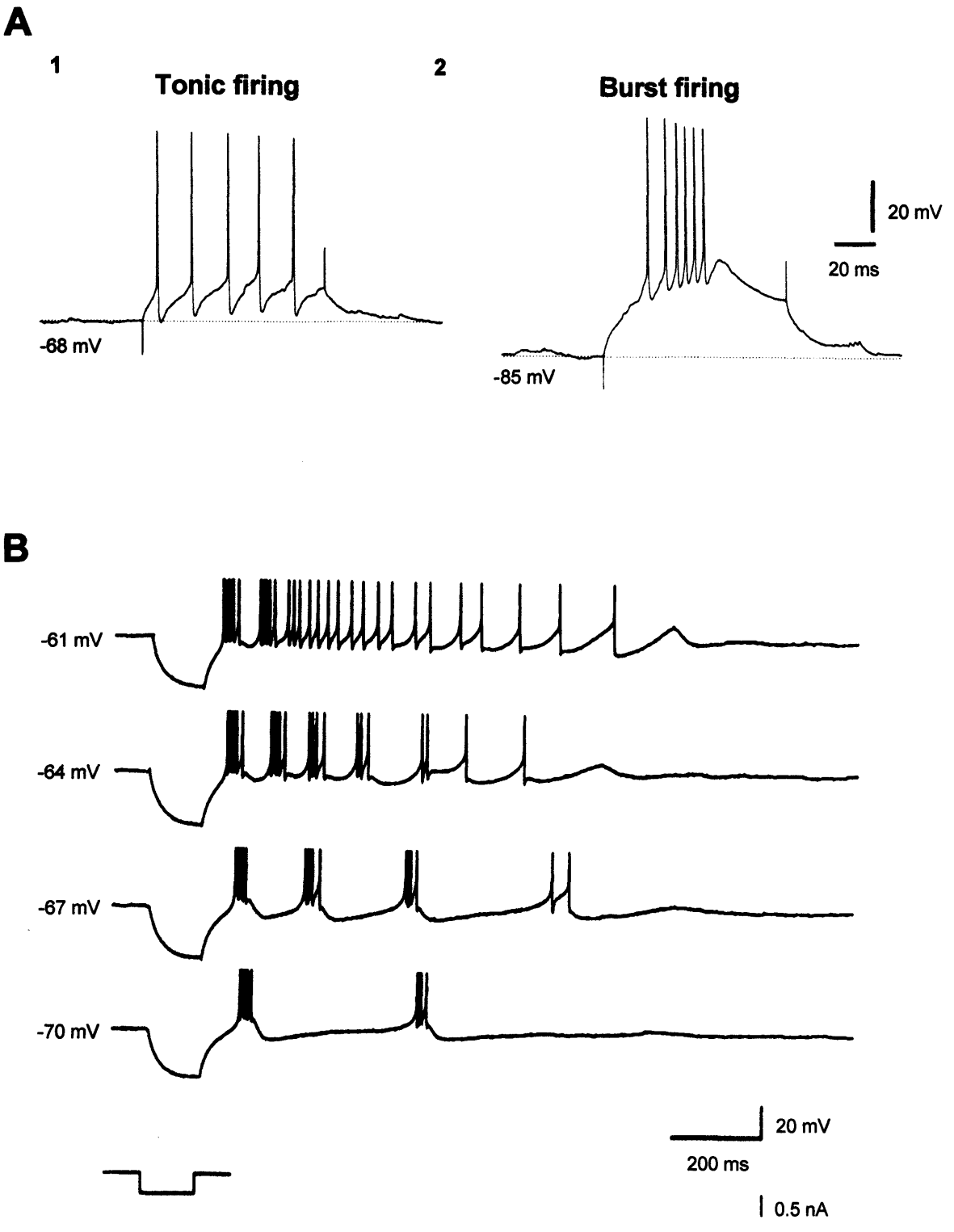

Figure 1.7 Intrinsic electrophysiological properties of NRT neurones.

Figure 1.7 Intrinsic electrophysiological properties of NRT neurones.
(A) The burst and tonic firing modes in a NRT neurone. Injection of a constant amplitude depolarising current step from two different levels of membrane potential. From a fairly depolarised membrane potential, the current step evokes a train of action potentials (1). From a more hyperpolarised membrane potential the depolarising current step leads to the generation of a LTCP-mediated burst of action potentials with a characteristic accelerating-decelerating action potential firing pattern (2). (from Contreras et al. 1992).
(B) Voltage-dependence of rebound burst firing in an NRT neurone. Injection of a hyperpolarizing current step at –61mV results in a sequence of rebound bursts at ~ 11-15Hz followed by a tonic tail of action potentials. Hyperpolarisation of the cell to –64 mV reduces the tonic tail of activity and reveals rhythmic bursting at ~ 7-11Hz. Further hyperpolarisation of the cell (-67mV and –70mV) further reduces the sequence of activity and slows the frequency of rebound bursting. (from Bal and McCormick 1993).

in NRT neurones where α1I was also highly expressed (Talley et al. 1999; Perez-Reyes 2003). When expressed in HEK-293, cloned α1G, α1H and α1I subunits all produced functional T-Type Ca^{2+} currents but with distinctive biophysical properties. Steady-state activation and inactivation kinetics were shifted 7 and 6 mV positively for α1I compared to α1G and α1H, respectively. Additionally, α1I activates and inactivates more slowly than either α1G or α1H although removal of inactivation was faster for α1I. Given the steady-state activation – inactivation kinetics of the cloned channels, a widow component was predicted for each current, but was largest and shifted positively for α1I (Chemin et al. 2002; Perez-Reyes 2003). Additionally simulation of characteristic neuronal activities indicated that the α1G kinetics reproduced TC activity whilst α1I kinetics more accurately reproduced NRT activity (Chemin et al. 2002).

HVA Ca^{2+} currents have been identified in NRT neurones of neonatal rats, functionally found to be partly mediated by N and P/Q-type currents (Sun et al. 2001) and suggested to play a role in Ca^{2+} influx at GABAergic presynaptic terminals. L-type Ca^{2+} channels have been identified at predominantly somatic regions by fluorescence labelling in thalamic slices (Budde et al. 1998).

1.6.3 K^+ currents.

NRT neurones also have an array of K^+ currents (Llinas and Geijo-Barrientos 1988; Avanzini et al. 1989; Bal and McCormick 1993). These contribute to stabilising and repolarising the membrane potential as in TC neurones. Of note however is the particular interaction of a Ca^{2+}-activated-K^+ current and I_T that gives rise to an NRT specific bursting pattern (Avanzini et al. 1989; Bal and McCormick 1993). Activation of I_T typically generates a LTCP and burst of action potentials, that may be followed by additional rhythmic rebound bursts, each separated by a transient AHP (Fig. 1.7B). The number and frequency of rebound bursting events is dependent on membrane potential (Bal and McCormick 1993) and presumably arises as activation of I_T is more depolarised in NRT neurones thus allowing the interaction of these currents (a detailed description of this bursting activity is given in section 1.7.2). Additionally a Na^+-dependent-K^+ current (I_{KNa}) is present in NRT neurones and produces a pronounced and long-lasting hyperpolarisation after persistent tonic firing or repetitive bursting activity (Kim and McCormick 1998a).

1.6.4 Hyperpolarisation-activated mixed cation current.

In NRT neurones, extracellular caesium (Cs^+) application does not apparently block or alter rhythmic activity and thus I_h is thought not to have a significant role in intrinsically generating rhythmic activities (Bal and McCormick 1993).

1.6.5 Ca^{2+}-activated non-selective cation current.

The presence of a Ca^{2+} activated non-selective cation current (I_{CAN}) (Partridge and Swandulla 1988) has been documented in NRT neurones and underlies a large afterdepolarising potential (ADP), that becomes pronounced after blockade of Ca^{2+}-activated-K^+ currents and in the presence of TTX (Bal and McCormick 1993). I_{CAN} in NRT neurones underlies the tonic tail of action potential firing that typically followed rebound burst firing (Fig. 1.7B) (a detailed description of this bursting activity is given in section 1.7.2).

1.7 ELECTROPHYSIOLOGY OF NEURONES OF THE NUCLEUS RETICULARIS THALAMI

NRT neurones are also capable of two distinct modes of firing: a "tonic" and a "burst" mode (Llinas and Geijo-Barrientos 1988; Spreafico et al. 1988; Contreras et al. 1993). Again induction of bursting activity in NRT neurones, as in TC neurones, is achieved by membrane hyperpolarisation and the de-inactivation of I_T (see section 1.6.2) (Llinas and Geijo-Barrientos 1988; Bal and McCormick 1993). As in TC neurones the tonic mode characterised by sustained tonic firing of action potentials predominated during wakefulness, whilst bursting activity is associated with decreased arousal and sleep (Steriade et al. 1986). Despite these similarities, NRT and TC neurones display marked differences in activity particularly during sleep states (see section 1.8).

1.7.1 Tonic firing.

The sustained single action potential firing pattern of NRT neurones during the awake state is similar in TC and NRT neurones. However it was noted that NRT neurones reached much higher firing frequencies (50-100Hz) during arousal than TC neurones during the same state (Steriade et al. 1986). Sustained tonic firing of action potentials can be induced in NRT neurones above around -50 to -45 mV (Fig. 1.7A_1) (Llinas and Geijo-Barrientos 1988; Bal and McCormick 1993)

and are typical Na^+/K^+ regenerative events, each followed by a transient Ca^{2+} - dependent AHP (Avanzini et al. 1989).

1.7.2 Burst firing.

As in TC neurones, burst firing in NRT neurones predominantly occurs during states of decreased arousal and sleep (Steriade et al. 1986). In NRT neurones, burst firing can be evoked from fairly hyperpolarised membrane potentials following activation of I_T, although at more depolarised levels than TC neurones (see section 1.6.2), Burst responses with a characteristic decelerating-accelerating action potential pattern can be evoked through depolarisation from hyperpolarised membrane potentials (Fig. 1.7A_2) or hyperpolarisations from depolarised membrane potentials (Llinas and Geijo-Barrientos 1988; Spreafico et al. 1988; Contreras et al. 1993). However, the manifestation of the burst responses is very voltage-dependent and can comprise a variable number of rhythmic rebound bursts, characteristically at 7-14Hz and followed by a tonic tail of action potential firing (Fig. 1.7B, -61mV and –64mV) (Bal and McCormick 1993; Contreras et al. 1993). The rhythmic rebound bursting results from the interaction of I_T and Ca^{2+} activated K^+ currents (Bal and McCormick 1993), whilst the induction of tonic firing either following or replacing rebound bursts is dependent on a prolonged, but transient ADP that is dependent on I_{CAN} (Bal and McCormick 1993) and presumably I_{Nap} (see section 1.6.1) as it has an activation threshold below that of action potentials (Jahnsen and Llinas 1984b; Jahnsen and Llinas 1984a). As the membrane potential is hyperpolarised, the frequency of rebound bursting is decreased both in frequency and number of bursts that are less likely to be followed by a tonic tail of action potentials (Fig. 1.7B, -67mV and –70mV).

1.8 SLEEP

In adults and children over 3-4 years of age, normal sleep consists of two distinctive sleep states: non-rapid eye movement sleep (NREM) or slow-wave sleep (SWS) and rapid eye movement (REM) sleep or paradoxical sleep. These sleep states have been distinguished and so-called because they can be defined on the basis of different neurophysiological and behavioural markers. In addition, NREM is also characterised by different Stages, 1-4, with stages 1 and 4 representing the lightest and deepest sleep stages, respectively. A whole night of

sleep comprises cyclical transitions through light and deep NREM stages and NREM and REM states (Fig. 1.8) (Kandel et al. 1991; Cooper 1994).

1.8.1 EEG sleep rhythms.

The principal way of determining the type and depth of sleep is through monitoring the EEG, along with the electromyogram (EMG) to monitor muscle tone, and behavioural observations. The following description highlights defining features in the human EEG during sleep. However, it is clear that these defining EEG features are common to both humans and some animals, particularly cats (Steriade et al. 1993d; Contreras and Steriade 1997).

Stage 1: A normal subject, on closing the eyes, will show a dominant post central rhythm in the 8-13 Hz frequency range. This is the posterior alpha rhythm that is characteristically seen during quite wakefulness. As the subject becomes drowsier, the alpha rhythm decreases in amount and amplitude and may slow slightly. Subsequently, the alpha rhythm is replaced by a pattern of mixed low-amplitude components on transition into the first stage of sleep. These components characterising Stage 1 occur in the fast (14Hz and above), θ (4-7 Hz) and δ (0.5-4 Hz) frequency ranges and the criteria for this sleep stage is the appearance of this mixed frequency pattern for greater than 50% of the observed epoch (typically, epochs of 20-30 seconds in duration are used for sleep scoring under experimental conditions). In addition, slow eye-rolling movements, often fairly regularly and typically lasting 2-4 seconds are also observed particularly at the onset of Stage 1. Slow components and fast activity show a gradual increase during Stage 1 (Cooper 1994).

Stage 2: This stage is characterised by the presence of K-complexes (KCs) and sleep spindles and with increasing slow activity in the θ and δ frequency ranges. KCs and sleep spindles may be separated by a long duration although they are distinctive features (Fig. 1.9A, Stage 2). KCs are discrete complex waveforms that have a high-amplitude surface-positive transient followed by a slower surface-negative transient (Fig. 1.9A, expanded KC). KCs can occur spontaneously or in response to stimuli and have an identical appearance regardless of their mode of origin or the modality of the stimulus used. KCs are often associated with sleep spindles (Fig. 1.9A, expanded KC+spindle). Sleep

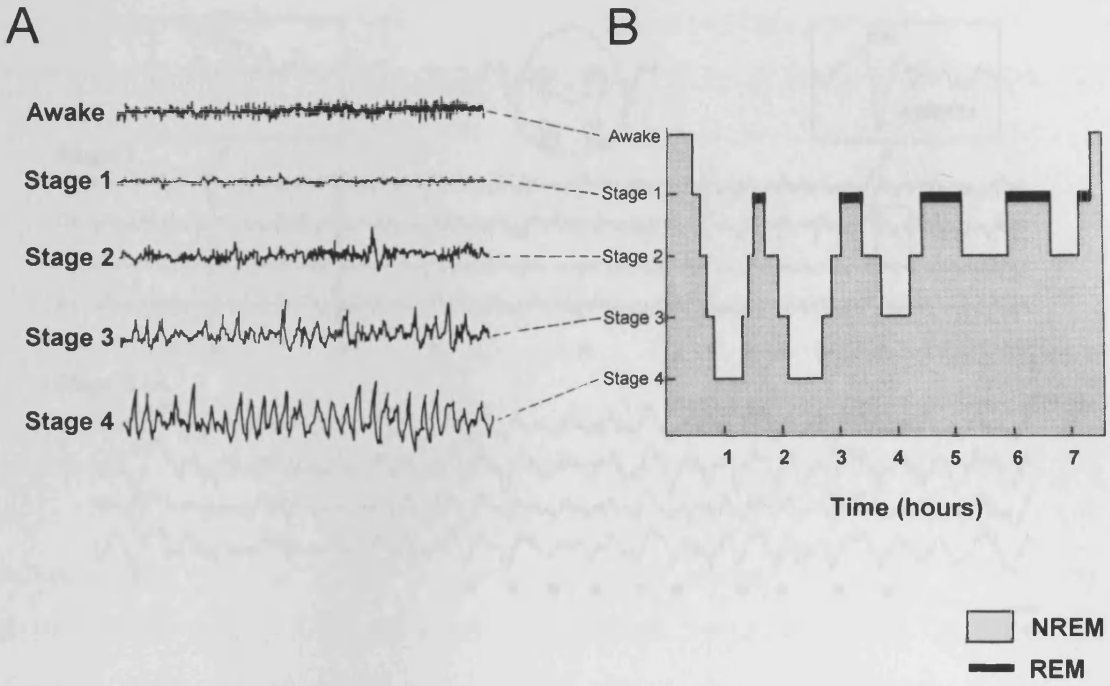

Figure 1.8 Sleep stages form a cyclical pattern.

(A) EEG recordings during wakefulness (Awake) and different sleep stages (Stages 1-4). Each record spans 30 seconds. Note the presence of several characteristic bursts of waxing and waning waves (sleep spindles) lasting 1-2 seconds in Stage 2. Also note the presence of large amplitude slow waves in the EEG recording of Stage 3 and the increasing amplitude and regularity of the slow waves in Stage 4.

(B) A typical night's pattern of sleep in a young adult. The duration spent in REM is indicated by the black bar. During the night many transitions through different non-rapid eye movement (NREM) sleep stages and NREM and rapid eye movement (REM) sleep are made. The first REM period is usually short (5-10 min) but tends to progressively lengthen during successive cycles. Stage 3 and 4 dominate in the first third of the night, but are often completely absent during the later early morning cycles. The duration of Stage 2 sleep increases progressively towards the end of the night.

(from Kandel et al. 1991).

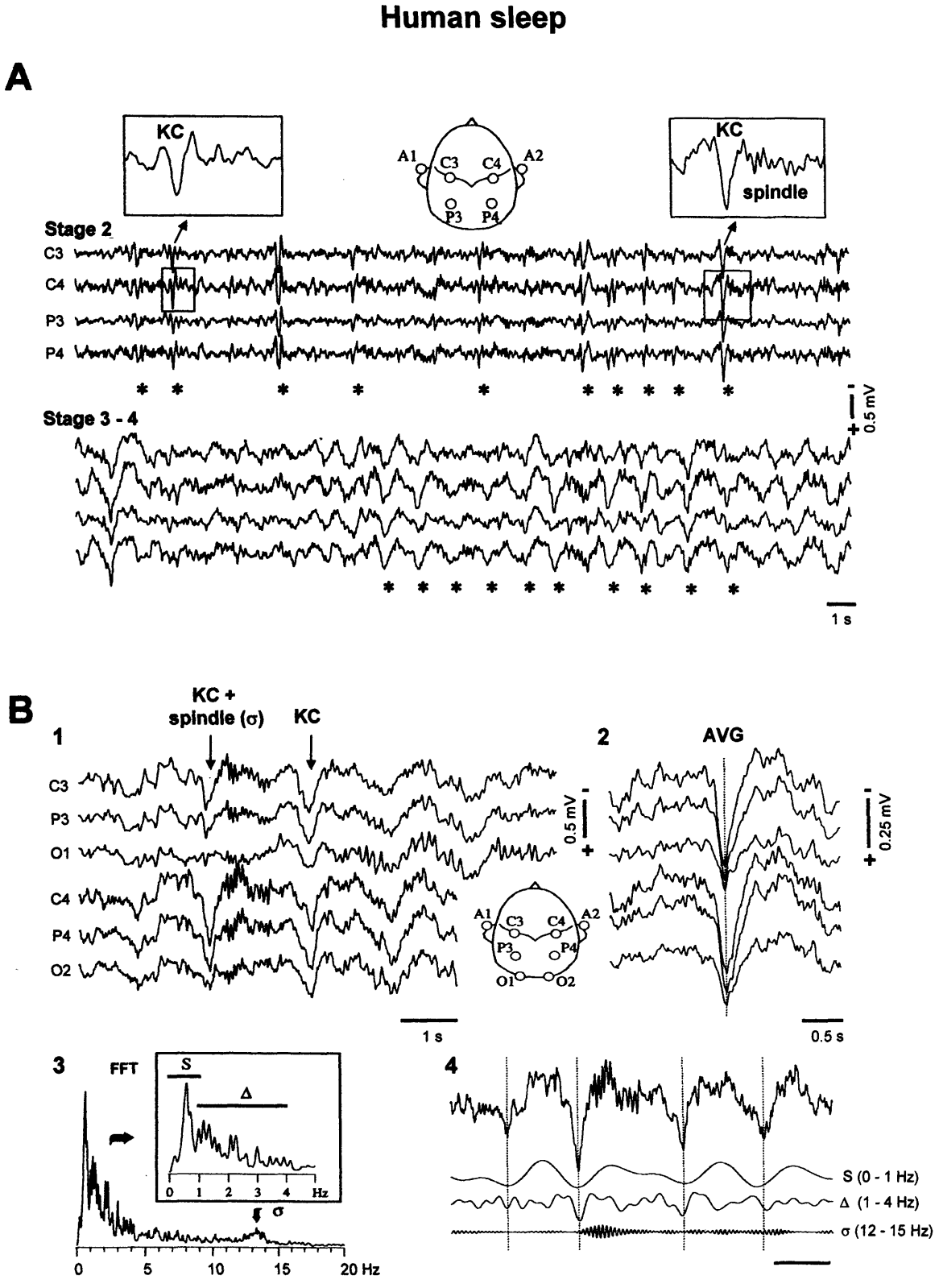

Figure 1.9 Human EEG during sleep stages.

Figure 1.9 Human EEG during sleep stages.

(A) Rhythmic K-Complexes (KCs) in human EEG during natural NREM sleep. Scalp monopolar recordings with respect to the contralateral ear (as indicated on the figurine). Stage 2: Four lead recorded from the two hemispheres show quasi-rhythmic KCs ~0.5Hz. The expanded insets display a simple KC and a KC followed by a spindle. Stage 3-4: is characterised by a more regular oscillation of the KCs (~0.7Hz). Asterisks mark the most obvious KCs in order to suggest their rhythmicity.

(B) NREM sleep of a normal human subject. Scalp monopolar recordings with respect to the contralateral ear (as indicated on the figurine). Short episode from sleep stage 3. The two arrows point to a KC followed by a spindle and an isolated KC. The two KCs are embedded in a slow rhythm of ~0.6Hz. Note the synchrony of the KCs in all recorded sites (1). Average of 50 KCs aligned on the positive peak of the upper channel (vertical dotted line) (2). Frequency decomposition of the C3 lead (upper trace) into three frequency bands (S 0-0.1Hz, Δ (1-4Hz) and σ (12-15Hz). It is shown that the KC results from a combination of S and Δ waves (3). Power spectrum of the C3 lead for a period of 80 seconds of the stable stage 3 activity containing the traces shown in (1) and clearly representing the three frequency bands shown in (3). Note the S activity displays high peaks distinct from those of the Δ activity.

(from Amzica and Steriade 1997).

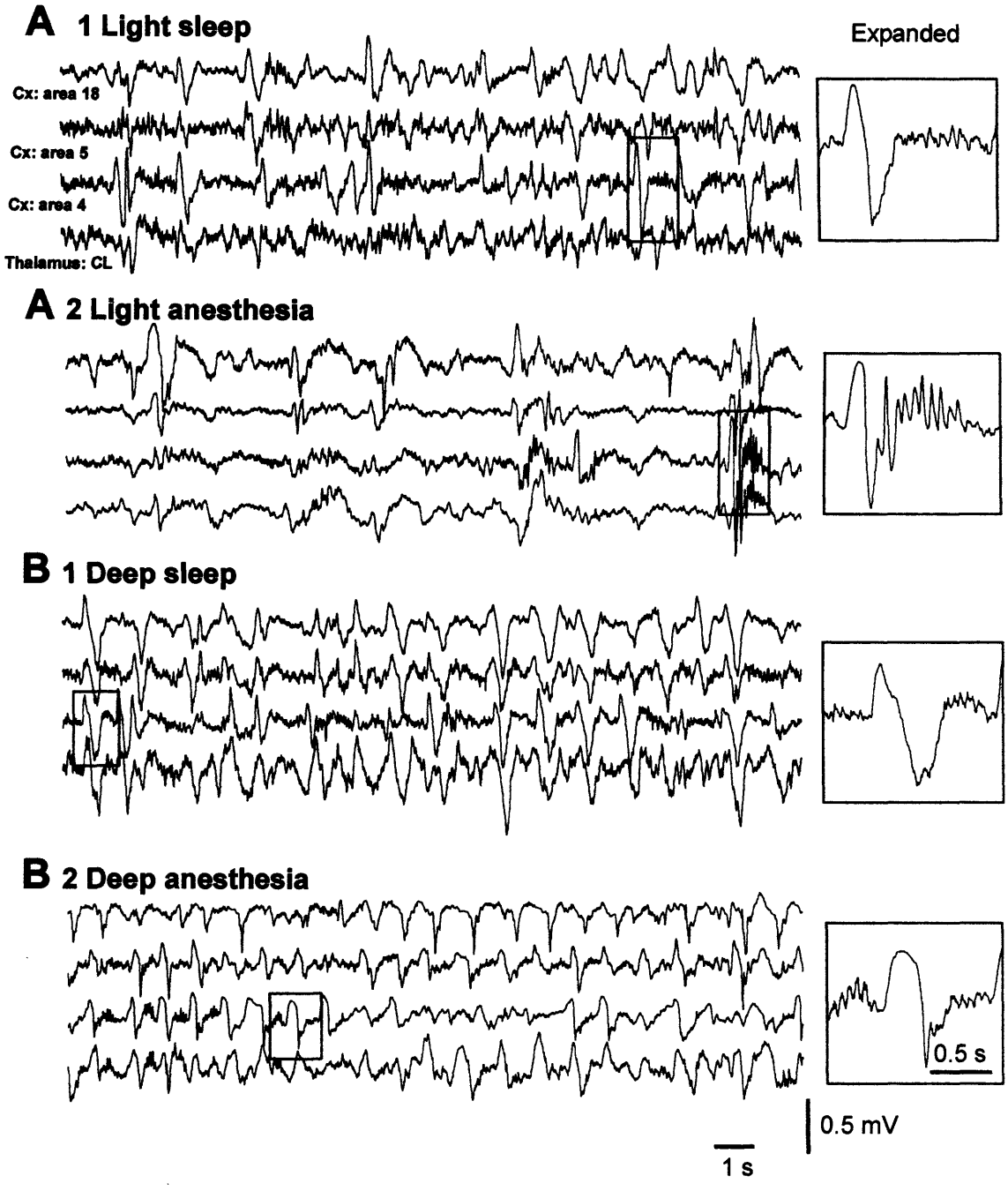

Figure 1.10 EEG spindle waves during light and deep sleep stages in cats.

Figure 1.10 EEG spindle waves during light and deep sleep stages in cats.
Comparison of the features of the EEG recorded during natural sleep (A1, B1) and under ketamine and xylazine anaesthesia (A2, B2) in a chronically implanted cat. Recordings were made using monopolar electrode from deep cortical layers (Cx: area 18, 5 and 4) and the centrolateral thalamus (Thalamus: CL), negativity of field potentials is downwards. The enclosed region (boxed) in each condition is expanded to the right in each case. Note the almost synchronous occurrence of slow waves in the cortex and thalamus.
(A) Spindles commonly occur both during light natural sleep (1) and light anaesthesia (2).
(B) As sleep deepens EEG recorded slow-waves become more rhythmic and the incidence of spindle waves is reduced, both during deep natural sleep (1) and deep anaesthesia (2).
(from Amzica and Steriade 1998a).

concurrent EMG. Saw-toothed waves are commonly seen usually just before or overlapping the onset of REM (Cooper 1994).

1.8.2 Cellular correlates of low frequency EEG activity during sleep.

It is already apparent from the descriptions given above that large-amplitude waves are a dominant feature of the EEG during NREM sleep stages: KCs in Stage 2 and large amplitude slow-waves during Stage 3 and 4. KCs and slow waves are generally described independently. However, recent investigations have shown that both these types of waves are associated with similar patterns of activity in cortical neurones (see section 1.8.2.1). KCs are thought to represent the forerunner of slow-waves. During Stage 2 KC are fairly arrhythmic and often separated by long durations (up to 3 seconds) (Cooper 1994; Amzica and Steriade 1997). Stages 3 and 4 are dominated by large slow waves that increase in rhythmicity as sleep deepens (Steriade et al. 1993d; Cooper 1994; Amzica and Steriade 1998a). The transitions from KCs to slow-waves is thought to reflect the increasing rhythmicity and global synchronisation in the cortex as sleep deepens (Amzica and Steriade 1998a). Given the dense interconnectivity of the cortex and thalamus, global synchrony of neuronal activity exists within the whole corticothalamic network in phase with the cortical rhythm (Fig. 1.10, Thalamus: CL) (Amzica and Steriade 1995b; Timofeev and Steriade 1996; Amzica and Steriade 1998a). The following sections provide a description of the activity of different neuronal elements within the corticothalamic network that are believed to underlie various EEG sleep rhythms.

1.8.2.1 Cortical correlates of the slow (<1Hz) sleep rhythm.

Large-amplitude slow waves at <4Hz in the EEG have been shown to comprise 2 components: a slow (0.1-1 Hz) component and the δ (1-4Hz) component. The <1Hz component is manifested as large-amplitude slow waves in the EEG and this pattern of rhythmic activity is described as the slow <1Hz sleep rhythm (Steriade et al. 1993d). The slow <1Hz sleep rhythm is a dominant feature in the EEG as it serves to group other EEG sleep rhythms including δ waves (typically 1-4Hz) and sleep spindles (typically 7-14Hz), into coherent, repeating episodes (Steriade et al. 1993c; Steriade et al. 1993d). These faster EEG sleep rhythms are in part of thalamic origin. The origin of δ (1-4Hz) rhythms in the EEG is presently uncertain. Both cortical and TC neurones have the ability to intrinsically

generate rhythmic activity at 1-4Hz (Connors et al. 1982; McCormick and Pape 1990; Leresche et al. 1991). Thus both neuronal population could contribute to underlying this activity in the EEG (Amzica and Steriade 1998b) (see section 1.8.2.2). Sleep spindles (7-14Hz) are generated by NRT neurones and projected to the cortex via interconnections with underlying thalamic territories (see section 1.8.2.3).

The EEG slow <1Hz sleep rhythm is generated in neocortical networks and is believed to impinge upon the thalamus, driving the thalamic <1Hz sleep rhythm. The thalamic slow <1Hz sleep rhythm is abolished following destruction of cortical inputs (Timofeev and Steriade 1996). Experiments *in vivo* following unilateral decortication, with most of one cortical hemisphere removed, but leaving intact a cortical area not connected with the thalamic regions investigated (Timofeev and Steriade 1996) showed 1) normal slow <1Hz rhythm in the intact cortex and absence of this oscillation ipsilateral to the ablated neocortex, 2) brief waning sequences of sleep spindles in the intact hemisphere following the depth negative (i.e. onset of cortical activation) component of the EEG slow rhythm, but prolonged waxing and waning sequences of sleep spindles on the partially ablated cortical hemisphere, 3) synchronous <1Hz rhythmic activity in area 4 of the intact cortex and ipsilateral VL nucleus, but an absence of the slow <1Hz rhythm in the decorticated VL thalamic nucleus, 4) synchronous spindles in cortical and thalamic areas in the intact hemisphere within the frequency of the slow <1Hz rhythm, but no synchrony between spindles between the two thalamic nuclei. Spindle in the decorticated hemisphere displayed a waxing and waning pattern, were 5-6 times longer (2.5-3 seconds) than in the cortex of the intact hemisphere, occurred with a periodicity of 10-12 seconds and were not related to a cortical slow <1Hz rhythm (Timofeev and Steriade 1996). So by way of its dense thalamic projections, the cortical <1Hz sleep rhythm is thought to trigger thalamic activity that is then projected back to the cortex and contributes to faster EEG rhythms and aid global synchronisation of cortical activity (Contreras et al. 1996; Contreras and Steriade 1996; Timofeev and Steriade 1996).

At the cellular level, the slow <1Hz sleep rhythm is evident in all types of cortical neurones and is manifested as recurring sequences of synaptic barrages, that can lead to epochs of sustained action potential firing, interspersed with periods

of quiescence (Steriade et al. 1993c; Steriade et al. 1993d; Steriade et al. 2001). This pattern of activity leads to the prominent appearance of depolarised 'up' and hyperpolarised 'down' states of the membrane potential and is described as the slow <1Hz oscillation (Fig. 1.11). The generation of this rhythm is thought to be through a combination of the intrinsic properties of cortical neurones and synaptic interactions (Amzica and Steriade 1995a; Sanchez-Vives and McCormick 2000). The periods of quiescence interposed between periods of action potential firing are associated with membrane hyperpolarisation and are though to be periods of disfacilitation of the cortical network (Timofeev et al. 2001). This suggests that synchronous global activation of cortical neurones arises on a background of depressed cortical activity. Such disfacilitation is hypothesised to arise through the depression of intracortical and thalamocortical synapses and the hyperpolarisation of TC neurones during decreased arousal (Timofeev et al. 1996; Gil et al. 1997; Timofeev et al. 2001).

This same type of activity is seen in cortical neurones during KCs. The depth negative component of the KC is associated with the onset of a depolarised "up" state in cortical neurones as seen in the slow <1Hz rhythm (Amzica and Steriade 1997). Additionally cortical neurones show transitions between a depolarised "up" state and hyperpolarised "down" state in synchrony with spontaneous KCs, exactly like that occurring during the slow <1Hz sleep rhythm. Therefore it is proposed that the slow <1Hz oscillation in fact underlies the genesis of KCs with increasing rhythmicity reflecting increasing global synchronisation as sleep deepens (Amzica and Steriade 1997; Amzica and Steriade 1998a).

1.8.2.2 Thalamocortical correlates of the slow (<1Hz) sleep rhythm.

In TC neurones, the intracellular correlate to the slow <1Hz sleep rhythm is also characterized by repeating depolarised 'up' and hyperpolarised 'down' states described as the slow <1Hz oscillation (Fig. 1.12) and which often demonstrates a stereotypical waveform (Steriade et al. 1993a). In particular, the transition from 'up' to 'down' state is commonly initiated by a pronounced inflection point, whereas the transition from 'down' to 'up' state is marked by a LTCP and accompanying high-frequency burst of action potentials (Steriade et al. 1993a). In addition, this slow <1Hz oscillation can also group LTCP-mediated bursts of

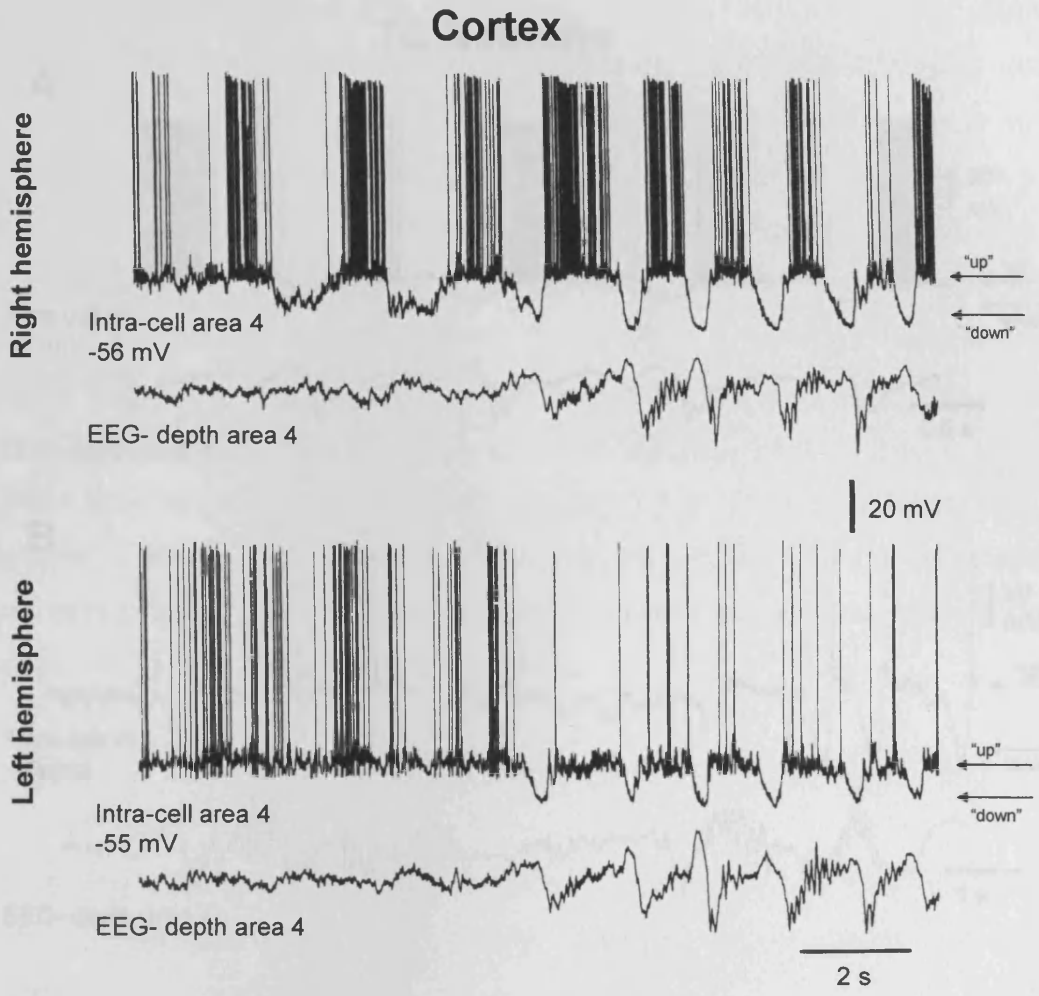

Figure 1.11 Intracellular correlates of the slow <1Hz sleep rhythm in cortical neurones *in vivo*.

Neurones were recorded from cats under ketamine and xylazine anesthesia. In EEG recordings, the negativity of field potentials is downwards.

The slow <1Hz oscillation in cortical neurones. Simultaneous intracellular recording of two neurones from the right (upper) and left (lower) precruciate areas 4 along with the depth EEG recordings from the same areas. Note the development from a non-oscillatory state to oscillatory state in close time relation with large slow-waves (~0.7 Hz) of the EEG in both cortical areas.

The slow <1Hz oscillation observed during intracellular recording of the cortical neurone is characterised by cyclical hyperpolarisations giving the appearance of rhythmic transitions between a depolarised "up" state, that can support action potential firing, and a hyperpolarised "down" quiescent state.

(from Steriade et al. 1994)

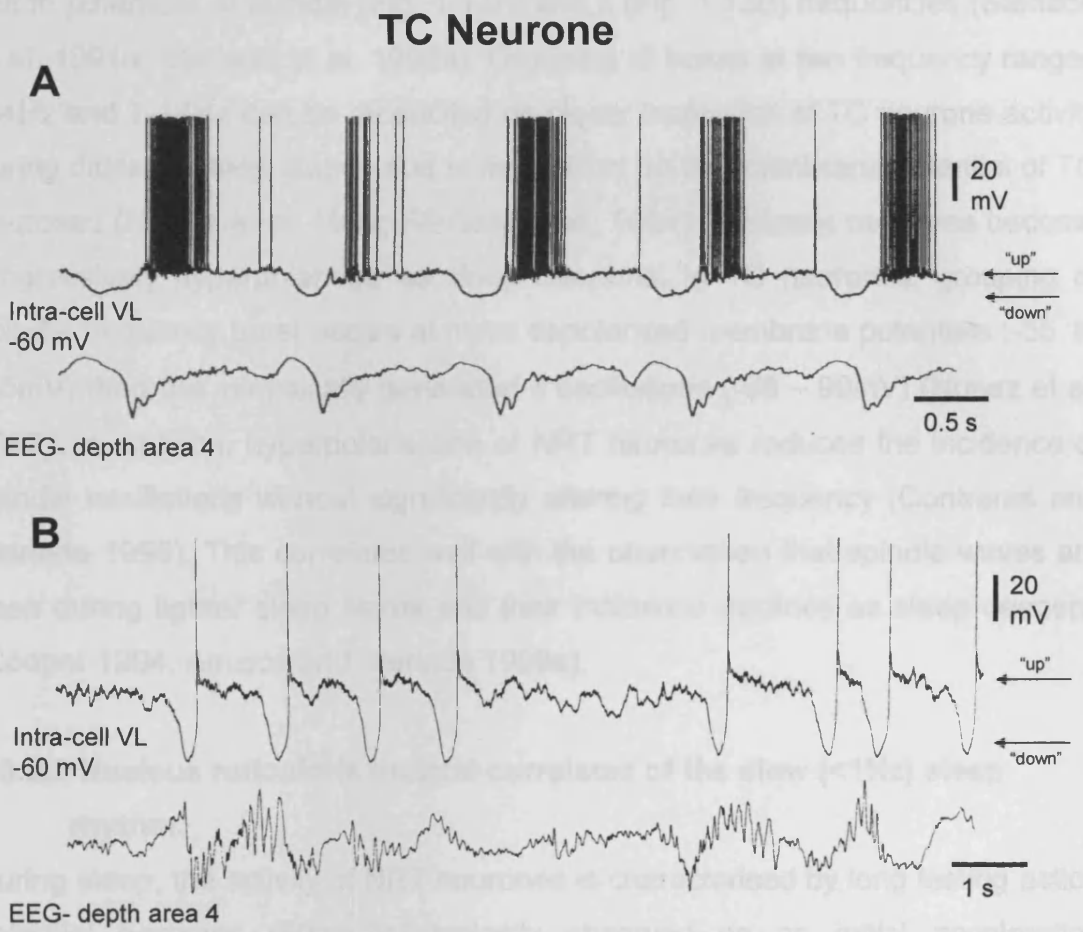

Figure 1.12 Intracellular correlates of the slow <1Hz sleep rhythm in TC neurones *in vivo*.

Neurones were recorded from cats under ketamine and xylazine anesthesia. In EEG recordings, the negativity of field potentials is downwards.

(A) The slow <1Hz oscillation in a VL TC neurone. Simultaneous intracellular recording of a neurone in the VL nucleus and depth EEG in cortical area 4. Note the close phase-relation between the negativity of the EEG waves and the onset of firing in the TC neurone. The slow <1Hz oscillation (0.7-0.8 Hz) has a similar manifestation to that of cortical neurones, with cyclical transitions between a depolarised "up" state interspersed with large hyperpolarisations. (from Steriade et al, 1996).

(B) The slow <1Hz oscillation in another VL TC neurone and simultaneously recorded depth EEG from the same area. Note the transitions between a depolarised "up" phase and a hyperpolarised "down" phase and stereotypical waveform. (from Steriade et al. 1993a).

action potentials at spindle (Fig. 1.13A) and δ (Fig. 1.13B) frequencies (Steriade et al. 1991a; Steriade et al. 1993a). Grouping of bursts at two frequency ranges 1-4Hz and 7-14Hz can be reconciled on closer inspection of TC neurone activity during different sleep stages and is dependent on the membrane potential of TC neurones (Nunez et al. 1992; Steriade et al. 1994). Thalamic neurones become progressively hyperpolarised as sleep deepens. In TC neurones, grouping of spindle frequency burst occurs at more depolarised membrane potentials (-55 to -65mV) than the intrinsically generated δ oscillations (-68 – 90mV) (Nunez et al. 1992). In addition, hyperpolarisation of NRT neurones reduces the incidence of spindle oscillations without significantly altering their frequency (Contreras and Steriade 1996). This correlates well with the observation that spindle waves are seen during lighter sleep states and their incidence declines as sleep deepens (Cooper 1994; Amzica and Steriade 1998a).

1.8.2.3 Nucleus reticularis thalami correlates of the slow (<1Hz) sleep rhythm.

During sleep, the activity of NRT neurones is characterised by long lasting action potential barrages (50ms-2s) typically observed as an initial acceleration followed by a deceleration that recurs at 0.1-0.2 Hz. In a subset of neurones (~15%) with very long spike barrages, the initial acceleration can take the form of repetitive distinct burst that typically occur at 7-14Hz. (Steriade et al. 1986). The initial rhythmic bursting is described as the spindle oscillation because it is believed that this component of NRT activity, through projections to TC neurones (the output neurones of the thalamus), leads to the generation of EEG recorded sleep spindles that typically occur at 7-14 Hz. In this way the spindle oscillations are grouped within a <1Hz frequency (Contreras and Steriade 1996).

That EEG recorded spindle waves originate from the NRT derives from a number of experimental observations *in vivo*. The thalamic origin of spindle rhythmicity was shown following its survival in thalamic nuclei after decortication (Morison and Bassett 1945). Subsequent findings have shown that abolition of NRT inputs in one hemisphere results in the lack of spindling activity in TC neurones in related thalamic nuclei and a lack of spindle waves in the EEG recordings from the contralateral hemisphere even though EEG spindle waves were still present

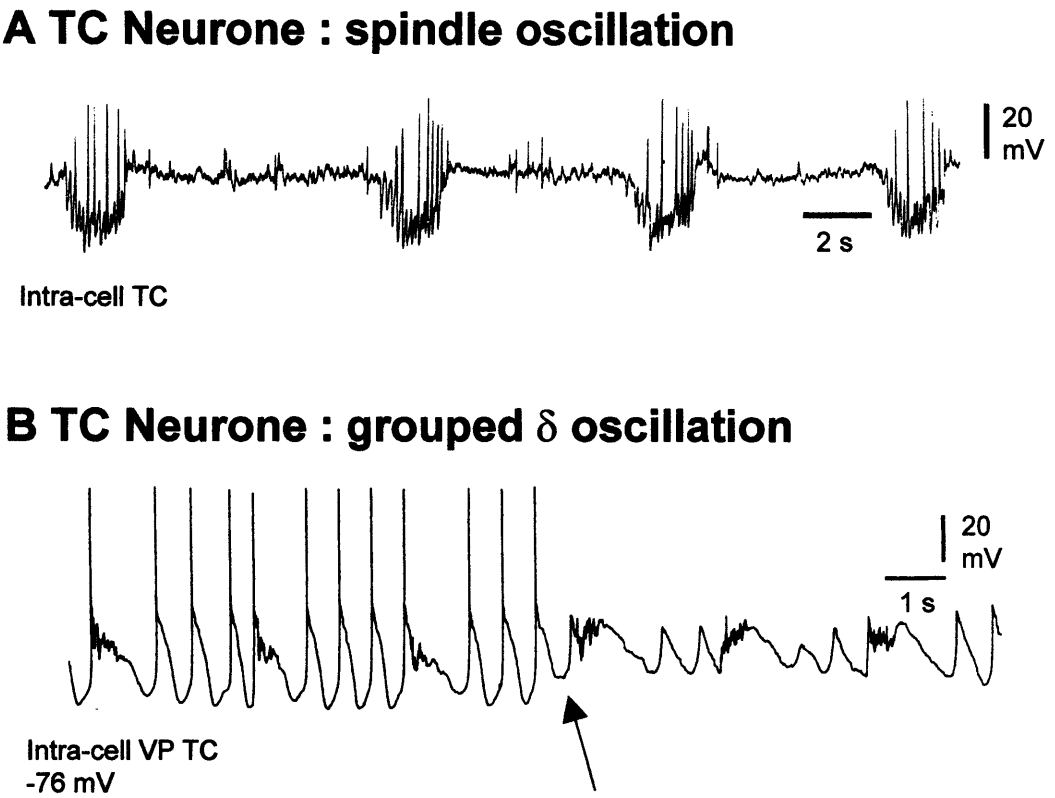

Figure 1.13 Grouped activity in TC neurones during sleep.

(A) Activity in a cat TC neurone showing spindle sequences. In TC neurones spindle sequences are characterised by rhythmic barrages of IPSPs that may evoke rebound LTCP-mediated bursts of action potentials and typically recur at 0.1-0.2 Hz. This neuronal activity was recorded during administration of barbiturate (Nembutal, sodium pentobarbital) anesthesia. (from Steriade et al. 1985).

(B). Activity in a cat TC neurone showing sequences of δ oscillation (1.5-2 Hz) grouped within the slow <1Hz oscillation (0.4 Hz). Note that grouping of the δ oscillation leading to action potential firing within the 1.5-2 Hz range occurred when the neurone was hyperpolarised below –75 mV, but was diminished by removal of hyperpolarizing d.c.current (arrow). Neuronal activity recorded under ketamine and xylazine anesthesia. (from Steriade et al. 1993a).

in the hemisphere receiving TC inputs from the intact thalamus (Steriade et al. 1985). Additionally, anterior thalamic nuclei that do not receive NRT inputs do not display spindling activity (Mulle et al. 1985). Finally, in isolated regions of NRT, extracellularly recorded neurones display rhythmic occurrence of spindle oscillations occurring in good time-relation to focally recorded NRT spindling at 7-14Hz although with a waxing and waning pattern and a recurring over a larger frequency range 0.1-0.3 Hz) (Steriade et al. 1987).

This intracellular correlate of the slow <1Hz sleep rhythm in NRT neurones thus can lead to a similar manifestation as in cortical neurones, that is the appearance of pronounced depolarised "up" and hyperpolarised "down" states of the membrane potential (Fig. 1.14). Contrary to the view that <1Hz rhythmic activity is generated in the cortex and drives thalamic activity, a number of observations suggest that a slow <1Hz oscillation can occur in NRT neurones in the absence of cortical input. These include the persistence of spindle oscillations in NRT and TC neurones, albeit sometimes at a slightly faster frequency (0.1-0.3Hz). In addition, the same pattern of activity is observed in the intact and isolated NRT, that is rhythmic spindle frequency bursting leading to a "tonic tail" of action potentials (Steriade et al. 1987). Additionally, in a small subset of NRT neurones without intact cortical inputs a <1Hz oscillation was observed (Timofeev and Steriade 1996). These observations indicates that a slow < 1Hz rhythm can arise in the thalamus in the absence of cortical input and given that spindle oscillations persist in the NRT in the absence of TC inputs (Steriade et al. 1987), suggests that NRT neurones generate a <1Hz oscillation. The depolarising plateau which characterised the "up" phase of the slow <1Hz oscillation in NRT neurones and therefore spindle oscillations that are superimposed on this depolarising phase are distinctly voltage-dependent. This depolarising envelope increases with hyperpolarisation down to –75 or –80mV and then decreases with further hyperpolarisation along with the incidence of spindle oscillations (Contreras and Steriade 1996). Whether this manifestation is a result of synaptic interactions within the NRT (Contreras and Steriade 1996) or is due to the intrinsic properties of NRT neurones is unknown. Hyperpolarisation of NRT neurones de-inactivates I_T and so synaptic inputs, IPSPs or reversed IPSPs (Bazhenov et al. 1999; Shu and McCormick 2002), may trigger bursting activity leading to the depolarising "up" phase of the slow <1Hz oscillation. Alternatively, hyperpolarisation of NRT

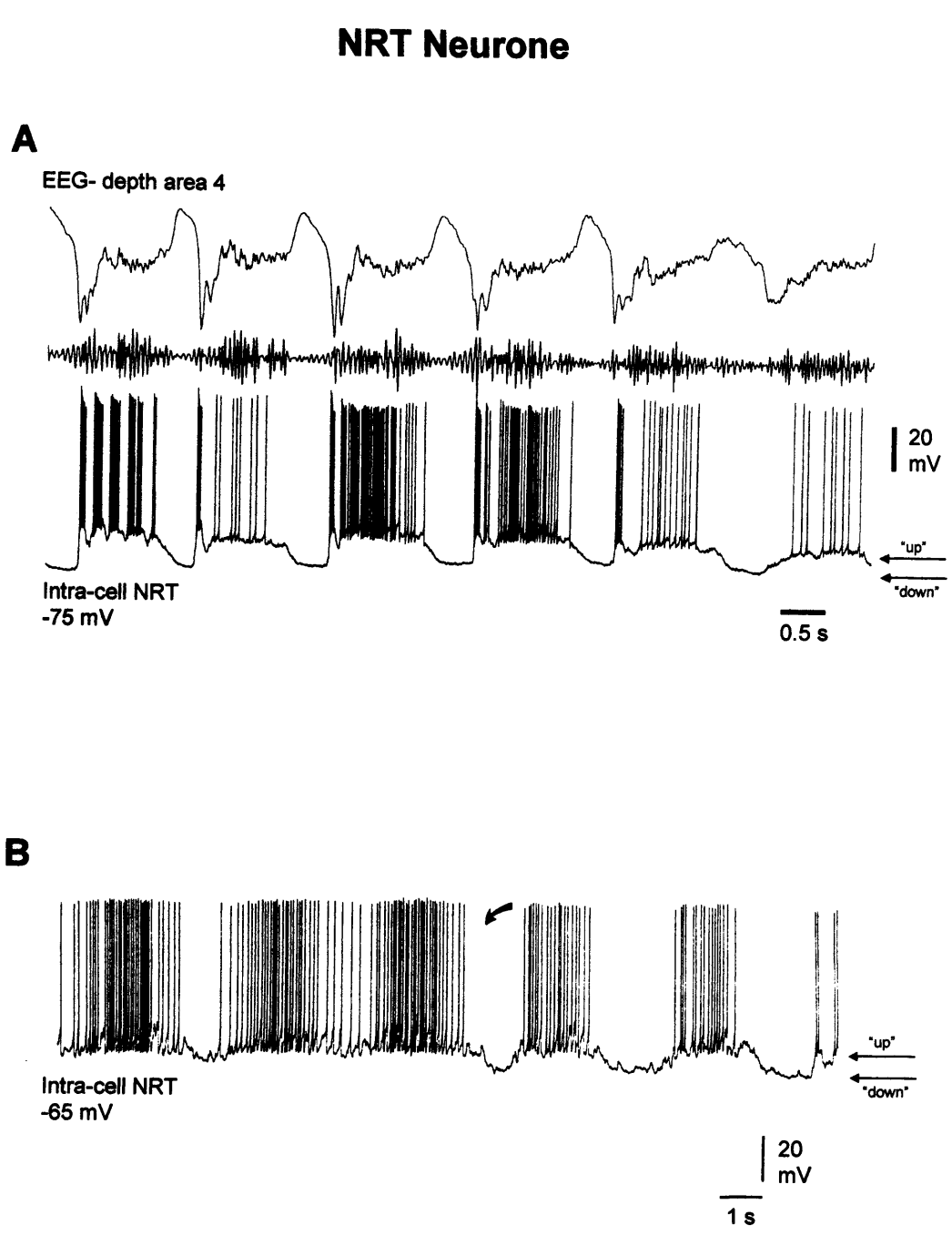

Figure 1.14 Intracellular correlates of the slow <1Hz sleep rhythm in NRT neurones *in vivo*.

Figure 1.14 Intracellular correlates of the slow (<1Hz) sleep rhythm in NRT neurones *in vivo*.

(A) The slow <1Hz oscillation in a NRT neurone. Simultaneous intracellular recording of a neurone in the peri-ventrolateral (VL) sector of the NRT and depth EEG in cortical area 4. (The EEG record filtered at 20-60 Hz is shown below the EEG) Note the close phase-relation between the negativity of the EEG waves and the onset of firing in the NRT neurone. The slow <1Hz oscillation in this NRT neurone has a similar manifestation to that of cortical neurones, with barrages of sustained firing during the "up" phase interspersed by large hyperpolarisations comprising quiescence or the "down" state. Note that the beginning of each oscillation cycle is marked by a LTCP-mediated burst of action potentials. Neurone was recorded from a cat under ketamine and xylazine anaesthesia. In the EEG recording, the negativity of field potentials is downwards.(from Steriade et al. 1996).

(B) Intracellular recording of a cat NRT neurone under urethane anaesthesia. Note the development of a slow <1Hz oscillation following the injection of hyperpolarizing d.c. current (oblique arrow). (from Steriade et al. 1993a).

neurones could trigger intrinsically generated rebound LTCP-mediated bursts followed by.a tonic tail of action potential firing (see section 1.7.2)(Avanzini et al. 1989; Bal and McCormick 1993) leading to the "up" phase of the slow (<1Hz) sleep oscillation. The termination of this firing and subsequent hyperpolarisation of the neurone may be sufficient to re-start the cycle again. The inability to eliminate synaptic interactions between NRT neurones *in vivo* prevents conclusive determination of this question.

The spindle oscillation generated in NRT neurones is projected to the cortex via TC neurones (Steriade et al. 1985). In TC neurones IPSPs arriving from the NRT can evoke rebound LTCP-mediated bursts at spindle (7-14Hz) frequencies that presumably impinge on cortical activity and is reflected in the EEG activity. As such TC neurones display spindle frequency bursts grouped within the <1Hz frequency. (Manifestation of spindle oscillations in TC neurones is described in relation to the slow <1Hz rhythm in section 1.8.2.2).

1.8.3 Summary.

Expression of the slow <1Hz oscillation in TC neurones is dependent on cortical input as it is abolished following removal of cortical inputs (see section 1.8.2.1) (Timofeev and Steriade 1996). However, the stereotypical waveform of the slow <1Hz oscillation in TC neurones is very similar to slow oscillatory activity intrinsically generated in TC neurones as part of the bistability-mediated repertoire of activities following reduction of I_{KLeak} (Williams et al. 1997a; Hughes et al. 1999). A major effect of corticothalamic input onto TC neurones is to reduce I_{KLeak} via the activation of mGluRs (McCormick and von Krosigk 1992). Thus reduction of I_{KLeak} via corticothalamic inputs may be sufficient to induce a slow (<1Hz) oscillation in TC neurones.

In NRT neurones, activation of mGluRs also leads to a reduction of I_{KLeak} (Lee and McCormick 1997). Given that NRT neurones have a similar complement of ionic conductances as TC neurones and that a window component of I_T is predicted (Chemin et al. 2002), it may be possible to unmask bistability-mediated activities in NRT neurones including slow (<1Hz) oscillatory activity.

1.9 ELECTROTONIC COUPLING IN THE THALAMUS

In the course of the experiments detailed in this thesis, small depolarising potentials were apparent in a subset of thalamic neurones in the presence of glutamatergic and GABAergic synaptic receptor antagonists. Given that these depolarising potentials had similar properties and waveforms to electrotonic coupling potentials observed in other neurones (see section 1.9.2), an analysis of these depolarising potentials was performed in order to establish their origin and possible role in modulating thalamic output. Therefore this section aims to introduce electrotonic coupling as a form of intercellular communication and to provide details of the current knowledge regarding electrotonic communication in the thalamus.

1.9.1 Electrotonic coupling.

In the adult vertebrate nervous system, the predominant mechanism of interneuronal signalling is via conventional synaptic transmission (Bennett 1996). However, interactions between neurones occur via both synaptic and non-synaptic mechanisms (Jefferys 1995). Direct, non-synaptic communication between cells can occur via specialised intercellular junctions, gap junctions (GJs), which allow the direct intercellular transfer of ions and signalling molecules of up to 1KD. As such, GJs provide a mechanism for both electrotonic and metabolic intercellular coupling (Dermietzel and Spray 1993; Simon and Goodenough 1998; Rozental et al. 2000). GJs and electrotonic coupling in the nervous system are receiving greater attention as increasingly sensitive or novel techniques have demonstrated their greater abundance in the adult nervous system of mammals than previously recognised. GJs and electrotonic coupling in neurones are associated with synchronised neuronal activity as both have been demonstrated in neuronal populations that display rhythmic oscillatory activity (Logan et al. 1996; Draguhn et al. 1998; Galarreta and Hestrin 1999; Beierlein et al. 2000).

1.9.2 Gap junctions.

GJs are specialised, low-resistance intercellular junctions, forming an aqueous pore between two closely apposed membranes and are considered the ultrastructural substrate of direct intercellular coupling. The principle structural components of vertebrate GJs are membrane-spanning proteins called connexins (Cxs). It is believed that each GJ is constructed as follows: six Cxs

aggregate to form a hemi-channel, or connexon, within each of the opposed membranes, and the Cx hemi-channels are connected extracellularly to form the complete intercellular channel (Fig. 1.15A). Assemblies of GJs tend to be clustered together forming GJ plaques (Fig. 1.15B). Cx expression decreases during development along with GJ intercellular communication: however neuronal coupling persists in many brain regions in adults (MacVicar and Dudek 1981; Rozental et al. 2000; Rouach et al. 2002).

A number of Cx proteins have been identified in neurones in the central nervous system including Cx26, 32, 36 and 43 and 47 (Dermietzel and Spray 1993; Simon and Goodenough 1998; Rozental et al. 2000). Although each of these Cx types has been detected in neurones by a variety of techniques, much attention has focused on Cx36. The use of freeze-fracture electron microscopy showed that Cx36 was the only neuronal connexin whilst Cx32 and Cx43 are localised to glia and astrocytes (Rash et al. 2000; Rash et al. 2001). In addition, Cx 36 is highly expressed in brain areas where electrical coupling has been functionally demonstrated, including the cortex (Galarreta and Hestrin 1999; Gibson et al. 1999; Tamas et al. 2000), hippocampus (Venance et al. 2000; Bartos et al. 2001), cerebellum (Mann-Metzer and Yarom 1999), and thalamic reticular nucleus (Landisman et al. 2002). Cx36 may predominate in networks of electrotonically coupled inhibitory neurones (Galarreta and Hestrin 2001). This does not exclude the participation of other Cx subtypes in interneuronal electrical communication as electrotonic communication is not restricted to inhibitory neurones and has been observed in excitatory neurones in the CNS, including the hippocampus (MacVicar and Dudek 1981; Nunez et al. 1990; Draguhn et al. 1998) and cortex (Venance et al. 2000). Cx47 is a newly discovered member of the mouse Cx family and consequently has received less attention. However, Cx 47 has been localised to cells within areas of grey matter in the spinal cord and brain, forms functional intercellular junctions when transfected into oocytes or HeLa cells (communication-deficient mammalian cell line) and are gated by transjunctional voltage differences and chemical uncouplers (Teubner et al. 2001).

Direct evidence for the existence of intercellular electrotonic communication in a neuronal population comes from dual electrophysiological recordings where pairs

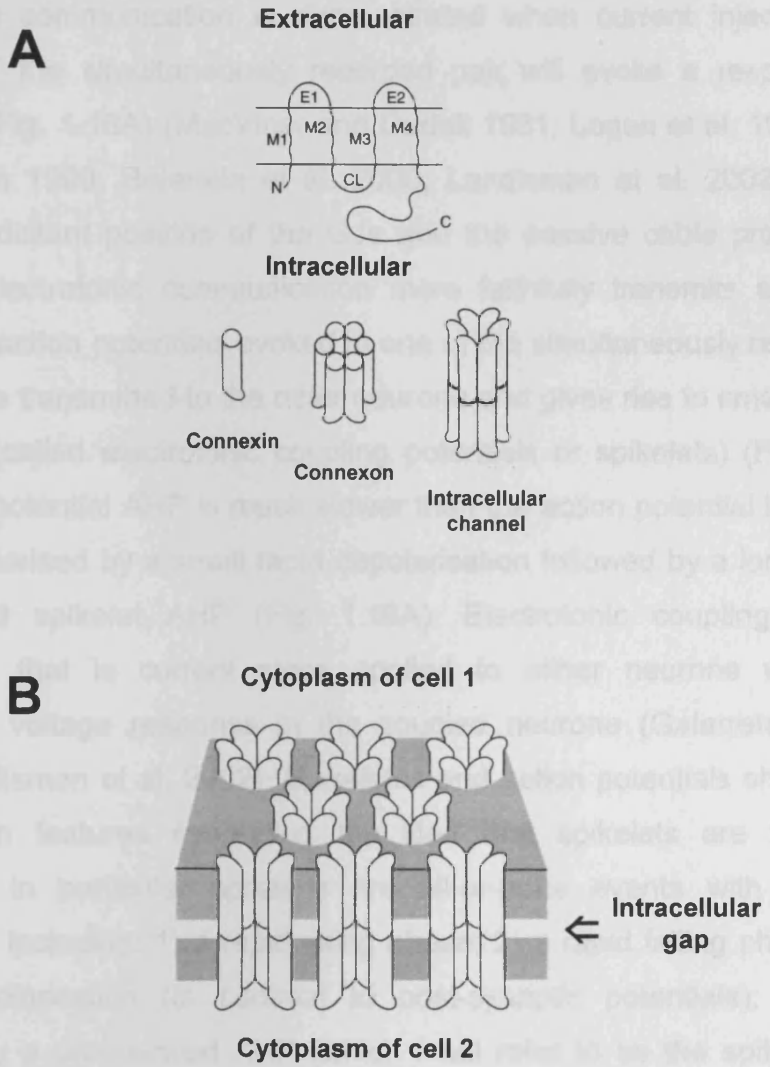

Figure 1.15 Schematic structure of Gap Junctions.

(A) The transmembrane topology of a generic connexin polypeptide creates four membrane domains (M1-M4), one cytoplasmic (CL) and two extracellular (E1 and E2) loops, and the N- and C-termini face the cytoplasm. Fourier microscopy shows that M1-M4 are packed helices, creating a single connexin subunit. Six subunits oligomerize into a connexon within the membrane of a single cell, which docks with a counterpart in an adjacent cell to form the intercellular channel.

(B) Gap junction plaques are variable numbers of intercellular channels clustered at close appositions of the plasma membranes of two cells, leaving a 3-nm `intercellular gap' and forming axial channels connecting the cytoplasms of the cells. The shaded planes represent the lipid bilayer.

(from Simon and Goodenough 1998).

of electrically coupled neurones are recorded simultaneously. Interneuronal electrotonic communication is demonstrated when current injection into one neurone of the simultaneously recorded pair will evoke a response in both neurones (Fig. 1.16A) (MacVicar and Dudek 1981; Logan et al. 1996; Galarreta and Hestrin 1999; Beierlein et al. 2000; Landisman et al. 2002). Due to the presumed distant position of the GJs and the passive cable properties of the dentrites electrotonic communication more faithfully transmits slower signals. Therefore, action potentials evoked in one of the simultaneously recorded pair of cells can be transmitted to the other neurone and gives rise to small depolarising potentials (called electrotonic coupling potentials or spikelets) (Fig. 1.16A). As the action potential AHP is much slower than the action potential itself, spikelets are characterised by a small rapid depolarisation followed by a longer and often pronounced spikelet AHP (Fig. 1.16A). Electrotonic coupling is often bi-directional, that is current steps applied to either neurone will evoke an attenuated voltage response in the coupled neurone (Galarreta and Hestrin 2001; Landisman et al. 2002). Spikeletes and action potentials share a number of common features supporting the idea that spikelets are filtered action potentials. In particular spikelets are all-or-none events with characteristic waveforms including: 1) a rapid rising phase; 2) a rapid falling phase indicating active repolarisation (in contrast to post-synaptic potentials); 3) are often followed by a pronounced AHP (which I will refer to as the spikelet AHP); 4) generation is often dependent on neuronal depolarisation, however the amplitude and duration are relatively insensitive to changes in membrane potential (MacVicar and Dudek 1981; Logan et al. 1996; Gibson et al. 1999; Galarreta and Hestrin 2001).

Intracellular injection of low molecular weight dyes such a Biocytin, Neurobiotin or Lucifer yellow (molecular weights: 372.5, 322.8 and 457.2 respectively), into a single neurone can result in the spread of dye-into other neurones (MacVicar and Dudek 1981; Nunez et al. 1990; O'Donnell and Grace 1993; Valiante et al. 1995; Mann-Metzer and Yarom 1999). This effect is referred to as dye-coupling and a correlation between the occurrence of spikelets and dye-coupling in neuronal populations is also taken as an indication of the presence of electronic coupling via GJs (Nunez et al. 1990; Valiante et al. 1995; Mann-Metzer and Yarom 1999). Interestingly, not all populations of neurones that have directly

A Electrotonic coupling between NRT neurones *in vitro*

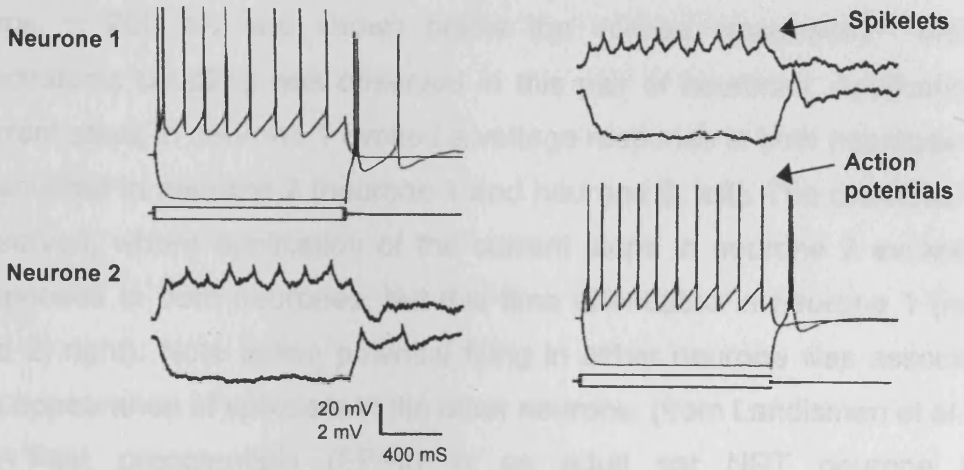

B Fast prepotentials in an NRT neurone *in vivo*

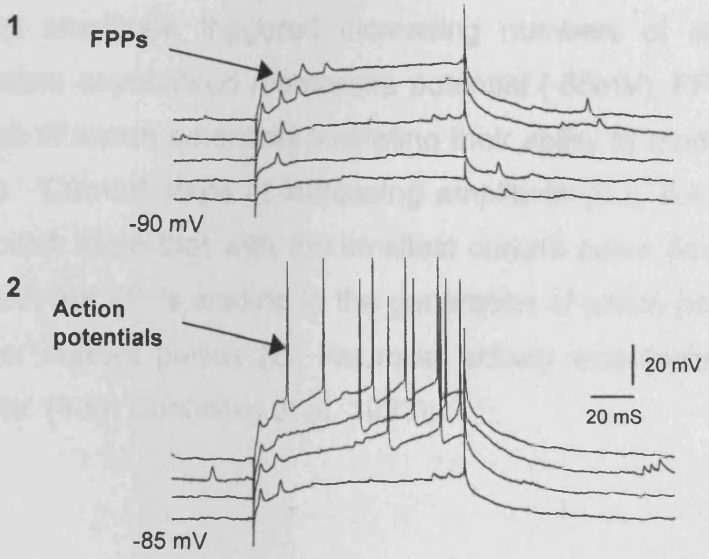

Figure 1.16 Electrotonic coupling and fast prepotentials in NRT neurons.

Figure 1.16 Electrotonic coupling and fast prepotentials in NRTneurones.
(A) A pair of simultaneously recorded NRT neurones in rat (age: 14-21 days) thalamic slices. (Neurone 1, left: the applied d.c. current steps, ± 200 pA, are shown below the voltage responses. Neurone 2, right: the applied d.c. current steps, ± 200 pA, are shown below the voltage responses). Bidirectional electrotonic coupling was observed in this pair of neurones. Application of d.c. current steps in neurone 1 evoked a voltage response in both neurones although attenuated in neurone 2 (neurone 1 and neurone 2, left). The converse was also observed, where application of the current steps in neurone 2 evoked voltage responses in both neurones, but this time attenuated in neurone 1 (neurone 1 and 2, right). Note action potential firing in either neurone was associated with the appearance of spikelets in the other neurone. (from Landisman et al. 2002).
(B) Fast prepotentials (FPPs) in an adult cat NRT neurone recorded intracellularly *in vivo*. FPPs evoked by application of depolarising current steps of increasing amplitude (0.6, 0.8, 0.9 and 1nA) from a hyperpolarised membrane (-90mV) potential are shown. Each trace is offset in order to clearly see the voltage response to each current step. Note that depolarising pulses of increasing amplitude triggered increasing numbers of all-or-none FPPs (1). From a more depolarised membrane potential (-85mV), FPPs could lead to the generation of action potentials indicating their ability to modify the output of NRT neurones. Current steps of increasing amplitude (0.2, 0.4, 0.6, 0.8 and 0.9nA) were applied. Note that with the smallest current pulse (lower trace) FPPs only are evoked, but FPPs leading to the generation of action potentials were evoked with larger current pulses (2). Neuronal activity was recorded under urethane anesthesia. (from Contreras et al. 1993).

been demonstrated to communicate electrotonically display dye-coupling (Logan et al. 1996; Galarreta and Hestrin 2001; Landisman et al. 2002). This may be due to methodological constraints or through the type of Cx involved, as it is thought that inhibitory interneurones that are associated with Cx36 do not demonstrate dye-coupling (Galarreta and Hestrin 2001; Landisman et al. 2002). In addition GJ communication in various systems may be sensitive to a number of factors. In various systems, GJs are modulated by transjunctional voltage, intracellular acidification and a number of pharmacological agents. Agents known to reduce coupling include: 1) lipophiles such as arachidonic acid, octanol, halothane, oleic acid and carbenoxolone; 2) acidifiers such as weak acids like lactate or agents that disrupt oxidative phosphorylation like dinitrophenol or nigeriacin; 3) antibodies or peptides targeted towards a particular region of the connexin protein; and 4) other molecules such as glycyrrhetinic acids (Rozental et al. 2001).

1.9.3 Electrotonic coupling in thalamic neurones.

The presence of electrotonic coupling has been directly demonstrated in the NRT of neonatal rats or mice (31% of recorded pairs (28 of 90) at postnatal days 14-21) (Landisman et al. 2002). Observed electrotonic coupling among pairs of simultaneously recorded neurones had the following characteristics: 1) symmetrical bi-directional coupling; 2) not obviously gated by transjunctional voltage; and 3) electrical signals were filtered and action potentials in one neurone gave rise to characteristic spikelets in the recorded coupled neurone (Fig. 1.16A). In addition, electrotonic coupling was dependent on the presence of Cx36 as demonstrated by the virtual absence of electrotonically coupled pairs of neurones in Cx36 null mice. Replacement of Cx36 with β-galactosidase (β-gal) in the Cx36 knockout mice (Deans et al. 2001) indicated that Cx36 expression is apparently restricted to subsets of NRT neurones. As previously described in populations of electrotonically coupled inhibitory neurones, no dye-coupling was observed in NRT neurones. (Landisman et al. 2002). Previously, NRT neurones recorded both *in vitro* and *in vivo* have been shown to display small depolarising potentials that have a similar appearance to spikelets and often give rise to action potentials (Fig. 1.16B) (Llinas and Geijo-Barrientos 1988; Amzica et al. 1992; Contreras et al. 1993). These small depolarising potentials have been referred to as small spikes or fast prepotentials (FPPs) and some have similar

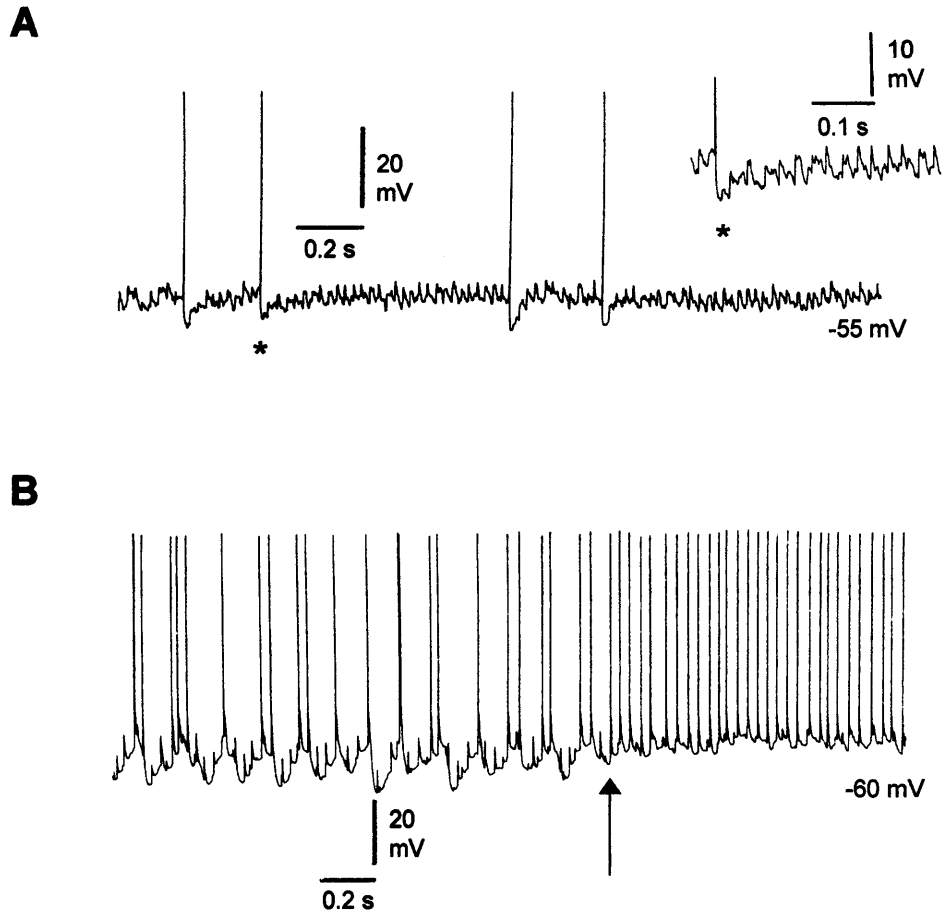

Figure 1.17 Fast prepotentials in TC neurones.

Fast prepotentials (FPPs) in 2 different cat TC neurones (A and B) recorded *in vivo*. The resting membrane potential is indicated below and to the right of the main trace for each neurone.

(A) A TC neurone in the ventrolateral (VL) nucleus. * indicates the action potential expanded in the trace to the upper right of the main trace. Action potential is truncated in the expanded trace. FPPs recurring rhythmically at 30-40 Hz and occasionally giving rise to a single action potential are shown here (main trace).

(B) A TC neurone in the centrolateral (CL) nucleus at two levels of injected d.c. current (arrow indicates removal of hyperpolarizing d.c. current). At the most hyperpolarised level, FPPs could sometimes give rise to action potentials. At the more depolarised level, action potentials firing dominated.

(from Steriade et al. 1991b).

properties to spikelets observed in electrotonically coupled neurones. These FPPs were 3-10mV in amplitude, and 3-6ms in duration (measured at the base) and were triggered by depolarisation. In addition, they had an all-or-none appearance as the amplitude did not change if the neurone was progressively hyperpolarised, had a short falling phase suggesting active repolarisation and were sometimes followed by an obvious AHP. These FPPs could give rise to full action potentials and were presumed to be of dendritic origin as they were triggered by depolarisation or could appear on the falling phase of a LTCP. In addition, these FPPs were Na^+-dependent as they were abolished in the presence of TTX *in vitro* (Llinas and Geijo-Barrientos 1988; Contreras et al. 1993). The similarity of these FPPs and spikelets in electrotonically coupled neurones suggests that they may indeed represent attenuated action potentials arising in coupled neurones. In which case, the ability of spikelets to give rise to action potentials suggests that electrotonic coupling has a role in determining NRT output.

A variety of *in vivo* studies have also described the presence of these so called FPPs in TC neurones (Deschenes et al. 1984; Steriade et al. 1991b; Timofeev and Steriade 1997). In these cases the amplitude of FPPs was insensitive to changes of the membrane potential, but their appearance was critically dependent on neuronal depolarisation. These FPPs (Fig. 1.17) were apparent in various forms and could consist of single component, short duration (4-10ms) rhythmic potentials (Deschenes et al. 1984; Steriade et al. 1991b), in combination with EPSPs (Timofeev and Steriade 1997) or as longer duration (10-20ms) events which exhibit multiple components (Steriade et al. 1991b). These properties are consistent with the properties of spikelets in neurones that are electrotonically coupled. In addition, *in vivo* FPPs are involved in synchronising oscillatory activity potentiated by stimulation of cholinergic inputs which are known to depolarise TC neurones (McCormick 1992), a role consistent with the role of electrotonic coupling in synchronising neuronal activity (see section 1.9.1). However, dye-coupling has not been observed in association with these FPPs *in vivo* when injected with Lucifer Yellow (Deschenes et al. 1984) and as yet there is no direct demonstration of electrotonic coupling between TC neurones. Cx36 expression has been reported in dorsal thalamic and other thalamic nuclei, but at lower levels than in the thalamic reticular nucleus and is

reportedly absent in some thalamic nuclei (Condorelli et al. 2000; Parenti et al. 2000; Liu and Jones 2003). However, other reports suggest that other Cx subtypes are present in neurones of thalamic relay nuclei of rodents (Micevych and Abelson 1991).

1.10 AIMS AND OBJECTIVES

The data in the following chapters aims to meet the following objectives.

1) A method is sought to induce slow (<1Hz) oscillatory activity in TC neurones using a physiologically relevant technique. Stimulation of corticothalamic fibres in thalamic slices is predicted to be the method most appropriate for mimicking cortical activation of mGluR receptor on TC neurones and therefore inducing slow (<1H) oscillatory activity *in vitro*. In addition, a simpler method of mimicking mGluR activation using pharmacological tools is required that mimics both cortical activation of TC neurones *in vivo* and corticothalamic stimulation *in vitro*.

2) With a simple pharmacological method of inducing slow (<1Hz) oscillatory activity in TC neurones it will be possible to investigate the mechanism by which this type of oscillatory activity arises. A full characterisation of the slow (<1Hz) oscillation in TC neurons *in vitro* is required.

3) It is predicted that mGluR activation of NRT neurones will lead to the induction of oscillatory activity at <1Hz in this neuronal type. Therefore an investigation of the effect of mGluR activation on NRT neurones is required.

4) The presence of spikelets in TC and NRT neurones is a novel electrophysiological finding. These spikelets are hypothesised to be a manifestation of electrotonic coupling between TC-TC and NRT-NRT neurones. An investigation into the origin of these spikelets is required.

CHAPTER 2

MATERIALS AND METHODS

2.1 *IN VITRO* TISSUE SLICE PREPARATION

All tissue slices were obtained following previously described methods (Crunelli et al. 1987a; Turner et al. 1994; Turner et al. 1997) and in accordance with the UK Animals (Scientific procedures) Act 1996 and Cardiff University Ethical Committee regulations. Male and female cats (0.5-2.5Kg) were placed in an anaesthetic delivery chamber and deeply anaesthetised with a mixture of O_2 and NO_2 (2:1) and halothane (5%). Animals were considered deeply anaesthetised when postural and withdrawal reflexes were abolished. At this point, the animal was transferred to the dissection area and positioned lying prone with the head supported from underneath. Anaesthesia was maintained with a reduced concentration of halothane (1-2%) delivered via a facemask for the duration required to remove the brain from the cranium (2-3 minutes). The absence of a withdrawal reflex was ensured before the procedure to remove the brain from the cranium was commenced. Further checking of the depth of anaesthesia was not performed as anaesthesia was maintained only for a short time following this point.

Following a caudorostral midline incision through the skin along the dorsal surface of the head, the skin was reflected and surrounding muscles removed by blunt dissection to expose the underlying cranium. A wide craniotomy was performed, taking care to avoid damaging the underlying cerebral hemispheres, and the meninges reflected. At this point (and thereafter until the brain was removed from the cranium), the brain was cooled by slowly pouring over aerated (95% O_2, 5% CO_2), iced (<4°C) solution of composition: (mM) sucrose (250), $NaHCO_3$ (16), KCl (2), KH_2PO_4 (1.25), $MgSO_4$ (5), $CaCl_2$ (2), glucose (10), indomethacin (0.045) (Pakhotin et al. 1997; Pakhotin et al. 1999) ascorbic acid (0.4) (Rice 1999). The use of indomethacin (cyclo-oxygenase inhibitor) and ascorbic acid (anti-oxidant) were utilised here as the cutting phase of the tissue preparation is suggested to be a critical point for triggering pathological events leading to slice degradation (Pakhotin et al. 1997) and aid electrophysiological and morphological preservation of brain slices (Pakhotin et al. 1997; Pakhotin et al. 1999; Rice 1999). The brain was lifted at its rostral end to expose the optic tracts. Following sectioning of the optic tracts, a coronal cut was made through the brainstem at the level of the inferior colliculus and the brain was rapidly removed from the cranium and placed in the same aerated (95% O_2, 5% CO_2),

iced (<4°C) solution described above. The brain was then placed in a petri dish, and bisected along the midline. The following procedure was then applied simultaneously to both halves of the brain. Tissue overlying the thalamus was removed by careful dissection revealing the dorsolateral surface of the thalamus and allowing positive identification of the surface of the LGN. Using the identified LGN as a reference to ensure correct orientation of the thalamus for slicing, a tissue block containing the dorsal thalamus was cut and subsequently adhered (using a cyanoacrylate adhesive) to the stage of a Vibroslice (Camden Instruments, UK). The Vibroslice stage was then immersed in the continually aerated, iced solution described above, and 450-500μM thalamic slices were cut.

In the majority of cases the block of tissue containing the dorsal thalamus was adhered to the Vibroslice stage on the midline and sagittal slices were cut starting from the lateral aspect and moving downward towards the midline. Using this orientation it was possible to obtain thalamic slices that contained the LGN or MGN and then the VB or VL as they were exposed during progression towards the midline. In sagittal slices containing the LGN, VB and VL care was taken to ensure that the surrounding nucleus reticularis thalamus (PGN or NRT) and corticothalamic fibres were left intact. In some cases, coronal LGN slices were obtained by adhering the block of thalamic tissue to the Vibroslice stage on the caudal surface, with subsequent slicing performed in the rostrocaudal direction. The locations of thalamic nuclei were identified following Berman and Jones, 1982.

2.2 TISSUE SLICE MAINTENANCE

Once cat thalamic slices were obtained they were treated in the following way: Newly cut slices were placed in a storage bath containing modified aCSF (storage solution) of composition: (mM) NaCl (134), $NaHCO_3$ (16), KCl (5), KH_2PO_4 (1.25), $MgSO_4$ (5), $CaCl_2$ (2), glucose (10) and ascorbic acid (0.4) at 30-32°C. After 1 hour the storage solution was allowed to cool slowly to room temperature, around 20°C, and slices were used for intracellular or extracellular electrophysiological recording. Slices remained under these conditions until used on that day or any unused slices were kept over night at 9 ± 1 °C (without additional aeration) for use on the following day. This procedure was implemented as overnight hypothermic storage of brain slices following treatment

of indomethacin has previously been shown to prolong slice viability for 3-5 days (Pakhotin et al. 1997; Pakhotin et al. 1999). On the following day slices remained cooled at 9°C without additional aeration and were used as required.

Tissue slices were transferred to an interface-style recording well and maintained in a manner suitable for electrophysiological recordings based on methods originally described by Yomamoto and McIlwain (1966) and later developed by Haas et al. (1979). The tissue slice was placed on a nylon mesh that overlays the surface of the perspex recording well and allows the slice to be maintained at the interface between the perfusion medium and a warmed, humidified atmosphere (water maintained at 35 ± 1 °C aerated with 95% O_2, 5% CO_2). Continually aerated (95% O_2, 5% CO_2) artificial cerebrospinal fluid (aCSF) of composition (mM): NaCl (134), $NaHCO_3$ (16), KCl (2), KH_2PO_4 (1.25) $MgSO_4$ (1), $CaCl_2$ (2), glucose (10), pH 7.4, was passed through a tube submerged in warmed water (35 ± 1 °C) and introduced at one end of the recording well, moved along the nylon mesh and subsequently removed from the other end by capillary action. This process was accelerated by the use of paper wicks. The tissue was therefore subjected to continual perfusion at a rate in the order of 1-2ml / min. This perfusion rate was formed by the action of gravity and controlled by the height of perfusion solution reservoirs above the recording well and by the incorporation of a precision variable valve (Dail-A-Flow, Abbot, Ireland). Since there is a dead space of ~2mm between the reservoirs and the recording well inlet, the exchange of the perfusion solution would be expected to occur in less than 5 minutes. However, the time taken for pharmacological agents to exert a noticeable effect was consistently greater than this time (around 10-15 minutes). After placement in the recording well, slices were left for 30 minutes prior to the commencement of recording.

2.3 ELECTROPHYSIOLOGICAL RECORDING TECHNIQUES

2.3.1 Intracellular Recordings.

Intracellular recordings were made with sharp glass microelectrodes pulled on a horizontal puller (P-97, Sutter Instruments Co.) from standard (GC 120F) or thin (GC 120TF) walled borosilicate glass capillaries (Harvard Apparatus). Electrodes were filled with 1M KAc and 0.5-2% Biocytin or 2% Neurobiotin, producing

subsequent d.c. resistances of 80-120 and 40-60 MΩ for standard and thin walled microelectrodes, respectively. The electrode was fixed in an electrode holder (HL-U, Axon) filled with 3M NaCl, and this assembly was subsequently attached to a headstage (HS-2, gain 0.1L, Axon instruments) of a voltage/current amplifier (Axoclamp A2, Axon Instruments). The headstage was mounted on a custom-built electrode advancing system, which allowed both gross manual positioning and accurate positioning by use of a servo mechanism. When the electrode came in contact with the tissue slice, the amplifier offset circuitry was adjusted so that the voltage offset read zero. At the termination of intracellular recordings, the offset from zero was noted and membrane voltage-measurements were adjusted to account for this factor during subsequent offline analysis.

2.3.1.1 Current-clamp recordings.

Under-current clamp, the membrane potential of the neurones is initially set to a level by the application of current through the recording electrode and is then free to vary from this set point either spontaneously or, for example, in response to stimulation of afferent pathways. Moreover, stepped d.c. changes in injected currents allow the examination of membrane charging behaviour and on-line estimates of the apparent input resistance of the neuronal membrane. Current clamp recordings were made with a bridge balance circuit allowing, via the principle of the Wheatstone bridge, the finite voltage deviations produced by current injection through an electrode with a finite value of d.c resistance to be magnified by a balance resistor. Furthermore, the finite capacitance of the recording electrode may be compensated for by additional circuitry that, in effect, produces a compensatory value of negative capacitance. Thus the voltage responses to stepped d.c. changes are a product of the resistive and capacitive elements of the neuronal membrane. Experimentally, these procedures were accomplished by adjustments made to the bridge balance resistor and the capacitance neutralisation control, thus minimising the fast voltage transits at the onset and offset of voltage responses evoked by stepped d.c. changes. After implementation of these procedures, the maximum apparent input resistance of the impaled neurone (R_N) could be estimated by determining the magnitude of the voltage deflection elicited from the resting membrane potential or between -60 to -70mV in response to small d.c. stepped changes (typically 10-100pA).

Under all experimental conditions, neurones were left for a maximum of 5 minutes at a given level of injected d.c. current, in order to see if they would generate an intrinsic oscillation at that injected d.c. current level.

2.3.1.2 Voltage-clamp recordings.

The voltage clamp technique involves the initial setting of the value of the membrane potential, but in contrast to current-clamp, the voltage is not allowed to move from this initial set point. Conductance alterations of the neuronal membrane associated with a shift from one voltage set point to another predetermined set point are estimated from the value of the injected current required to achieve transition between the two voltage set points. Voltage clamp recordings were made using the discontinuous single electrode voltage clamp (dSEVC) method. The dSEVC method relies on the principle of task sharing between periods of voltage sampling and current injection, thus allowing the voltage clamp to be achieved with a single microelectrode. The frequency of periods of voltage sampling and current injection is set experimentally and ranged between 2.5-3.5 kHz. In this scheme, a sample and hold circuitry initially samples the membrane potential value, which is retained for a cycle. This value is compared, within the comparator circuitry, to a value determined by the experimenter. The comparator output becomes the input for the controlled current source circuitry, which produces a current directly proportional to the value of comparator output that is conveyed to, and irrespective of the finite resistance of the recording electrode. Repetition of this cycle is made and the value of output current is automatically adjusted in each cycle to maintain a close correspondence between the measured value of membrane potential and the ideal command potential. Experimentally neurones were impaled under current clamp and maintained until steady values of membrane potential and apparent input resistance were achieved. The transition from current-clamp to dSEVC modes was achieved using the procedures described by Finkel and Redman (1984). This involved the optimal adjustment of capacitance neutralisation, phase, gain and sampling rate controls of the amplifier so that settling of the continuously monitored headstage voltage was achieved within switching cycles.

2.3.1.3 Dynamic clamp.

Dynamic clamp is a variation on intracellular sharp electrode current clamp recording whereby computer generated conductances can be injected into real neurones. Any conductance that can be mathematically modelled can be intrduced into a neurone and specific paramenters of a given conductance can be altered to investigate its function (Sharp et al. 1993; Prinz et al. 2004). The dynamic clamp system used here was implemented as previously described (Hughes et al. 1999). This system was utilised following microelectrode impalement of a neurone: The membrane potential (Vm) of the real neurone is continuously sampled by the Axoclamp 2A amplifier in bridge mode and the voltage signal is transferred to a personal computer running the dynamic-clamp software via an analogue to digital converter. Based on this Vm and a set of equations describing the kinetics, maximal conductance and voltage dependence of different conductances, a current command signal (V1) was calculated representing the current that would flow through the membrane if specified currents were present. V1 was then transferred back to the recording amplifier following conversion from a digital to analogue signal and applied to the real neurone as a transmembrane current signal (I_{inj}). The software design allowed all or any properties of a computer generated conductance to be manipulated as required for various experiments. The recorded current and voltage traces were stored directly on the computer. A Digidata 1200 interface (Axon Instruments) was used to perform analogue to digital or digital to analogue conversions enabling a sampling rate of 50KHz.

2.3.2 Extracellular recordings.

Extracellular recordings were made using modified patch clamp electrodes pulled on a horizontal puller (P-97, Sutter Instruments Co.) from standard (GC 120F) walled borosilicate glass capillaries (Harvard Apparatus). Electrodes were filled with 0.5M NaCl with subsequent resistances of 1-5MΩ. The electrode was fixed in an electrode holder (HL 1, Axon Instruments) filled with 3M NaCl and this assembly was subsequently attached to a headstage (NL 100, Digitimer) attached to a differential amplifier (Neurolog 104, Digitimer). As for intracellular recordings, the headstage was mounted on a custom built electrode advancing system, which allowed both gross manual positioning and accurate positioning by use of a servo mechanism. Extracellular recordings were used to observe spontaneous action potential firing under different experimental conditions.

2.3.3 Stimulation protocol.

Electrical stimulation of corticothalamic fibres in sagittal thalamic slices was performed using an isolated stimulator (DS2A, Digitimer Ltd, UK) connected to a tungsten bipolar electrode placed in the optic radiations. Corticothalamic fibres were stimulated at 25-100 Hz for 100-600 ms with each stimulus comprising a 50-300 μA pulse lasting 0.2 ms.

2.3.4 Data capture, analysis and statistics.

For intracellular recording, the output from the Axoclamp 2A was low pass filtered (to 30 kHz) and for extracellular recording, the output or the Neurolog 104 was filtered at 0.1-20kHz. Subsequently, signals were digitised at 48 KHz and recorded with a digital audio tape (DAT) recorder (DTR-1204, Biologic, France). Recorded data stored on DAT was then re-digitised via a Digidata 1200 interface using pClamp software (Axon Instruments) running on a standard personal computer. Offline analysis was performed also using pClamp software (Axon Instruments) and graphics were produced using Sigmaplot (SPSS Inc.), Origin 7 (OriginLab Co.) or Prism (Graphpad) software. In most cases, statistical analysis was performed using a t-test selected for paired or unpaired observations after checking that the data sets were normally distributed and of equal variance. Other statistical tests were used when the data sets analysed did not meet the criteria for analysis using a t-test and are indicated in the relevant results chapters. A Mann-Whitney test was used for unpaired data sets that were not normally distributed. *P* was considered significant when <0.05 for 2-tailed *P*-values. Autocorrelograms were computed using discretised action potential trains and normalised to the value obtained at 0ms. Other analysis protocols are listed in the relevant results chapters. All quantitative results in the text and figure legends are expressed as mean ± SEM.

2.3.5 Electrophysiological identification of thalamic neurones.

Intracellularly recorded TC neurones and NRT neurones were identified by their position in the slice and characteristic voltage responses following injection of depolarising or hyperpolarising d.c. current steps (Jahnsen and Llinas 1984b; Jahnsen and Llinas 1984a; Llinas and Geijo-Barrientos 1988; Avanzini et al. 1989; Crunelli et al. 1989; Bal and McCormick 1993). In particular, TC and NRT

neurones could be distinguished according to the structure of the LTCP-mediated burst of action potentials. LTCP-mediated burst in TC neurones were characterised by a decelerating action potential pattern (Fig. 2.1A) (Jahnsen and Llinas 1984a; Jahnsen and Llinas 1984c; Crunelli et al. 1987b; Llinas and Geijo-Barrientos 1988; Crunelli et al. 1989), whilst in NRT neurones the LTCP-mediated bursts had an accelerating then decelerating action potential pattern (Fig. 2.1B) (Llinas and Geijo-Barrientos 1988; Avanzini et al. 1989; Bal and McCormick 1993). Positive identification of extracellularly recorded TC or NRT units was made by their position in the tissue slice and observation of the structure of action potential burst firing. As for intracellular recordings, TC units were identified with a decelerating pattern of burst firing (Fig. 2.2A) and NRT units were identified with an accelerating then decelerating pattern of burst firing (Fig. 2.2B) (Domich et al. 1986).

2.4 MORPHOLOGICAL PROCEDURES.

2.4.1 Tissue slice processing.

Impaled neurones were morphologically identified following the intracellular injection of the low-molecular weight biotinylated compounds: Biocytin (a biotin-lysine complex, MW=372) or Neurobiotin (a biotin derivative, N-(2-aminoethyl) biotinamide hydrochloride, MW= 286) dissolved in the electrode solution (1M KAc). In order to allow positive identification of recorded neurones after morphological recovery, typically 2-3 impalements were made per tissue slice and the position of each was recorded on a schematic drawing of the brain slice during experimental procedures. Movement of the biotinylated compounds Biocytin and Neurobiotin is aided by the application of an active injection protocol: Biocytin can be electrophoresed with either positive or negative current, where as Neurobiotin is selectively ejected by positive current (Kita and Armstrong 1991). However, an active injection protocol was not employed here as the combination of current steps applied during intracellular recording to examine various parameters of the membrane properties and the duration of recordings was sufficient to allow the recovery of well-filled cells when either Biocytin or Neurobiotin were used. The same visualisation protocol was followed

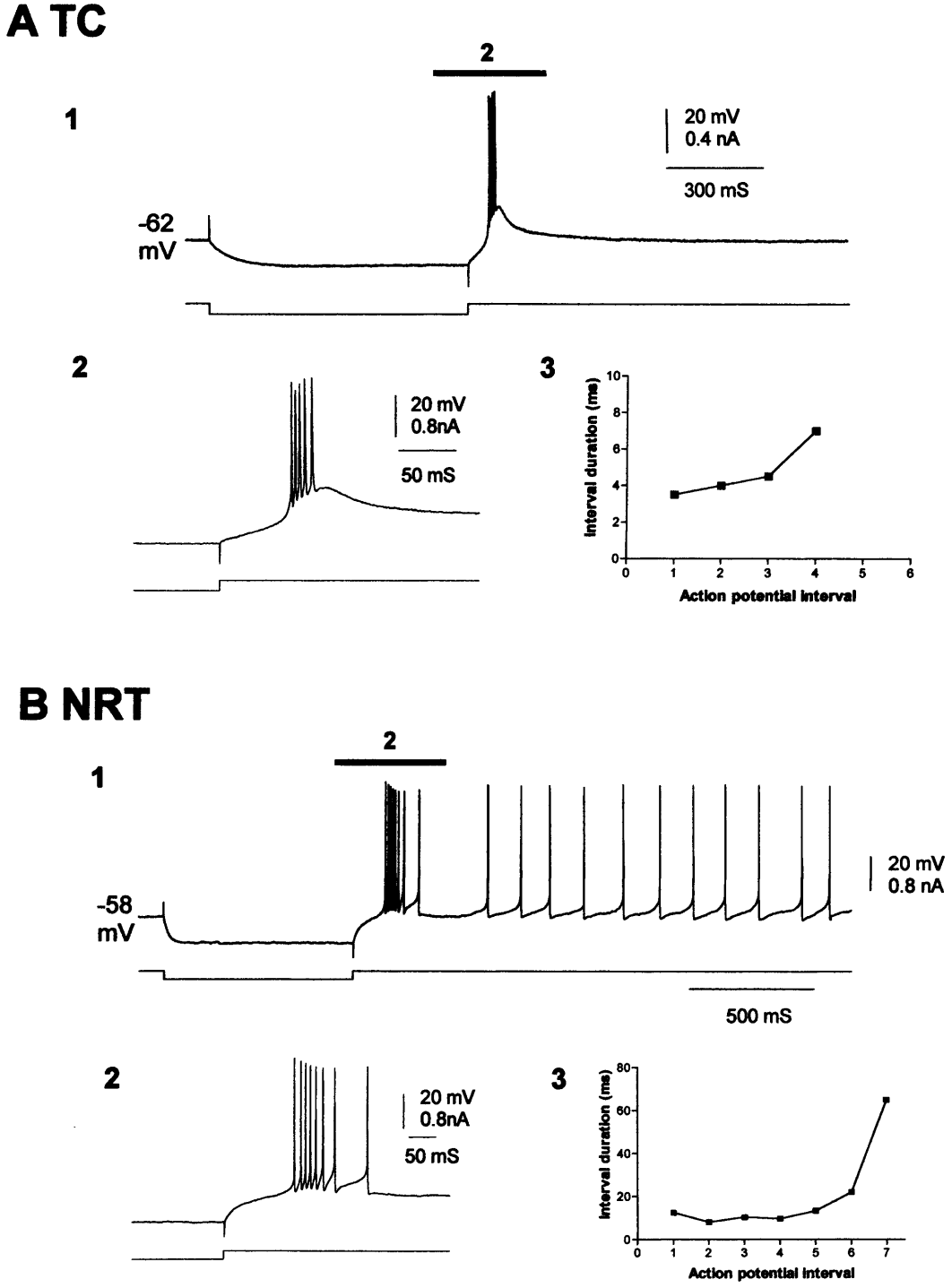

Figure 2.1 Characteristic intracellular burst pattern in thalamic neurones.
(A) Evoked LTCP-mediated burst of action potentials in a TC neurone (1) and expanded below (2). Note the increase in successive action potential intervals (3) indicating a decelerating action potential firing pattern.
(B) Evoked LTCP-mediated burst of action potentials in a NRT neurone (1) and expanded below (2). Note the decrease then increase in successive action potential intervals (3) indicating an accelerating-decelerating action potential firing pattern.

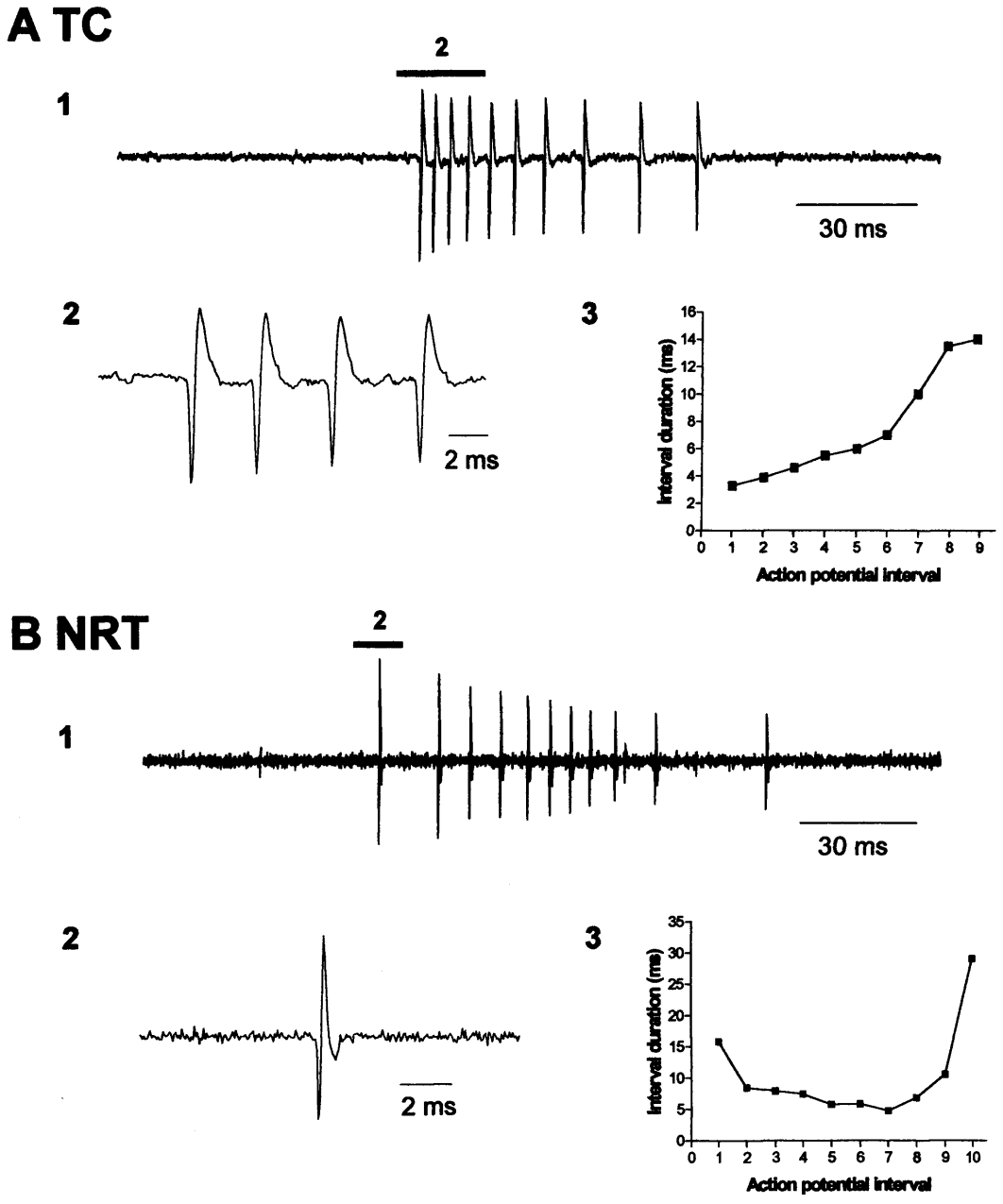

Figure 2.2 Characteristic extracellular burst pattern in thalamic neurones.
(A) Spontaneous burst of action potentials in a TC neurone (1) and expanded below (2). Note the increase in successive action potential intervals (3) indicating a decelerating action potential firing pattern and indicative of a LTCP-mediated burst of action potential in TC neurones.
(B) Spontaneous burst of action potentials in a NRT neurone (1) and expanded below (2). Note the decrease then increase in successive action potential intervals (3) indicating an accelerating-decelerating action potential firing pattern and indicative of a LTCP-mediated burst of action potentials in NRT neurones.

for both Biocytin and Neurobiotin, following the procedure described by Horikawa and Armstrong (1988) and as previously detailed (Williams et al. 1996; Turner et al. 1997). This procedure utilises the high affinity of biotin for avidin and consequently if avidin is conjugated with light emitting or light absorbing markers, the resulting avidin-biotin complex can be visualised (Horikawa and Armstrong 1988). At the end of impalement, the microelectrode was gently removed and slices were allowed to rest in the recording chamber for at least 30 minutes prior to being placed in fixative (4% paraformaldehyde in 0.1M phosphate buffered saline (PBS) (pH 7.4) overnight (8-14 hours) and subsequently into 0.1M PBS until further processing. Slices were then embedded in 4% agar and re-sectioned at 100μm. All subsequent morphological procedures were carried out at room temperature. Re-sectioned slices were incubated in 3% H_2O_2 in 0.1M PBS with 0.4% Triton X-100 (Sigma) for 12 minutes to quench background peroxidase activity and permeablise the tissue and then rinsed (3 x 10 minutes) in 0.1M PBS with 0.4% Triton X-100. Following a 3 hour incubation period with an avidin-biotin-horseradish peroxidase complex (Vectastain Elite ABC kit, Vector Laboratories) in 0.1M PBS with 0.4% Triton X-100, re-sectioned slices were again rinsed (3 x 10 minutes) in 0.1M PBS with 0.4% Triton X-100. Filled neurones were developed, under visual control, by incubating the re-sectioned slices in 0.1M 3,3-diaminobenzidine (DAB) in 0.1M Tris buffer (pH 7.2 at 25°C) and 0.03% H_2O_2 for about 10-12 minutes. Re-sectioned slices were again rinsed in 0.1M PBS with 0.4% Triton X-100, then arranged on slides with gelatine (2%) mounting solution, air dried, defatted in Xylene and permanently mounted in DPX neutral mounting solution (Aldrich).

Recovered neurones were viewed and analysed under a light microscope (Labophot-2, Nikon). Measurements of somal diameter, dendritic length and inspection of dendritic appendages were made at x100 magnification. No correction was made for tissue shrinkage. Presentation of neuronal morphology was achieved by digital photography (LEITZ DMRD, Leica, UK) using Spotcam software (Diagnostic Instruments Ltd, UK).

2.4.2 Morphological identification of thalamic neurones.

Following morphological recovery, neurones were identified as TC neurones due to their position in the tissue slice and according to previously described criteria:

That is a centrally located soma with radially extending dendrites or fairly polarised dendritic field, that is a typically "bushy" appearance (Fig. 2.3A) (Friedlander et al. 1981; Stanford et al. 1981; Spreafico et al. 1983; Stanford et al. 1983; Winer 1985; Yen et al. 1985b; Sawyer et al. 1994; Turner et al. 1997). TC neurones could be morphologically distinguished from local interneurones as interneurones typically have a smaller soma, more polarised dendritic fields and much finer and more sinuous dendrites (Fig. 2.3B) (Majorossy and Kiss 1976; Spreafico et al. 1983; Sherman and Friedlander 1988). Only in the LGN were TC neurones morphologically subclassified as X, Y or W-cell according to previously described criteria (Friedlander et al. 1981; Stanford et al. 1983) (Fig. 2.3A).

Following morphological recovery, neurones were identified as NRT/PGN neurones due to their position in the tissue slice and according to previously described criteria: That is with a typically oval shaped soma and polarised, discoidal shaped dendritic field (Fig. 2.3C) (Houser et al. 1980; Yen et al. 1985a; Yen et al. 1985b; Llinas and Geijo-Barrientos 1988).

2.5 DRUG CONCENTRATIONS AND SOURCES

All drugs were bath applied, that is added to the aCSF at their final concentrations for application to tissue slices. In experiments using $NiCl_2$, $CdCl_2$ or $BaCl_2$, KH_2PO_4 was omitted, but the K^+ concentration was maintained by increasing the KCl concentration to 3.25 mM, and $MgSO_4$ was omitted and replaced by equimolar MgCl. Nifedipine was dissolved in 100% ethanol and added to the aCSF such that the final ethanol concentration did not exceed 0.1% and experiments were performed in semi-darkness to minimise degradation of the compound due to exposure to light.

Drugs were obtained from the following sources and used at the following concentration unless otherwise stated elsewhere: (RS)-1-aminoindan-1,5-dicarboxylic acid (AIDA) (250 μM), L(+)-2-amino-4-phosphonobutyric acid (L-AP4) (100-200 μM), (2R, 4R)-4-aminopyrrolidine-2,4-dicarboxylate (APDC) (100-200 μM), DL-2-amino-5-phosphonovaleric acid (APV) (50-100 μM), (+)-2-methyl-4-carboxyphenylglycine (LY 367385) (250 μM), P-(3-aminopropyl)-P-diethoxymethyl-phosphinic acid (CGP 56999A) (20 μM), [S-(R*,R*)]-[3-[[1-(3,4-dicholorophenyl)ethyl]amino]-2-hydroxypropyl](cyclohexylmethyl)phosphotinic

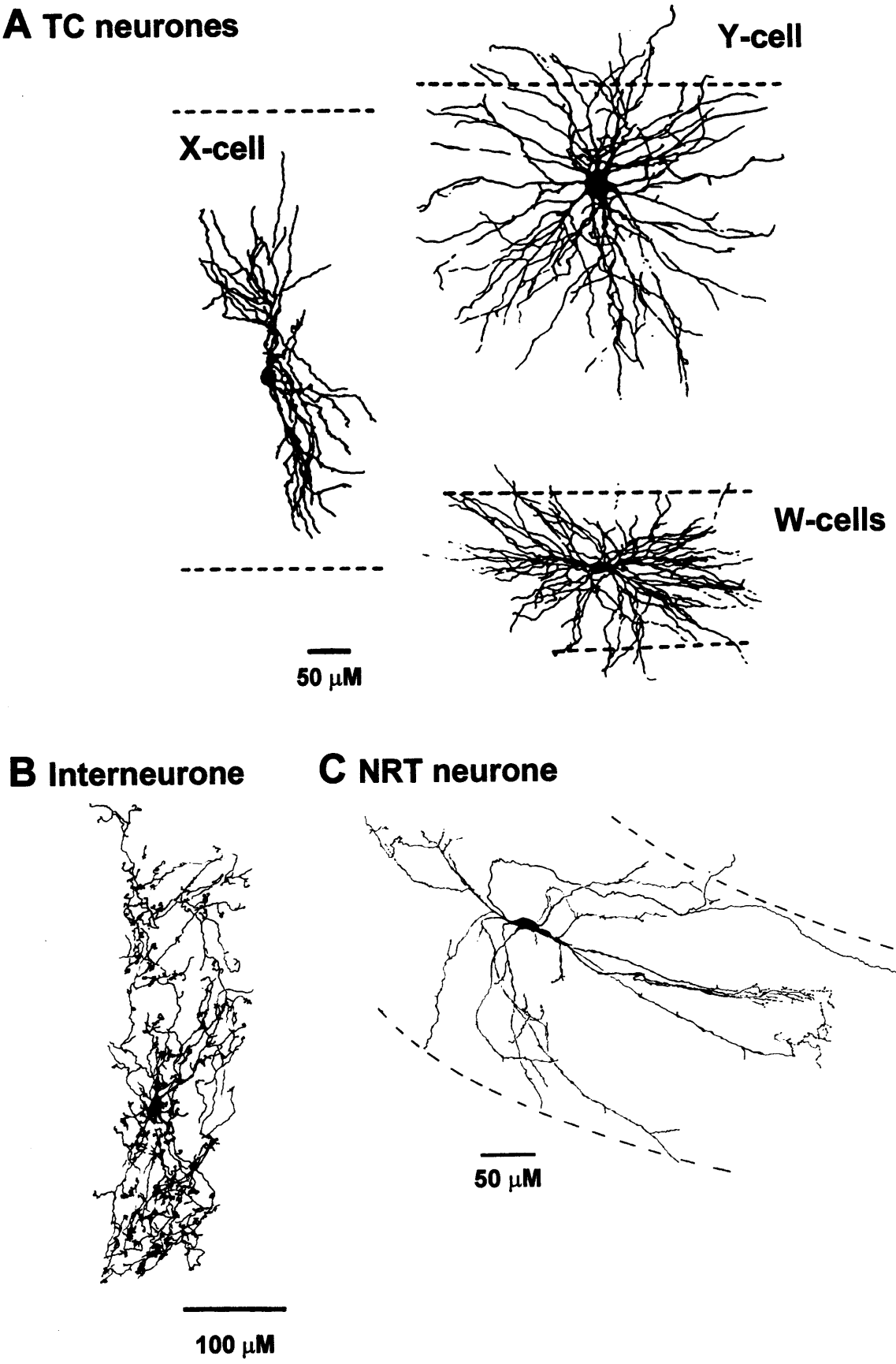

Figure 2.3 Representative morphology of thalamic neurones.

Figure 2.3 Representative morphology of thalamic neurones.

Thalamic neurone types can be identified according to distinctive morphological characteristics.

(A) Morphological characteristics of physiologically identified TC neurones in the lateral geniculate nucleus of the cat: X cells have polarised dendritic arbours that are confined within laminar boarders (dashed lines). Y cells are larger with radial dendritic arbours and the dendrites may cross laminar boarders. W-cells may have fairly polarised dendritic arbours that generally run horizontally with laminar borders. (from Stanford et al. 1983).

(B) Morphological characteristics of an inteneurone in the lateral geniculate nucleus of the cat. Typically, interneurones have compact dendritic arbours comprising fine, convoluted dendrites. (from Sherman and Friedlander 1988).

(C) Morphological characteristics of a NRT neurone projecting to the ventral posterior lateral nucleus of the cat. Typically, NRT neurones have a discoidal dendritic arbour. (from Yen et al. 1985a).

acid (CGP 54626) (20μM), 6-cyano-7-nitroquinoxaline-2,3-dione (CNQX) (10 μM), 7-(hydroxyimino)-cyclopropa[b]chromen-1a-carboxylate ethyl ester (CPCCOEt) (300 μM), (RS)-α-cyclopropyl-4-phosphonophenylglycine (CPPG) (50 μM), ω-conotoxin-MVIIC (2-3 μM), ω-conotoxin-GVIA (3 μM), (+/-)-1-aminocyclopentane-*trans*-1,3-dicarboxylic acid (*trans*-ACPD) (50-120 μM), (RS)-2-chloro-5-hydroxyphenylglycine (CHPG) (1 mM), (2S,2'R,3'R)-2-(2'3'-dicarboxy-cyclopropyl)glycine (DCG-IV) (10-100 μM), (S)-3,5-dihydroxyphenylglycine (DHPG) (50-100 μM), (2S)-α-ethylglutamic acid (EGLU) (250 μM), 2-methyl-6-(phenylethynyl)pyridine (MPEP) (30-50 μM), 4-(N-ethyl-N-phenylamino)-1,2-dimethyl-6-(methylamino)-pyrimidinium chloride (ZD 7288) (50-300 μM) and Tetrodotoxin (TTX) (1 μM) were obtained from Tocris-Cookson, Bristol, UK. 4-aminopyridine (4-AP) (100-250 μM), bis-(*o*-aminophenoxy)-*N,N,N',N'*,-tetraacetic acid (BAPTA) (100 mM), bicuculline methiodide (BMI) (30 μM), ethylene glycol-bis(b-aminoethyl ether)-*N,N,N',N'*-tetraacetic acid (EGTA) (134 mM), nifedipine (1-10 μM), 2-(3-Carboxypropyl)-3-amino-6(4-methoxyphenyl) pyridazinium bromide (SR 95531) (20 μM), 3β-Hydroxy-11-oxoolean-12-en-30-oic acid 3-hemisuccinate (carbenoxolone) (100-200 μM), Nε-Biotinyl-L-lysine (Biocytin) (0.5-2 %), L-threoascorbic acid (400 μM) and 1-(P-Chlorobenzoyl)-5-methoxy-2-methylindole-3-acetic acid (Indomethacin) (45 μM) were obtained from Sigma, UK. N-(2-aminoethyl) biotinamide hydrochloride (Neurobiotin) (2 %) was obtained from Vector Laboratories, UK.

CHAPTER 3

INDUCTION AND NUCLEUS-SPECIFIC PROPERTIES OF THE SLOW (<1Hz) OSCILLATION IN THALAMOCORTICAL NEURONES *IN VITRO*

3.1 INTRODUCTION

During all stages of resting sleep, the electroencephalogram (EEG) of humans and animals is dominated by large amplitude, slow waves that recur every 1-10 seconds (Steriade et al. 1993b; Steriade et al. 1993c; Steriade et al. 1993d; Achermann and Borbely 1997; Timofeev et al. 2001). This so-called slow (<1Hz) rhythm is generated in neocortical networks (Steriade et al. 1993c; Steriade et al. 1993d; Sanchez-Vives and McCormick 2000) and organizes other sleep rhythms, such as spindle and δ waves, into coherent, repeating episodes (Steriade et al. 1993a; Steriade et al. 1993c). At the cellular level, the slow rhythm is evident in all types of cortical neurones and is manifested as recurring sequences of synaptic barrages, that can lead to epochs of sustained action potential firing, interspersed with periods of disfacilitation or quiescence (Steriade et al. 1993d; Timofeev et al. 2001). This pattern of activity leads to prominent 'up' and 'down' states of the membrane potential, and is thought to be generated by a combination of extensive interconnectivity in the neocortex and the intrinsic properties of cortical neurones (Amzica and Steriade 1995a; Sanchez-Vives and McCormick 2000).

In thalamocortical (TC) neurones, the intracellular correlate to the slow rhythm is also characterized by repeating 'up' and 'down' states, which often demonstrate a stereotypical waveform (Steriade et al. 1993a; Contreras and Steriade 1995). In particular, the transition from 'up' to 'down' state is commonly initiated by a pronounced inflection point, whereas the transition from 'down' to 'up' state is marked by a low-threshold Ca^{2+} potential (LTCP) and accompanying high-frequency burst of action potentials (see Fig. 1.14) (Steriade et al. 1993a; Steriade et al. 1996). The slow (<1Hz) oscillation in TC neurones is dependent on corticothalamic input since it is abolished following decortication (Timofeev and Steriade 1996). This has led to the belief that the slow (<1Hz) oscillation in TC neurones is primarily a simple reflection of rhythmic cortical activity.

However, in TC neurones maintained *in vitro*, where corticothalamic input is absent, slow oscillatory activity at <1Hz has been described possessing a similar appearance to that observed *in vivo* (Williams et al. 1997a). This oscillation is present in a subset (< 15%) of neurones and is generated by a bistable interaction between the "window" (i.e. steady-state) component of the T-type

Ca^{2+} current, I_T, $I_{Twindow}$, and the leak K^+ current, I_{KLeak} (Williams et al. 1997a). Since this bistable interaction only occurs if g_{Leak} is below a specific threshold, this slow oscillatory activity has been demonstrated in every TC neurone *in vitro* following the artificial reduction of g_{Leak} using a dynamic clamp system (Hughes et al. 1999).

As a major effect of corticothalamic input onto TC neurones is to reduce g_{Leak} via the activation of metabotropic glutamate receptors (mGluRs) (McCormick and von Krosigk 1992), the ability to unmask slow oscillatory activity through corticothalamic stimulation was investigated. In addition a pharmacological protocol was sought to mimic corticothalamic stimulation in order to investigate the properties of the induced oscillatory activity in TC neurones of modality specific relay nuclei including the LGN (visual), VB (somatosensory), VL (motor) or MGN (auditory).

3.2 METHODS

3.2.1 Electrophysiology.

Intracellular and extracellular electrophysiological recordings were performed in adult cat slices containing the LGN, VB, VL and MGN as described in Chapter 2.

3.2.2 Data analysis.

Data analysis was performed as described in Chapter 2 except:

3.2.2.1 Analysis of the "up" and "down" states of the slow (<1Hz) oscillation.

The duration of the "up" state was measured as the time between the peak of the first action potential of the LTCP-mediated burst to the following inflection point marking the start of the large hyperpolarising potential (LHP) (Fig. 3.1↔). The duration of the "down" state was measured as the time between the inflection point marking the start of the LHP to the peak of the first action potential of the following LTCP-mediated burst (Fig. 3.1↔). The inflection point was taken as the membrane potential where the second derivative of the voltage with respect to time was 0 ($d^2v/dt^2=0$) in the region where the LHP began (Fig. 3.1).

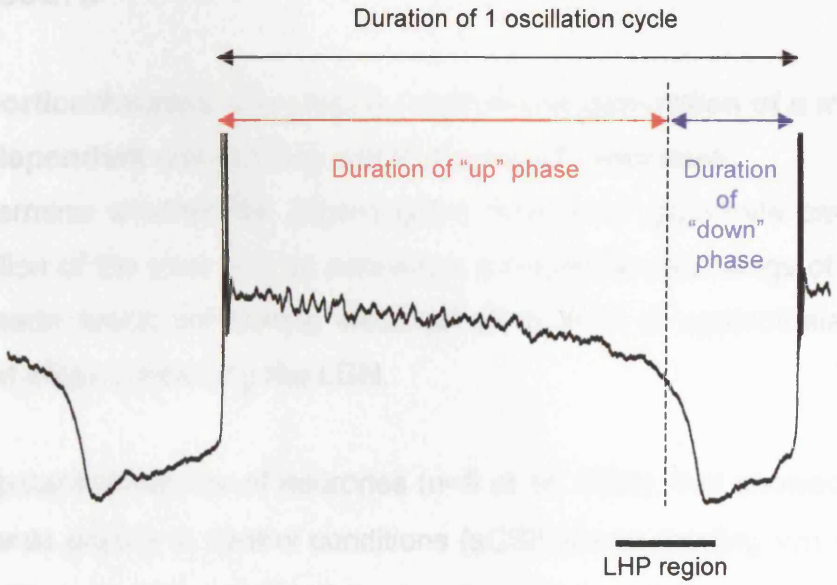

Figure 3.1 Analysis of the "up" and "down" phases of the slow (<1Hz) oscillation.

The duration of 1 oscillation cycle was measured from the peak of the first action potential in the LTCP-mediated burst of action potentials to the peak of the first action potential in the following LTCP-mediated burst of action potentials. The inflection point was taken as the membrane potential where the second derivative of the voltage with respect to time was zero in the region where the LHP occurred (LHP region). Subsequently the duration of the "up" phase was measured from the start of the oscillation cycle to the inflection point (←→) and the "down" phase was measured from the inflection point to the end of the oscillation cycle (←→).

3.2.3 Drugs.

Drugs were obtained, applied and used at concentrations described in Chapter 2.

3.3 RESULTS

3.3.1 Corticothalamic stimulation leads to the generation of a mGluR1a-dependent slow (<1Hz) oscillation in TC neurones.

To determine whether the physiological release of glutamate can lead to the generation of the slow (<1Hz) oscillation, intracellular recordings of TC neurones were made whilst performing electrical stimulation of corticothalamic fibres in thalamic slices containing the LGN.

In a substantial number of neurones (n=9 of 16; 56%), that showed no evidence of rhythmic activity in control conditions (aCSF alone) (resting Vm = -65 ± 1 mV, R_N = 155 ± 16 MΩ, n= 16), following the offset of the stimulation epoch (50-300μA for 0.2ms, at 25-100Hz for 100-600ms), a damped oscillation was generated that consisted of rhythmic LTCP-mediated bursts that recurred with an initial frequency <1Hz (0.91 ± 0.07 Hz). In addition, in the first few cycles of this oscillation, the LTCP-mediated bursts were followed by a prolonged 'up' state that was terminated by a characteristic inflection point (Fig. 3.2B). This unmasking of the slow (<1Hz) oscillation by physiological stimuli was critically dependent on membrane potential, requiring the initial resting value to be in the region -65 to -60 mV. In contrast, stimulation from an initial value > -60 mV typically led to action potential firing (Fig. 3.2A), whilst stimulation from an initial value of between -70 and -65 mV usually led to the generation of a damped δ oscillation (Fig. 3.2C). Stimulation of corticothalamic fibres whilst TC neurones were held at an initial membrane potential negative to -70 mV led simply to a long-lasting EPSP (amplitude = 4.5 ± 0.4 mV; n=6) (Fig. 3.2D).

The amplitude of the slow EPSP was enhanced by the presence of blockers of GABA and ionotropic glutamate receptors (i.e. CNQX, APV, BMI and CGP 56999A) (7.8 ± 1.0 mV; n=10) (P<0.01) (Fig. 3.3A and C_1) (Turner and Salt 1998; von Krosigk et al. 1999). Accordingly, the prevalence of the slow (<1Hz)

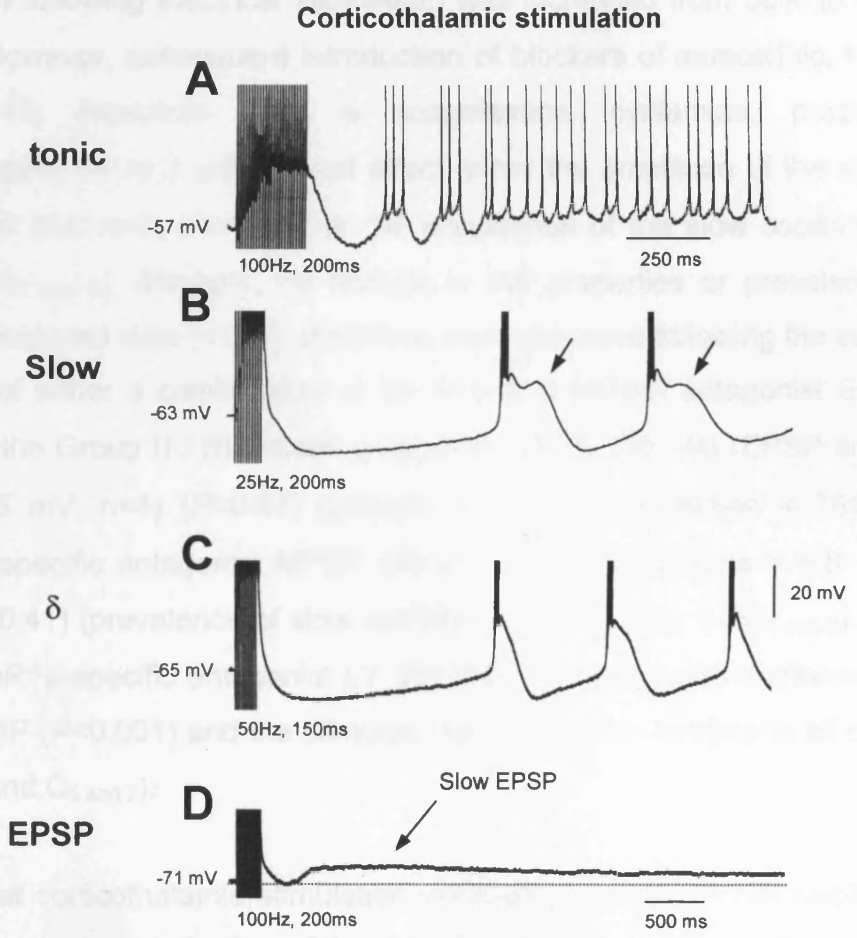

Figure 3.2 Corticothalamic stimulation leads to the generation of a slow (<1Hz) oscillation.

(A) Stimulation of corticothalamic inputs from an initial holding potential of -57 mV gives rise to a period of action potential firing.

(B) Stimulation from a more hyperpolarised membrane potential (-63mV) brings about a slow (<1Hz) oscillation. Note the prolonged depolarised phase following the LTCPs and the ensuing characteristic inflection point (arrows).

(C) Stimulation from a more hyperpolarised membrane potential (-65mV) brings about a δ oscillation only.

(D) Stimulation from an even more hyperpolarised membrane potential (-71mV) brings about a long-lasting slow EPSP (arrow).

In all traces, the stimulation epoch comprised stimuli of 200μA for 0.2ms with the frequency and duration of simulation indicated.

Published in Hughes et al. 2002b

oscillation following electrical stimulation was increased from 56% to 80% (Fig. 3.3C_2). However, subsequent introduction of blockers of muscarinic, H_1, α_1 and 5-HT_1/5-HT_2 receptors (that is scopolamine, pyrilamine, prazosin and methysergide, all at 3 μM) did not affect either the amplitude of the slow EPSP (6.9 ± 0.6 mV; n=4) (*P*=0.51), or the prevalence of the slow oscillation (75%) (Fig. 3.3$C_{1\ and\ 2}$). Similarly, no change in the properties or prevalence of the stimulus-induced slow (<1Hz) oscillation were observed following the subsequent addition of either a combination of the Group II mGluR antagonist EGLU (250 μM) and the Group II / III mGluR antagonist CPPG (50 μM) (EPSP amplitude = 7.6 ± 0.5 mV; n=4) (*P*=0.97) (prevalence of slow oscillation = 75%), or the mGluR5-specific antagonist MPEP (50 μM) (EPSP amplitude = 6.8 ± 0.3 mV; n=4) (*P*=0.41) (prevalence of slow oscillation = 67%) (Fig. 3.3$C_{1\ and\ 2}$). However, the mGluR1a-specific antagonist LY 367385 (250 μM) (n=6) abolished both the slow EPSP (*P*<0.001) and the stimulus-induced slow oscillation in all cases (Fig. 3.3A, B and $C_{1\ and\ 2}$).

Given that corticothalamic stimulation unmasked a slow (<1Hz) oscillation that was dependent on activation of the mGluR1a receptor subtype, the non-specific mGluR receptor agonist *trans*-ACPD was applied to thalamic slices in order to mimic the effects of corticothalamic stimulation and thus to enable investigation of the slow (<1Hz) oscillation. The following sections provide a description of the properties of the slow (<1Hz) oscillation in LGN TC neurones and then a comparison of the properties of the slow (<1Hz) oscillation in the thalamic relay nuclei examined.

3.3.2 Properties of the slow (<1Hz) oscillation in LGN TC neurones.

3.3.2.1 *Trans*-ACPD induces an mGluR1a-dependent slow (<1Hz) oscillation in LGN TC neurones.

Under control conditions (aCSF alone) TC neurones recorded intracellularly from the LGN had relatively hyperpolarised membrane potentials (-66.0 ± 1.1 mV, n=83) in the absence of injected d.c. current (Fig. 3.4A_1). R_N of neurones recorded under control conditions was = 192 ± 15 MΩ (n = 83). LGN TC neurones recorded intracellularly in the presence of *trans*-ACPD (100 μM) and

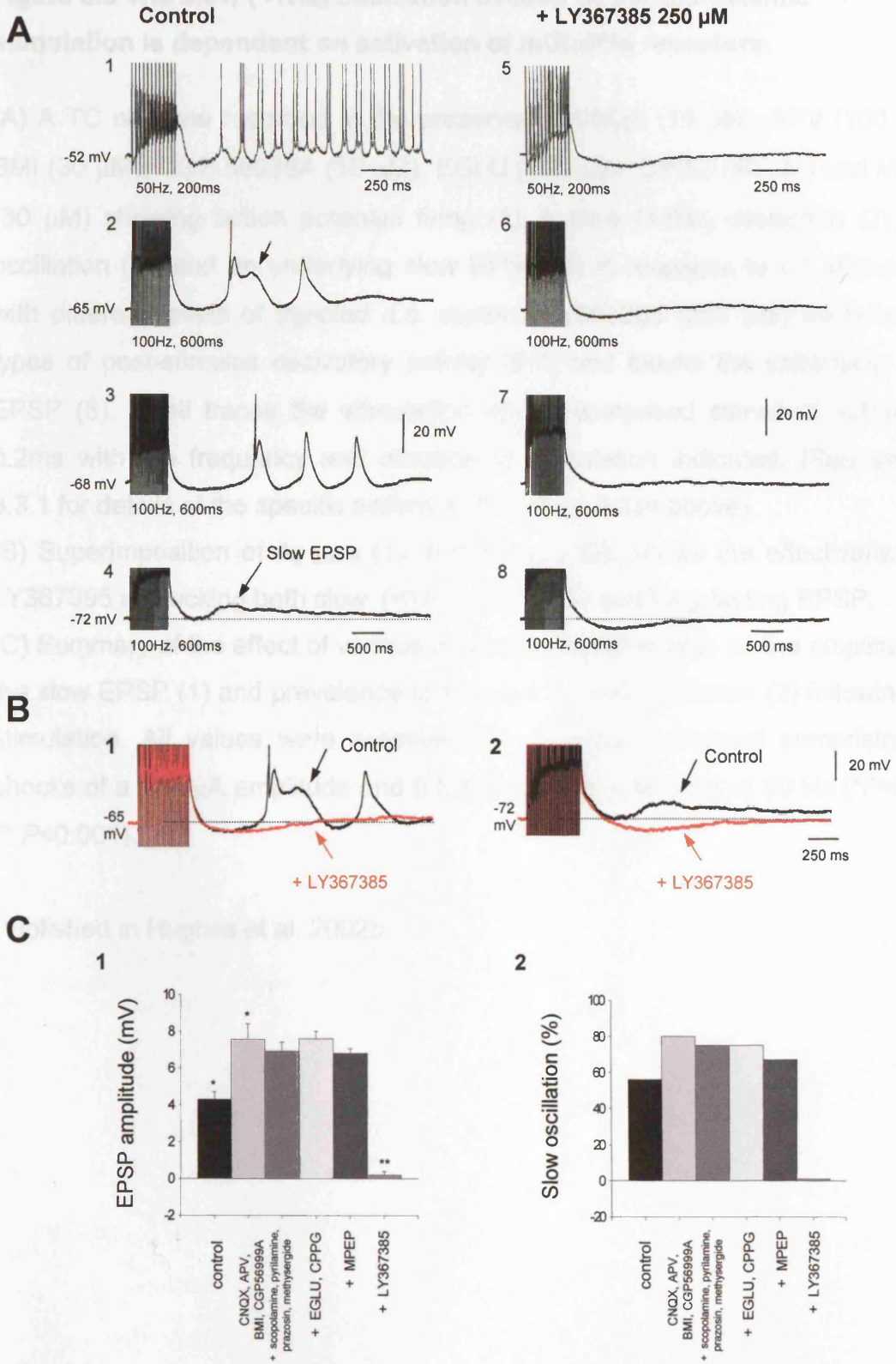

Figure 3.3 The slow (<1Hz) oscillation evoked by corticothalamic stimulation is dependent on activation of mGluR1a receptors.

Figure 3.3 The slow (<1Hz) oscillation evoked by corticothalamic stimulation is dependent on activation of mGluR1a receptors.

(A) A TC neurone recorded in the presence of CNQX (10 μM), APV (100 μM), BMI (30 μM), CGP 56999A (10 μM), EGLU (250 μM), CPPG (50 μM) and MPEP (30 μM) showing action potential firing (1), a slow (<1Hz) oscillation (2), a δ oscillation (3), and an underlying slow EPSP (4) in response to CT stimulation with different levels of injected d.c. current. LY367385 (250 μM) abolishes all types of post-stimulus oscillatory activity (5-7) and blocks the underlying slow EPSP (8). In all traces the stimulation epoch comprised stimuli of 100μA for 0.2ms with the frequency and duration of stimulation indicated. (See section 3.3.1 for details of the specific actions of the drugs listed above).
(B) Superimposition of $A_{2 \text{ and } 6}$ (1), and $A_{4 \text{ and } 8}$ (2), shows the effectiveness of LY367395 in blocking both slow (<1Hz) oscillation and long-lasting EPSP.
(C) Summary of the effect of various pharmacological agents on the amplitude of the slow EPSP (1) and prevalence of the slow (<1Hz) oscillation (2) following CT stimulation. All values were assessed for a stimulus protocol comprising 25 shocks of a 100 μA amplitude and 0.2 ms duration delivered at 50 Hz (*P<0.01; ** P<0.001).

Published in Hughes et al. 2002b

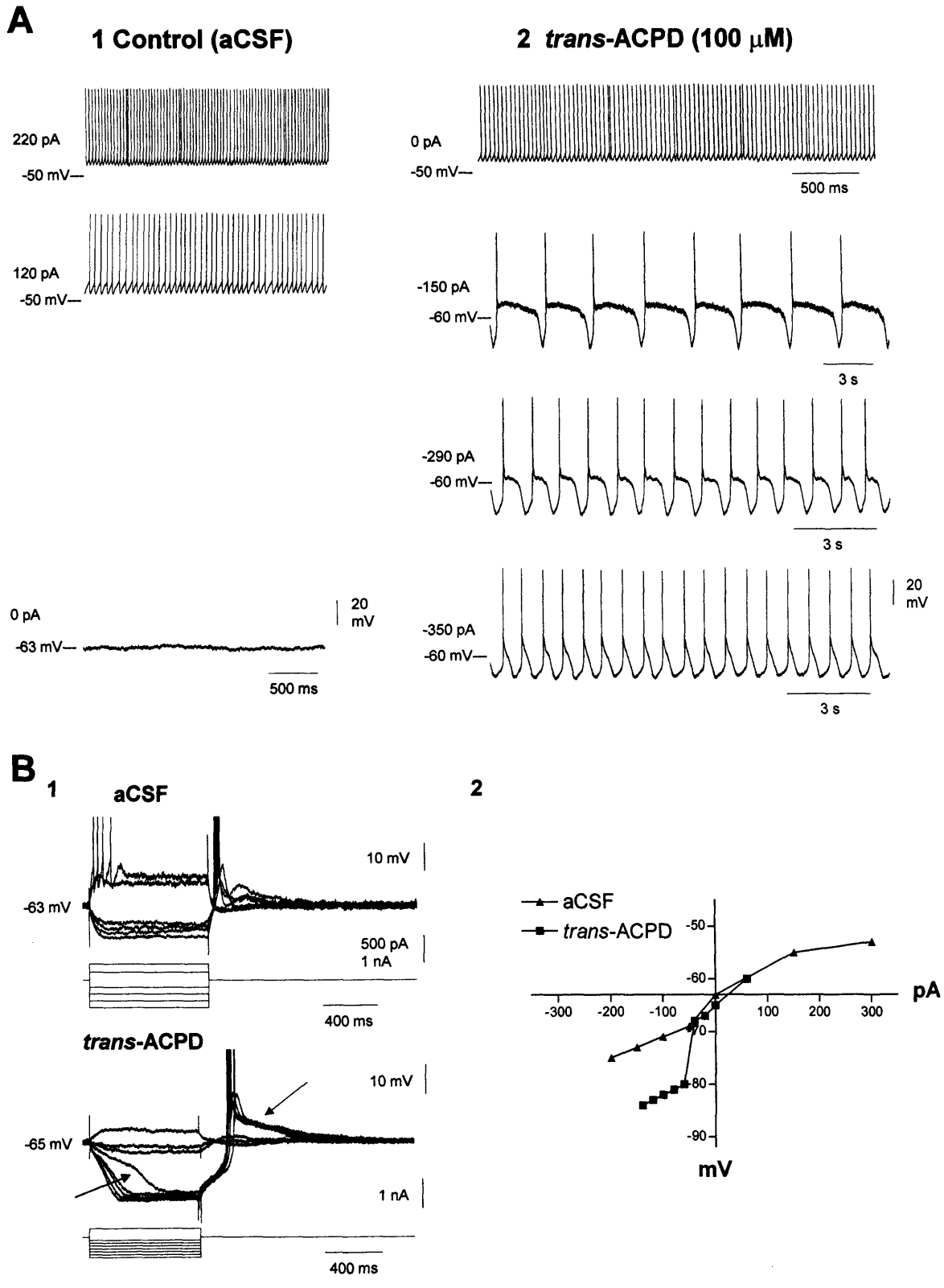

Figure 3.4 *Trans*-ACPD induces a slow (<1Hz) oscillation in LGN TC neurones.

Figure 3.4 *Trans*-ACPD induces a slow (<1Hz) oscillation in LGN TC neurones.

(A) An LGN TC neurone exhibiting no spontaneous activity in the absence of injected d.c. current (0pA) and tonic firing of increasing frequency during application of depolarising d.c. current (120pA, 220pA) (1). Application of *trans*-ACPD (100μM) unmasks a range of oscillatory activity in this neurone. In the presence of *trans*-ACPD and the absence of injected d.c. current (0pA), this neurone displayed sustained tonic action potential firing. With injection of hyperpolarising injected d.c. current a slow (<1Hz) oscillation is revealed (-150pA, -290pA). With further injection of hyperpolarising d.c. current this neurone exhibits a δ oscillation (-350pA) (2).

(B) Voltage responses to negative and positive current steps of the LGN TC neurone shown in (A). Note the linear increase in the amplitude of the voltage response to negative current steps in aCSF. In contrast, in the presence of *trans*-ACDP the voltage responses to the applied negative current steps display non-linear increase in amplitude sometimes with the presence of a clear inflection point (black arrow). In addition, the evoked LTCPs were followed by an ADP (red arrow). Action potentials are truncated (1). These characteristic voltage responses in the presence of aCSF or *trans*-ACPD are also reflected in the steady-state current-voltage plots under these conditions. The plot representing the current-voltage relationship in aCSF is fairly linear (▲). In contrast, the plot representing the current-voltage relationship in *trans*-ACPD (■) has a characteristic S-shape (2).

without application of injected d.c. current displayed tonic action potential firing (11.6 ± 3.4 Hz, n=34), high-threshold (HT) bursting at α or θ frequencies (6.5 ± 1.2 Hz, n= 8) or displayed no spontaneous activity (resting membrane potential: -52.0 ± 0.1 mV, n=13) (see Table 3.1). Application of hyperpolarising d.c. current revealed oscillatory activity in 65% of neurones: at slow (<1Hz) and δ (1-2 Hz) frequencies (n= 34) (Fig. 3.4A_2) or at δ (1-2 Hz) frequencies only (n=2). Oscillatory activity as associated with a high R_N: non-oscillating neurones: R_N = 147.9 ± 14.8 MΩ (n=19), oscillating neurones: R_N = 614.2 ± 92.6 MΩ (n=36) (*P* = 0.001). The ability to generate a slow (<1Hz) oscillation was dependent on the concentration of *trans*-ACPD with a lower concentration (50 μM) leading to a reduced prevalence of the slow (<1Hz) oscillation (n=4 of 20; 20%) accompanied by a smaller depolarisation (ΔV_m = 11 ± 3 mV), whilst a higher concentration (125 μM) led to an increased prevalence of the slow (<1Hz) oscillation (n=8 of 10; 80%) accompanied by a larger depolarisation (ΔV_m = 21 ± 3 mV).

Under control conditions, LGN TC neurones displayed fairly linear voltage responses to applied hyperpolarising or depolarising current pulses (Fig. 3.4B_1). In contrast, neurones displaying a slow (<1Hz) oscillation in the presence of *trans*-ACPD displayed voltage responses mediated by a bistable interaction between $I_{Twindow}$ and $I_{KLeak,}$ including input amplification and the presence o a clear inflection point during hyperpolarising voltage excursions (Fig. 3.4B_1 ➔) (Williams et al. 1997a; Hughes et al. 1999). In addition, a clear afterdepolarising potential (ADP) followed the evoked LTCPs at the offset of hyperpolarising current steps (Fig. 3.4B_1 ➔) (Hughes et al. 1999). These voltage responses under control conditions (aCSF) and in the presence of *trans*-ACPD also gave rise to different steady-state current-voltage relationships (Fig. 3.4B_2) with a more linear relationship observed in aCSF, but a distinctive S-shape in the current-voltage plot in the presence of *trans*-ACPD.

The slow (<1Hz) oscillation was apparent during the transition between a depolarised state, where either tonic action potential or HT bursting at α or θ bursting can occur, and a pure δ oscillation at hyperpolarised membrane potentials (Fig. 3.5A). Transition from a pure δ oscillation to the slow (<1Hz)

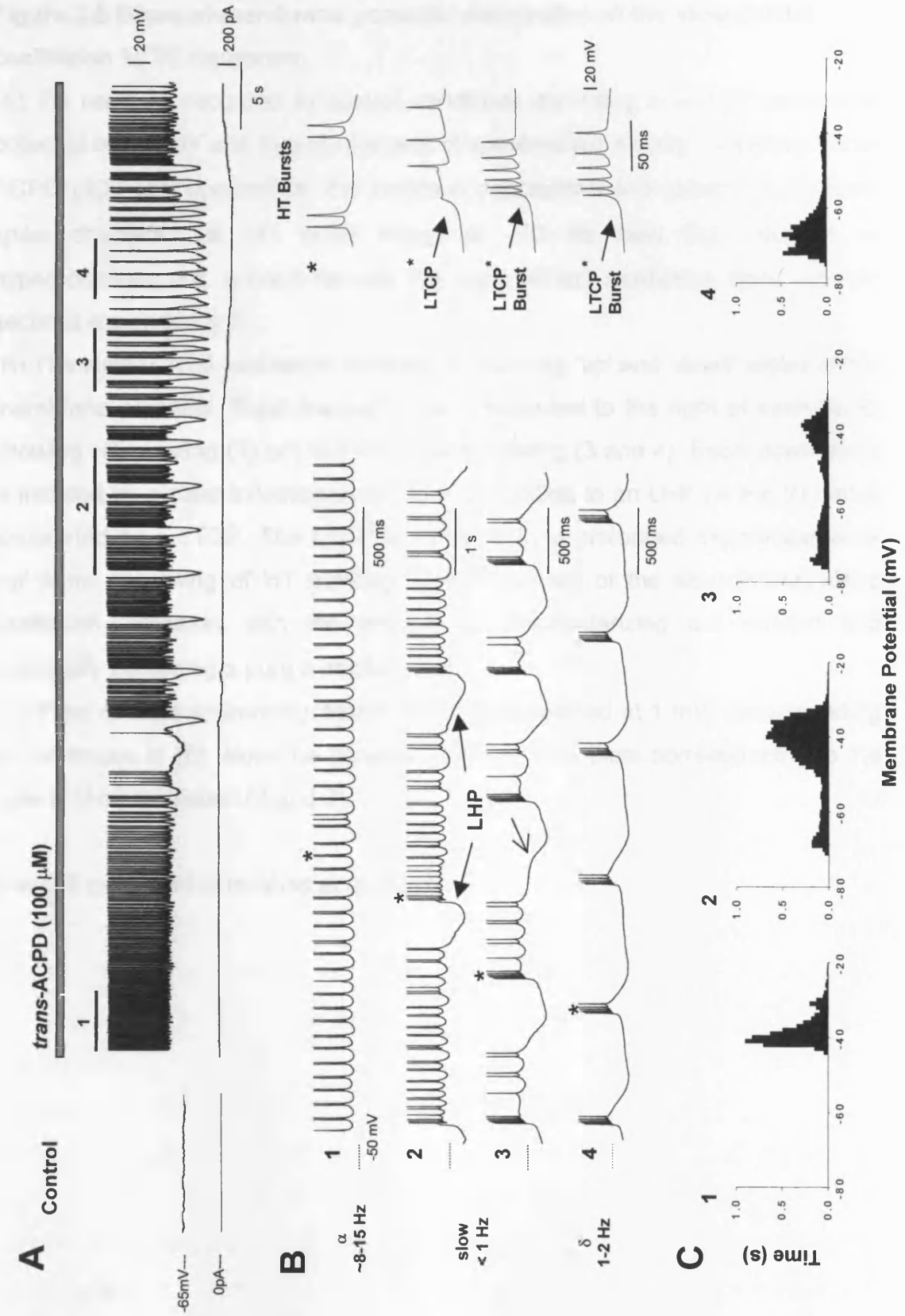

Figure 3.5 Bimodal membrane potential distribution of the slow (<1Hz) oscillation in LGN TC neurones.

Figure 3.5 Bimodal membrane potential distribution of the slow (<1Hz) oscillation in TC neurones.

(A) TC neurone recorded in control conditions exhibiting a resting membrane potential of -65 mV and therefore a lack of spontaneous activity. Following *trans*-ACPD (100 μM) application, the neurone depolarises and generates rhythmic spike doublets (i.e. HT burst firing) at ~10 Hz (see B_1). Injection of hyperpolarizing d.c. current reveals the slow (<1Hz) oscillation. Bars indicate sections expanded in B.

(B) The slow (<1Hz) oscillation consists of recurring 'up' and 'down' states of the membrane potential. Burst marked (*) are expanded to the right of each trace, showing HT bursting (1) or LTCP-mediated bursting (3 and 4). Each 'down' state is initiated by a clear inflection point (↙ in 3) leading to an LHP (◄►in 2) that is terminated by a LTCP. The LTCP is followed by a prolonged depolarisation or 'up' state consisting of HT bursting. The frequency of the slow (<1Hz) sleep oscillation increases with the amount of hyperpolarizing d.c. current and eventually becoming a pure δ oscillation (4).

(C) Plots of the membrane potential distribution (binned at 1 mV) corresponding to the traces in (B). Note the bimodal distribution in plots corresponding to the slow (<1Hz) oscillation (2 and 3).

A and B published in Hughes et al. 2002b

oscillation was achieved by the unmasking of the depolarised "up" phase leading to oscillatory activity at <1Hz as neurones were depolarised (Fig. 3.5B). Consequently, the slow (<1Hz) oscillation was manifested as rhythmic transitions between a depolarised "up" phase and a hyperpolarised "down" phase separated by a maximum range of ~ 15 - 35 mV (maximum change: 26.9 ± 1.0 mV, n=34) at frequencies from 0.01 - 0.8 Hz (minimum frequency = 0.30 ± 0.04 Hz, n= 34). Each "down" phase was encompassed in a stereotypical large hyperpolarising potential (LHP, Fig. $3.5B_2$ ◄►) that was characteristically initiated by a clear inflection point (Fig. $3.5B_3$ ↙). Following the peak of the LHP, the membrane potential exhibited a slow depolarisation, which eventually gave rise to a LTCP. Interestingly, this LTCP did not always support a typical high-frequency burst of action potentials (Fig. $3.5B_2$), which probably reflects an increased inactivation of T-type Ca^{2+} channels due to a mGluR-induced dendritic depolarisation (Zhan et al. 2000). The LTCP was followed by a prolonged depolarisation of variable duration, which comprised the 'up' state of the oscillation (Fig. $3.5B_{2 \text{ and } 3}$). This led to a bimodal distribution of membrane potential with two modes located between ~-70 to -65 mV and ~-55 to -45 mV (Fig. 3.5C).

Given that corticothalamic stimulation leads to the generation of a slow (<1Hz) oscillation that is dependent on activation mGluR1a receptors (section 3.3.1), it was predicted that *trans*-ACPD effectively induced a slow (<1Hz) oscillation via the same receptors. The actions of *trans*-ACPD in bringing about the slow (<1Hz) oscillation were mimicked by the Group I mGluR (i.e. mGluR1a and mGluR5) specific agonist, DHPG (50 μM) (n=6 of 9) (Fig. 3.6A and B_3). Correspondingly, DHPG also led to a depolarisation (ΔV_m = 11 ± 2 mV; n=9) of TC neurones as well as an increase in R_N (463 ± 275%; n=9) (Fig. $3.6B_{1 \text{ and } 2}$). In contrast, neither the mGluR5-specific agonist, CHPG (1 mM) (n=4), the Group II mGluR-specific agonists, APDC (100-200 μM) (n=5) and DCG-IV (10-100 μM), nor the Group III mGluR-specific agonist, L-AP4 (100-200 μM) (n=4), were able to cause either a slow (<1Hz) oscillation, a change in membrane potential or an increase in R_N (P>0.75) (Fig. 3.6B).

These results strongly suggested that *trans*-ACPD brings about a slow (<1Hz) oscillation through the activation of mGluR1a. To further confirm this observation

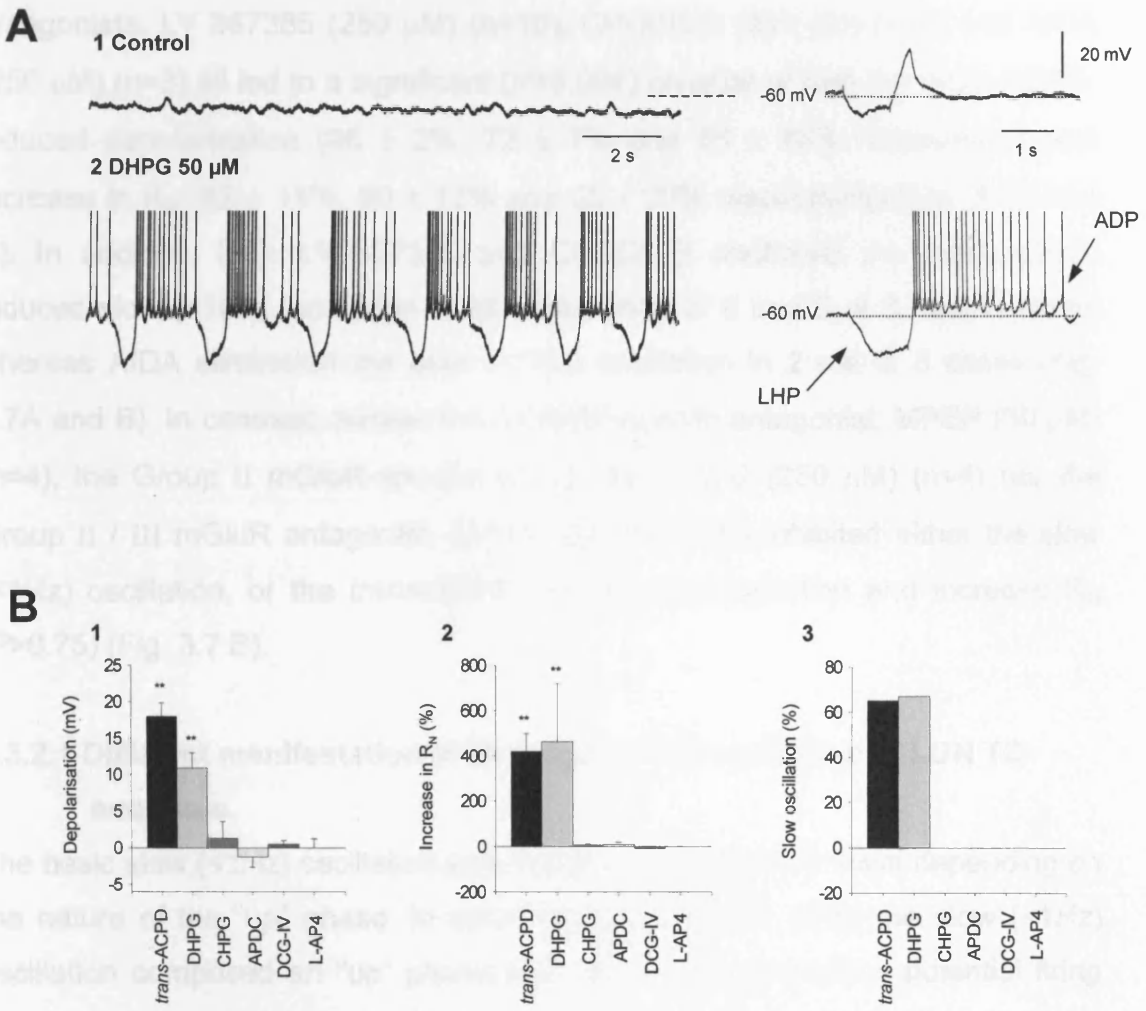

Figure 3.6 The *trans*-ACPD induced slow (<1Hz) oscillation arises due to the activation of mGluR1 receptors.

(A) Application of the group 1 mGluR agonist DHPG (50 µM) to a TC neurone leads to the generation of a slow (<1Hz) oscillation (left trace) and a characteristic LHP-ADP sequence in response to a small hyperpolarising current pulse (40 pA) (right trace).

(B) Summary of the response of LGN TC neurones to the application of various mGluR agonists (** P<0.001).

Published in Hughes et al. 2002b

the effect of a number of mGluR subtype-specific antagonists on the response of TC neurones to 100 μM *trans*-ACPD was examined. The mGluR1a-specific antagonists, LY 367385 (250 μM) (n=10), CPCCOEt (300 μM) (n=4) and AIDA (250 μM) (n=3) all led to a significant (P<0.001) reversal of both the *trans*-ACPD-induced depolarisation (96 ± 2%, 72 ± 7% and 65 ± 12% respectively) and increase in R_N (82 ± 11%, 80 ± 12% and 55 ± 30% respectively) (Fig. 3.7A and B). In addition, both LY 367385 and CPCCOEt abolished the *trans*-ACPD-induced slow (<1Hz) oscillation in all cases (n=8 of 8 and 3 of 3, respectively), whereas AIDA eliminated the slow (<1Hz) oscillation in 2 out of 3 cases (Fig. 3.7A and B). In contrast, neither the mGluR5-specifc antagonist, MPEP (30 μM) (n=4), the Group II mGluR-specific antagonist, EGLU (250 μM) (n=4) nor the Group II / III mGluR antagonist, CPPG (50 μM) (n=3) inhibited either the slow (<1Hz) oscillation, or the *trans*-ACPD-induced depolarisation and increase R_N (P>0.75) (Fig. 3.7 B).

3.3.2.1 Different manifestation of the slow (<1Hz) oscillation in LGN TC neurones.

The basic slow (<1Hz) oscillation was manifested in different ways depending on the nature of the "up" phase. In some neurones (n=23, 68%) the slow (<1Hz) oscillation comprised an "up" phase that did not support action potential firing (quiescent "up" phase, Fig. 3.8A). In other neurones (n=11, 32%) the "up" phase that could support action potential firing (active "up" phase, Fig. 3.8B). Activity supported by the "up" phase could be either tonic firing (maximum frequency = 10.2 ± 1.2 Hz, n=7) (Fig. 3.8B_1), HT bursting (maximum frequency = 6.7 ± 1.1 Hz n=2) (Fig. 3.8B_2) or a combination of both with tonic firing transiently transformed into HT bursting (n=2) (Fig. 3.8B_3).

Sequences of the intrinsically generated δ oscillation (see section 1.5.3) (McCormick and Pape 1990; Leresche et al. 1991; Soltesz et al. 1991) could also be grouped within the <1Hz frequency ("δ grouping" or "grouped δ", Fig. 3.9) and replaced the LHP encompassing the "down" phase. "δ grouping" was observed in 28% (n= 8) of neurones (maximum number of grouped events: 5.5 ± 1.14 (n=48), frequency = 1.7 ± 0.2 Hz, n= 120), appearing in neurones with both

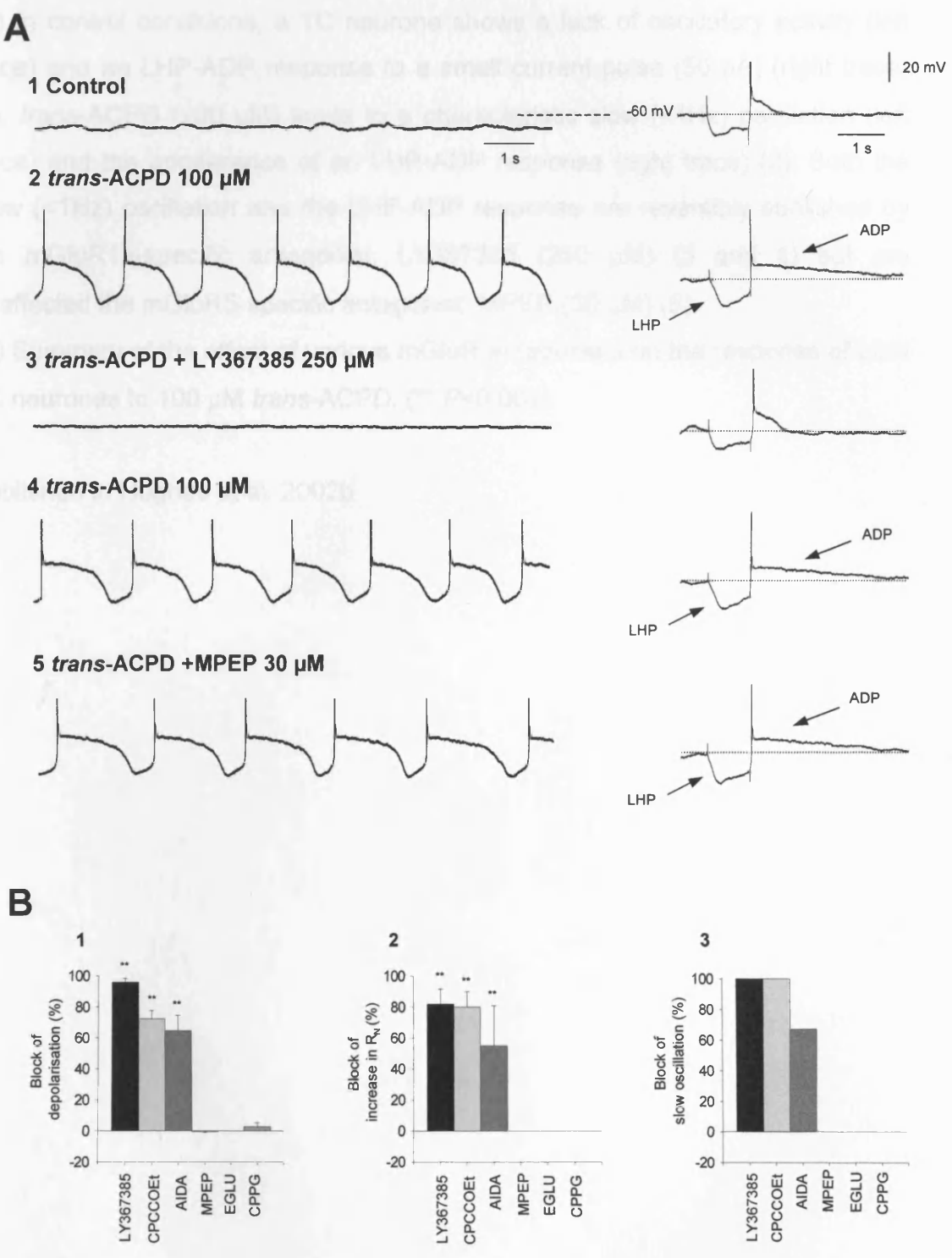

Figure 3.7 The *trans*-ACPD induced slow (<1Hz) oscillation is abolished by mGluR1a receptor antagonists.

Figure 3.7 The *trans*-ACPD induced slow (<1Hz) oscillation is abolished by mGluR1a receptor antagonists.

(A) In control conditions, a TC neurone shows a lack of oscillatory activity (left trace) and no LHP-ADP response to a small current pulse (50 pA) (right trace) (1). *trans*-ACPD (100 μM) leads to a characteristic slow (<1Hz) oscillation (left trace) and the appearance of an LHP-ADP response (right trace) (2). Both the slow (<1Hz) oscillation and the LHP-ADP response are reversibly abolished by the mGluR1a-specific antagonist, LY367385 (250 μM) (3 and 4) but are unaffected the mGluR5-specific antagonist, MPEP (30 μM) (5).

(B) Summary of the effect of various mGluR antagonists on the response of LGN TC neurones to 100 μM *trans*-ACPD. (** $P<0.001$).

Published in Hughes et al. 2002b

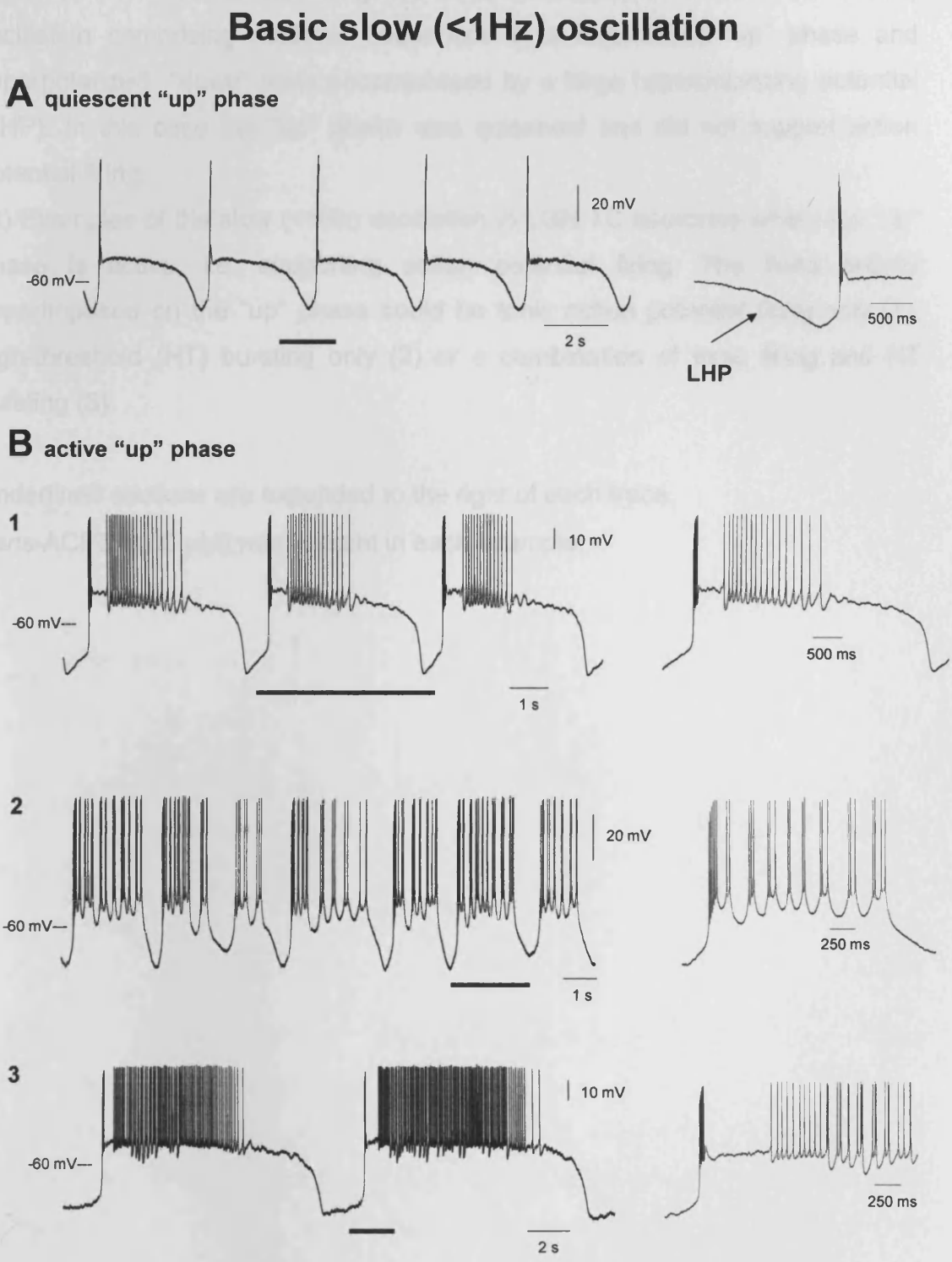

Figure 3.8 Manifestation of the slow (<1Hz) oscillation in LGN TC neurones.

Figure 3.8 Manifestation of the slow (<1Hz) oscillation in LGN TC neurones.
(A) LGN TC neurone exhibiting the basic manifestation of the slow (<1Hz) oscillation comprising rhythmic sequences of a depolarised "up" phase and hyperpolarized "down" state encompassed by a large hyperpolarizing potential (LHP). In this case the "up" phase was quiescent and did not support action potential firing.
(B) Examples of the slow (<1Hz) oscillation in LGN TC neurones where the "up" phase is active, i.e. supporting action potential firing. The firing activity superimposed on the "up" phase could be tonic action potential firing only (1), high-threshold (HT) bursting only (2) or a combination of tonic firing and HT bursting (3).

Underlined sections are expanded to the right of each trace.
trans-ACPD (100 μM) was present in each example.

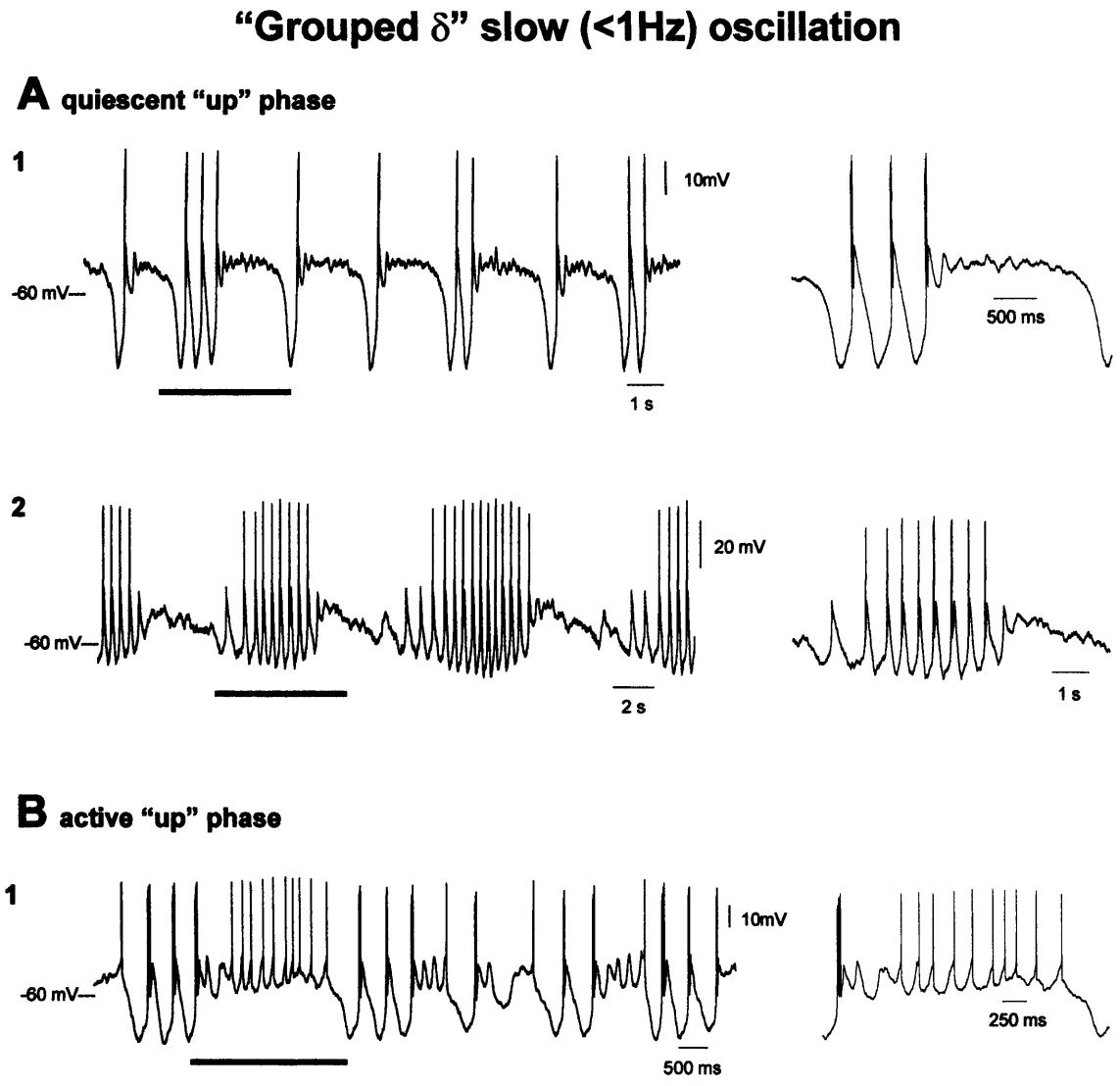

Figure 3.9 Manifestation of "grouped δ" subtypes of the slow (<1Hz) oscillation in LGN TC neurones.

(A) Examples of the slow (<1Hz) oscillation with a quiescent "up" phase in LGN TC neurones where sequences of δ oscillation were grouped within the <1Hz frequency. The grouped sequences of the δ-oscillation replaced the LHP encompassing the "down" phase.

(B) Grouping of sequences of δ oscillation within the slow (<1Hz) oscillation in an LGN TC neurone with an "up" phase supporting action potential firing.

Underlined sections are expanded to the right of each trace.

T*trans*-ACPD (100 μM) was present in each example.

a quiescent "up" phase (n=4) (Fig. 3.9A) and an active "up" phase (n=4) (Fig. 3.9B). In all recorded neurones, neuronal depolarisation decreased the frequency of the slow (<1Hz) oscillation (Fig. 3.10A). In neurones displaying the basic slow (<1Hz) oscillation, the decrease in frequency of the oscillation resulted from a lengthening of the "up" phase (from 1.4 ± 0.2 to 11.3 ± 2.4 seconds, n=26 neurones, P < 0.0001, see Table 3.3) whilst the LHP encompassing the "down" phase show a smaller change (from 1.0 ± 0.2 to 1.4 ± 0.2 seconds, n=26 neurones, P = 0.05, see Table 3.3) as the hyperpolarising injected d.c. current was removed (Fig. 3.10B). In neurones where sequences of δ oscillation were grouped within the slow (<1Hz) oscillation, the duration of the "down" phase was increased, accommodating the "grouped δ" sequence, and contributed to the decrease in the frequency of the slow (<1Hz) oscillation in combination with a lengthening of the "up" phase (Fig. 3.10C –260pA). However, as grouping was reduced or abolished during neuronal depolarisation (Fig. 3.10C), the further lengthening of the "up" phase outweighed this factor and the frequency of the slow (<1Hz) oscillation was further reduced (Fig. 3.10C –230pA and C_2).

In neurones displaying a slow (<1Hz) oscillation with a quiescent "up" phase, in addition to lengthening of the duration of the "up" phase, the maximum membrane potential reached during the "up" phase was also increased with neuronal depolarisation (Fig. 3.11A) (maximum "up" phase: -53.3 ± 0.7 mV, n=23). This effect also presumably underlies the effect of neuronal depolarisation seen in neurones displaying a slow (<1Hz) oscillation with an active "up" phase. In these latter cases, further depolarisation changed the nature of the firing activity with an increase in both the duration and frequency of the firing activity (Fig. 3.11B). Notably, the frequency of activity during the "up" phase could reach values that were observed when neurones were depolarised beyond the range where the slow (<1Hz) oscillation occurred (Fig. 3.11B_2). Additionally the mean rate of action potential firing during the "up" phase of the slow (<1Hz) oscillation was comparable to that observed in neurones displaying spontaneous action potential firing in the absence of injected d.c. current: Tonic firing = 11.6 ± 3.4Hz (n= 34) and 10.2 ± 1.2 Hz (n=7), respectively, P = 0.61. HT bursting = 6.5 ± 1.2 Hz (n=8) and 6.7 ± 1.1 Hz (n=2), respectively, P = 0.91. statistical analysis was performed using a Mann-Whitney test.

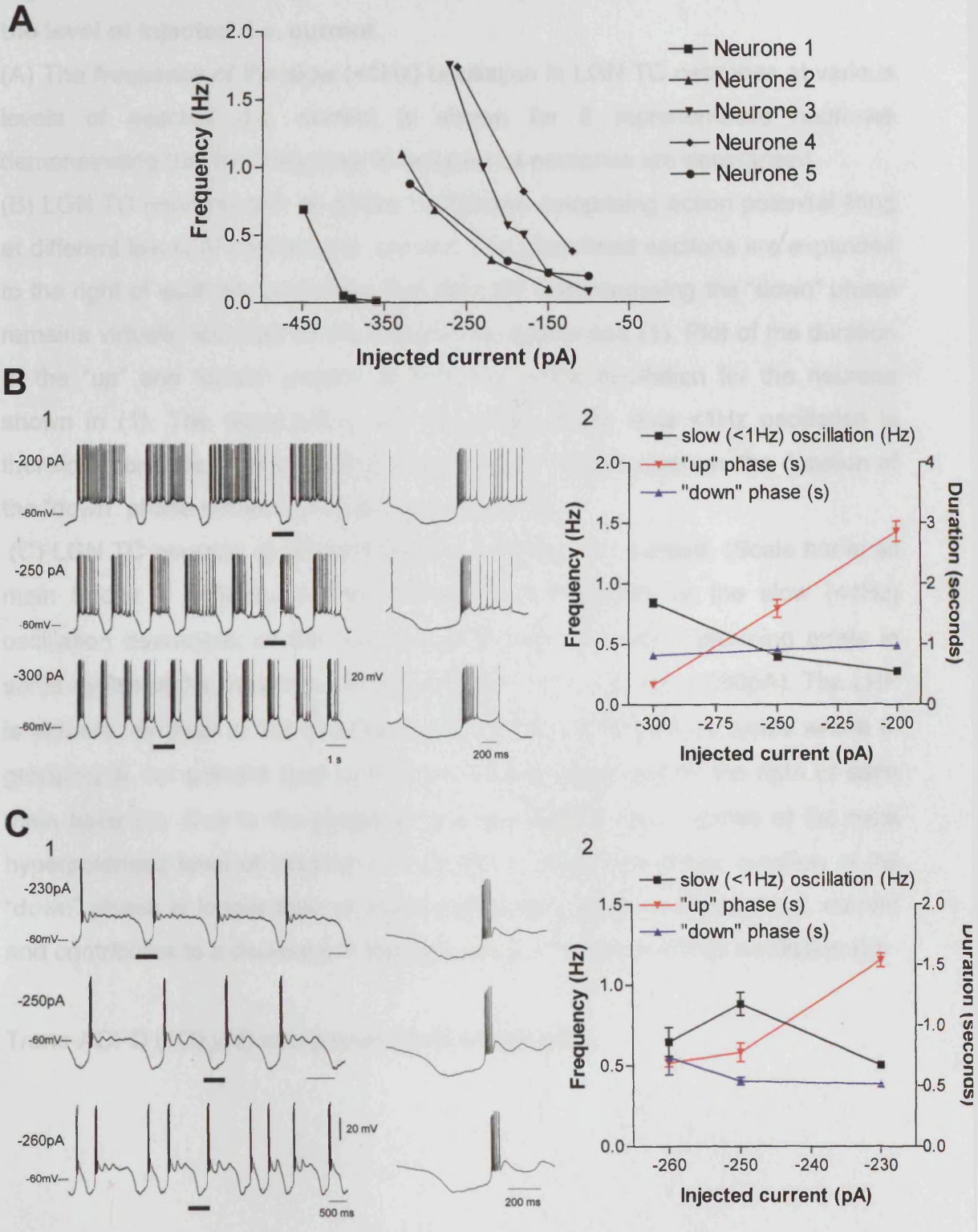

Figure 3.10 The frequency of the slow (<1Hz) oscillation is dependent on the level of injected d.c. current.

Figure 3.10 The frequency of the slow (<1Hz) oscillation is dependent on the level of injected d.c. current.

(A) The frequency of the slow (<1Hz) oscillation in LGN TC neurones at various levels of injected d.c. current is shown for 5 representative neurones demonstrating that the frequency is reduced as neurones are depolarised.

(B) LGN TC neurone with an active "up" phase comprising action potential firing at different levels of injected d.c. current. The underlined sections are expanded to the right of each trace showing that the LHP encompassing the "down" phase remains virtually identical as the neurone is depolarised (1). Plot of the duration of the "up" and "down" phases of the slow <1Hz oscillation for the neurone shown in (1). The decrease in the frequency of the slow <1Hz oscillation is therefore dependent on a lengthening of the "up" phase whereas the duration of the "down" phase remains virtually unchanged (2).

(C) LGN TC neurone at different levels of injected d.c. current. (Scale bar in all main traces = 500ms). In this neurone, the frequency of the slow (<1Hz) oscillation decreases as the neurone is depolarised and δ grouping exists in some cycles at the most hyperpolarised level of d.c. current (-260pA). The LHP is virtually identical at the different levels of injected current in cycles where δ-grouping is not present (see underlined section expanded to the right of each main trace (1). Due to the presence of δ grouping in some cycles at the most hyperpolarised level of injected d.c. current (-260pA) the mean duration of the "down" phase is longer than at more depolarised levels of injected d.c. current and contributes to a decrease in the frequency of the slow (<1Hz) oscillation (2).

T*rans*-ACPD (100 μM) was present in all examples.

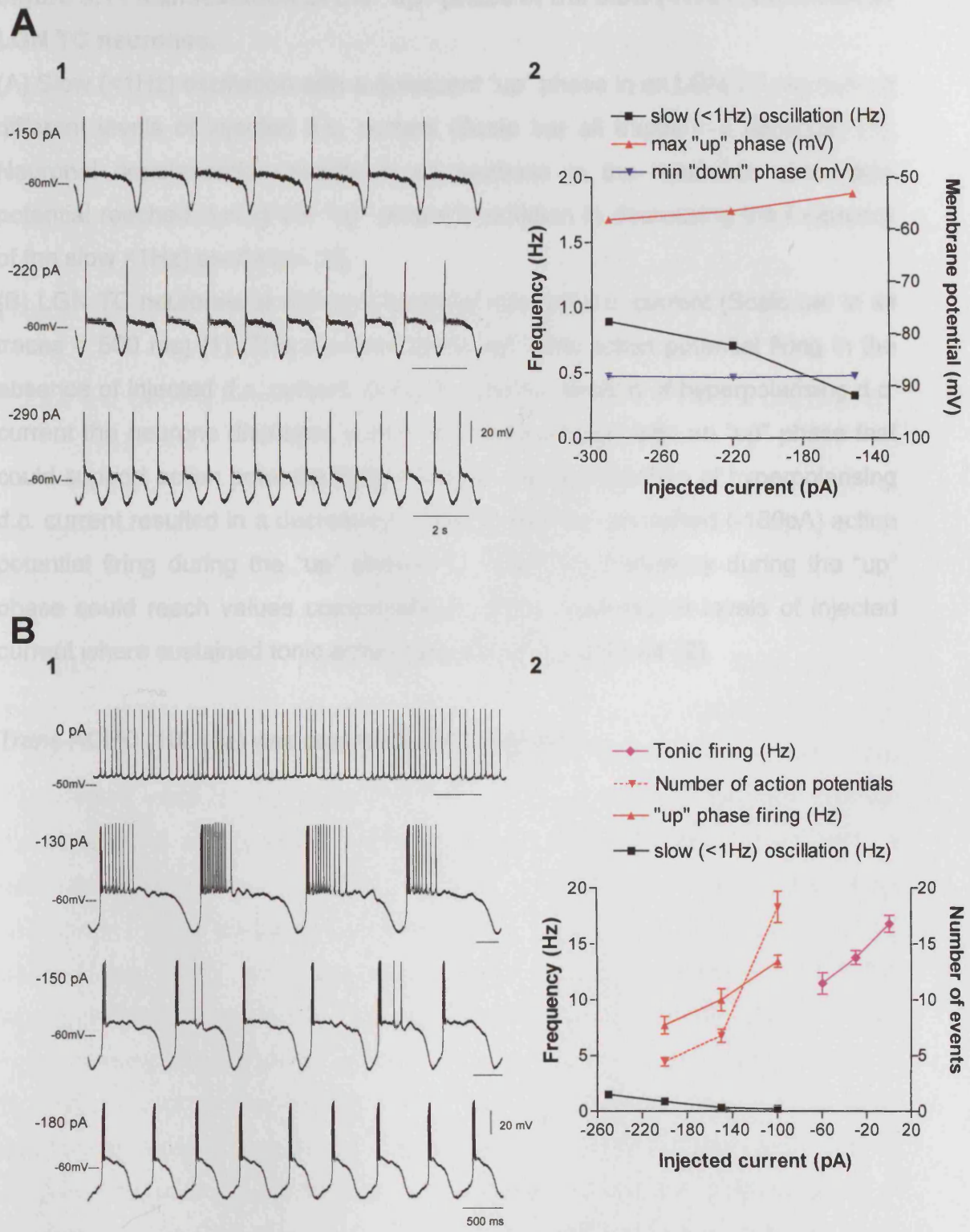

Figure 3.11 Properties of the "up" phase of the slow (<1Hz) oscillation in LGN TC neurones.

Figure 3.11 Manifestation of the "up" phase of the slow (<1Hz) oscillation in LGN TC neurones.

(A) Slow (<1Hz) oscillation with a quiescent "up" phase in an LGN TC neurone at different levels of injected d.c. current (Scale bar all traces = 2 seconds) (1). Neuronal depolarisation results in an increase in the maximum membrane potential reached during the "up" phase in addition to decreasing the frequency of the slow <1Hz) oscillation (2).

(B) LGN TC neurones at different levels of injected d.c. current (Scale bar in all traces = 500 ms) (1). This neurone displayed tonic action potential firing in the absence of injected d.c. current (0pA). Following injection of hyperpolarising d.c. current the neurone displayed a slow (<1Hz) oscillation with an "up" phase that could support action potential firing (-130pA). Further injection of hyperpolarising d.c. current resulted in a decrease (-150pA), and then abolished (-180pA) action potential firing during the "up" phase (1). The firing frequency during the "up" phase could reach values comparable to those observed at levels of injected current where sustained tonic action potential firing occurred (2).

Trans-ACPD (100 μM) was present in each example.

The manifestation of grouping of sequences of δ oscillation within the slow (<1Hz) oscillation was also dependent on neuronal depolarisation (Fig. 3.12) and occurred during the transition from a pure δ oscillation to a pure slow (<1Hz) oscillation (see Fig. 3.5, Fig. 3.12A). With neuronal depolarisation, as the frequency of the slow (<1Hz) oscillation decreased, the percentage of oscillation cycles where grouping occurred were reduced (Fig. 3.12B) along with the number of grouped δ events per oscillation cycle, although the frequency of grouped δ events remained consistent (Fig. 3.12C).

3.3.2.3 Extracellular manifestation of the slow (<1Hz) oscillation in LGN TC neurones.

To ascertain whether TC neurones normally exhibit slow (<1Hz) oscillations in the absence of manipulation of their membrane potential, extracellular single unit recordings were performed. In control conditions (aCSF alone) these recordings exhibited a lack of spontaneous activity (n=109) (Fig. 3.13A). However, application of *trans*-ACPD (125μM) led to either continuous tonic firing (n=72) or rhythmic bursts of action potentials in the α or θ frequency bands (n=27) (Fig. 3.13B_1). Both of these activity patterns reflect a state where neurones are depolarised beyond the region where the slow (<1Hz) oscillation can be observed and are consistent with the effects of *trans*-ACPD observed in intracellular recordings (see Fig. 3.4A_2 and 3.5A). Since with extracellular recordings it is not possible to apply hyperpolarising d.c. current in order to bring about a slow (<1Hz) oscillation (see Fig. 3.5A), the concentration of *trans*-ACPD was gradually decreased to achieve a similar effect (n=15). This involves compromising the enhanced effect of higher concentrations of *trans*-ACPD in facilitating the generation of the slow (<1Hz) oscillation with attempting to attain the correct level of membrane polarisation necessary for the slow (<1Hz) oscillation to occur. Using this approach, it was noted that during the reduction of the *trans*-ACPD concentration, TC neurones could continue to generate tonic firing (n=4) or α/θ bursting (n=4) patterns of activity, but in isolated episodes that, 1) recurred rhythmically at low frequencies (i.e. <1 Hz) (Fig. 3.13B_{2-4}), 2) were often initiated by a clearly identifiable LTCP-mediated burst (Fig. 3.13B_4) (Domich et al. 1986), and 3) whose occurrence increased in frequency as the concentration of *trans*-ACPD was reduced, culminating in the rhythmic generation of isolated LTCP-mediated bursts at δ (1-2 Hz) frequencies (i.e. a

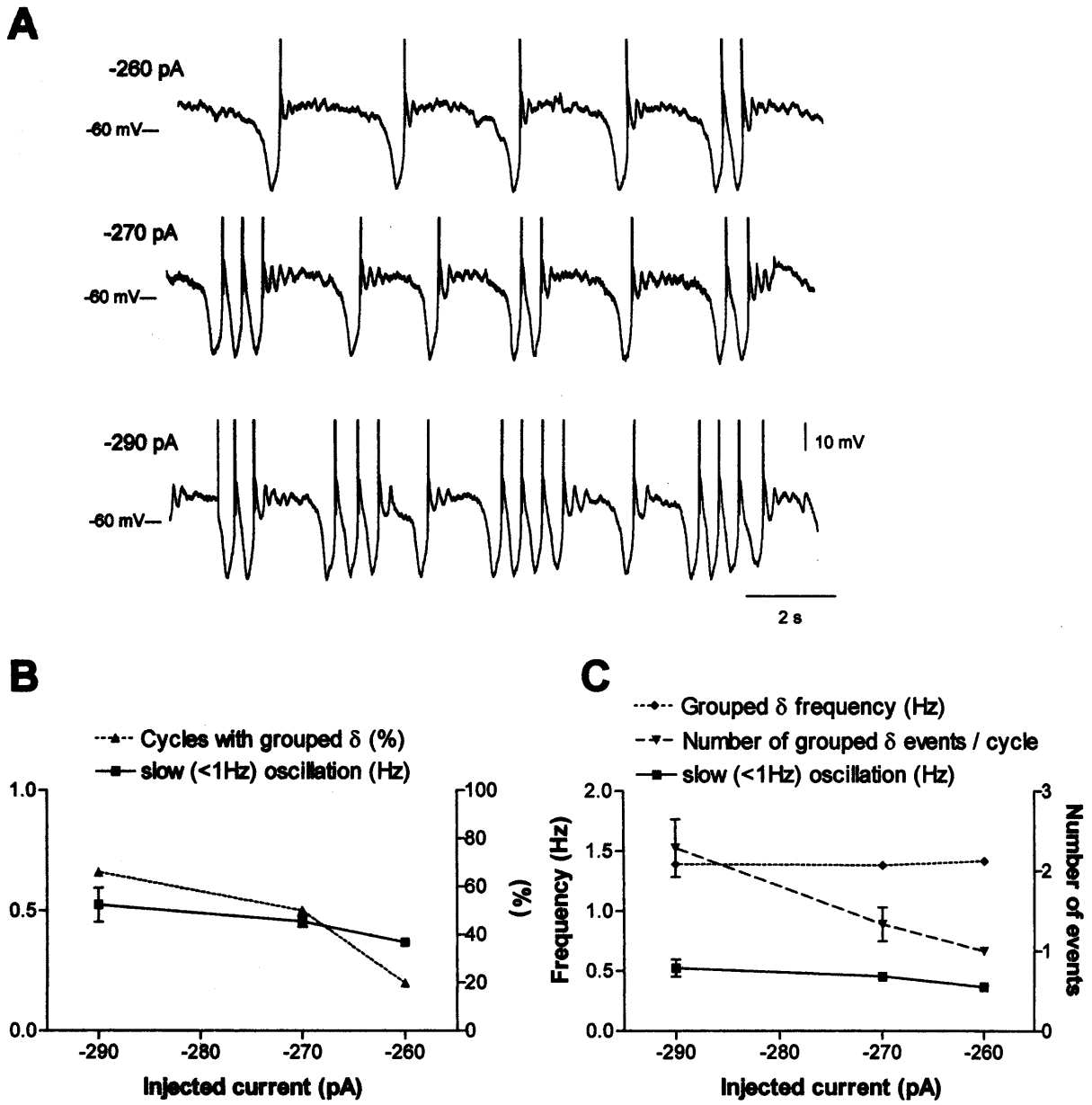

Figure 3.12 Properties of "δ grouping" during the "down" phase of the slow (<1Hz) oscillation.

Figure 3.12 Properties of "δ grouping" during the "down" phase of the slow (<1Hz) oscillation.

(A) LGN TC neurones at different levels of injected d.c. current showing the effect of neuronal depolarisation on the nature of δ grouping.

(B) Removal of hyperpolarising d.c. current results in a decrease in the number of cycles where δ grouping exists.

(C) In addition, removal of hyperpolarising d.c. current results in a decrease in the number of grouped δ events, although the frequency of the grouped δ oscillation increased slightly.

Data in plots (B and C) is derived from 10 consecutive cycles at each of the levels of injected d.c. current shown in (A).

Action potentials are truncated in this example.

Trans-ACPD (100 μM) was present.

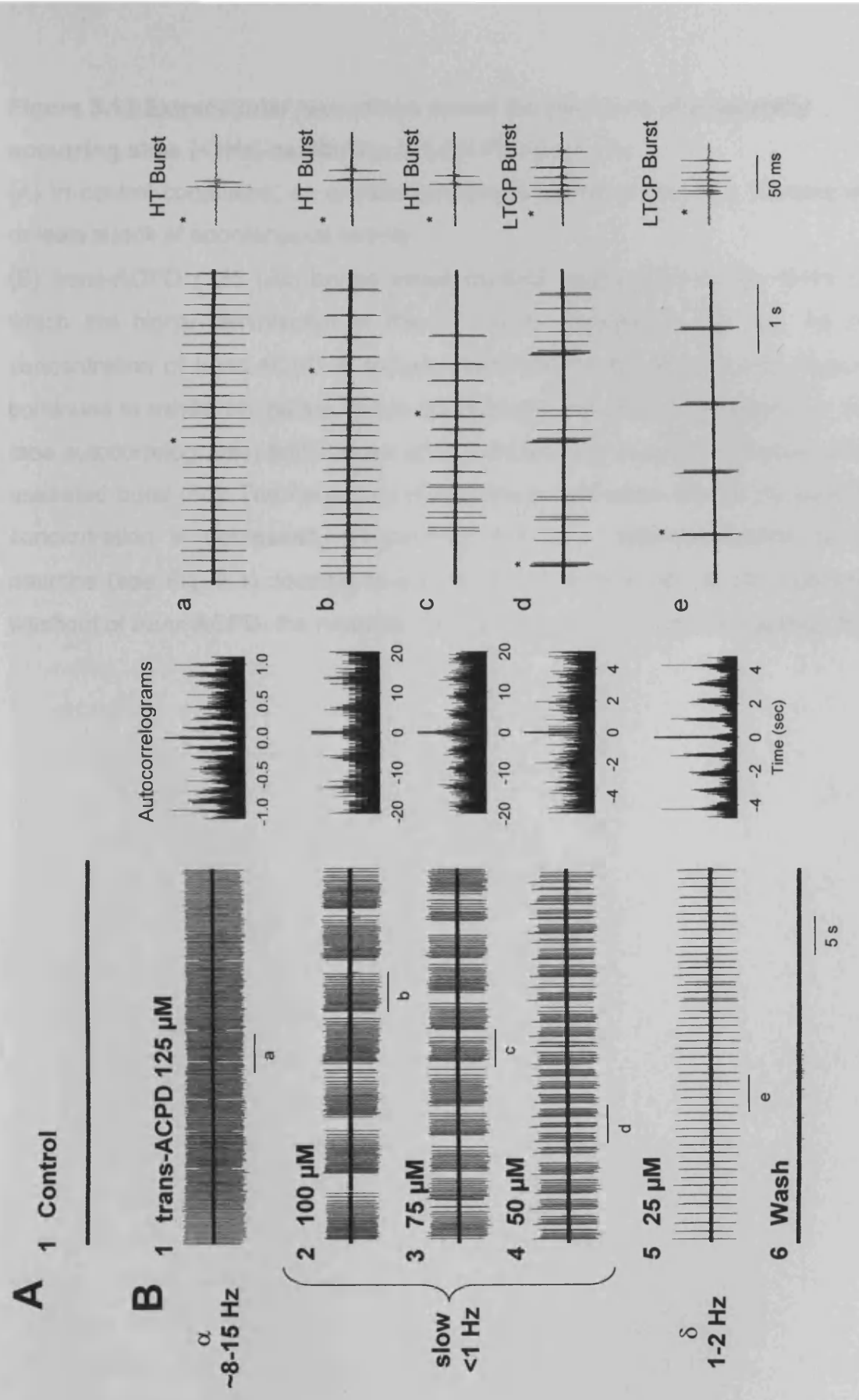

Figure 3.13 Extracellular recordings reveal the presence of naturally occurring slow (<1Hz) oscillation in LGN TC neurones.

Figure 3.13 Extracellular recordings reveal the presence of a naturally occurring slow (<1Hz) oscillation in LGN TC neurones.

(A) In control conditions, an extracellular single unit recording of a TC neurone reveals a lack of spontaneous activity.

(B) *trans*-ACPD (125 μM) brings about rhythmic spike doublets at ~8 Hz (1) which are highly reminiscent of the HT bursts depicted in Fig. 3.4. As the concentration of *trans*-ACPD is reduced from 125 to 50 μM (1-4), the neurone continues to exhibit HT bursts, but in discrete episodes that recur slowly (<1 Hz) (see autocorrelograms) and that are often initiated by a clearly identifiable LTCP-mediated burst (4d). The frequency of recurrence increases as the *trans*-ACPD concentration is decreased, presumably due to a hyperpolarisation of the neurone (see Fig. 3.4), leading to a pure δ oscillation at 25 μM (5). Following washout of *trans*-ACPD, the neurone returns to a state of electrical inactivity (6).

δ oscillation) (Fig. 3.13B_5), just prior to returning to the control scenario of no spontaneous activity (Fig. 3.13B_6). In some cases, the low-frequency (<1Hz) activity brought about by a controlled reduction in *trans*-ACPD concentration consisted simply of rhythmic LTCP-mediated bursts (but at a frequency too low to be considered a δ oscillation) with a lack of subsequent tonic firing or α/θ bursting activity (n=6).

In the presence of *trans*-ACPD the same manifestations of the slow (<1Hz) oscillation were observed during extracellular recordings of LGN TC neurones as occurred during intracellular recordings. <1Hz rhythmic activity occurred at frequencies from 0.59 – 0.01 Hz (minimum = 0.28 ± 0.03 Hz, n=28). In 46% (n=13) of neurones, oscillatory activity was manifested as characteristic LTCP-mediated action potential bursts only and presumably represented a slow (<1Hz) oscillation where the "up" phase of the oscillation was quiescent (Fig. 3.14A). In the remaining cases (n=15), rhythmic LTCP-mediated bursts were followed by transient action potential firing manifested as either tonic firing (Fig. 3.14B_1) (12.2 ± 2.3 Hz, n=10), HT bursting (Fig. 3.14B_2) (5.9 ± 0.08 Hz, n=3) or a combination of tonic firing and HT bursting (n= 2) (Fig. 3.14B_3) and presumably represented a slow (<1Hz) oscillation where the "up" phase was active. Grouping of sequences of δ oscillation (number of grouped events: 3.2 ± 0.4, n= 72, frequency of grouped events: 1.2 ± 0.1 Hz, n=72) occurred in 29% (n=8) of neurones. In some cases (n=5) only sequences of δ grouping were apparent and thus it was not possible to ascertain whether or not this was a true slow (<1Hz) oscillation displaying "δ grouping" with a quiescent "up" phase as seen during intracellular recordings (see Fig. 3.9A) or simply recurring sequences of the δ oscillation at <1Hz as previously observed during intracellular recordings of TC neurones (Leresche et al, 1991). In other cases (n=3), "δ grouping" was followed by transient action potential firing and thus was presumed to be a slow (<1Hz) oscillation displaying both "δ grouping" and an active "up" phase (Fig. 3.14C). Thus, extracellular recordings show that TC neurones in the LGN can naturally generate slow (<1Hz) oscillatory activity with indistinguishable properties to those observed during intracellular recordings.

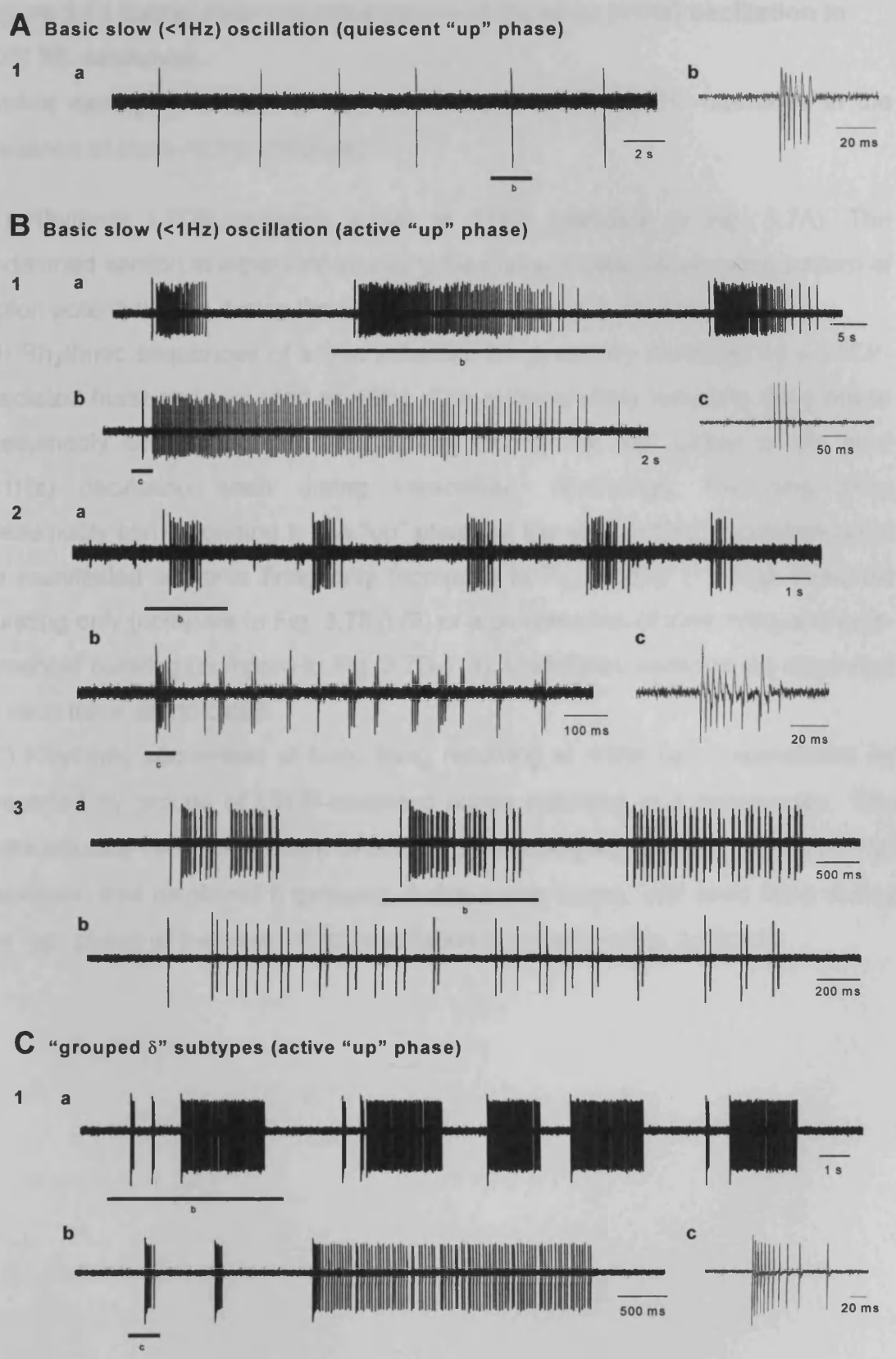

Figure 3.14 Extracellular manifestations of the slow (<1Hz) oscillation in LGN TC neurones.

Figure 3.14 Extracellular manifestations of the slow (<1Hz) oscillation in LGN TC neurones.

Typical examples of the slow (<1Hz) oscillation in LGN TC neurones in the presence of *trans*-ACPD (100 μM).

(A) Rhythmic LTCP-mediated bursts at <1Hz (compare to Fig. 3.7A). The underlined section is expanded showing the characteristic decelerating pattern of action potential firing during the LTCP-mediated burst in TC neurones (1).

(B) Rhythmic sequences of action potential firing, usually preceded by a LTCP-mediated burst and recurring at <1Hz. The extracellularly recurring firing phase presumably corresponds to firing activity during the "up" phase of the slow (<1Hz) oscillation seen during intracellular recordings. Recurring firing presumably corresponding to the "up" phase of the slow (<1Hz) oscillation could be manifested as tonic firing only (compare to Fig. 3.7B_1) (1), high-threshold bursting only (compare to Fig. 3.7B_2) (2) or a combination of tonic firing and high-threshold bursting (compare to Fig. 3.7B_3) (3). Underlined sections are expanded in each trace as indicated.

(C) Rhythmic sequences of tonic firing recurring at <1Hz could sometimes be preceded by groups of LTCP-mediated bursts recurring at δ frequencies. This extracellularly recorded pattern of activity presumably represented a slow (<1Hz) oscillation that displayed δ grouping during some cycles, and tonic firing during the "up" phase of the slow (<1Hz) oscillation (compare to Fig. 3.8B) (1).

3.3.3 Nucleus-specific comparison of the properties of the slow (<1Hz) oscillation in TC neurones.

3.3.3.1 Induction of the slow (<1Hz) oscillation.

As seen in LGN TC neurones, application of *trans*-ACPD (100 μM) to intracellularly recorded TC neurones in the VB, VL and MGN resulted in a similar depolarisation and increase in R_N (see Table 3.1). In addition, consistent with observation in the LGN, application of *trans*-ACPD (100 μM) was also effective in unmasking a slow (<1Hz) oscillation in VB (12 of 26, 46%), VL (8 of 15, 53%) and MGN (14 of 27, 52%) TC neurones. As observed in LGN TC neurones, the slow (<1Hz) oscillation in VB, VL and MGN TC neurones existed between the transition from a hyperpolarised membrane potential, where a pure δ oscillation existed, to a depolarised membrane potential were tonic firing only occurred (see Fig. 3.15 for example in the VB). Again, as observed in LGN TC neurones, higher R_N values were associated with neurones that displayed oscillatory activity (see Table 3.2). In concordance with this observation, those neurones that displayed a slow (<1Hz) oscillation also displayed voltage responses characteristically due to a bistable interaction between I_{KLeak} and $I_{Twindow}$, including input amplification and the presence of a clear inflection point during hyperpolarising voltage excursions (Fig. 3.15B_1 →) (Williams et al. 1997a; Hughes et al. 1999). In addition, a clear ADP was followed the evoked LTCPs at the offset of the hyperpolarising current step (Fig. 3.15B_1 ←) (Hughes et al. 1999). These voltage responses under control conditions (aCSF) and in the presence of *trans*-ACPD also gave rise to different steady-state current-voltage relationships (Fig. 3.15B_2) with a more linear relationship observed in aCSF, but a distinctive S-shape in the current-voltage plot in the presence of *trans*-ACPD (Hughes et al. 1999).

3.3.3.2 Properties of the slow (<1Hz) oscillation.

In contrast to the observations made in LGN TC neurones, during intracellular recordings of VB, VL and MGN TC neurones, the "up" state of the slow (<1Hz) oscillation was always quiescent and appeared as long-lasting plateaus (Fig. 3.15 and Fig. 3.16), but sequences of δ oscillation could sometimes replace the LHP to comprise the down state (Fig. 3.15A_2 –190pA): (VB: 4 of 12, 33%, maximum number of grouped events: 7.2 ± 1.0, n=12, frequency = 1.58 ± 0.14

	Vm (mV)	δ (Hz)	Slow (Hz)	Action potential firing (Hz)	HT bursting (Hz)	R_N (MΩ)
Control (aCSF)						
LGN	-66.0 ± 1.1 (n=83)	-	-	-	-	192 ± 15.0 (n=83)
VB	-68.5 ± 1.7 (n=4)	1.38 ± 0.1 (n=6)	-	-	-	195.8 ± 30.3 (n=10)
VL	-68.3 ± 2.3 (n=7)	1.84 ± 0.03 (n=1)	-	-	-	157.5 ± 27.8 (n=8)
MGN	-64.4 ± 0.9 (n=12)	1.6 ± 0.1 (n=5)	-	-	-	216.2 ± 25.2 (n=17)
***Trans*-ACPD**						
LGN	-52.0 ± 0.1 (n=13) $P = 0.003$	-	-	11.6 ± 3.4 (n=34)	6.5 ± 1.2 (n=8)	1010 ± 100.0 (n=55) $P = 0.002$
VB	-56.5 ± 1.5 (n=21) $P = 0.007$	-	0.19 ± 0.1 (n=5)	-	-	474.6 ± 159.5 (n=26) $P = 0.26$
VL	-56.5 ± 1.5 (n=13) $P < 0.001$	1.34 ± 0.02 (n=1)	0.32 ± 0.01 (n=1)	-	-	552.8 ± 205.9 (n=15) $P = 0.24$
MGN	-55.3 ± 0.7 (n=20) $P < 0.001$	-	0.1 ± 0.01 (n=5)	12.5 ± 4.3 (n=2)	-	546.3 ± 119.8 (n=27) $P = 0.039$

Table 3.1 Effect of *trans*-ACPD application on TC neurones.

Comparison of the activity of TC neurones in different thalamic relay nuclei under control conditions and in the presence of *trans*-ACPD.

All data were collected under the indicated experimental conditions in the absence of injected d.c. current.

The *P*-values given were calculated by analysing the data obtained for each parameter, as specified, under control conditions and in the presence of *trans*-ACPD.

	Oscillation			No oscillation	
	Slow (<1Hz)	δ			
	Min Frequency (Hz)	Min Frequency (Hz)	Max IR (MΩ)	Max IR (MΩ)	*P*
LGN	0.3 ± 0.04 (n=34)	1.25 ± 0.2 (n=2)	614.2 ± 92.6 (n=36) *P* = 0.001	147.9 ± 14.8 (n=19) *P* = 0.35	<0.0001
VB	0.12 ± 0.04 (n=12)	1.04 ± 0.04 (n=4)	758.6 ± 255.2 (n=16) *P* = 0.049	143.3 ± 18.9 (n=10) *P* = 0.17	0.049
VL	0.04 ± 0.02 (n=8)	1.49 ± 0.2 (n=5)	766.7 ± 272.5 (n=13) *P* = 0.152	125.2 ± 14.4 (n=2) -	-
MGN	0.06 ± 0.01 (n=14)	1.53 ± 0.1 (n=3)	723.1 ± 151.9 (n=17) *P* = 0.004	163.3 ± 23.3 (n=10) *P* = 0.47	0.025

Table 3.2 Oscillatory activity in TC neurones is associated with higher apparent input resistances in TC neurons.

The following data were obtained from TC neurons in different thalamic relay nuclei recorded in the presence of *trans*-ACPD as shown in Table 3.1. Slow (<1Hz) = indicated those neurons displaying a slow (<1Hz) oscillation (but also could be displaying δ frequency activity). δ =those neurons only displaying a δ oscillation. n = the number of neurones.

P-values included in the "Max IR" column refer to a statistical comparison between the maximum R_N values of TC neurones indicated an those in the presence of aCSF alone as shown in Table 1: control.

The *P*-value in the final column refers to a statistical comparison between the maximum R_N values of oscillating and non-oscillating TC neurones in the presence of *trans*-ACPD.

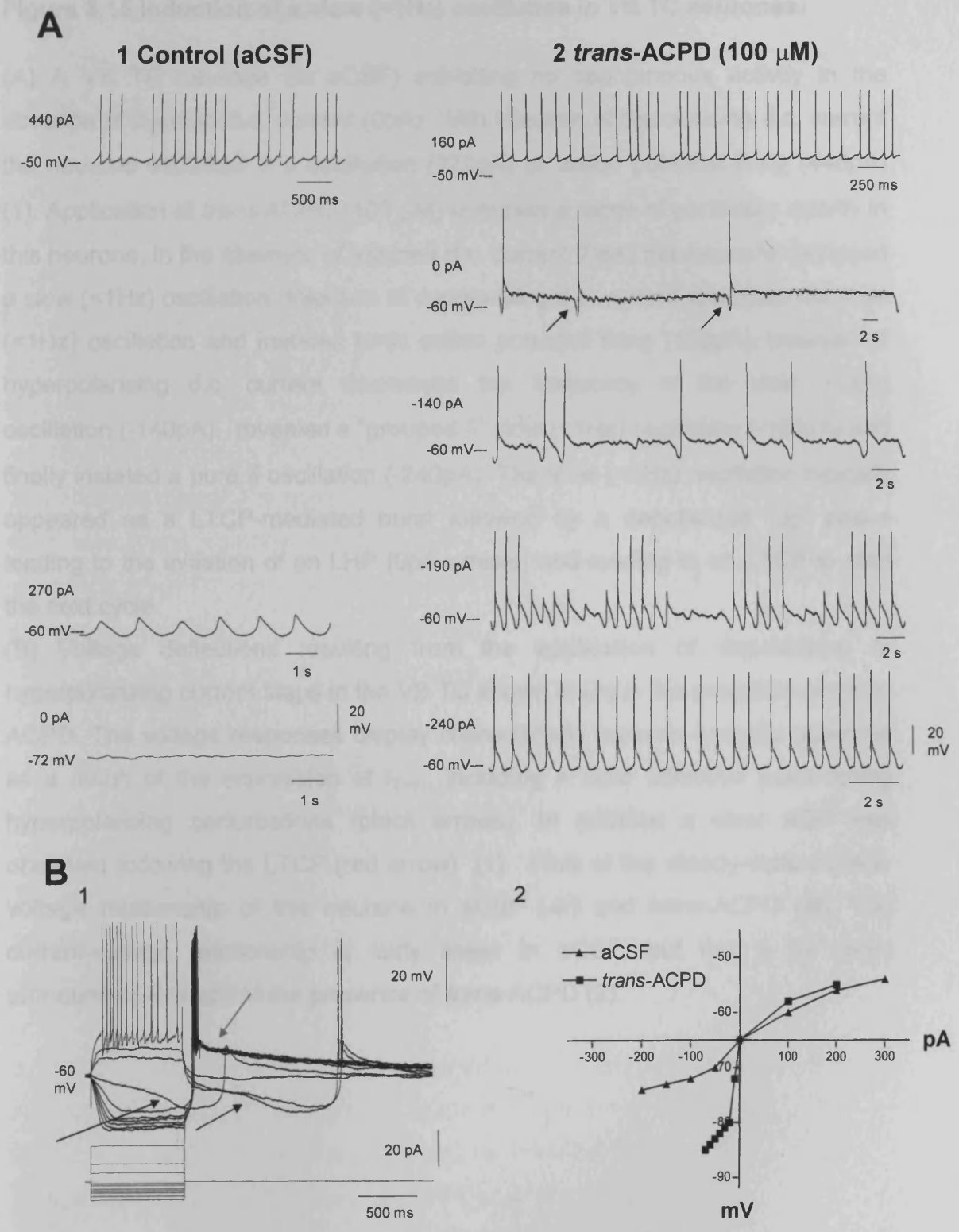

Figure 3.15 Induction of a slow (<1Hz) oscillation in VB TC neurones.

Figure 3.15 Induction of a slow (<1Hz) oscillation in VB TC neurones.

(A) A VB TC neurone (in aCSF) exhibiting no spontaneous activity in the absence of injected d.c. current (0pA). With injection of depolarising d.c. current the neurone exhibited a δ oscillation (270pA) or action potential firing (440pA) (1). Application of *trans*-ACPD (100 μM) unmasks a range of oscillatory activity in this neurone. In the absence of injected d.c. current (0pA) this neurone displayed a slow (<1Hz) oscillation. Injection of depolarising d.c. current abolished the slow (<1Hz) oscillation and instated tonic action potential firing (160pA). Injection of hyperpolarising d.c. current decreased the frequency of the slow (<1Hz) oscillation (-140pA), revealed a "grouped δ" slow (<1Hz) oscillation (-190pA) and finally instated a pure δ oscillation (-240pA). The slow (<1Hz) oscillation typically appeared as a LTCP-mediated burst followed by a depolarised "up" phase leading to the initiation of an LHP (0pA arrows) and leading to an LTCP to start the next cycle.

(B) Voltage deflections resulting from the application of depolarising or hyperpolarizing current steps in the VB TC shown in (A) in the presence of *trans*-ACPD. The voltage responses display characteristic features typically observed as a result of the expression of I_{Twin}, including a clear inflection point during hyperpolarising perturbations (black arrows). In addition a clear ADP was observed following the LTCP (red arrow) (1). Plots of the steady-state current-voltage relationship of this neurone in aCSF (▲) and *trans*-ACPD (■). The current-voltage relationship is fairly linear in aCSF, but has a far more pronounced S-shape in the presence of *trans*-ACPD (2).

Hz, n=12, VL: 2 of 8, 25%, maximum number of grouped events: 15.4 ± 3.2, n=12, frequency = 1.4 ± 0.1 Hz, n=52, MGN: 7 of 14, 50%, maximum number of grouped events: 10.8 ± 5.3, n=21, frequency = 1.2 ± 0.07 Hz, n=56.

The properties of the slow (<1Hz) oscillation in TC neurones in the VB, VL and MGN were fully consistent with those observed in LGN TC neurones. The slow (<1Hz) oscillation in VB, VL and MGN TC neurones always comprised a rhythmic transition between a depolarised "up" state and a hyperpolarised "down" state although separated by a smaller maximum membrane potential range than in LGN TC: LGN = 26.9 ± 1.0 mV (n=34), VB = 17.4 ± 4.3 mV (n=12), P <0.001, VL = 19.6 ± 2.1 mV (n=8), P = 0.002 and MGN = 19.3 ± 1.7 mV (n=14), P = 0.002. This reduced membrane potential range was accounted for by a decrease in the peak membrane potential reached during the "up" phase of the slow (<1Hz) oscillation when TC neurones in the LGN (-53.3 ± 0.7 mV, n=23 were compared with those in the VB (-62.1 ± 1.8 mV, n=11, P <0.001), VL (-59.3 ± 1.6 mV, n=8, P = 0.001) and MGN (-60.7 ± 1.6 mV, n=14, P <0.001).

In all neurones displaying the slow (<1Hz) oscillation, the frequency of the slow (<1Hz) oscillation was decreased during neuronal depolarisation (Fig. 3.16). As described in the LGN, in VB, VL and MGN TC neurones, the decrease in the frequency of the slow (<1Hz) oscillation was manifested as an increase in the duration of the "up" phase with usually no change in the duration of the "down" phase (Fig. 3.16, Table 3.3).

3.3.3.3 Extracellular manifestations of the slow (<1Hz) oscillation.

As was observed in LGN slices, application of *trans*-ACPD resulted in an increase in observed spontaneous activity and the induction of slow (<1Hz) oscillatory activity. Under control conditions, spontaneous activity was seen in 11 of 30 VB slices and comprised δ (1-2Hz) frequency rhythmic LTCP-mediated bursts of action potentials (1.2 ± 0.2 Hz, n=16). In the presence of *trans*-ACPD, 7% of units recorded in VB slices displayed rhythmic LTCP-mediated events at δ frequencies (1.1±0.05 Hz, n=4), 75% of the recorded activity comprised rhythmic LTCP-mediated bursts occurring at <1Hz frequencies (0.32 ± 0.04 Hz, n=43) that presumably represented the slow (<1Hz) oscillation, and the remainder of

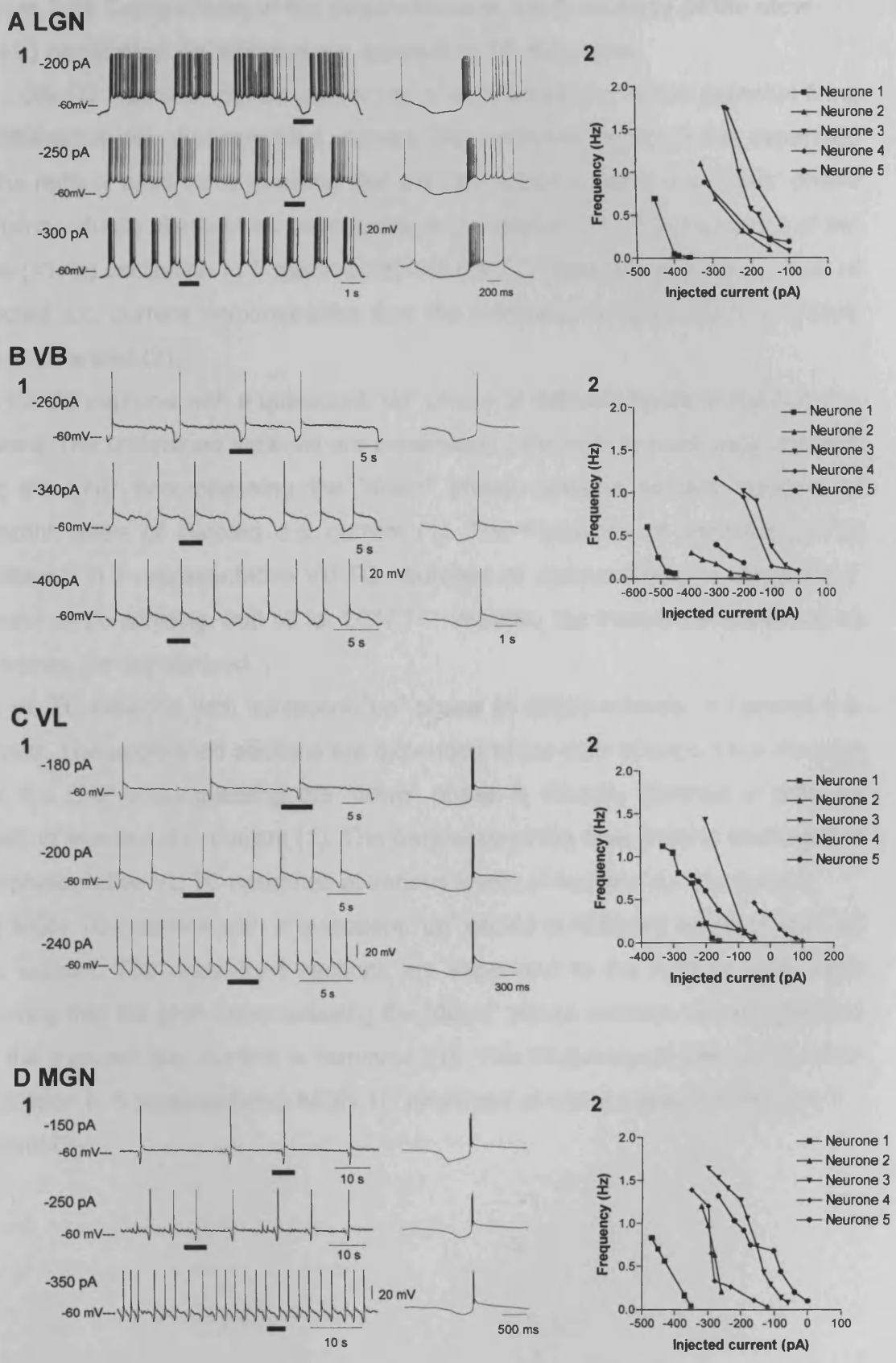

Figure 3.16 Comparison of the dependence of the frequency of the slow (<1Hz) oscillation on injected d.c. current in TC neurones.

Figure 3.16 Comparison of the dependence of the frequency of the slow (<1Hz) oscillation on injected d.c. current in TC neurones.

(A) LGN TC neurone with an active "up" phase comprising action potential firing at different levels of injected d.c. current. The underlined sections are expanded to the right of each trace showing that the LHP encompassing the "down" phase remains virtually identical as the neurone is depolarised (1). The frequency of the slow (<1Hz) oscillation in 5 representative LGN TC neurones at various levels of injected d.c. current demonstrating that the frequency is reduced as neurones are depolarized (2).

(B) VB TC neurone with a quiescent "up" phase at different levels of injected d.c. current. The underlined sections are expanded to the right of each trace showing that the LHP encompassing the "down" phase remains virtually identical at different levels of injected d.c. current (1). The frequency of the slow (<1Hz) oscillation in 5 representative VB TC neurones at various levels of injected d.c. current demonstrating, that as for LGN TC neuones, the frequency is reduced as neurones are depolarised.

(C) VL TC neurone with quiescent "up" phase at different levels of injected d.c. current. The underlined sections are expanded to the right of each trace showing that the LHP encompassing the "down" phase is virtually identical at different levels of injected d.c. current (1). The frequency of the slow (<1Hz) oscillation in 5 representative VL TC neurones at various levels of injected d.c. current (2).

(D) MGN TC neurone with a quiescent "up" phase at different levels of injected d.c. current. The underlined sections are expanded to the right of each trace showing that the LHP encompassing the "down" phase remains virtually identical as the injected d.c. current is removed (1). The frequency of the slow (<1Hz) oscillation in 5 representative MGN TC neurones at various levels of injected d.c current (2).

	"up" phase (seconds)				"down" phase (seconds)			
	Min	**Max**	***P***	**Increase**	**Min**	**Max**	***P***	**Increase**
LGN	1.4 ± 0.2 (0.3-2.7) n = 26	11.3 ± 2.4 (1.7-46.6) n = 26	0.0006*	9.8 ± 2.4 (1.2-45.9) n = 26	1.0 ± 0.2 (0.3-3.8) n = 26	1.4 ± 0.2 (0.5-3.9) n = 26	0.0003*	0.4 ± 0.1 (0.02-1.7) n = 26
VB	1.5 ± 0.4 (0.5-3.3) n = 8	14.1 ± 5.6 (1.5-40.6) n = 8	0.07	12.6 ± 5.5 (0.7-38.8) n = 8	1.0 ± 0.2 (0.5-1.5) n = 8	1.2 ± 0.2 (0.6-2.1) n = 8	0.09	0.2 ± 0.1 (0.1-0.6) n = 8
VL	3.9 ± 1.3 (0.7-8.5) n = 6	48.5 ± 14.2 (5.9-82.4) n = 6	0.03*	44.6 ± 13.3 (5.2-78.8) n = 6	1.2 ± 0.4 (0.5-2.5) n = 6	1.3 ± 0.3 (0.8-2.7) n = 6	0.08	0.2 ± 0.1 (0.1-0.4) n = 6
MGN	2.3 ± 0.6 (0.9-4.9) n = 7	17.1 ± 3.7 (3.9-31.3) n = 7	0.0051*	14.8 ± 3.4 (3.0-29.0) n = 7	0.9 ± 0.1 (0.6-1.1) n = 7	1.2 ± 0.2 (0.7-2.3) n = 7	0.09	0.4 ± 0.2 (0.1-1.3) n = 7

Table 3.3 Duration of the "up" and "down" phases of the basic slow (<1Hz) oscillation in TC neurones.

Summary of the durations of the "up" and "down" phases of the slow (<1Hz) oscillation in LGN, VB, VL and MGN TC neurones. For each parameter the mean value is followed by the range and the number of neurones. Minimum (Min) values correspond to the most hyperpolarised level of injected d.c. current where the "up" or "down" phases were measured. Maximum (Max) values correspond to the most depolarised level of injected d.c. current where the "up" or "down" phases were measured. The increase in duration (Increase) corresponds to the increase in duration of the "up" or "down" phase between the most hyperpolarised and most depolarised levels of injected d.c. current where these parameters of the slow (<1Hz) oscillation were measured.

The *P*-values given were calculated using the Min and Max values for the "up" or "down" phase for TC neurones in each thalamic relay nucleus (* = $P<0.05$).

recorded neurones either showed spontaneous tonic firing (8.5 ± 1.8 Hz n =6) or HT bursting (2.4 ± 0.19 Hz, n=4). Similar activity was seen in VL slices, under control conditions, spontaneous activity was sometimes seen in VL slices (n=9 of 25) and consisted of LTCP-mediated bursts occurring at δ (1-2 Hz) frequencies (1.5 ± 0.5 Hz, n=2) or <1Hz frequencies (0.6 ± 0.1 Hz, n=8). In the presence of *trans*-ACPD, units recorded in VL slices predominantly showed oscillatory activity comprising LTCP-mediated bursts at slow (<1Hz) frequencies (0.27 ± 0.04 Hz, n=28, 74%) or δ frequencies (n = 1 neurone, 1.2 ± 0.01 Hz, n=6 cycles, 3%) and the remainder of recordings comprised either spontaneous tonic firing (9.7 ± 2.8 Hz, n=6) or HT bursts (6.4 ± 2.5 Hz, n=3). Under control conditions in MGN slices spontaneous activity was occasionally seen (n=10 of 27) and consisted of LTCP-mediated bursts occurring at δ (1-2 Hz) frequencies (1.6 ± 0.1 Hz, n=10) or <1Hz frequencies (0.7 ± 0.1 Hz, n=3). In the presence of *trans*-ACPD, oscillatory activity comprised LTCP-mediated bursts at slow (<1Hz) frequencies (72 %, 0.25 ± 0.03 Hz, n=42) or, δ frequencies (7%, n = 4, 1.1 ± 0.04 Hz, n=4) and the remainder of recordings comprised spontaneous tonic action potential firing (17.2 ± 5.5 Hz, n=9) or HT bursts (3.2 ± 0.2 Hz, n=3).

Extracellular recordings in VB, VL and MGN slices (Fig. 3.17) showed a similar pattern of expression of the slow (<1Hz) oscillation as was observed during intracellular recordings. That is, in VB, VL and MGN slices, in the majority of cases the slow (<1Hz) oscillation comprised a quiescent "up" phase (Fig. 3.17B, see Table 3.4). In a number of cases sequences of δ (1-2Hz) frequency bursts were grouped within the <1Hz frequency and presumed to represent a "grouped δ" slow (<1Hz) oscillation (Fig. 3.17C): VB = 3 of 43, 7%, maximum number of grouped events = 4.3 ± 1.3 (n=18), maximum frequency of grouped events = 1.3 ± 0.03 Hz (n=18), VL = 2 of 28, 7%, maximum number of grouped events = 5.6 ± 0.4 (n=12), maximum frequency of grouped events = 1.1 ± 0.1 Hz (n=30) and MGN = 7 of 42, 17%, maximum number of grouped events = 7.8 ± 2.1 (n=21), maximum frequency of grouped events = 1.1 ± 0.2 Hz (n=60). However, in the few cases where the slow (<1Hz) oscillation appeared to comprise action potential firing during the "up" phase (Fig. 3.17A), the appearance was much the same as that observed during extracellular recording in LGN slices: VB = 8 of 43, 19%, action potential firing = 12.8 ± 2.0 (n=24), VL = 2 of 28, 7%, action potential

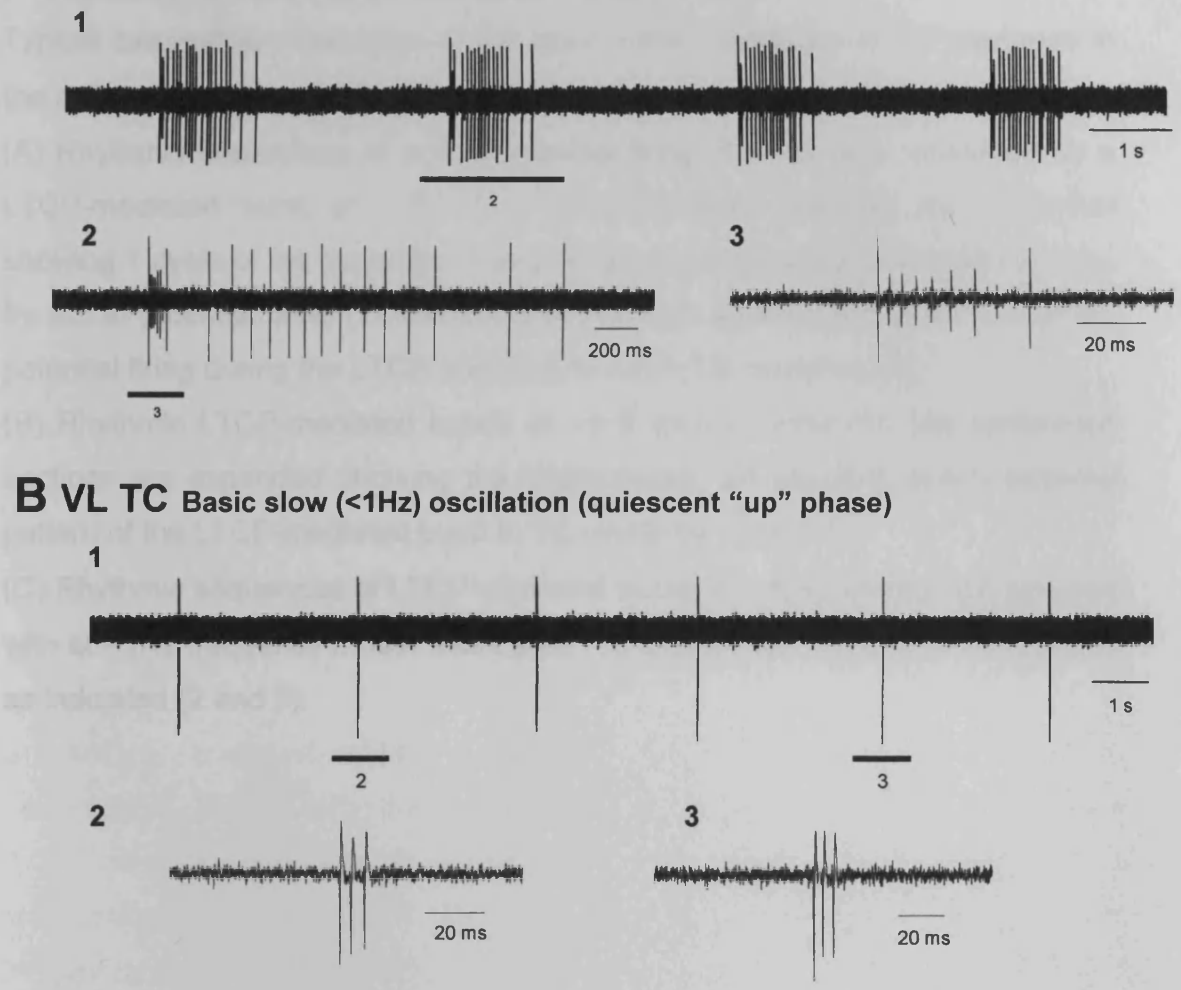

Figure 3.17 Examples of typical extracellular manifestation of the slow (<1Hz) oscillation in VB, VL and MGN TC neurons.

Figure 3.17 Examples of typical extracellular manifestation of the slow (<1Hz) oscillation in VB, VL and MGN TC neurones.

Typical extracellular examples of the slow (<1Hz) oscillation in TC neurones in the presence of *trans*-ACPD (100 μM).

(A) Rhythmic sequences of action potential firing in a VB slice, preceded by a LTCP-mediated burst at <1Hz (1). The underlined sections are expanded showing 1 cycle of the oscillation comprising a burst of action potentials followed by action potential firing (2) and the characteristic decelerating pattern of action potential firing during the LTCP-mediated burst in TC neurones (3).

(B) Rhythmic LTCP-mediated bursts at <1Hz in a VL slice (1). The underlined sections are expanded showing the characteristic decelerating action potential pattern of the LTCP-mediated burst in TC neurones (2 and 3).

(C) Rhythmic sequences of LTCP-mediated bursts at δ frequencies and grouped with at <1Hz frequency in and MGN slice (1). Underlined sections are expanded as indicated (2 and 3).

firing = 12.4 ± 7.9 (n=12) and MGN = 6 of 42, 14%, action potential firing = 19.5 ± 9.4 (n=18).

3.3.5 Summary of the nucleus-specific properties of the slow (<1Hz) oscillation in TC neurones.

A number of manifestations of the slow (<1Hz) oscillation were observed in TC neurones (Table 3.4). In the LGN the full range of manifestations were observed during both intracellular and extracellular recordings. In contrast, a more limited range of manifestations were observed in TC neurones of the other nuclei examined and predominantly observed as a slow (<1Hz) oscillation that did not support action potential firing during the "up" phase following the LTCP-mediated burst of action potentials. However, in a small number of cases VB, VL and MGN TC neurones did display a slow (<1Hz) oscillation during the presumed "up" phase during extracellular recordings.

In most relay nuclei examined the frequency range of the slow (<1Hz) oscillation was broadly similar during both intracellular and extracellular recordings (Table 3.5). The only exception is the faster range of frequencies encompassed by the extracellularly recorded VB TC neurones, however, the mean minimum frequency during extracellular recordings was very similar (see Table 3.5). The minimum frequencies of the slow (<1Hz) oscillation recorded intracellularly and extracellularly were not found to be significantly different except in the case of the VL (see Table 3.5).

3.4 DISCUSSION

The novel findings described in this chapter are 1) the induction in TC neurones, maintained *in vitro*, of a slow (<1Hz) oscillation with a number of very similar properties to those observed in TC neurones *in* vivo during sleep, 2) the slow (<1Hz) oscillation observed *in vitro* is induced following corticothalamic stimulation or pharmacological manipulation is dependent on activation of mGluR 1a receptors in both cases, and 3) the slow (<1Hz) oscillation can support action potential firing during the "up" phase, with the highest proportion of neurones displaying this characteristic being observed in the LGN, the thalamic relay nucleus subserving the visual system in the intact brain.

	Active "up" phase			Silent "up" phase		
	Basic	**Grouped**	**Total**	**Basic**	**Grouped**	**Total**
LGN						
Intracellular (n=34)	7	4	11 (32%)	19	4	23 (68%)
Extracellular (n=28)	12	3	15 (54%)	8	5	13 (46%)
VB						
Intracellular (n=12)	–	–	–	8	4	12 (100%)
Extracellular (n=43)	8	–	8 (9%)	32	3	35 (81%)
VL						
Intracellular (n=8)	–	–	–	6	2	8 (100%)
Extracellular (n=28)	2	–	2 (7%)	24	2	26 (93%)
MGN						
Intracellular (n=14)	–	–	–	7	7	14 (100%)
Extracellular (n=42)	5	1	6 (14%)	29	7	36 (86%)

Table 3.4 Expression of different sub-types of the slow (<1Hz) oscillation in TC neurones.

Summary of the proportion of different sub-types of the slow (<1Hz) oscillation exhibited by TC neurones in the LGN, VB, VL and MGN. Note that only during intracellular recordings of LGN TC neurones was the slow (<1Hz) oscillation with an active "up" phase observed. During extracellular recordings, the slow (<1Hz) oscillation with an active "up" phase was observed in all thalamic relay nuclei examined, however was far more prevalent in the LGN than in the VB, VL or MGN.

		Intracellular	Extracellular	
LGN	Minimum frequency (Hz)	0.30 ± 0.04 Hz (n=34)	0.28 ± 0.03 Hz (n=28)	$P = 0.73$
	Frequency range (Hz)	0.01- 0.80 Hz	0.01- 0.59 Hz	
VB	Minimum frequency (Hz)	0.12 ± 0.04 Hz (n=11)	0.32 ± 0.04 Hz (n=43)	$P = 0.05$
	Frequency range (Hz)	0.02 - 0.82 Hz	0.17 - 0.81 Hz	
VL	Minimum frequency (Hz)	0.04 ± 0.02 Hz (n=8)	0.27 ± 0.04 Hz (n=28)	$P = 0.03$*
	Frequency range (Hz)	0.01 - 0.82 Hz	0.01 - 0.7 Hz	
MGN	Minimum frequency (Hz)	0.06 ± 0.01 Hz (n=14)	0.25 ± 0.03 Hz (n=42)	$P = 0.21$
	Frequency range (Hz)	0.02 - 0.8 Hz	0.01 - 0.8 Hz	

Table 3.5 Comparison of the minimum frequencies of the slow (<1Hz) oscillation during intracellular and extracelular recordings.

Summary of the frequency range and minimum frequency of the slow (<1Hz) oscillation in TC neurones in the LGN, VB, VL and MGN during intacellular and extracellular recordings.

The *P*-values given were calculated using the minimum frequencies of the slow (<1Hz) oscillation recorded intracellularly and extracellularly.

3.4.1 Induction of a slow (<1Hz) oscillation in TC neurones.

In TC neurones of the thalamic relay nuclei examined maintained *in vitro*, exogenous or synaptic activation of the mGluR associated with cortical input, mGluR1a (Godwin et al. 1996), leads to the generation of a slow (<1Hz) oscillation. The properties of the slow (<1Hz) oscillation described in this chapter are entirely consistent with those observed *in vivo* during sleep (Fig. 3.18) (Steriade et al. 1993a; Contreras and Steriade 1995; Steriade et al. 1996; Contreras and Steriade 1997; Steriade et al. 2001) in that, 1) the frequency ranges of the slow (<1Hz) oscillation in the two conditions are virtually identical; 2) in both cases, the slow (<1Hz) oscillation is characterized by prominent 'up' and 'down' states separated by ~20-25 mV; 3) in both scenarios the transition from 'up' to 'down' state is commonly characterized by a marked inflection point whilst the transition from 'down' to 'up' state is punctuated by a LTCP; 4) the slow (<1Hz) oscillation *in vitro* is able to group sequences of δ oscillation in an indistinguishable manner to that observed *in vivo*; 5) as with the slow (<1Hz) oscillation observed *in vivo*, the slow (<1Hz) oscillation *in vitro* exists at a level of depolarisation between that of a sustained firing and a continuous δ oscillation; 6) *in vitro*, action potential firing during the "up" phase of the slow (<1Hz) oscillation reached frequencies observed when sustained tonic firing occurred, consistent with the observation *in vivo* that activity during depolarised phase of the slow (<1Hz) oscillation can reach frequencies observed during the awake state (Steriade et al. 1993d; Steriade et al. 2001) and 7) *in vivo*, the slow (<1Hz) oscillation is dependent on an intact cortex (Timofeev and Steriade 1996) whereas *in vitro*, the slow (<1Hz) oscillation is unmasked when cortical input is mimicked through either the exogenous or endogenous activation of mGluR1a. Thus these observations strongly suggest that the slow (<1Hz) oscillation unmasked in TC neurones *in vitro* does indeed represent the slow (<1Hz) oscillation observed in TC neurones during the slow (<1Hz) rhythm in the thalamus *in vivo*.

3.4.2 A role for mGluR1a in the regulation of slow (<1Hz) sleep rhythms.

Tonic activation of mGluR receptors in TC neurones is sufficient to induce a self-sustained slow (<1Hz) sleep oscillation as demonstrated by the persistence of oscillatory activity in the absence of any other synaptic influences. This is in accordance with the necessity for intact corticothalamic inputs to the thalamus

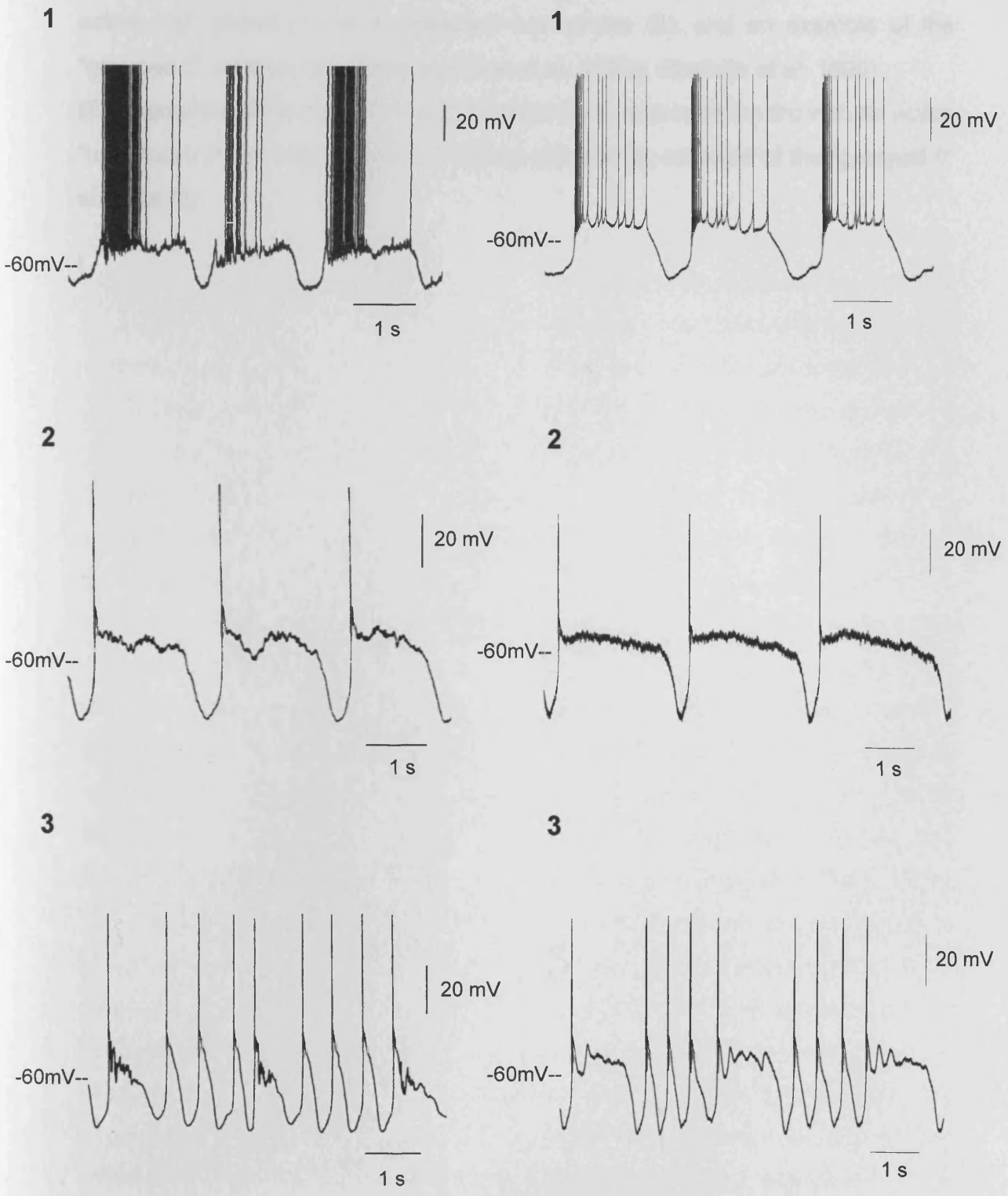

Figure 3.18 Comparison of the slow (<1Hz) sleep oscillation in TC neurones *in vivo* and *in vitro*.

Figure 3.18 Comparison of the slow (<1Hz) oscillation in TC neurones *in vivo* and *in vitro*.

(A) Examples of the basic slow (<1Hz) oscillation in TC neurones *in vivo* with an active "up" phase (1) or a quiescent "up" phase (2), and an example of the "grouped δ" subtype (3). (From Steriade et al. 1993a, Steriade et al, 1996).

(B) Examples of the slow (<1Hz) oscillation in TC neurones *in vitro* with an active "up" phase (1) or a quiescent "up" phase (2), and an example of the "grouped δ" subtype (3).

for the generation of the slow (<1Hz) sleep oscillation in TC neurones *in vivo* (Timofeev and Steriade 1996). However, it is in contrast to the view that the thalamic slow (<1Hz) sleep oscillation is a reflection of the cortical slow (<1Hz) oscillation (Steriade et al. 1993a; Steriade et al. 1993c; Steriade et al. 1993d; Amzica and Steriade 1995b; Contreras and Steriade 1997). In addition, extracellular investigations demonstrate that in addition to effecting a fundamental change in basic neuronal dynamics, mGluR1a activation can efficiently promote slow (<1Hz) oscillatory activities under natural conditions by facilitating an appropriate membrane potential depolarisation to within the voltage range where the slow (<1Hz) oscillation can occur. Moreover, my study shows that different intensities of mGluR1a-activation facilitate different types of oscillatory activity in TC neurones. The idea that corticothalamic mGluRs are substantially activated during sleep is well supported by numerous studies showing that in this behavioural state, cortical neurones are far from inactive and continue to generate sustained periods of action potential firing (Steriade et al. 1993c; Steriade et al. 1993d; Steriade et al. 1996; Steriade et al. 2001). Indeed, during sleep, although the rhythmic recurrence of hyperpolarising episodes (i.e. the 'down' states of the slow oscillation, see section 1.8.2.1) in cortical neurones will lessen the overall output of the cortex to the thalamus in comparison to wakefulness, the 'up' state of the slow oscillation in cortical neurones supports action potential firing rates that are actually comparable to those observed during the wake state (Steriade et al. 1993d; Steriade et al. 2001). The mGluR component of the corticothalamic input is a long-lasting depolarisation (see section 3.3.1) (McCormick and von Krosigk 1992; von Krosigk et al. 1999; Turner and Salt 2000) and therefore cortical activity would maintain tonic activation of mGluR receptors on TC neurones and therefore prolonged depolarisation of TC neurones *in vivo.* During decreasing arousal, cortical activity is deceased but not abolished (Steriade et al. 1993d; Steriade et al. 2001) and presumably glutamate released from corticothalamic afferent continues to provide tonic activation of mGluR receptors on TC neurones. However, the reduction of depolarising influences both from the cortex and brainstem (Steriade and Glenn 1982; Steriade et al. 1990; Steriade 1993) resulting in hyperpolarisation of TC neurones presumably allows the membrane potential of TC neurones to move to a range where the slow (<1Hz) sleep oscillation will be generated. In this way, the slow (<1Hz) oscillation in TC neurones may contribute to the initial

organisation of the cortical slow (<1Hz) sleep oscillation as sleep deepens as well a contributing to the maintenance of the cortical slow (<1Hz) oscillation during deep sleep (Steriade et al. 1993a; Steriade et al. 1993c).

3.4.3 Modality-specific properties of the slow (<1Hz) oscillation.

Although the slow (<1Hz) oscillation was induced in TC neurones of all thalamic nuclei examined, the depolarised "up" phase of the slow (<1Hz) oscillation supported action potential firing predominantly in LGN TC neurones. The following points suggest that this finding is not an artefact produced by the experimental techniques: 1) this observation was also made during extracellular recordings where the neuronal membrane should not sustain any substantial damage due to impalement, 2) during intracellular recordings, an active "up" phase was only observed in LGN TC neurones and not in VB, VL and MGN TC neurones. This could, in part, have been due to the smaller number of TC neurones recorded, but unlikely to be due to damage caused by neuronal impalement as oscillatory activity was associated with high input resistances and 3) the maximum membrane potential during the "up" phase of the slow (<1Hz) oscillation was more depolarised in LGN TC neurones (-53.3 ± 0.7 mV) compared to VB (-62.1 ± 1.8 mV), VL (-59.3 ± 1.6 mV) or MGN (-60.7 ± 1.5 mV) TC neurones. Given that the maximum membrane potential reached during the "up" phase increased as the frequency of slow (<1Hz) oscillation decreased when neurones were depolarised and that the frequency ranges of the slow (<1Hz) oscillation were similar in TC neurones of all nuclei examined (and notably longer in the VL), this observation was not due to a restricted frequency range in the VB, VL and MGN.

In VB, VL and MGN TC neurones the "up" phase of the slow (<1Hz) oscillation was always observed as a long-lasting plateau following the LTCP, suggesting that activation of K^+ channels provided an opposing rectification that effectively clamped the membrane potential at a given value before termination of the "up" phase. Greater rectification at depolarised membrane potentials is reported in VB TC neurones compared to LGN TC neurones (Turner et al. 1997) and so could also be operating in VL and MGN TC neurones. This is consistent with the observation that *trans*-ACPD effectively depolarised neurones beyond the threshold for action potential generation in a greater proportion of LGN TC

neurones than in TC neurones of the other nuclei which could also be due to the greater rectification at depolarised membrane potentials. However, another possible explanation for the greater depolarisation observed in LGN TC neurones in the presence of *trans*-ACPD is that LGN TC neurones are more sensitive to *trans*-ACPD than TC neurones in the other nuclei. This can not be excluded, but given that induction of the slow (<1Hz) oscillation and voltage responses typically observed due to a bistable interaction between I_{KLeak} and $I_{Twindow}$ (Williams et al. 1997a; Hughes et al. 1999) occured in TC neurones in all nuclei with the same concentration of *trans*-ACPD, this is unlikely to be the case.

As thalamocortical activity evokes excitatory monosynaptic responses in cortical neurones (Salt et al. 1995; Gil and Amitai 1996) and repetitive thalamic stimulation results in an augmented excitatory response in cortical neurones (Steriade et al. 1998), the contribution of action potential firing during the "up" phase of the slow (<1Hz) oscillation in TC neurones is presumably to drive cortical activity during this phase and thus reinforce the slow (<1Hz) oscillation in the cortex. However, the results described here suggest that the LGN TC neurones will be substantially more active during the slow (<1Hz) oscillation than in the other modality specific nuclei examined (>50% compared to <10%). As the LGN is the major thalamic nucleus receiving subcortical visual inputs, projecting to the visual cortical areas and also receiving substantial inputs from visual cortical areas (see section 1.3), this suggests that during sleep and particularly during SWS the corticothalamic network involved in processing visual information may be more active than other modality-related brain areas.

CHAPTER 4

CELLULAR MECHANISMS OF THE SLOW (<1Hz) SLEEP OSCILLATION IN THALAMOCORTICAL NEURONES *IN VITRO*

4.1 INTRODUCTION

In Chapter 3, the induction of the slow (<1Hz) sleep oscillation in TC neurones *in vitro* with identical properties as those observed in *vivo* was described following corticothalamic stimulation and using a pharmacological protocol i.e. application of *trans*-ACPD that successfully mimics the corticothalamic stimulation. Therefore using this pharmacological manipulation to induce <1Hz oscillatory activity, the cellular mechanisms of the slow (<1Hz) sleep oscillation in LGN TC neurones maintained *in vitro* were investigated.

4.2 METHODS

4.2.1 Electrophysiology.

Intracellular recordings were performed in adult cat thalamic slices containing the LGN as described in Chapter 2.

4.2.2 Data analysis.

Data analysis was performed and presented as described in Chapter 2.

4.2.3 Drugs.

Drugs were obtained, applied and used at the concentrations described in Chapter 2.

4.3 RESULTS

4.3.1 The intrinsic nature of the slow (<1Hz) sleep oscillation in TC neurones.

As described in Chapter 3, application of *trans*-ACPD induced a slow (<1Hz) sleep oscillation in TC neurones (n=34). In some neurones (n=14), the slow (<1Hz) sleep oscillation served to group periods of δ oscillations into short recurring episodes ("grouped δ" subtype of the slow (<1Hz) oscillation) (Fig. 4.1 and see Chapter 3). Both the slow (<1Hz) sleep oscillation and its ability to "group" δ oscillations occurred independently of the activation of non-NMDA, NMDA, $GABA_A$ and $GABA_B$ receptors since they persisted in the presence of CNQX (10 μM), APV (100 μM), BMI (30 μM) and CGP 56999A (10 μM) (n=16 of 16) (Fig. 4.1A). In addition, the slow (<1Hz) sleep oscillation and "grouping" of δ

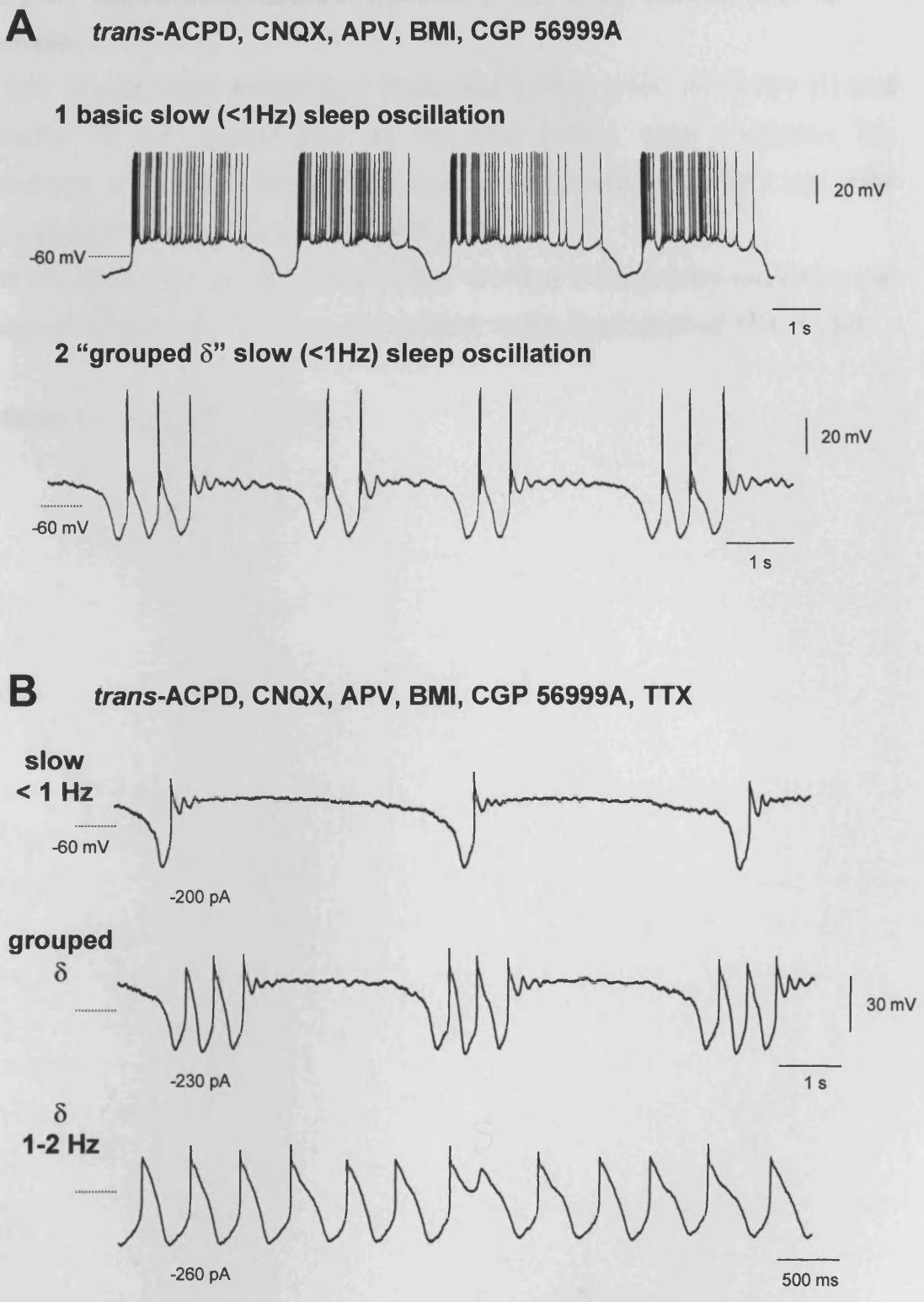

Figure 4.1 The intrinsic nature of the slow (<1Hz) sleep oscillation in TC neurones.

Figure 4.1 The intrinsic nature of the slow (<1Hz) sleep oscillation in TC neurones.

(A) Two TC neurones exhibiting a basic slow (<1Hz) sleep oscillation (1) and "grouping" of the δ oscillation by the slow (<1Hz) sleep oscillation (2), respectively, in the presence of the receptor antagonists CNQX (10 μM), APV (100 μM), BMI (30 μM) and CGP 56999A (10 μM).

(B) In the same neurone as shown in (A_2), the slow (<1Hz) sleep oscillation and "grouping" of the δ oscillation are not affected by the application of TTX (1 μM).

Published in Hughes et al. 2002b

oscillations were insensitive to tetrodotoxin (TTX) (1 μM) (n=9 of 9) (Fig. 4.1B). Thus, the slow (<1Hz) sleep oscillation, and its ability to "group" δ oscillations in TC neurones are generated by intrinsic mechanisms and result from a direct postsynaptic effect of *trans*-ACPD.

4.3.2 The effect of *trans*-ACPD in TC neurones is fully accounted for by a reduction of g_{Leak}.

As described in Chapter 3, in control conditions, the voltage response of TC neurones to the injection of small (10-50 pA) hyperpolarising d.c. current pulses elicited from -60 mV consisted of a typical monophasic charging pattern with cells exhibiting an R_N of 192 ± 15 MΩ (n=83) (see Fig. 3.4B_1 aCSF, Fig. 4.2A_1 and 4.2B_1). Following the application of 100 μM *trans*-ACPD, in neurones that exhibited the slow (<1Hz) sleep oscillation, this response was markedly altered with small current pulses giving rise to a stereotypical hyperpolarising voltage waveform that was the same as the LHP evident during the slow (<1Hz) sleep oscillation (see Fig. 3.4B_1 *trans*-ACPD, Fig. 4.2$A_{2 \text{ and } 3}$). In these neurones, the apparent input resistance in the range -60 to -80 mV could be as high as 2.5 GΩ (1.01 ± 0.1 GΩ; n=34), leading to an overall increase following *trans*-ACPD application of 419 ± 81% (n=34). The current pulse-induced LHP was always terminated by a LTCP that, in turn, was always followed by a slowly decaying (up to 30 sec) afterdepolarisation (ADP). This transient ADP is clearly apparent during the 'up' state of the slow (<1Hz) sleep oscillation (see Chapter 3 and Fig. 4.2A_3). Thus the essential features of the slow (<1Hz) sleep oscillation were reproduced through the injection of hyperpolarising current pulses. In neurones that did not exhibit the slow (<1Hz) sleep oscillation following application of 100 μM *trans*-ACPD application, an LHP response was never observed, with cells continuing to exhibit a linear charging pattern albeit with a 50 ± 12% (n=21) increase in apparent input resistance (Fig. 4.2$B_{1 \text{ and } 2}$). These cells did however display a prominent ADP following *trans*-ACPD application (Fig. 4.2B_2), which is consistent with observations in rat TC neurones (Turner and Salt 2000), and suggested that different cellular mechanisms may underlie the LHP and ADP. As expected from previous studies (Williams et al. 1997a; Hughes et al. 1999), the apparent input resistance in control conditions was found to be a good predictor of whether or not TC neurones would exhibit an LHP-ADP sequence, and thus a slow (<1Hz) sleep oscillation, following *trans*-ACPD application, with non-

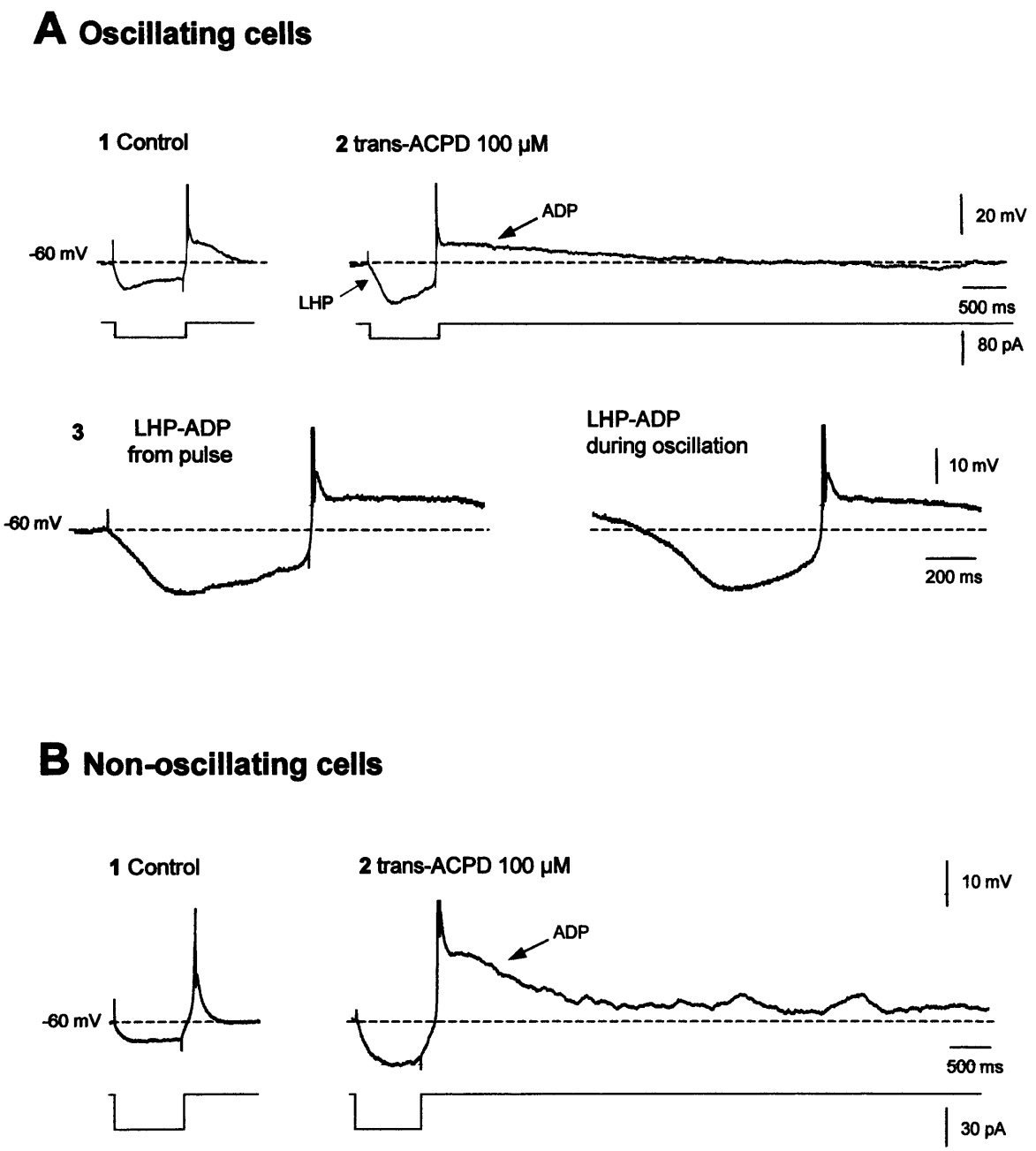

Figure 4.2 *Trans*-ACPD unmasks a LHP and ADP in TC neurones displaying the slow (<1Hz) sleep oscillation.

Figure 4.2 *Trans*-ACPD unmasks a LHP and ADP in TC neurones displaying the slow (<1Hz) sleep oscillation.

(A) In control conditions, the voltage response of a TC neurone, that displayed the slow (<1Hz) oscillation following *trans*-ACPD application, to a small hyperpolarizing current pulse (-40 pA) applied from -60 mV consists of a monophasic charging pattern (1). *trans*-ACPD (100 μM) causes an increase in apparent input resistance (2) and a modified charging pattern comprising a stereotypical LHP. The LHP is followed by a LTCP and subsequent ADP (expanded in 3). The current pulse-induced LHP-ADP sequence (3, left trace) is equivalent to the activity evident during a cycle of the slow (<1Hz) sleep oscillation (3, right trace).

(B) In a TC neurone that did not display the slow (<1Hz) sleep oscillation, *trans*-ACPD (100 μM) causes an increase in apparent input resistance (1 and 2) and unmasks a prominent ADP (2) but not does not lead to the appearance of an LHP (2).

(Note: action potentials in A and B have been truncated for clarity).

Published in Hughes et al. 2002b

oscillating cells displaying a significantly lower pre-drug value (113 ± 19 MΩ; n=21) than oscillating cells (220 ± 17 MΩ; n=34) (P<0.001). Accordingly, the likelihood of observing a slow (<1Hz) sleep oscillation following the application of 100 μM *trans*-ACPD increased as a function of apparent input resistance in control conditions. Neurones exhibiting values <100 MΩ were never able to generate a slow (<1Hz) sleep oscillation, whilst neurones exhibiting values in the ranges 100-150 MΩ and 151-200 MΩ were able to generate a slow (<1Hz) sleep oscillation in 42% and 75% of cases respectively, and neurones exhibiting values > 200 MΩ were able to generate a slow (<1Hz) sleep oscillation in 92% of cases.

In order to demonstrate that the appearance of the LHP and ADP can be entirely explained by a simple reduction in g_{Leak}, the outcome of applying *trans*-ACPD and the effect of artificially reducing g_{Leak} with a dynamic clamp system (Hughes et al. 1999) were compared in the same TC neurone (n=5). By performing this procedure it was shown that for certain levels of artificial g_{Leak}-reduction (g_{Leak} = -4.0 ± 0.7 nS) and *trans*-ACPD concentration (125 μM), the resulting effects of the two approaches were indistinguishable. In both situations, injection of small hyperpolarising d.c. current pulses from -60 mV led to the generation of an identical LHP that was terminated by a LTCP, which in turn was followed by a prominent, long-lasting ADP (Fig. 4.3). In addition, these effects of *trans*-ACPD could be fully reversed following an equivalent dynamic clamp-induced artificial increase in g_{Leak} (g_{Leak} = +4.0 ± 0.7 nS) (Fig. 4.3B). Thus, the appearance of the LHP and ADP following the application of *trans*-ACPD can be fully accounted for by a reduction in g_{Leak}.

4.3.3 Bistability brought about by the interaction of $I_{Twindow}$ and I_{Kleak} underlies the mGluR1a-induced slow (<1Hz) oscillation.

As expected from previous studies (Williams et al. 1997a), the I_h channel blocker, ZD 7288 (50-300 μM) abolished the slow "sag" potential apparent during the LHP, leading to an *uncoupling* of the "up" and "down" states of the slow (<1Hz) sleep oscillation and the appearance of two distinct, stable resting membrane potentials, i.e. membrane potential bistability (n=19 of 19) (Fig. 4.4A). This membrane potential bistability is generated by a peculiar interaction between $I_{Twindow}$ and I_{KLeak} that occurs when g_{Leak} falls below a well-defined threshold

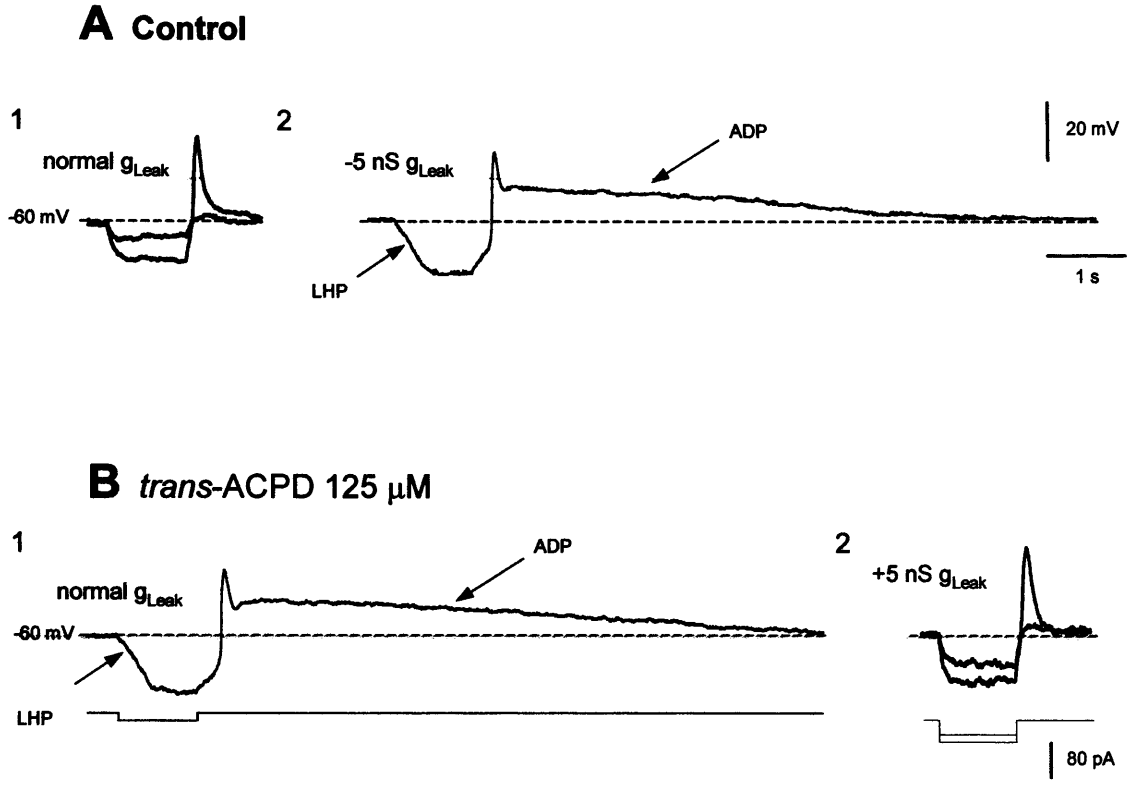

Figure 4.3 The effects of *trans*-ACPD are fully accounted for by a reduction in g_{Leak}.

(A) TC neurone exhibiting a conventional charging pattern in response to small hyperpolarizing current steps (-20 and -40 pA) (1). Following an artificial reduction in g_{Leak} (artificial g_{Leak} = -5 nS) using a dynamic clamp system, the neurone displays a characteristic LHP-ADP sequence in response to a 20 pA current step (2).

(B) An identical LHP-ADP sequence is apparent following *trans*-ACPD application (1). A subsequent artificial increase in g_{Leak} causes the neurone to exhibit identical behaviour to that observed in control conditions (2).

Note TTX (1 μM) was also present in the recording medium.

Published in Hughes et al. 2002b

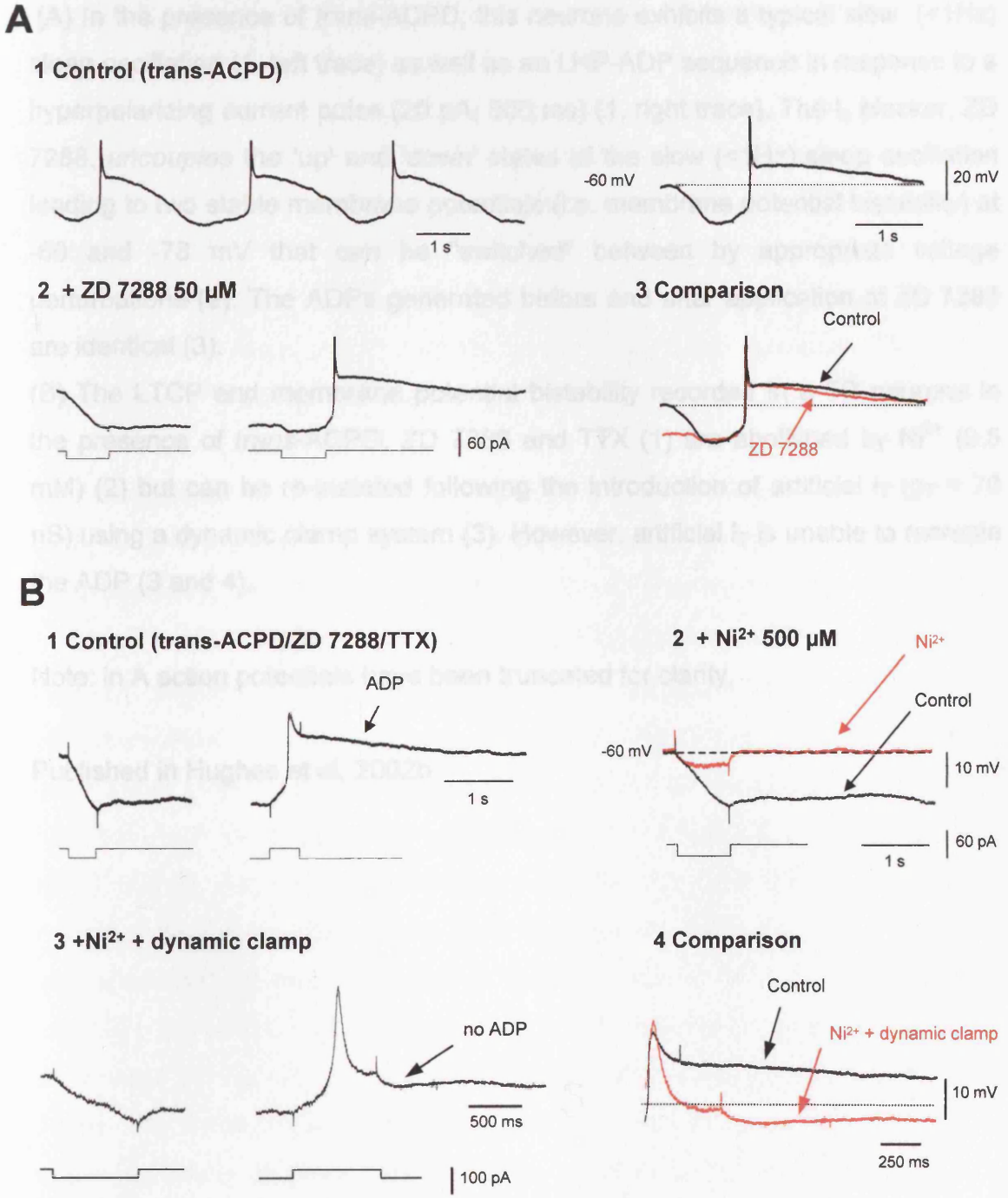

Figure 4.4 A bistable interaction between $I_{Twindow}$ and I_{KLeak} underlies the slow (<1Hz) sleep oscillation in TC neurones.

Figure 4.4 A bistable interaction between $I_{Twindow}$ and I_{KLeak} underlies the slow (<1Hz) sleep oscillation in TC neurones.

(A) In the presence of *trans*-ACPD, this neurone exhibits a typical slow (<1Hz) sleep oscillation (1, left trace) as well as an LHP-ADP sequence in response to a hyperpolarizing current pulse (20 pA, 800 ms) (1, right trace). The I_h blocker, ZD 7288, *uncouples* the 'up' and 'down' states of the slow (<1Hz) sleep oscillation leading to two stable membrane potentials (i.e. membrane potential bistability) at -60 and -78 mV that can be "switched" between by appropriate voltage perturbations (2). The ADPs generated before and after application of ZD 7288 are identical (3).

(B) The LTCP and membrane potential bistability recorded in a TC neurone in the presence of *trans*-ACPD, ZD 7288 and TTX (1) are abolished by Ni^{2+} (0.5 mM) (2) but can be re-instated following the introduction of artificial I_T (g_T = 70 nS) using a dynamic clamp system (3). However, artificial I_T is unable to recreate the ADP (3 and 4).

Note: in A action potentials have been truncated for clarity.

Published in Hughes et al. 2002b

(Williams et al. 1997a; Toth et al. 1998; Hughes et al. 1999). The two stable "up" and "down" states comprising the membrane potential bistability could be "switched" between by small membrane potential perturbations (Williams et al. 1997a; Hughes et al. 1999). As with the slow (<1Hz) sleep oscillation, the transition from "up" to "down" stable state was initiated by a marked inflection point, whilst the shift from "down" to "up" stable state was characterised by the generation of a LTCP and subsequent transient ADP (Fig. 4.4A_2). A comparison of the ADP generated in normal conditions with that exhibited following a block of I_h with ZD 7288 revealed no differences in either amplitude (14.3 ± 1.4 mV *vs* 14.8 ± 1.3 mV respectively; *P*=0.78) or duration (3.8 ± 0.5 s *vs* 3.9 ± 0.6 s respectively; *P*=0.86) (n=10 neurones) (Fig. 4.4A_3).

Membrane potential bistability and the LTCP were unaffected by TTX (1 μM) (n=6) (Fig. 4.4B_1), as expected from its lack of effect on the slow (<1Hz) sleep oscillation (see Fig. 4.1B) and by either of the K^+ channel blockers Ba^{2+} (1 mM) (n=5) or 4-AP (100-250 μM) (n=3). The high-voltage activated (HVA) Ca^{2+} channel blockers, Cd^{2+} (250-400 μM) (n=3), nifedipine (1-10 μM) (n=3), ω-conotoxin-MVIIC (3 μM) (n=6) or ω-conotoxin-GVIA (3 μM) (n=3) also failed to affect either membrane potential bistability or the LTCP. However, both bistability and the LTCP were selectively abolished by the T-type Ca^{2+} channel blocker, Ni^{2+} (350-500 μM) (n=4) (Fig. 4.4B_2) confirming that they are dependent on I_T and, in particular, that membrane potential bistability relies on $I_{Twindow}$. This point was supported by observing that in the presence of Ni^{2+}, introduction of an artificial I_T (g_T = 124 ± 36 nS; n=5) using a dynamic clamp system led to the re-apperance of membrane potential bistability (Fig. 4.4$B_{3\ and\ 4}$) (Hughes et al. 1999). The fundamental reliance of the slow (<1Hz) sleep oscillation on $I_{Twindow}$ was conclusively illustrated by noting its abolition by Ni^{2+} (350-500 μM) (n=5) (Fig. 4.5A), but not by either the high-voltage activated (HVA) Ca^{2+} channel blocker Cd^{2+} (250-400 μM) (n=4) (Fig. 4.5B), nifedipine (1-10 μM) (n=4), Ba^{2+} (1 mM) (n=4) or 4-AP (100-250 μM) (n=2).

4.3.4 A Ca^{2+}-activated, non-selective cation current underlies the ADP.

In addition to blocking both membrane potential bistability and the slow (<1Hz) sleep oscillation, Ni^{2+} also always abolished the ADP (n=9 of 9) (Fig. 4.4B_2 and

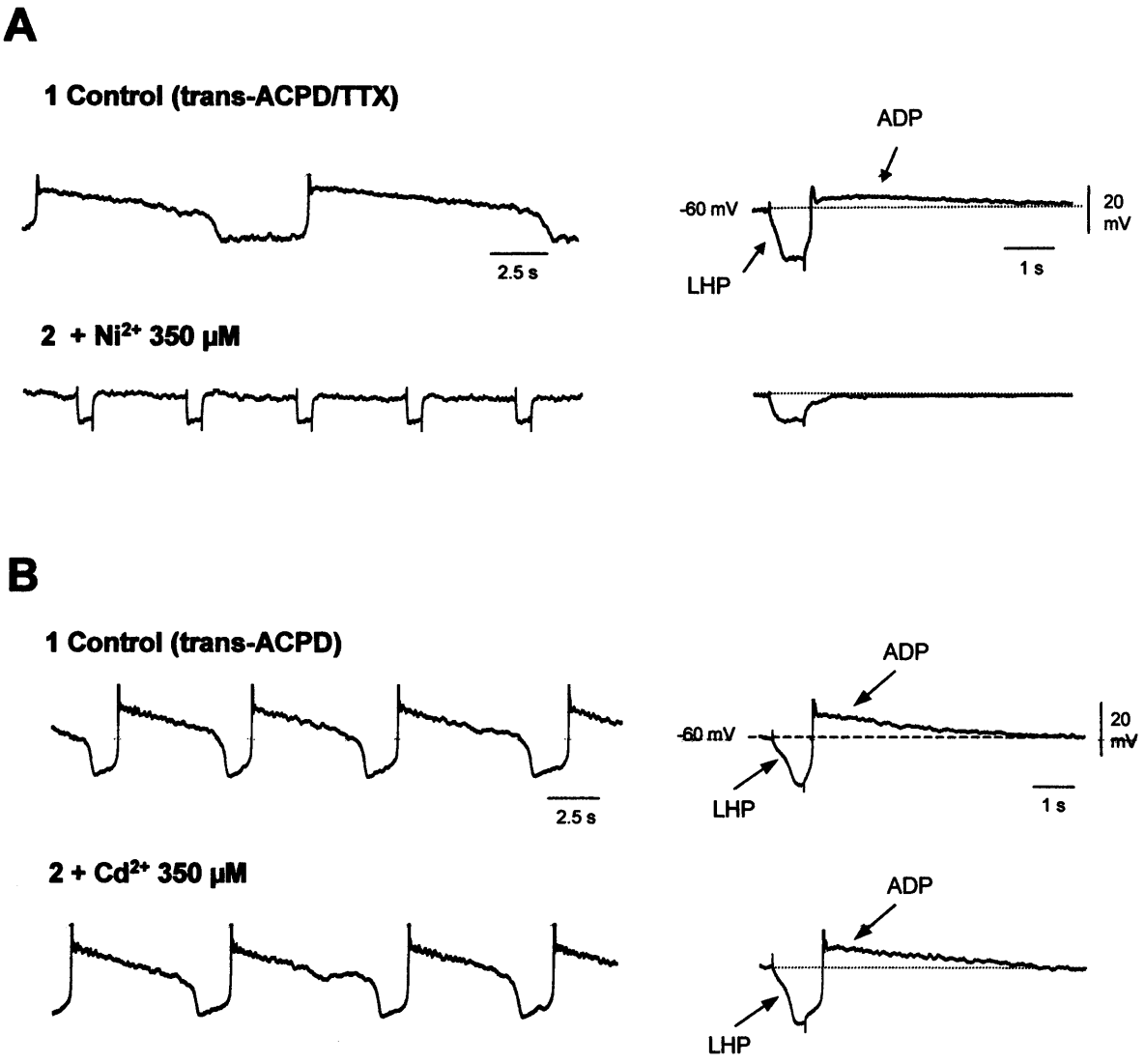

Figure 4.5 The slow (<1Hz) sleep oscillation is dependent on T-type Ca^{2+} channels.

(A) The slow (<1Hz) sleep oscillation recorded in the presence of *trans*-ACPD and TTX (1, left trace) and the LHP-ADP response of the neurone to a small hyperpolarizing current pulse (50 pA, 1 s) (1, right trace) are eliminated by Ni^{2+} (350 µM) (left trace) (2, left and right traces).

(B) Both the slow (<1Hz) oscillation and the pulse-induced LHP and ADP are unaffected by Cd^{2+} (350 µM).

Note: in B action potentials have been truncated for clarity.

Published in Hughes et al. 2002b

4.5A_2). Furthermore, whilst artificial I_T was able to restore bistability following its block by Ni^{2+}, it was unable to recreate the ADP (Fig. 4.4$B_{3 \text{ and } 4}$). Since artificial I_T fully replicates the biophysical properties of endogenous I_T (Hughes et al. 1999) except that it is not carried by Ca^{2+}, it was reasoned that the ADP must involve a Ca^{2+}-dependent conductance. This conclusion was supported by the observation: that the inclusion of either of the Ca^{2+} chelators, BAPTA (100 mM) (n=3) or EGTA (50-100 mM) (n=5) in the intracellular electrode abolished the ADP without any loss in R_N (Fig. 4.6A).

The ADP was unchanged by either TTX (1 μM) (n=21) (Fig. 4.1B, 4.3 and 4.5A), Cd^{2+} (250-400 μM) (n=10) (Fig. 4.5B), nifedipine (1-10 μM) (n=6), ω-conotoxin-MVIIC (3 μM) (n=6) or ω-conotoxin-GVIA (3 μM) (n=3) (P>0.5) illustrating that it does not involve TTX-sensitive Na^+ channels and is not dependent on Ca^{2+} entry through HVA Ca^{2+} channels. In addition, Ba^{2+} (1 mM) (n=5) and 4-AP (100-250 μM) (n=3) either did not affect the ADP, or led to its enhancement due to an increase in R_N. This result indicated that suppression of K^+ currents due to Ca^{2+} influx during the LTCP was not the major mechanism responsible for the generation of the ADP (Tokimasa 1985; Chen 1991). Replacement of NaCl with choline chloride failed to affect the generation of the ADP (n=5). However, substitution of the majority (134 mM) of Na^+ with $NMDG^+$ reversibly inhibited the ADP (n=7) (Fig. 4.6B). These properties strongly suggested that the ADP is generated by a Ca^{2+}-activated, non-selective cation current, I_{CAN} (Partridge and Swandulla 1988), as is the case for similar behaviour in other types of thalamic neurones (Bal and McCormick 1993; Zhu et al. 1999). In order to test this hypothesis, a hybrid current/voltage clamp protocol was employed that enabled a direct measurement of the current underlying the ADP. Switching the amplifier from current to voltage clamp at the peak of the ADP revealed a small, slowly decaying inward current (Fig. 4.7B). By measuring the difference in current between the peak of the ADP and at steady-state when the ADP has decayed, it was found that the current responsible for the ADP 1) exhibited an amplitude (-21.7 ± 6.4 pA at -60 mV; n=5) that was linearly related to membrane potential (Fig. 4.7C), 2) showed an extrapolated reversal potential of 8.7 ± 1.1 mV (n=5) (Fig. 4.7C), and 3) displayed a time-course that decayed mono-exponentially in a voltage-independent manner with τ_{decay} = 1.44 ± 0.3 s (n=5) (Fig. 4.7B). These measurements were unaffected by TTX (1 μM) and Ba^{2+} (1-2 mM) (amplitude at

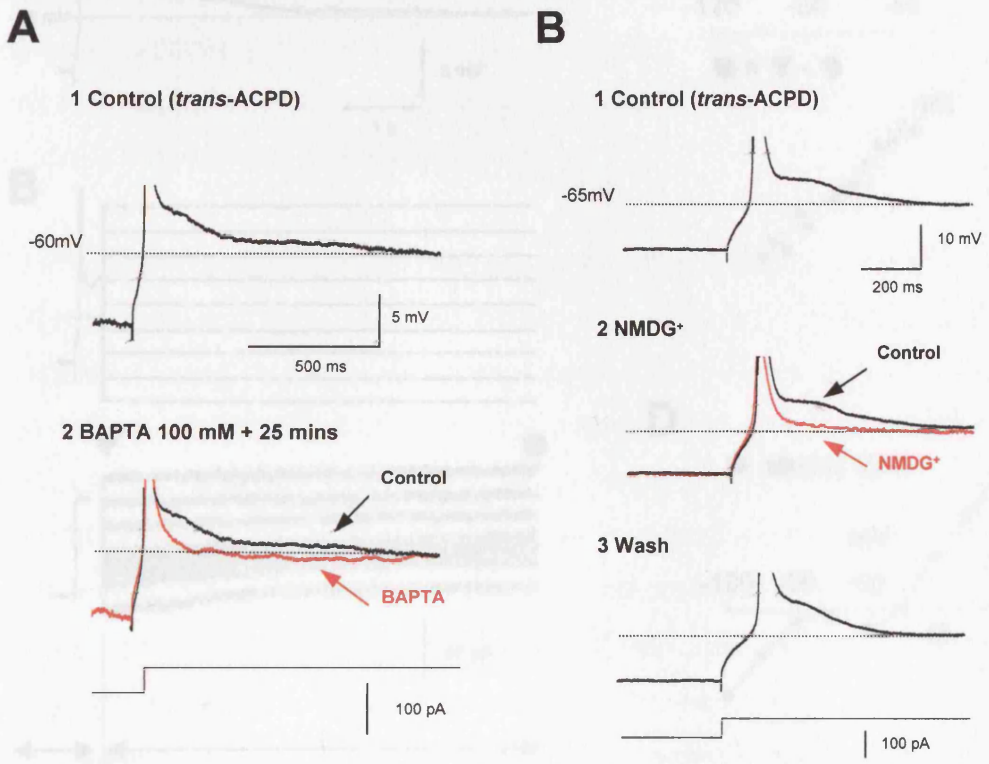

Figure 4.6 The ADP is generated by a Ca^{2+} and Na^{+} dependent mechanism.
(A) Releasing a TC neurone from hyperpolarization leads to the generation of a LTCP followed by an ADP. (1, recorded directly after impalement). The ADP is abolished by inclusion of BAPTA (100 mM) in the recording electrode (2, recorded 25 minutes after neuronal impalement).
(B) The ADP in TC neurones (1) is reversibly blocked by substituting extracellular Na^{+} (134 mM) with equimolar $NMDG^{+}$ (2 and 3).

(Note: ZD 7288, 50 μM, was present in all experiments depicted in this figure. LTCPs have been truncated for clarity).

Published in Hughes et al. 2002b

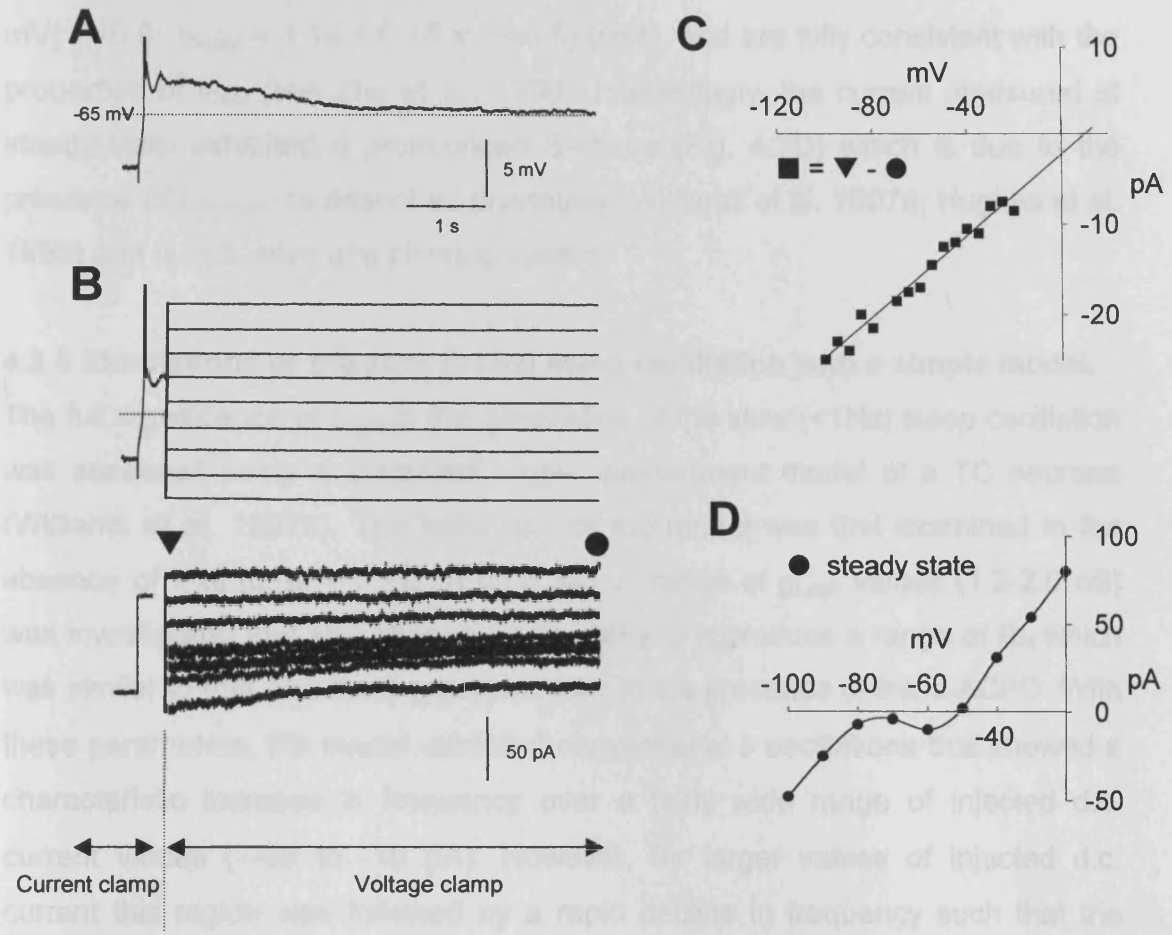

Figure 4.7 The ADP is generated by a slowly decaying inward current.

(A) Typical example of the ADP following a LTCP in a TC neurone.

(B) Switching the recording amplifier from current to voltage clamp at the peak of the ADP reveals the presence of a slow inward current.

(C) The "difference-current" (■) measured between the peak of the ADP (▼) and at steady-state (●), i.e. the current underlying the ADP, possesses an amplitude that is linearly related to membrane potential and exhibits an extrapolated reversal potential of +10 mV.

(D) The steady-state I-V relationship exhibits a pronounced 'S' shape, which is due to $I_{Twindow}$ and indicates an underlying bistable system (Hughes et al 1999).

(Note: ZD 7288, 50 μM, was present in all experiments depicted in this figure. Action potentials have been truncated for clarity).

Published in Hughes et al. 2002b

-60 mV = -24.3 ± 10.5 pA; *P*=0.5; extrapolated reversal potential = 11.7 ± 4.7 mV; *P*=0.8; τ_{decay} = 1.14 ± 0.16 s; *P*=0.5) (n=4), and are fully consistent with the properties of I_{CAN} (see Zhu et al., 1999). Interestingly, the current measured at steady-state exhibited a pronounced S-shape (Fig. 4.7D) which is due to the presence of $I_{Twindow}$ as described previously (Williams et al. 1997a; Hughes et al. 1999) and is indicative of a bistable system.

4.3.5 Simulations of the slow (<1Hz) sleep oscillation with a simple model.

The full significance of I_{CAN} in the generation of the slow (<1Hz) sleep oscillation was assessed using a simplified single compartment model of a TC neurone (Williams et al. 1997a). The behaviour of the model was first examined in the absence of I_{CAN} (g_{CAN} = 0 nS) (Fig. 4.8A). A range of g_{Leak} values (1.2-2.0 nS) was investigated that was chosen for its ability to reproduce a range of R_N which was similar to that observed experimentally in the presence of *trans*-ACPD. With these parameters, the model exhibited conventional δ oscillations that showed a characteristic increase in frequency over a fairly wide range of injected d.c. current values (~-50 to -10 pA). However, for larger values of injected d.c. current this region was followed by a rapid decline in frequency such that the minimum frequency of the oscillation was achieved at the most positive level of injected d.c. current for which an oscillation existed (Fig. 4.8A_2). The voltage waveform of the oscillation at frequencies <1Hz was similar to that observed experimentally (Fig. 4.8A_1). However, the range of currents for which a slow oscillation could be produced by the model under these conditions was extremely narrow (<1.5 pA) (Fig. 4.8A_2). Thus, with g_{CAN} = 0 nS the model is unable to support the stable generation of a slow oscillation. In addition, with g_{CAN} = 0 nS the model does not exhibit "grouped" δ oscillations (Fig. 4.8C_1, middle trace; see also Fig. 4.1A_2 and B).

The model was next examined in the presence of I_{CAN} (Fig. 4.8B_1) using a range of maximal conductance values (g_{CAN} = 5-10 nS) that led to this current exhibiting similar properties to those observed in experiments. Under these conditions, although oscillatory frequency showed an initial increase, followed by a sharp decrease in response to increasing injected d.c. current, as witnessed with g_{CAN} = 0 nS, the sharp decrease was than followed by a region where

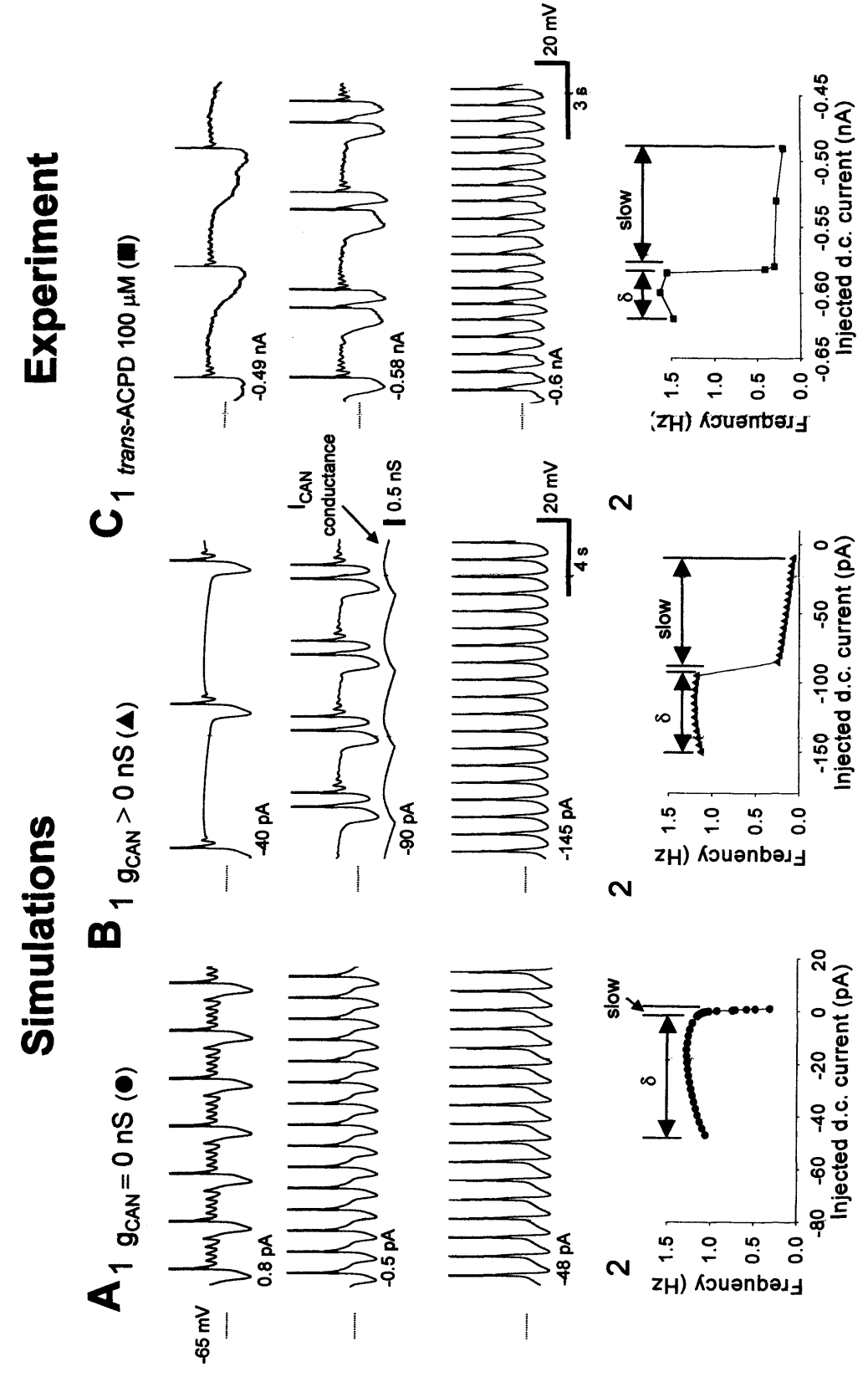

Figure 4.8 The slow (<1Hz) sleep oscillation in a simplified model of a TC neurone.

Figure 4.8. The slow (<1Hz) sleep oscillation in a simplified model of a TC neurone.

(A) In the absence of I_{CAN} (i.e. g_{CAN} = 0 nS), a model TC neuron with g_{Leak} = 1.5 nS exhibits a slow oscillation (1) but only for a very narrow range of d.c. current inputs (2).

(B) With g_{CAN} = 10 nS, the model exhibits a slow oscillation over a much greater range of d.c. current inputs (1 and 2). Furthermore, the model is able to exhibit "grouped" δ oscillations as a transition stage between a continuous δ oscillation and a pure slow (<1Hz) oscillation. The δ activity occurs whilst the conductance of I_{CAN} is accumulating to a point where it is able to facilitate the generation of a prolonged 'up' state.

(C) Experimental traces obtained in the presence of *trans*-ACPD show almost identical properties to those in B_1. Also, the current vs frequency plot for the experimental scenario possesses a similar form to that shown in B_2.

Published in Hughes et al. 2002b

oscillation frequency *gradually* decreased from 0.24 to 0.06 Hz over a relatively large range of injected d.c. currents (75 pA, i.e. -85 to -10 pA, for g_{CAN} = 10 nS) (Fig. 4.8B_2). The mean rate of decrease of frequency with respect to current for this "slow" region (0.0024 Hz pA^{-1}) was similar to that observed in experiments (e.g. 0.0023 Hz pA^{-1} or 0.41 to 0.2 Hz over 90 pA in Fig. 4.8C). Thus, I_{CAN} stabilises the slow (<1Hz) sleep oscillation over a wide range of conditions. I_{CAN} achieves this effect by transforming what would normally be a δ oscillation (see region labelled "δ" in Fig. 4.8A_2) into a slow oscillation by temporarily depolarising the cell following a LTCP into or beyond the region (labelled "slow" in Fig. 4.8A_2) where it can naturally exhibit a slow oscillation in the absence of I_{CAN} (i.e. top trace in Fig. 4.8A_1). The waveforms of the slow oscillation generated with g_{CAN} > 0 nS were very similar to those observed experimentally (Fig. 4.8C_1). Furthermore, for specific values of injected d.c. current, marking the transition between a continuous δ oscillation (Fig. 4.8B_1, bottom trace) and a pure slow (<1Hz) sleep oscillation (Fig. 4.8B_1, top trace), the model exhibited "grouped" δ activity (Fig. 4.8B_1, middle trace) that was similar to that observed in experiments (Fig. 4.8C_1, middle trace). The "grouped" δ activity occurs at a level of injected d.c. current where the effect of I_{CAN} following a single LTCP is just insufficient to force a prolonged depolarisation. However, since a second LTCP occurs before I_{CAN} has not significantly decayed, the conductance of I_{CAN} accumulates and becomes large enough to facilitate a prolonged depolarisation (Fig. 4.8B_1, middle trace).

4.4. DISCUSSION

The novel findings described in this chapter are 1) the slow (<1Hz) sleep oscillation in TC neurones is generated by a bistable interaction between $I_{Twindow}$ and a reduced I_{KLeak} and 2) I_{CAN} underlies the ADP in TC neurones and serves to enhance and stabilise the slow (<1Hz) sleep oscillation.

4.4.1 Biophysical mechanisms underlying the slow (<1Hz) sleep oscillation.

The slow (<1Hz) sleep oscillation in TC neurones induced following *trans*-ACPD application possesses almost identical properties to those observed in previous studies in a small sample of neurones with an unusually low g_{Leak} in control conditions (Williams et al. 1997a), or in all TC neurones following an artificial reduction in g_{Leak} (Hughes et al. 1999). In these neurones, slow oscillatory

activity depends on a bistable interaction between $I_{Twindow}$ and I_{KLeak}. The presence of this interaction in TC neurones can be easily detected since a pharmacological block of I_h instigates full membrane potential bistability (i.e. two distinct stable 'up' and 'down' states) in these cells (see Fig. 4.4A and B_2). Thus, based on the following evidence, the slow (<1Hz) sleep oscillation described here also results from an $I_{Twindow}$-I_{KLeak} bistable interaction; 1) the main reported effect of mGluR-activation in TC neurones is to reduce g_{Leak} (McCormick and von Krosigk 1992; Turner and Salt 2000) and as shown here, all the effects of *trans*-ACPD on the properties of TC neurones relevant to the slow (<1Hz) sleep oscillation could be mimicked by a simple artificial reduction in g_{Leak} (Hughes et al. 1999); 2) following the application of ZD 7288, neurones that exhibit the slow (<1Hz) sleep oscillation display full membrane potential bistability that is blocked by Ni^{2+}, and can be subsequently re-induced by artificial I_T; 3) the slow (<1Hz) sleep oscillation and membrane bistability are unaffected by other Ca^{2+} channel blockers; and 4) the slow (<1Hz) sleep oscillation is also selectively abolished by Ni^{2+}. Therefore, the most critical component in the generation of the slow (<1Hz) sleep oscillation in TC neurones is $I_{Twindow}$.

The likelihood that TC neurones exhibit the slow (<1Hz) sleep oscillation following mGluR-activation was dependent on their R_N in control conditions with larger values leading to an increased prevalence. This finding is consistent with the necessity for g_{Leak} to fall below a well-defined threshold before the slow (<1Hz) sleep oscillation can be observed (Toth et al. 1998; Hughes et al. 1999) and may explain why some previous investigations into the effects of *trans*-ACPD on TC neurones have failed to observe similar activities to those described here (McCormick and von Krosigk 1992; Lee and McCormick 1997; Tennigkeit et al. 1999; Zhan et al. 2000; Gutierrez et al. 2001), while others have (Turner and Salt 2000). Since the R_N of TC neurones recorded *in vivo* is much lower than that observed *in vitro*, it could be argued that the slow oscillation described here is unlikely to occur *in vivo*. However, TC neurones recorded *in vivo* readily exhibit the intrinsic δ oscillation (Steriade et al. 1991a; Curro Dossi et al. 1992) despite the fact that *in vitro* this activity is necessarily correlated with a large value of R_N (Turner et al. 1997). This suggests that it is meaningless to make predictions about the potential to exhibit oscillatory behaviour *in vivo* based

purely on a comparison of measurements of apparent input resistance obtained *in vitro* and *in vivo*.

4.4.3 The ADP and role of I_{CAN} in the generation of the slow (<1Hz) sleep oscillation.

Regardless of whether or not TC neurones displayed the slow (<1Hz) sleep oscillation following *trans*-ACPD application, the appearance of a pronounced ADP after a LTCP was always evident. Since an identical ADP could be brought about following a simple artificial reduction in g_{Leak}, its appearance is unlikely to be due to anything more than a reduction in g_{Leak} (McCormick and von Krosigk 1992; Lee and McCormick 1997) as opposed to a combination of other mGluR-related mechanisms that have been described (Tennigkeit et al. 1999; Chuang et al. 2000). The following experimental observations support the conclusion that the ADP is generated by I_{CAN} (Partridge and Swandulla 1988); 1) the inability of artificial I_T to promote an ADP; 2) the vulnerability of the ADP to intracellular Ca^{2+} chelation; 3) the insensitivity of the ADP to ZD 7288; 4) the dependence of the ADP on the presence of extracellular Na^+; and 5) the biophysical properties of the transient inward current generated following a LTCP. The reason this current has not been appreciated in previous studies of TC neurones is presumably due to its masking by a larger I_{KLeak} in control conditions.

Investigations using a biophysical model of a TC neurone confirmed that I_{CAN} is crucial to the generation of the slow (<1Hz) sleep oscillation. Indeed, in the absence of I_{CAN}, the model was unable to provide a full explanation for the slow (<1Hz) sleep oscillation observed experimentally, since oscillations at frequencies <1 Hz could only be observed for a very narrow range of injected d.c. currents. The presence of I_{CAN} modifies this scenario by transforming what would usually be a conventional δ oscillation into a slow (<1Hz) sleep oscillation by transiently depolarising the cell following a LTCP into or beyond the narrow region where a slow oscillation can exist in the absence of I_{CAN}. Thus whilst $I_{Twindow}$ is responsible for the basic "up" and "down" states of the slow (<1Hz) oscillation, the enhancement and prolongation of the 'up' state by I_{CAN} is crucial in order to stabilize and enhance the expression of the oscillation over a wide range of conditions. In addition, due to the ability of I_{CAN} to "build up" over a number of LTCP events, its inclusion in the model is also able to fully explain the

experimental observation of "grouped" δ oscillations (Steriade et al. 1993a). A similar ADP has recently been shown in LGN TC neurones of the ferret (Lüthi and McCormick 1998). In contrast with our results, this ADP is thought to be generated by a Ca^{2+}-mediated upregulation of I_h and is believed to be, at least in part, responsible for the waxing and waning of spindle-like oscillations in TC neurones in thalamic slices (Bal and McCormick 1996). However, the lack of effect of the specific I_h-blocker, ZD 7288, on the ADP observed in this study suggests that I_h has no involvement its generation. Rather, the role of I_h in the slow oscillation is to dictate the duration of the stereotypical "down" phase or LHP and facilitate the transition from the "down" to "up" state.

Therefore, the basic biophysical mechanism of the slow (<1Hz) slow sleep oscillation has been fully elucidated and is summarised in Fig. 4.9. That is, activation of I_T generates a LTCP, usually evoking a burst of action potentials and entry of Ca^{2+} into the neurone. Following the peak of the LTCP, $I_{Twindow}$ remains "switched on" effectively inducing the "up" phase. Ca^{2+} entry during the LTCP activates I_{CAN} that stabilises and enhances the "up" phase but then slowly decays. During decay of the "up" phase, the membrane potential slowly hyperpolarises, and at a critical point $I_{Twindow}$ subsequently "switches off" and an LHP is initiated. The LHP rapidly and sufficiently hyperpolarises the membrane potential to activate I_h which brings about the slow repolarisation of the membrane potential and the initiation of an subsequent LTCP. In this way rhythmic activity at (<1Hz) can be sustained.

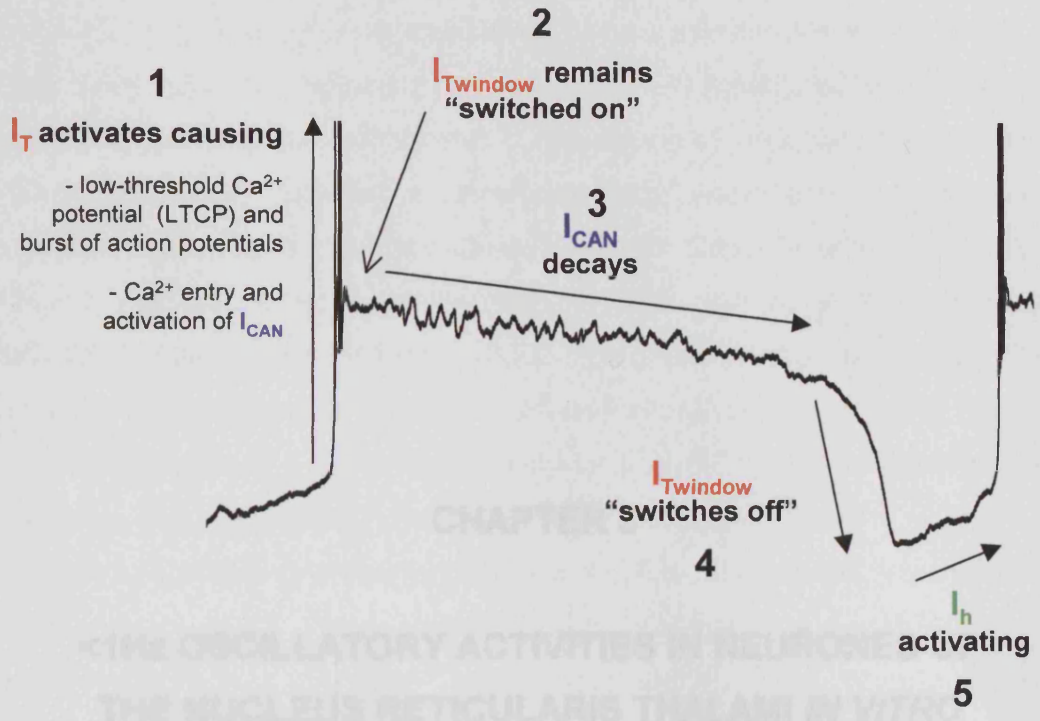

Figure 4.9 Mechanism of the slow (<1Hz) sleep oscillation in TC neurones.

Schematics figure showing the biophysical mechanism of the slow (<1Hz) sleep oscillation in TC neurons in *vitro*.

Activation of I_T (1) generates a LTCP, evoking a burst of action potentials in this case, and entry of Ca^{2+} into the neurone. $I_{Twindow}$ remains "switched on" effectively instating the "up" phase (2). Ca^{2+} entry during the LTCP activates I_{CAN} that stabalises and enhances the "up" phase but then slowly decays (3). During decay of the "up" phase, the membrane potential slowly hyperpolarises, and $I_{Twindow}$ subsequently "switches off" and an LHP is initiated (4). The LHP rapidly and sufficiently hyperpolarises the membrane potential to activate I_h which brings about the slow repolarisation of the membrane potential (5) and the initiation of an LTCP to restart the cycle again.

CHAPTER 5

<1Hz OSCILLATORY ACTIVITIES IN NEURONES OF THE NUCLEUS RETICULARIS THALAMI *IN VITRO*

5.1 INTRODUCTION

NRT neurones display rhythmic oscillatory activity at two distinct frequency ranges during sleep stages: a slow (<1Hz) oscillation and spindle oscillations typically occurring at (7-14Hz) (Mulle et al. 1986; Steriade et al. 1987; Steriade et al. 1993a). The slow (<1Hz) oscillation occurs in phase with the EEG slow (<1Hz) sleep rhythm (Steriade et al. 1993a) and is manifested in a very similar way to that observed in cortical and TC neurones *in vivo*: that is comprising of rhythmic transitions between a depolarised "up" state and a hyperpolarised "down" state (see Fig. 1.16) (Steriade et al. 1993a; Steriade et al. 1996). Like TC neurones, NRT neurones receive a major cortical input via corticothalamic axon collaterals (Robson 1984; Montero 1989). The mGluR component of this cortical input has been shown to induce a robust depolarisation of NRT neurones through modulation of I_{KLeak} (Lee and McCormick 1997; von Krosigk et al. 1999). In addition, the overlapping activation and inactivation kinetics of I_T in NRT neurones, predicting the existence of a window component for this current (Chemin et al. 2002; Perez-Reyes 2003), indicates that bistability-mediated activities may be present in NRT neurones. In addition, the presence of I_{CAN} in NRT neurones (Bal and McCormick 1993) suggests that NRT neurones have all the components that are responsible for the manifestation of a slow (<1Hz) oscillation (as in TC neurones, see Chapter 4). Therefore, given the similarity of the slow (<1Hz) oscillation in TC and NRT neurones *in vivo*, and that mGluR activation modulates I_{KLeak} in both NRT neurones (Lee and McCormick 1997; von Krosigk et al. 1999) and in TC neurones (McCormick and von Krosigk 1992), then mGluR activation alone may also induce a slow (<1Hz) oscillation in NRT neurones.

Spindle oscillations in NRT neurones are grouped within a <1Hz rhythm: occurring as discrete rhythmic events at 7-14Hz on a depolarising envelope typically recurring at 0.1-0.2 Hz (Steriade et al. 1986; Contreras and Steriade 1996). Spindle oscillations are generated by the NRT as they survive in isolated islands that are disconnected from TC and corticothalamic inputs (Steriade et al. 1987). Through their interconnections to TC neurones, spindle frequency inhibitory inputs impinge on TC neurones evoking rebound LTCPs in TC neurones (Mulle et al. 1985; Steriade et al. 1987) that are then transferred to the cortex giving rise to EEG spindle waves (Steriade et al. 1987). Corticothalamic

inputs are implicated in the organisation of spindle oscillations as both EEG sleep spindles and thalamic spindle oscillations are highly synchronised in the intact brain (Contreras and Steriade 1996; Contreras et al. 1997). In the absence of cortical inputs local, but not global, synchronisation of spindle oscillations occurs in the thalamus (Contreras and Steriade 1996; Contreras et al. 1997). The origin of this local synchronisation is thought to be the NRT given that spindles survive disconnection form TC neurones (Steriade et al. 1987). This again suggests that the NRT alone generates a <1Hz oscillation that groups spindle oscillation. Previous in *vitro* studies in thalamic slices with intact TC-NRT connections have demonstrated the presence of "spindle-like" oscillations in TC neurones (von Krosigk et al. 1993). This type of "spindle-like" oscillation in TC neurones is maintained through reciprocal burst firing in TC and NRT neurones and up regulation of I_h in TC neurones (Luthi et al. 1998; Lüthi and McCormick 1998), but the activity of the NRT neurones during these "spindle-like" oscillations does not reproduce that observed during spindle oscillations *in vivo*.

Therefore in light of the effect of postsynaptic mGluR activation in TC neurones in unmasking (<1Hz) oscillatory activity (see Chapters 3 and 4) (Williams et al. 1997a; Hughes et al. 1999), the effect of post-synaptic mGluR activation in NRT neurones maintained *in vitro* was investigated. In addition to the prediction that a slow (<1Hz) oscillation should be induced following mGluR activation, the ability of NRT neurones / networks to generate spindle oscillations *in vitro* isolated from other inputs was also of interest.

5.2 METHODS

5.2.1 Electrophysiology.

Intracellular and extracellular recordings were performed in adult cat thalamic slices containing the LGN, VB or VL with the associated portion of the NRT as described in Chapter 2. In the following descriptions, all neurones will be referred to as NRT neurones regardless of the associated thalamic relay nucleus.

5.2.2 Data analysis.

Data analysis was performed as described in Chapter 2.

5.2.3 Drugs.

Drugs were obtained, applied and used at concentrations as described in Chapter 2. The $GABA_A$ receptor antagonist SR 95531 was used during both intracellular and extracellular recordings from NRT neurones as BMI, the $GABA_A$ antagonist routinely used during electrophysiological recording of TC neurones, has been shown to block the AHP following LTCP-mediated bursts in NRT neurones (Debarbieux et al. 1998).

5.3 RESULTS

5.3.1 Application of *trans*-ACPD induces a slow (<1Hz) oscillation in NRT neurones.

NRT neurones recorded intracellularly under control conditions (in the presence of aCSF alone) predominantly showed no oscillatory activity and had stable resting membrane potentials below the threshold for action potential firing (mean resting potential = -63.4 ± 2.4 mV, n=17) (Fig. 5.1A). Other NRT neurones, recorded under the same conditions, displayed low frequency tonic action potential firing (mean tonic firing rate = 5.8 ± 1.7 Hz, n=4). Under these conditions, the R_N of recorded neurones was 130.7 ± 13.6 MΩ (n=21). All neurones displayed electrophysiological characteristics previously described in NRT neurones and were positively identified by the accelerating then decelerating LTCP-mediated burst (Fig. 5.1_{2b}) (Domich et al. 1986; Llinas and Geijo-Barrientos 1988; Avanzini et al. 1989; Bal and McCormick 1993; Contreras et al. 1993). In 33% of neurones (n=7), rebound bursting was evoked at the offset of hyperpolarising current steps and could be followed by a period of tonic firing (Avanzini et al. 1989; Bal and McCormick 1993; Contreras et al. 1993).

Application of the non-specific mGluR agonist *trans*-ACPD (100μM) to NRT neurones recorded in aCSF alone resulted in depolarisation such that in the absence of injected d.c. current neurones displayed tonic firing (39.0 ± 12.0 Hz, n=8). In addition, the R_N of recorded neurones was increased by the application of *trans*-ACPD (ΔR_N = 64.0 ± 29.1 MΩ, n= 8, 49.2%). In the absence of injected d.c. current, a depolarised state and thus tonic firing characterised the activity of the NRT neuronal population (n=37) recorded in the presence of *trans*-ACPD (Fig. 5.1B) (tonic firing rate = 37.8 ± 4.3 Hz, R_N = 162.7 ± 10.4 MΩ, n=37). NRT

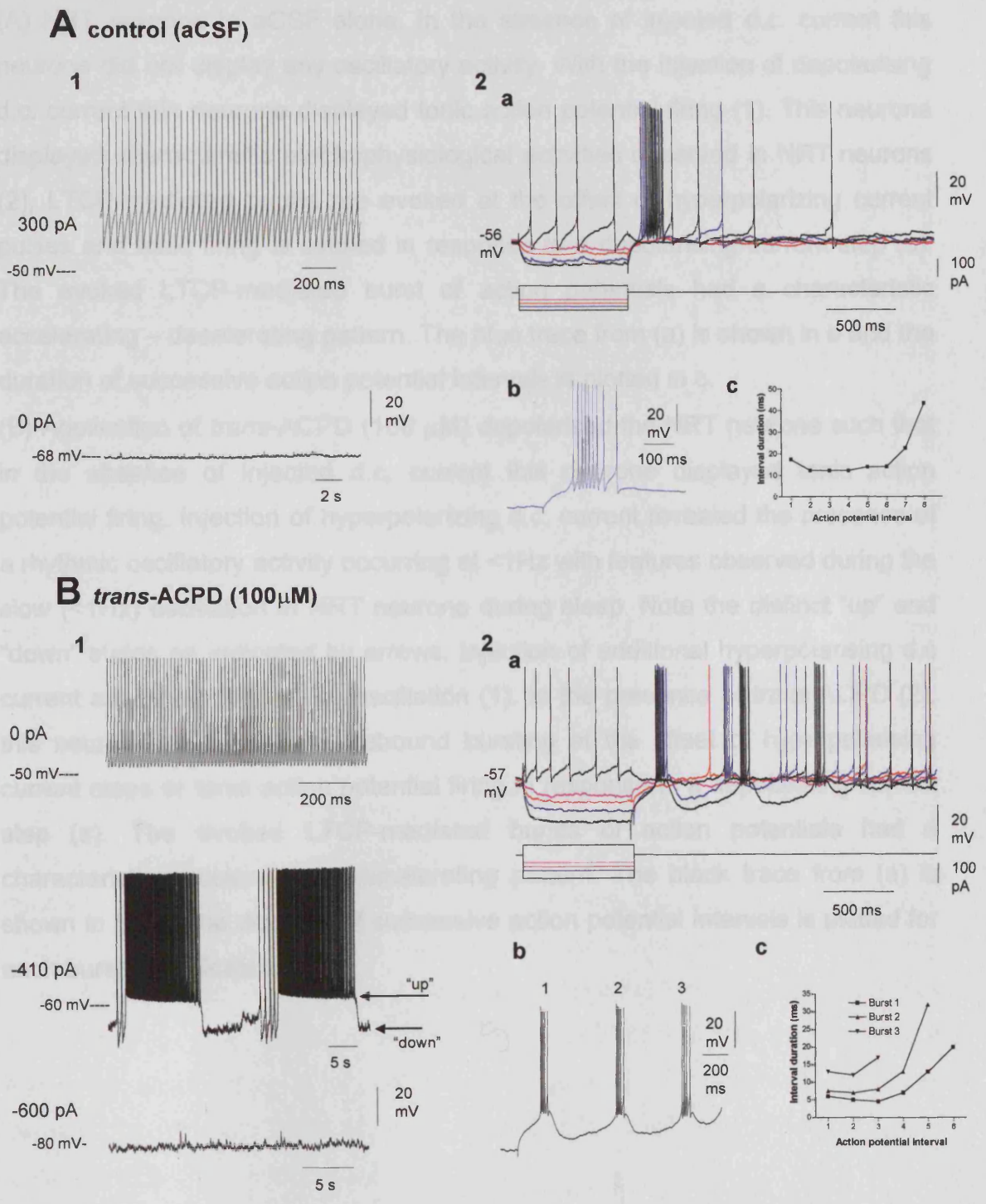

Figure 5.1 *Trans*-ACPD induces a slow (<1Hz) oscillation in NRT neurones.

Figure 5.1 *Trans*-ACPD induces a slow (<1Hz) oscillation in NRT neurones.

(A) NRT neurone in aCSF alone. In the absence of injected d.c. current this neurone did not display any oscillatory activity. With the injection of depolarising d.c. current thin neurone displayed tonic action potential firing (1). This neurone displayed characteristic electrophysiological activities observed in NRT neurons (2), LTCP-mediated bursts are evoked at the offset of hyperpolarizing current pulses and tonic firing is evoked in response to a depolarising current step (a). The evoked LTCP-mediated burst of action potentials had a characteristic accelerating – decelerating pattern. The blue trace from (a) is shown in b and the duration of successive action potential intervals is plotted in c.

(B) Application of *trans*-ACPD (100 μM) depolarised the NRT neurone such that in the absence of injected d.c. current this neurone displayed tonic action potential firing. Injection of hyperpolarizing d.c. current revealed the presence of a rhythmic oscillatory activity occurring at <1Hz with features observed during the slow (<1Hz) oscillation in NRT neurone during sleep. Note the distinct "up" and "down" states as indicated by arrows. Injection of additional hyperpolarising d.c current abolished the (<1Hz) oscillation (1). In the presence of *trans*-ACPD (2), this neurone also displayed rebound bursting at the offset of hyperpolarising current steps or tonic action potential firing in response to a depolarising current step (a). The evoked LTCP-mediated bursts of action potentials had a characteristic accelerating – decelerating pattern. The black trace from (a) is shown in b and the duration of successive action potential intervals is plotted for each burst as indicated in c.

neurones retained their identifying electrophysiological characteristics in the presence of *trans*-ACPD. An increase in the proportion of neurones displaying rebound bursts as the offset of hyperpolarising current pulses was also observed in the presence of *trans*-ACPD (51%, n=19) (Fig. 5.1B_2).

In addition to robust neuronal depolarisation and hence the induction of tonic action potential firing in NRT neurones, oscillatory activity at slow (<1Hz) frequencies was also apparent when neurones were hyperpolarised through injection of d.c. current in the presence of *trans*-ACPD (Fig. 5.1B). Slow (<1Hz) oscillatory activity was apparent in 43% of NRT neurones (16 of 37) and was manifested as rhythmic sequences of sustained action potential firing (the "up" phase) interspersed by quiescence (the "down" phase) that sometimes could be partly replaced by rhythmic bursting (Fig. 5.1B) and occurred at frequencies ranging from 0.02 – 0.7 Hz, minimum = 0.16 ± 0.04 Hz (n=16). A higher input resistance was associated with neurones displaying oscillatory activity at <1Hz (oscillating neurones: R_N = 156.7 ± 14.3 MΩ (n= 16), non-oscillating neurones: R_N = 132.0 ± 24.9 MΩ (n=21) although this was not statistically significant (P = 0.26).

In NRT neurones, in the presence of *trans*-ACPD, slow (<1Hz) oscillatory activity showed a clear dependence on the level of injected d.c. current, becoming apparent during removal of injected hyperpolarising d.c. current (Fig. 5.2) and therefore during the transition from a quiescent hyperpolarised membrane potential (Fig. 5.2A, -650pA) to a depolarised level where only tonic firing was apparent (Fig. 5.2, -400pA). Initially on removal of injected d.c. current, δ frequency activity (Fig. 5.2A, -530pA) was apparent. Subsequently as further injected d.c. current was removed slow (<1Hz) oscillatory activity became apparent (Fig. 5.2A, –480pA and -440pA).

5.3.2 Neuronal depolarisation decreases the frequency of the slow (<1Hz) oscillation.

The frequency of ongoing slow (<1Hz) oscillatory activity decreased during removal of injected hyperpolarising d.c. current (Fig. 5.2A, 5.3A and B, Fig. 5.5A). As neurones were released from injected hyperpolarising d.c. current, the "up" phase (measured as the duration of sustained action potential firing) was

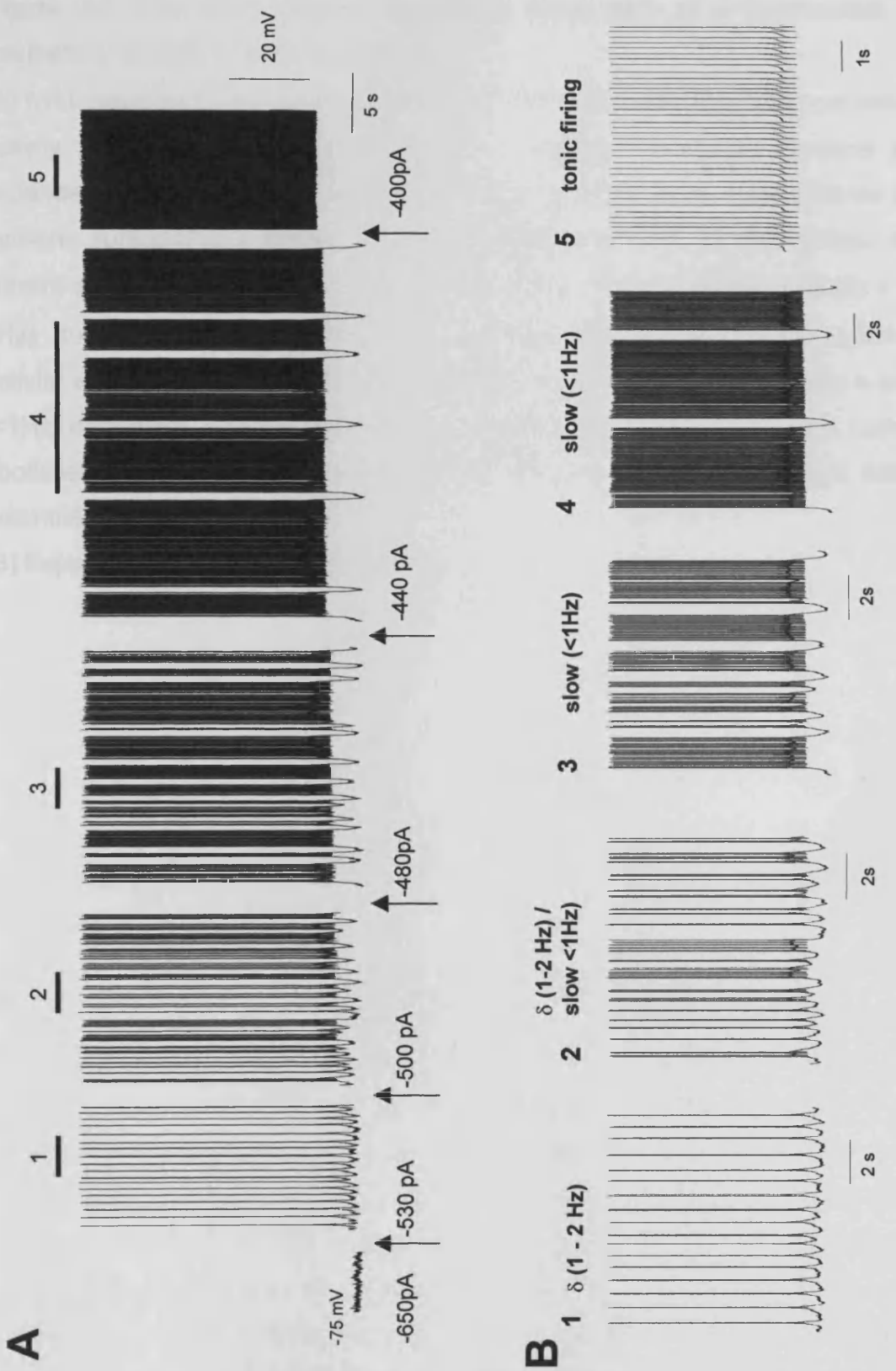

Figure 5.2 The slow (<1Hz) oscillation forms part of a continuum of oscillatory activity in NRT neurones.

Figure 5.2 The slow (<1Hz) oscillation form part of a continuum of oscillatory activity in NRT neurones.

(A) NRT neurone in the presence of *trans*-ACPD (100 μM) displaying oscillatory activity at different levels of injected d.c. current. Underlined sections are expanded in B. Injection of hyperpolarizing d.c current could hyperpolarise the neurone sufficiently to abolish oscillatory activity (-670pA). As the injected d.c. current was removed a range of oscillatory activity became evident. Initially δ (1-2Hz) bursts occurred (-530pA), later δ (1-2Hz) and slow (<1Hz) oscillatory activity was apparent (-500pA). As more d.c. current was removed only a slow (<1Hz) oscillation was present (-480pA, -440pA). Removal of further d.c. current abolished the slow (<1Hz) oscillation and the neurone displayed tonic action potential firing (-400pA).

(B) Expanded sections as indicated in A.

markedly increased both in duration and as a % of the oscillation cycle (Fig. 5.3B). Whilst the maximum and minimum action potential firing rates remained fairly consistent during the "up" phase, the mean action potential firing rate during the "up" phase decreased as injected d.c. current was removed (Fig. 5.3C). This effect occurred because there was a more rapid decline in the normalised firing rate during the "up" phase as injected d.c. current was removed (Fig. 5.3C).

5.3.3 Different manifestation of the slow (<1Hz) oscillation in NRT neurones.

A variety of manifestations of the slow (<1Hz) oscillation were seen in NRT neurones. The basic manifestation of the slow (<1Hz) oscillation comprised rhythmic sequences of sustained action potential firing (the "up" phase) interposed by a LHP that encompassed the "down" phase. The transition to the "up" phase was always marked by a LTCP-mediated burst of action potentials (Fig. 5.4A), whereas the transition to the "down" phase could be marked by a clear inflection point (see Fig. 5.13). The "up" phase always comprised sustained, but decelerating action potential firing: maximum frequency: 6.5 – 125 Hz, 50.1 ± 8.5 Hz (n=16), minimum frequency: 2.3 – 18.1 Hz, 9.4 ± 1.4 Hz (n=16) and comprised 21.3 – 90.4 %, 57.6 ± 5.9 % (n=16) of the oscillation cycle.

In addition, grouping of action potential bursts during the "down" phase of the slow (<1Hz) oscillation was sometimes observed (n=5, 31% of neurones displaying a slow (<1Hz) oscillation) leading to the manifestation of "grouped" subtypes (Fig. 5.4B_{1-2}). Grouping of bursts occurred at the beginning of each cycle of the slow oscillation and always led to the initiation of the "up" phase (Fig. 5.4B_{1-2}). These grouped bursts are presumably rhythmic LTCP-mediated events as both these spontaneous rhythmic bursts (Fig. 5.4B_{1d}, Fig. 5.4B_{2d}) and evoked LTCP mediated bursts (Fig. 5.1A_2 and B_2) have the same characteristic accelerating then decelerating action potential firing pattern. Under these conditions, grouped bursts occurred at frequencies within 1.3 – 4 Hz, 3.02 ± 0.4 Hz (n=5). In all cases there was an increase in the interburst frequency during each episode of "grouped" bursts (calculated using the interval between sequential bursts within a "grouped" episode) (Fig. 5.4B_3). In some neurones this increase was small (Fig. 5.4B_1: mean increase = 0.7 ± 0.2 Hz (153.8 ± 44.2 %)

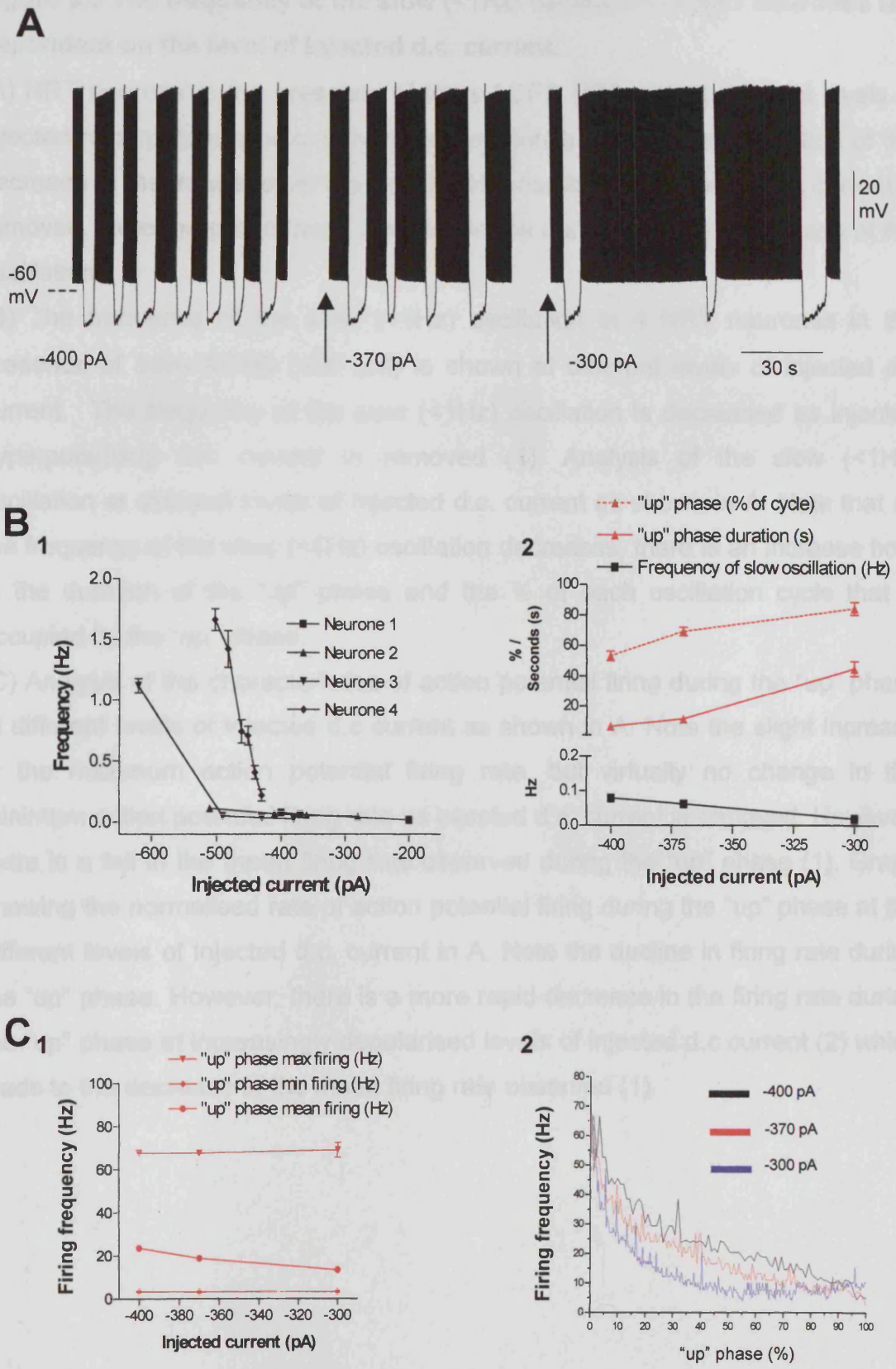

Figure 5.3 The frequency of the slow (<1Hz) oscillation in NRT neurones is dependent on the level of injected d.c. current.

Figure 5.3 The frequency of the slow (<1Hz) oscillation in NRT neurones is dependent on the level of injected d.c. current.

(A) NRT neurone in the presence of *trans*-ACPD (100 μM) at different levels of injected hyperpolarising d.c. current and demonstrating the manifestation of the decrease in the frequency of the slow (<1Hz) oscillation as injected d.c current is removed. Note the pronounced increase in the duration of the "up" phase of the oscillation.

(B) The frequency of the slow (<1Hz) oscillation in 4 NRT neurones in the presence of *trans*-ACPD (100 μM) is shown at different levels of injected d.c current. The frequency of the slow (<1Hz) oscillation is decreased as injected hyperpolarising d.c. current in removed (1). Analysis of the slow (<1Hz) oscillation at different levels of injected d.c. current as shown in A. Note that as the frequency of the slow (<1Hz) oscillation decreases, there is an increase both in the duration of the "up" phase and the % of each oscillation cycle that is occupied by the "up" phase.

(C) Analysis of the characteristics of action potential firing during the "up" phase at different levels of injected d.c current as shown in A. Note the slight increase in the maximum action potential firing rate, but virtually no change in the minimum action potential firing rate as injected d.c. current is removed. However, there is a fall in the mean firing rate observed during the "up" phase (1). Graph showing the normalised rate of action potential firing during the "up" phase at the different levels of injected d.c. current in A. Note the decline in firing rate during the "up" phase. However, there is a more rapid decrease in the firing rate during the "up" phase at increasingly depolarised levels of injected d.c current (2) which leads to the decrease in the mean firing rate observed (1).

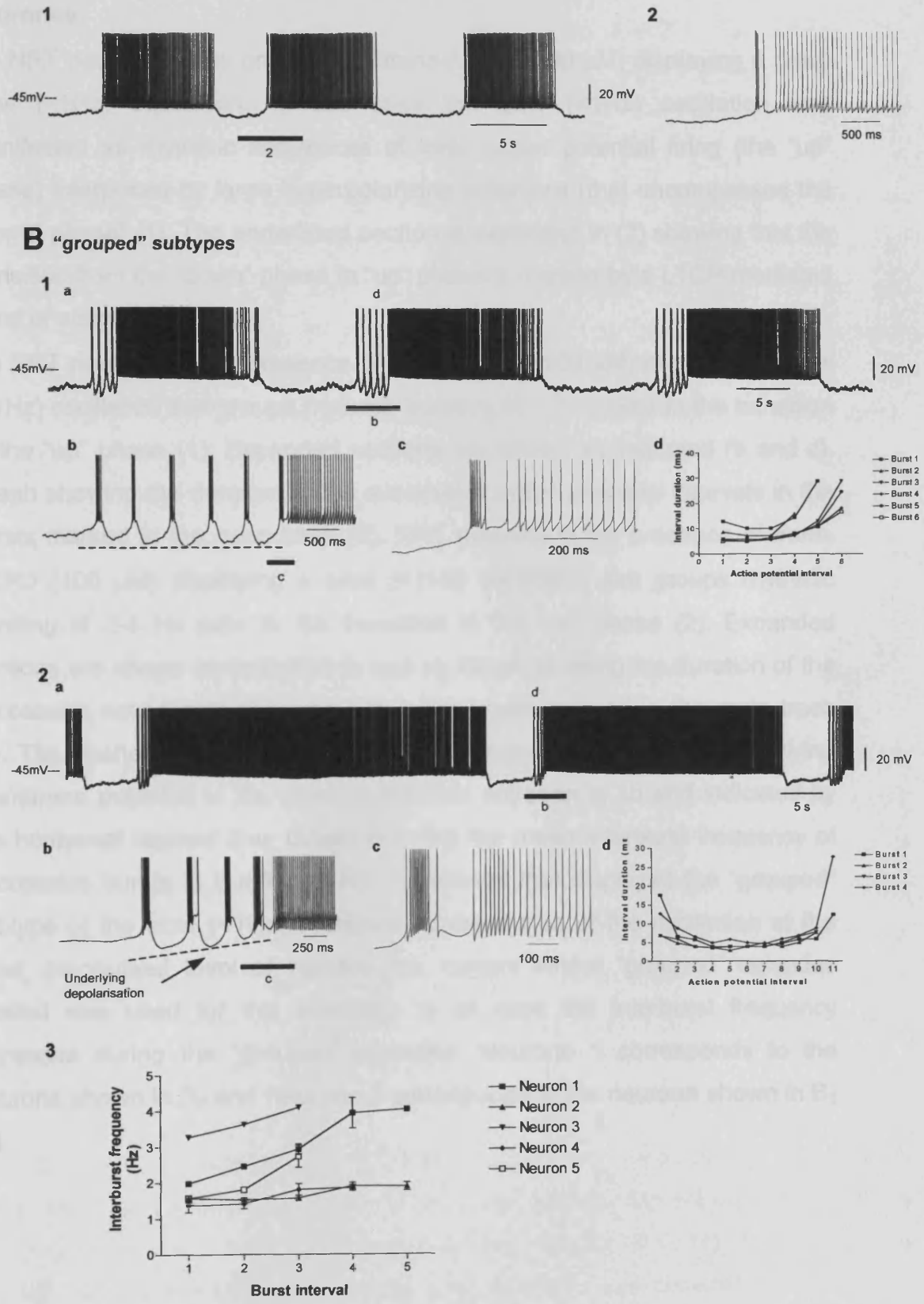

Figure 5.4 Different manifestations of the slow (<1Hz) oscillation in NRT neurones.

Figure 5.4 Different manifestations of the slow (<1Hz) oscillation in NRT neurones.

(A) NRT neurone in the presence of *trans*-ACPD (100 μM) displaying a basic slow (<1Hz) oscillation. In this case the slow (<1Hz) oscillation was manifested as rhythmic sequences of tonic action potential firing (the "up" phase) interposed by large hyperpolarizing potentials (that encompasses the "down" phase) (1). The underlined section is expanded in (2) showing that the transition from the "down" phase to "up" phase is marked by a LTCP-mediated burst of action potentials.

(B) NRT neurone in the presence of *trans*-ACPD (100 μM) displaying a slow (<1Hz) oscillation that groups rhythmic bursting at 1-2 Hz prior to the transition to the "up" phase (1). Expanded sections are shown as indicated (b and c). Graph showing the duration of the successive action potential intervals in the bursts marked in the main trace (d). NRT neurone in the presence of *trans*-ACPD (100 μM) displaying a slow (<1Hz) oscillation that groups rhythmic bursting at 2-4 Hz prior to the transition to the "up" phase (2). Expanded sections are shown as indicated (b and c). Graph showing the duration of the successive action potential intervals in the bursts marked in the main trace (d). The dashed line shows a pronounced depolarisation of the underlying membrane potential in 2b, whereas that this not seen in 1b and indicated by the horizontal dashed line. Graph showing the mean interburst frequency of successive bursts in 5 different NRT neurones that displayed the "grouped" subtype of the slow (<1Hz) oscillation (three cycles of the oscillation at the most depolarised level of injected d.c. current where "grouped" episodes existed was used for this analysis). In all case the interburst frequency increased during the "grouped" episodes. Neurone 1 corresponds to the neurone shown in B_2 and Neurone 2 corresponds to the neurone shown in B_1 (3).

(n=3) and Fig. 5.4B_3), but in others was more notable (Fig. 5.4B_2: mean increase = 2.2 ± Hz (198.6 ± 23.0 %) (n=3) and Fig. 5.4B_3) and was associated with an obvious depolarisation of the underlying membrane potential (Fig. 5.4B_{2b}). The increase in interburst frequency ranged from 0.3-2.2 Hz, 1.1 ± 0.3 Hz (n = 5 neurones).

In addition to variations in the extent and frequency of grouping in different neurones, the properties of grouped episodes could also depend on the level of injected d.c. current (Fig. 5.5). As the injected hyperpolarising d.c. current was decreased the number of grouped bursts per oscillation cycle decreased although the mean interburst frequency remained fairly consistent, only increasing slightly (Fig. 5.5C_1). Further analysis of the interburst frequency within episodes of "grouped" bursting, showed that both the minimum and maximum interburst frequencies increased as the level of injected hyperpolarising d.c. current was reduced thereby leading to a smaller increase in the interburst frequency (Fig. 5.5C_2).

5.3.4 Extracellular recordings indicate the normal occurrence of the slow (<1Hz) oscillation in NRT neurones.

Extracellular recordings revealed the same pattern of activity seen in NRT neurones as seen during intracellular recordings. In the majority of slices (n=51 of 62) no spontaneous activity was recorded extracellularly in the presence of aCSF alone. Only occasionally under these conditions was spontaneous activity recorded (n=11 slices) and predominantly comprised δ (1-2 Hz) frequency bursts of action potentials (0.65 – 2.0 Hz, 1.3 ± 0.1 Hz, n=10 sites), low frequency tonic firing (2.0 – 7.9 Hz, 4.1 ± 1.0 Hz, n=5 sites) or slow (<1Hz) oscillatory activity (0.14 - 0.05 Hz, 0.08 ± 0.03 Hz, n=4 sites).

Application of *trans*-ACPD (100μM) progressively led to an increase in spontaneous activity with slow (<1Hz) oscillation occurring between the transition from no activity to tonic action potential firing only (Fig. 5.6). This full repertoire of NRT activity was seen occasionally (n=4). In other cases *trans*-ACPD application or wash-off resulted in transitions between no activity, a slow (<1Hz) oscillation and tonic action potential firing (n=12) or from no activity to tonic action potential firing only (n=11). The predominant types of activity recorded extracellularly in

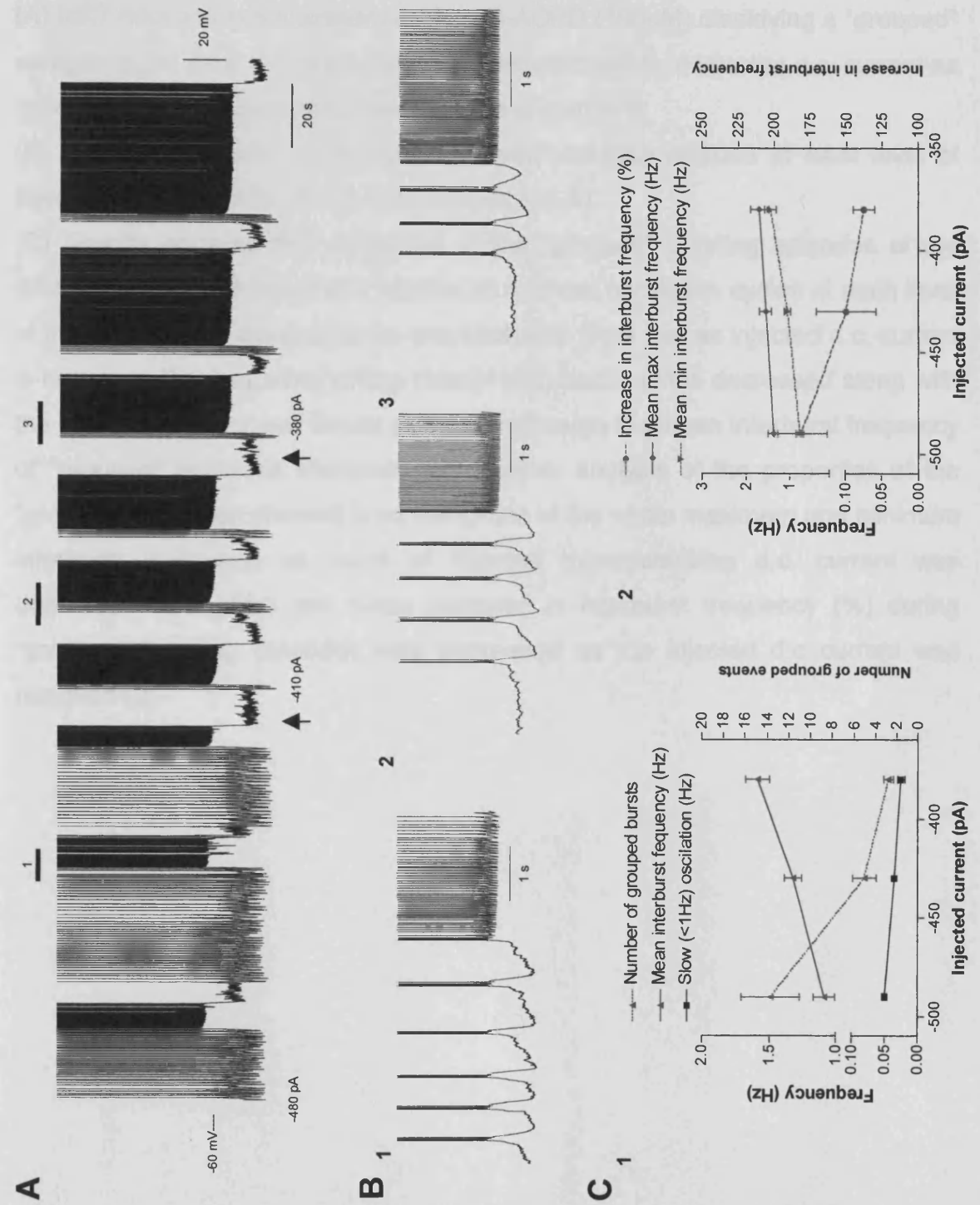

Figure 5.5 Properties of bursting episodes "grouped" by the slow (<1Hz) oscillation in NRT neurones.

Figure 5.5 Properties of bursting episodes "grouped" by the slow (<1Hz) oscillation in NRT neurones.

(A) NRT neurone in the presence of *trans*-ACPD (100μM) displaying a "grouped" subtype of the slow (<1Hz) oscillation at different levels of injected d.c. current as indicated. Bars indicate expanded regions shown in B.

(B) Expanded regions showing a "grouped" bursting episode at each level of injected d.c. current (1, 2 and 3 as indicated in A) .

(C) Graphs showing the properties of the "grouped" bursting episodes at the different levels of injected d.c. current in A (three oscillation cycles at each level of injected current were used fro this analysis). Note that as injected d.c. current is removed, the frequency of the slow (<1Hz) oscillation is decreased along with the number of "grouped" bursts per cycle although the mean interburst frequency of "grouped" episodes increases (1). Further analysis of the properties of the "grouped" episodes showed a convergence of the mean maximum and minimum interburst frequency as value of injected hyperpolarising d.c. current was decreased. Therefore the mean increase in interburst frequency (%) during "grouped" bursting episodes was decreased as the injected d.c current was removed (2).

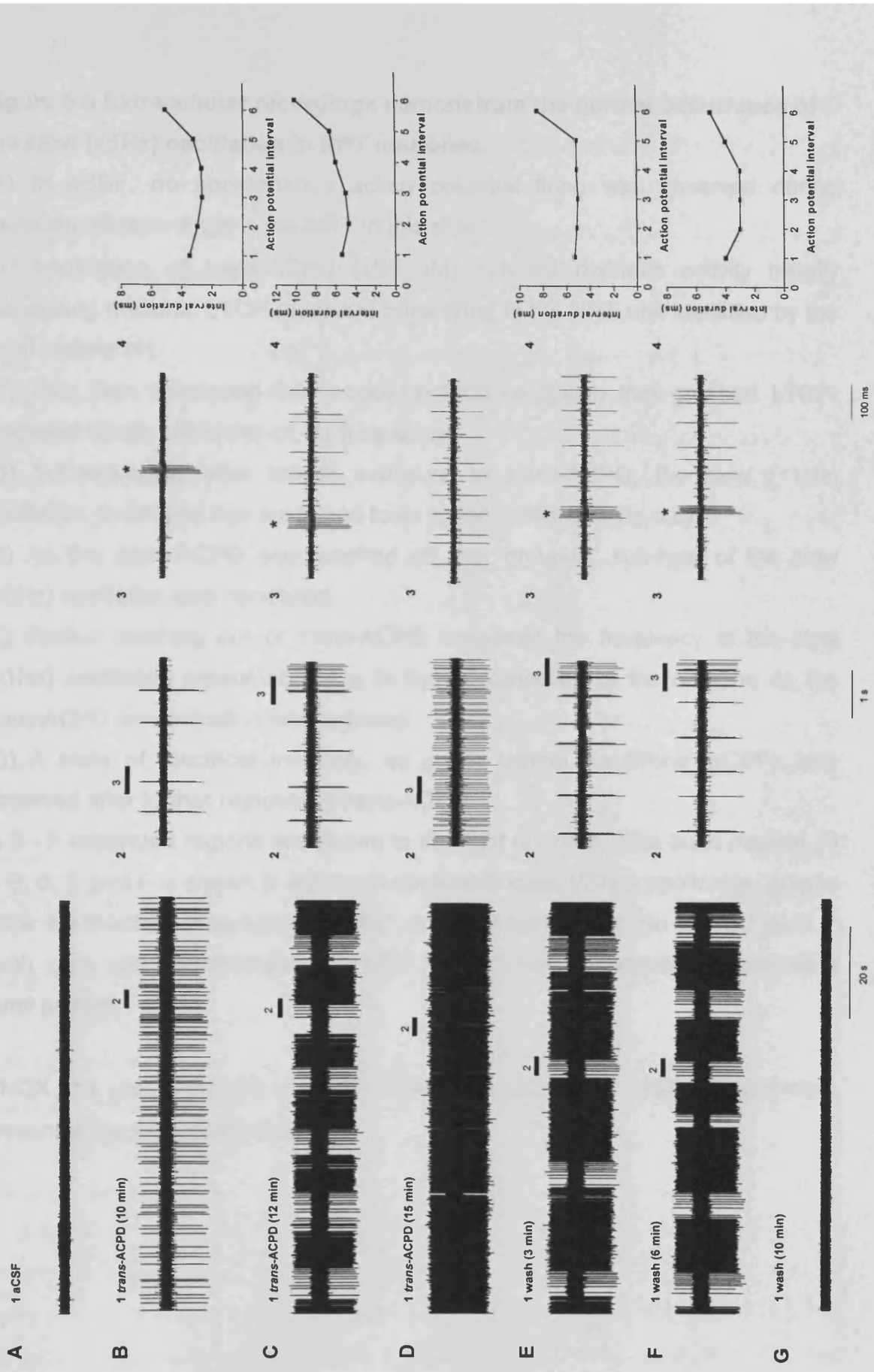

Figure 5.6 Extracellular recordings demonstrate the normal occurrence of the slow (<1Hz) oscillation in NRT neurones.

Figure 5.6 Extracellular recordings demonstrate the normal occurrence of the slow (<1Hz) oscillation in NRT neurones.

(A) In aCSF, no spontaneous action potential firing was observed during extracellular recordings in the NRT in this slice.

(B) Application of *trans*-ACPD (100 μM) induced rhythmic activity initially comprising rhythmic LTCP-mediated burst firing in the NRT unit identified by the burst pattern (4).

(C) This then developed into a slow (<1Hz) oscillation that grouped LTCP-mediated bursts within the <1 Hz frequency.

(D) Subsequently, after longer exposure to *trans*-ACPD, the slow (<1Hz) oscillation developed into sustained tonic action potential firing only.

(E) As the *trans*-ACPD was washed off the "grouped" sub-type of the slow (<1Hz) oscillation was reinstated.

(F) Further washing out of *trans*-ACPD increased the frequency of the slow (<1Hz) oscillation presumably due to hyperpolarisation of the neurone as the *trans*-ACPD concentration was reduced.

(G) A state of electrical inactivity, as under control conditions (aCSF), was observed after further removal of *trans*-ACPD.

In B - F expanded regions are shown to the right (2 and 3). The burst marked (*) in B, C, E and F is shown in 4 in each applicable case. Where applicable, graphs show the duration of successive action potential intervals for the marked burst in each case and demonstrates the NRT characteristic accelerating-decelerating burst pattern.

CNQX (10 μM), APV (50 μM), SR 95531 (20 μM), CGP 54626 (20μM) were present in the recording medium.

the NRT in the presence of *trans*-ACPD were the slow (<1Hz) oscillation (48% of recorded units, 0.01 to 0.57 Hz, 0.13 ± 0.02 Hz, n=16) or tonic firing only (33% of recorded units, 2.50 – 81.2 Hz, 13.4 ± 1.1 Hz, n=11). In a small number of cases (9%) sustained LTCP-mediated bursts of action potentials (0.9 – 12.8 Hz, 4.1 ± 0.8, n=6) were recorded in the presence of *trans*-ACPD.

The slow (<1Hz) oscillation was manifested as seen during intracellular recordings and comprised rhythmic sequences of sustained firing ("up phase") and quiescence ("down phase") (Fig. 5.7A) with the "up" phase dominated by a pattern of decelerating tonic firing (186.5 – 4.5 Hz, 27.7 ± 5.6 Hz, n= 16). Also, both the "basic" manifestation (Fig. 5.7A) and the "grouped" subtype (Fig. 5.7B) of slow (<1Hz) oscillation were observed during extracellular recordings. "Grouping" of bursts occurred in 63% (n=10) of units displaying slow (<1Hz) oscillatory activity, occurred at the start of each oscillatory cycle and were always followed by sustained firing comprising the "up" phase. Within "grouped" episodes, the frequency of grouping ranged from 0.9 – 8.1 Hz (Fig. 5.7B_3). In addition, the pattern of increasing interburst frequency was also apparent during the "grouped" bursting episodes: Minimum: 0.9 – 1.9 Hz, 1.6 ± 0.08 Hz (n=10), maximum: 1.3 – 8.1 Hz, 4.1 ± 0.4 Hz (n=10) with the increase in interburst frequency ranging from 0.2 – 6.3 Hz, 2.5 ± 0.4 Hz (n=10) (Fig. 5.7B_{1-2} and B_3).

5.3.5 The slow (<1Hz) oscillation arises through a mGluR1a dependent mechanism.

The specific mGluR1a receptor antagonist LY 367385 (250 μM) was effective in reversibly abolishing the *trans*-ACPD induced slow (<1Hz) oscillation (n=4) both during intracellular (Fig. 5.8) and extracellular recordings (not shown). In addition, the Group I mGluR specific agonist DHPG (100μM) was also effective in mimicking *trans*-ACPD. Application of DHPG during intracellular recordings depolarised NRT neurones such that in the absence of injected d.c. current neurones displayed tonic action potential firing (6.4 – 30.0 Hz, 13.7 ± 5.5 Hz, maximum apparent input resistance = 110 ± 16.4 MΩ, n=6). In addition, the slow (<1Hz) oscillation was induced in 50% (n=3) of neurones recorded intracellularly (frequency: range = 0.02 – 0.05 Hz, mean = 0.03 ± 0.013 Hz, n=3). Extracellular recordings in the presence of DHPG (100 μM) also mimicked the activity

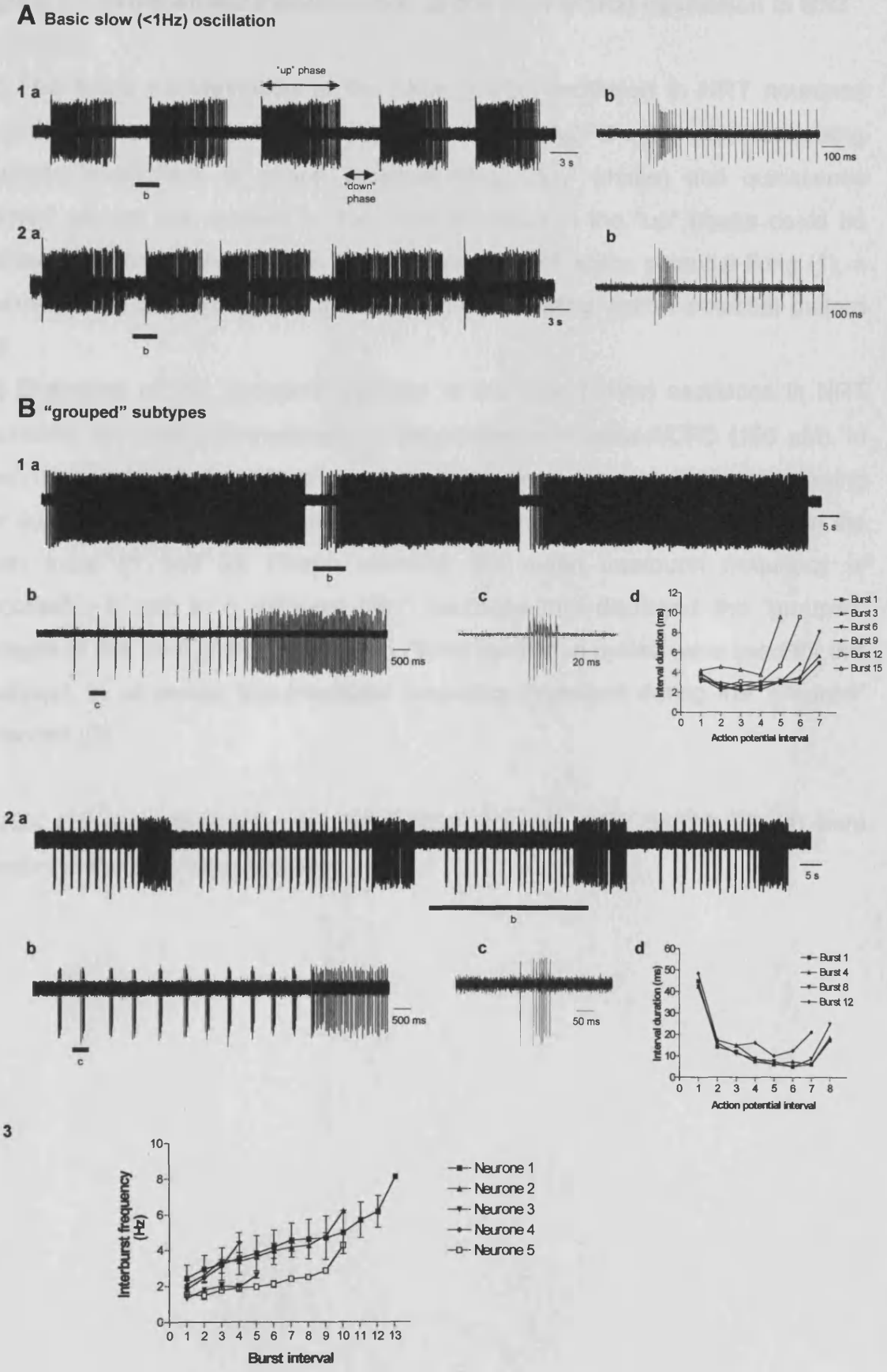

Figure 5.7 Extracellular manifestations of the slow (<1Hz) oscillation in NRT neurones.

Figure 5.7 Extracellular manifestation of the slow (<1Hz) oscillation in NRT neurones.

(A) The basic manifestation of the slow (<1Hz) oscillation in NRT neurones recorded extracellularly in the presence of *trans*-ACPD (100 μM) comprising rhythmic sequences of action potential firing ("up" phase) and quiescence ("down" phase) (as marked in 1a). The transition to the "up" phase could be marked by a clear acceleration than deceleration of action potential firing (1), a discrete burst comprising an accelerating-decelerating action potential pattern (2).

(B) Examples of the "grouped" subtype of the slow (<1Hz) oscillation in NRT neurones recorded extracellularly in the presence of *trans*-ACPD (100 μM). In each case, expanded sections are shown as indicated (b and c). Graph showing the duration of successive action potential intervals in the bursts marked in the main trace (1 and 2). Graph showing the mean interburst frequency of successive bursts in 5 different NRT neurones that displayed the "grouped" subtype of the slow (<1Hz) oscillation (three oscillation cycles were used for this analysis). In all cases, the interburst frequency increased during the "grouped" episodes (3).

CNQX (10 μM), APV (50 μM), SR 95531 (20 μM), CGP 54626 (20μM) were present in the recording medium.

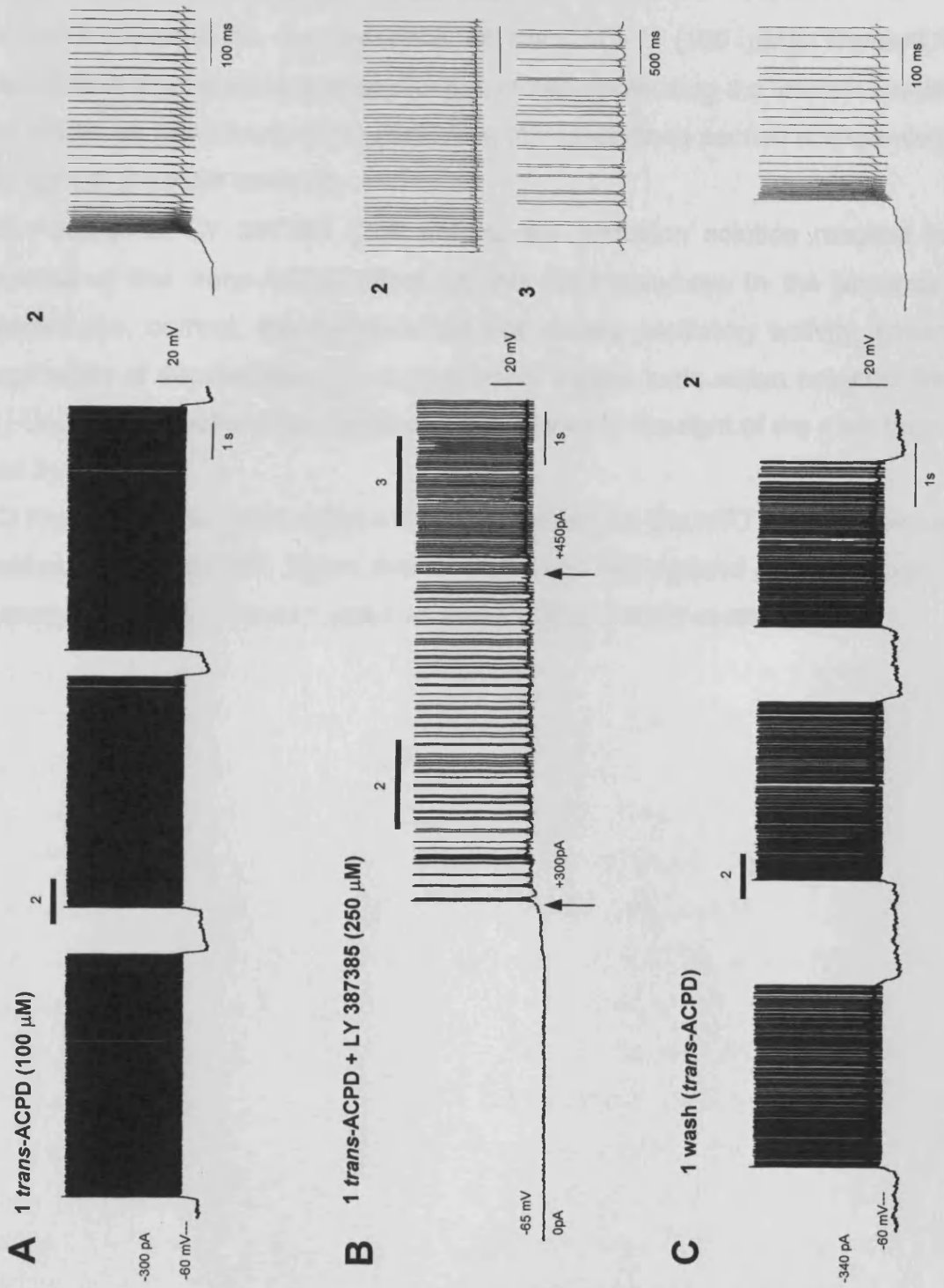

Figure 5.8 The slow (<1Hz) oscillation in NRT neurones is reversibly abolished by the mGluR1a specific antagonist LY387385

Figure 5.8 The slow (<1Hz) oscillation is reversibly abolished by the mGluR1a specific antagonist LY387385.

(A) NRT neurone in the presence of *trans*-ACPD (100 μM). *Trans*-ACPD depolarised this neurone and application of hyperpolarising d.c. current revealed the existence of a slow (<1Hz) oscillation (1). Underlined section is expanded to the right of the main trace (2).

(B) Addition of LY 387385 (250 μM) to the perfusion solution resulted in a reversal of the *trans*-ACPD effect on this NRT neurone. In the absence of injected d.c. current, this neurone did not display oscillatory activity, however application of depolarising d.c. current could instate tonic action potential firing. (1) Underlined sections are expanded and shown to the right of the main trace (2 and 3).

(C) Reversal of the block of the *trans*-ACPD effect on this NRT neurone following washout of LY 387385. Again this neurone was depolarised and application of hyperpolarizing d.c. current again revealed a slow (<1Hz) oscillation.

observed during extracellular recordings of NRT units in the presence of *trans*-ACPD. In the presence of DHPG, NRT activity recorded extracellular activity was predominantly seen as a slow (<1Hz) oscillation (0.1 - 0.02 Hz, 0.09 ± 0.03 Hz, n=8) (Fig. 5.9) with 50% of these cases being the "grouped bursts" subtype. The remaining units showed tonic firing (10.5 ± 4.4, n=2) or bursts of action potentials (2.2 ± 1.0, n=2).

5.3.6 The slow (<1Hz) oscillation is intrinsically generated in NRT neurones.
Application of TTX (1 μM) to NRT neurones displaying the slow (<1Hz) oscillation in the presence of *trans*-ACPD was effective in abolishing action potential firing and in the absence of injected d.c. current had a resting membrane potential of -48.5 ± 3.5 mV (n=2). However the waveform underlying the slow (<1Hz) oscillation persisted in the presence of TTX during application of hyperpolarising d.c. current (n=2) (Fig. 5.10A). The waveform persisting in the presence of TTX comprised rhythmic transitions between a depolarised "up" phase and hyperpolarised "down" phase as observed in the absence of TTX. The transition to the "up" phase was mediated by a LTCP and was followed by a long depolarised phase, the "up" phase, before a rapid transition back to a hyperpolarised "down" phase marked by a clear inflection point. The following "down" phase was manifested as a slow repolarisation, much like the slow repolarisation attributed to I_h in TC neurones (McCormick and Pape 1990; Soltesz et al. 1991) leading to the initiation of a LTCP and thus beginning another cycle of the oscillation. In this way the slow (<1Hz) oscillation persisting in the presence of TTX in NRT and TC neurones *in vitro* was very similar (see Chapter 3 and 4). In addition, negative current steps applied in the presence of *trans*-ACPD alone revealed waveforms that appeared to be very similar to the $I_{Twindow}$ mediated waveforms in TC neurones (Williams et al. 1997a; Hughes et al. 1999) including the presence of an inflection point (Fig. 5.10A_{1c}*) and input amplification. A pronounced ADP was present following the evoked LTCPs as previously described in NRT neurones (Bal and McCormick 1993) (Fig. 5.10A_{2c}). The R_N of NRT neurones increased in the presence of TTX in these neurones (Δ R_N = 98.7 ± 32.0 %, n= 2) and, in addition to the pronounced ADP, a slow "sag" potential was clearly evident in TTX (Fig. 5.10A_{2c}: black line). Application of TTX to NRT neurones not displaying a slow (<1Hz) oscillation in the presence of

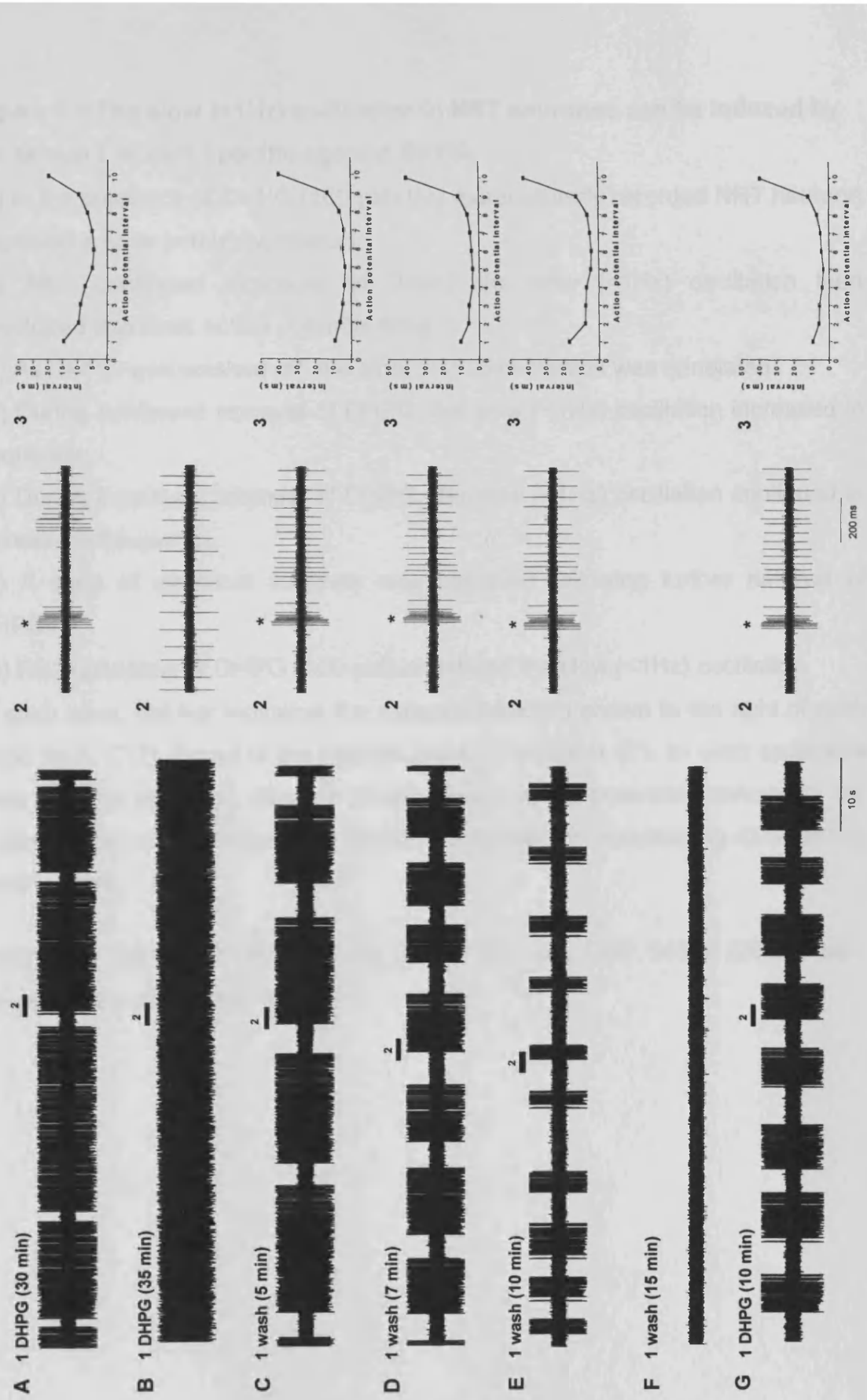

Figure 5.9 The slow (<1Hz) oscillation in NRT neurones can be induced by the Group I mGluR specific agonist DHPG

Figure 5.9 The slow (<1Hz) oscillation in NRT neurones can be induced by the Group I mGluR specific agonist DHPG.

(A) In the presence of DHPG (100 μM) this extracellularly recorded NRT neurone displayed a slow (<1Hz) oscillation.

(B) After continued exposure to DHPG the slow (<1Hz) oscillation then developed into tonic action potential firing.

(C) As DHPG was washed off, the slow (<1Hz) oscillation was reinstated.

(D) During continued removal of DHPG, the slow (<1Hz) oscillation increased in frequency.

(E) During continued removal of DHPG, the slow (<1Hz) oscillation continued to increase in frequency.

(F) A state of electrical inactivity was observed following further removal of DHPG.

(G) Re-application of DHPG (100 μM) reinstated the slow (<1Hz) oscillation.

In each case, the bar indicates the expanded section shown to the right of each trace. In A, C, D, E and G the marked burst (*) is shown in 3. In each applicable case, graphs show the duration of successive action potential intervals for the marked burst and demonstrates the NRT characteristic accelerating-decelerating burst pattern.

CNQX (10 μM), APV (50 μM), SR 95531 (20 μM), CGP 54626 (20μM) were present in the recording medium.

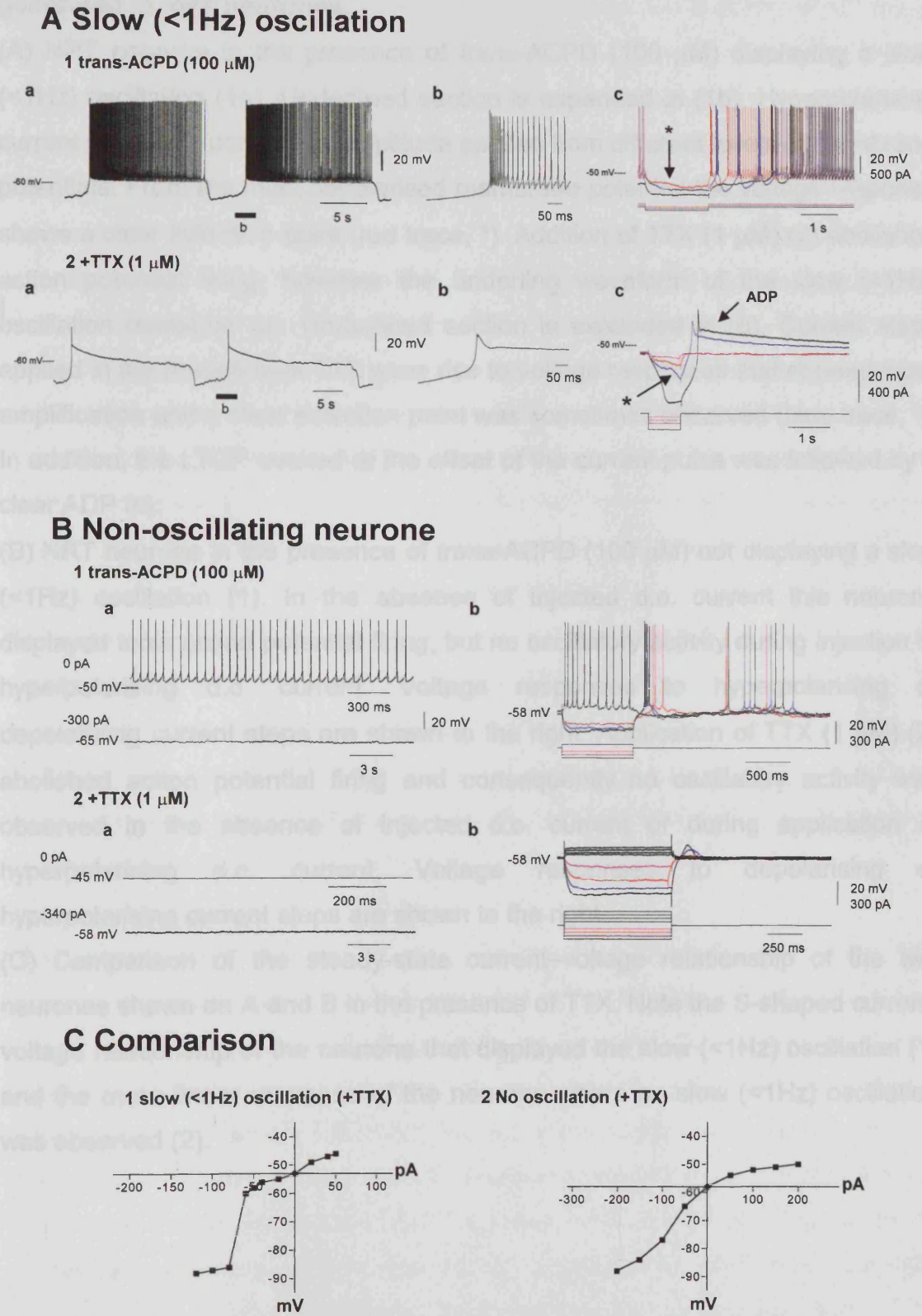

Figure 5.10 The *trans*-ACPD induced slow (<1Hz) oscillation is intrinsically generated in NRT neurones.

Figure 5.10 The *trans*-ACPD induced slow (<1Hz) oscillation is intrinsically generated in NRT neurones.

(A) NRT neurone in the presence of *trans*-ACPD (100 μM) displaying a slow (<1Hz) oscillation (1a). Underlined section is expanded in (1b). Hyperpolarising current steps of a consistent amplitude applied from different levels of membrane potentials. From the most depolarised membrane potential the voltage response shows a clear inflection point (red trace, *). Addition of TTX (1 μM) (2) abolished action potential firing, however the underling waveform of the slow (<1Hz) oscillation remained (a). Underlined section is expanded in (b). Current steps applied in the presence of TTX gave rise to voltage responses that showed input amplification and a clear inflection point was sometimes observed (blue trace, *). In addition, the LTCP evoked at the offset of the current pulse was followed by a clear ADP (c).

(B) NRT neurone in the presence of *trans*-ACPD (100 μM) not displaying a slow (<1Hz) oscillation (1). In the absence of injected d.c. current this neurone displayed tonic action potential firing, but no oscillatory activity during injection of hyperpolarising d.c. current. Voltage responses to hyperpolarising or depolarising current steps are shown to the right. Application of TTX (1 μM) (2) abolished action potential firing and consequently no oscillatory activity was observed in the absence of injected d.c. current or during application of hyperpolarising d.c. current. Voltage responses to depolarising or hyperpolarising current steps are shown to the right.

(C) Comparison of the steady-state current–voltage relationship of the two neurones shown on A and B in the presence of TTX. Note the S-shaped current-voltage relationship of the neurone that displayed the slow (<1Hz) oscillation (1) and the more linear response of the neurone where no slow (<1Hz) oscillation was observed (2).

trans-ACPD alone (n=3), but displaying the otherwise normal electrophysiological activity of NRT neurones (Fig. 5.10B_1) abolished action potential firing and in the absence of injected d.c. current showed a resting membrane potential of -45 ± 1.2 mV (n=3). In these neurones, the evoked waveforms during applied current steps did not indicate the presence of an obvious $I_{Twindow}$ component. In addition, linear responses to current steps were observed both in *trans*-ACPD and in TTX (Fig. 5.10B_{2b}), although a small "sag" potential was present both in *trans*-ACPD alone (Fig. 5.10B_{1a}: hyperpolarising black trace) and in the presence of TTX (Fig. 5.102B: hyperpolarising black trace). The difference between the evoked responses observed for neurones displaying a slow (<1Hz) oscillation and those not oscillating in the presence of TTX is shown in the steady-state current-voltage relationships (Fig. 5.10C). The neurone displaying a slow (<1Hz) oscillation has a S-shaped steady-state current-voltage relationship, much like that of TC neurones (see Chapter 3) and attributed to an underlying bistable system (Williams et al. 1997a; Hughes et al. 1999) (Fig. 5.10C_1). In contrast, the non-oscillating neurone has a far more linear current-voltage relationship (Fig. 5.10C_2). The R_N of the non-oscillating NRT neurones was also increased in the presence of TTX (ΔR_N = 73.19 ± 40.35, n= 3). In the presence of TTX, neurones not displaying a slow (<1Hz) oscillation prior to the application of TTX a pronounced ADP was present following evoked LTCPs (see Fig. 5.14 B_{2b}).

Given that in many of the NRT neurones recorded intracellularly a slow "sag" potential is present, as is similarly apparent in intracellular recording by others (Brunton and Charpak 1998; Debarbieux et al. 1998) and that a slow "sag" potential is indicative of the presence of I_h in TC neurones (McCormick and Pape 1988; Pape and McCormick 1989; Soltesz et al. 1991), the presence of an I_h current was suspected even though previously thought to be absent (Bal and McCormick 1993). In addition, the "grouped" episodes of bursting within the hyperpolarised phase of the slow (<1Hz) oscillation in NRT neurones often occurred at δ (1-2Hz) frequencies and this type of oscillatory activity in TC neurones is known to be intrinsically generated though the interplay of I_T and I_h (McCormick and Pape 1990; Leresche et al. 1991; Soltesz et al. 1991). Therefore, in order to investigate if the I_h current made a contribution to this slow "sag" potential, ZD 7288 (30 μM) was applied to neurones displaying the slow

(<1Hz) oscillation. Only in one neurone was this successfully achieved (Fig. 5.11), and application of ZD 7288 did block grouped activity and the slow (<1Hz) oscillation and also the slow "sag" potential that was observed prior to the application of ZD 7288.

5.3.7 Application of *trans*-ACPD induces an undulating (<1Hz) oscillation in NRT neurones.

In a small number of NRT neurones recorded in the presence of *trans*-ACPD (100 μM) (n=3 of 37, 8%) or DHPG (n=1) a second type of <1Hz oscillation was observed. I will refer to this as the undulating (<1Hz) oscillation due to its particular manifestation. The undulating (<1Hz) oscillation could either be the only <1Hz oscillatory activity in NRT neurones (n=3) or could be present along with the slow (<1Hz) oscillation (n=1) with the slow (<1Hz) oscillation transformed into the undulating (<1Hz) oscillation as injected hyperpolarising d.c. current was reduced (Fig. 5.12A) and was observed in the presence of the synaptic blockers (APV, CNQX, SR 95531 and CGP 54626, n=3).

Although both these types of <1Hz oscillation in NRT neurones comprised rhythmic barrages of sustained action potential firing interposed by periods of quiescence leading to a bimodal membrane potential distribution during the oscillation cycle (Fig. 5.12B), particular features of their manifestation were very different. The slow (<1Hz) oscillation was observed over a fairly large range of injected d.c. current values (see Fig. 5.2, 5.3 and 5.5), whereas the undulating (<1Hz) oscillation typically occurred when the membrane potential was initially moved to around -50 to -60mV. The slow (<1Hz) oscillation was characterised by the presence of a LHP that encompassed the "down" phase whereas the undulating (<1Hz) oscillation had a slowly developing and decaying hyperpolarising envelope interposed between the successive "up" phases. These differences led to a much wider range between the 2 membrane potential modes during the oscillatory cycles. The "up" and "down" states were separated by 10 – 25.2 mV (15.9 ± 1.4 mV, n=18) for the slow (<1Hz) oscillation, but separated by 4.0 – 11.0 mV (7.3 ± 1.9 mV, n=4, P = 0.006) for the undulating (<1Hz) oscillation (Fig. 5.12B). The frequency ranges encompassed by the two types of <1Hz oscillation differed, with the undulating (<1Hz) oscillation encompassing a slower range 0.01 – 0.04 Hz (0.02 ± 0.006 Hz, n=4) than the slow (<1Hz)

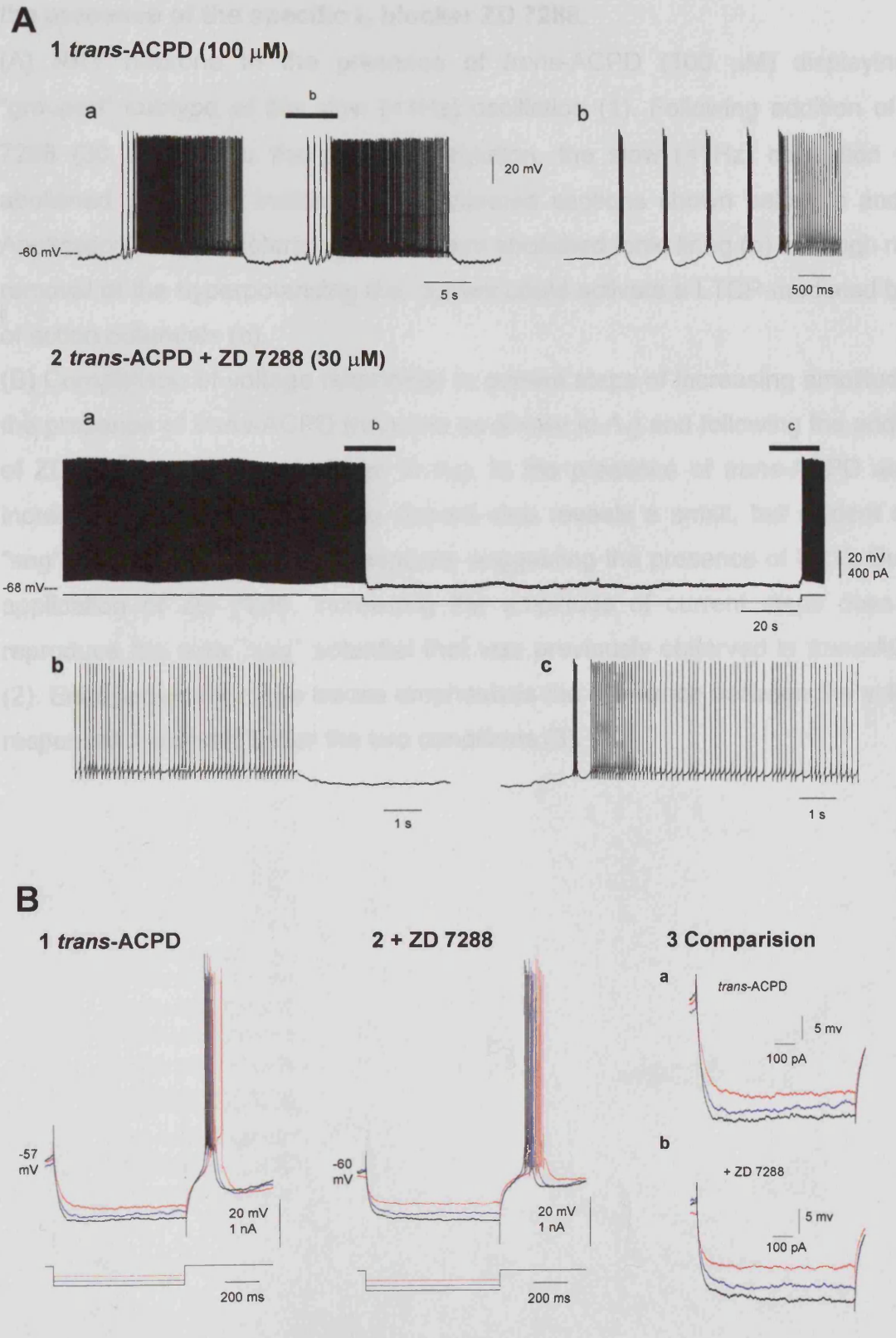

Figure 5.11 The *trans*-ACPD induced slow (<1Hz) oscillation in NRT neurones is abolished in the presence of the specific I_h blocker ZD 7288.

Figure 5.11 The *trans*-ACPD induced slow (<1Hz) oscillation is abolished in the presence of the specific I_h blocker ZD 7288.

(A) NRT neurone in the presence of *trans*-ACPD (100 μM) displaying a "grouped" subtype of the slow (<1Hz) oscillation (1). Following addition of ZD 7288 (30 μM) (2) to the perfusion solution, the slow (<1Hz) oscillation was abolished (a). Bars indicated the expanded sections shown below (b and c). Application of hyperpolarising d.c. current abolished tonic firing (b) although rapid removal of the hyperpolarising d.c. current could activate a LTCP-mediated burst of action potentials (c).

(B) Comparison of voltage responses to current steps of increasing amplitude in the presence of *trans*-ACPD (neurone as shown in A_1) and following the addition of ZD 7288 (neurone as shown in A_2). In the presence of *trans*-ACPD alone, increasing the amplitude of the current step reveals a small, but evident slow "sag" potential in the voltage response suggesting the presence of I_h (1). During application of ZD 7288, increasing the amplitude of current steps does not reproduce the slow "sag" potential that was previously observed in *trans*-ACPD (2). Enlargement of these traces emphasises the difference between the voltage responses observed under the two conditions (3).

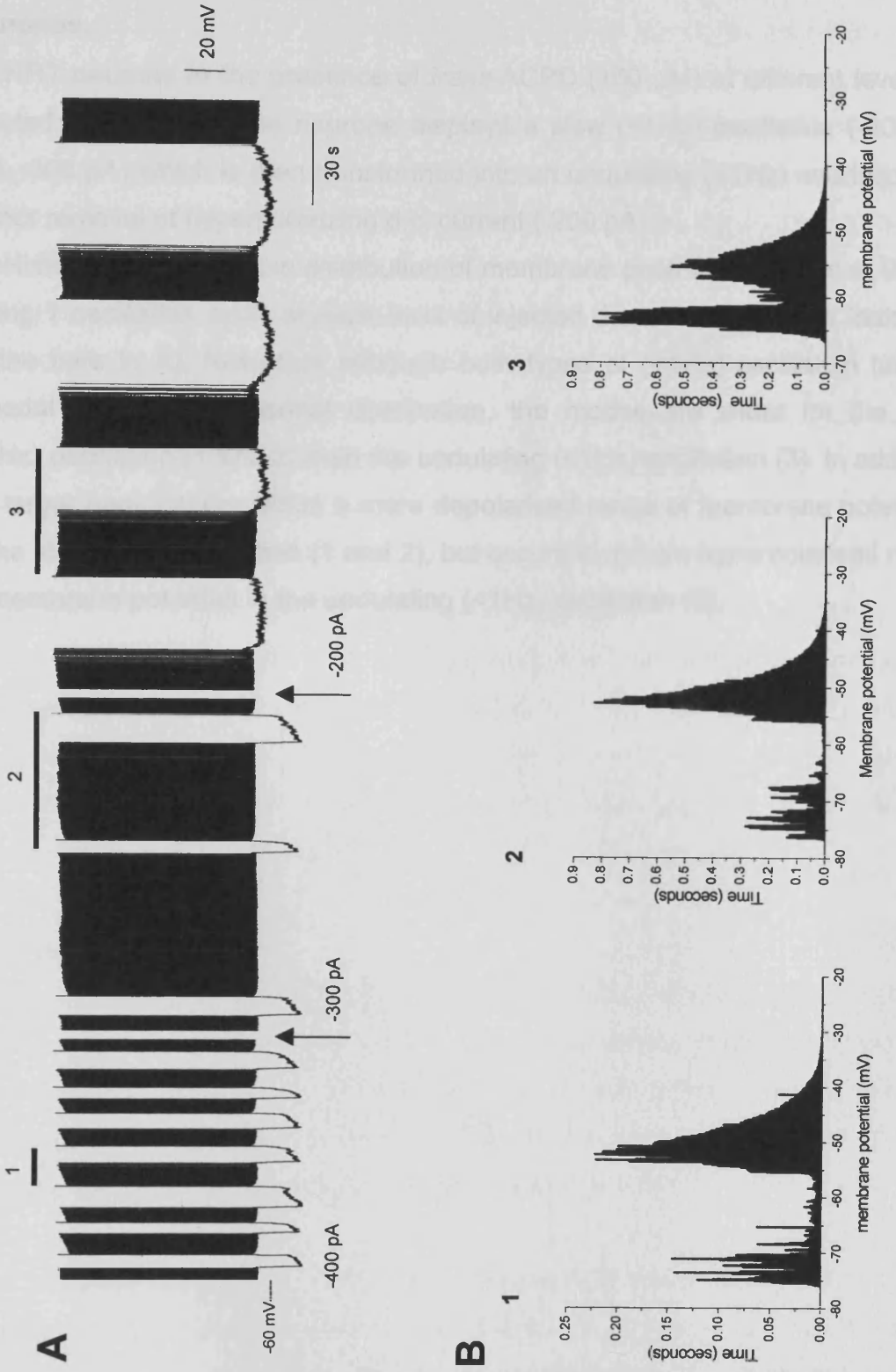

Figure 5.12 *Trans*-ACPD induces an undulating (<1Hz) oscillation in NRT neurones.

Figure 5.12 *Trans*-ACPD induces an undulating (<1Hz) oscillation in NRT neurones.

(A) NRT neurone in the presence of *trans*-ACPD (100 μM) at different levels of injected d.c. current. The neurone displays a slow (<1Hz) oscillation (-400 pA and –300 pA) which is then transformed into an undulating (<1Hz) oscillation on further removal of hyperpolarizing d.c. current (-200 pA).

(B) Histogram showing the distribution of membrane potentials (binned at 0.1 V) during 1 oscillation cycle at each level of injected d.c. current (and as indicated by the bars in A). Note that although both types of (<1Hz) oscillation have a bimodal membrane potential distribution, the modes are wider for the slow (<1Hz) oscillation (1 and 2) than the undulating (<1Hz) oscillation (3). In addition, the larger peak occurs within a more depolarised range of membrane potentials in the slow (<Hz) oscillation (1 and 2), but occurs in a more hyperpolarised range of membrane potential in the undulating (<1Hz) oscillation (3).

oscillation (0.7 – 0.02, 0.16 ± 0.04 Hz) that was found to be statistically significant (P = 0.0041). In contrast to the LTCP that marks the transition to the "up" phase during the slow <1Hz) oscillation (Fig. 5.13A), the "up" phase of the undulating (<1Hz) oscillation (measured as the duration of action potential firing) was manifested as slowly developing then decaying action potential firing (Fig. 5.13B). Additionally in contrast to the decelerating firing rate of the "up" phase observed during the slow (<1Hz) oscillation (Fig. 5.13A_3), the "up" phase of the undulating (<1Hz) oscillation was characterised by an accelerating and then decelerating firing rate (Fig. 5.13B_3): Maximum: 6.6 – 27.0 Hz, 14.9 ± 4.4 Hz (n=33), minimum frequency: 1.2 – 2.6 Hz, 1.8 ± 0.2 Hz (n=3), mean frequency: 5.0 – 9.1 Hz, 5.2 ± 1.3 Hz (n=3) and comprised 43.3 – 59.60 % (51.1 ± 3.0 %, n= 3) of the oscillation cycle.

Application of TTX (1μM) to neurones displaying the undulating (<1Hz) oscillation abolished both action potential firing and the waveform underlying the undulating (<1Hz) oscillation (n=3) (Fig. 5.14). In these cases, TTX increased the R_N of recorded neurones (ΔR_N =66.69 ± 8.38 %, n = 3) and both the slow "sag" potential indicative of the presence of I_h and an ADP following the LTCP were clearly visible in TTX (Fig. 5.14B_2).

5.4 DISCUSSION

The novel findings described in this chapter are 1) the induction of a slow (<1Hz) oscillation in NRT neurones *in vitro*, that has very similar properties to the slow (<1Hz) oscillation observed in NRT neurones *in vivo* during sleep; 2) the slow (<1Hz) oscillation *in vitro* can occur via mGluR1a activation; and 3) the induction of an undulating (<1Hz) oscillation in NRT neurones *in vitro*.

5.4.1 Induction of a slow (<1Hz) oscillation in NRT neurones.

As *trans*-ACPD application was used to pharmacologically mimic corticothalamic stimulation in TC neurones, the same mechanism was employed in NRT neurones in order to observe the effect of mGluR activation on NRT neurones. To date both Group I and Group II mGluR effect have been reported in NRT neurones: Group I activation causing a depolarisation via reduction of I_{KLeak} (McCormick and von Krosigk 1992; Lee and McCormick 1997) and Group II activation causing Hyperpolarisation (Cox and Sherman 1999). Application of

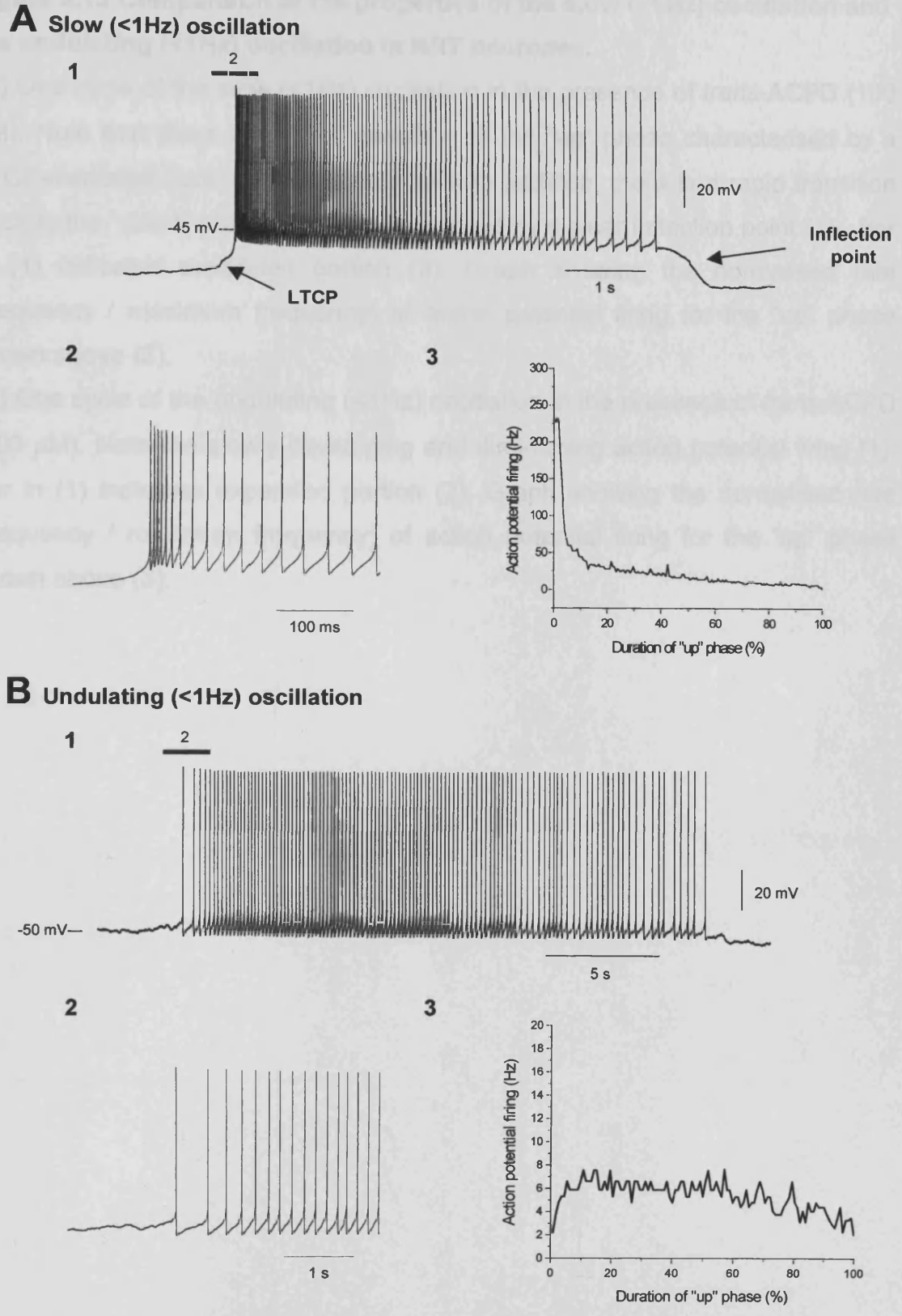

Figure 5.13 Comparison of the properties of the slow (<1Hz) oscillation and the undulating (<1Hz) oscillation in NRT neurones.

Figure 5.13 Comparison of the properties of the slow (<1Hz) oscillation and the undulating (<1Hz) oscillation in NRT neurones.

(A) One cycle of the slow (<1Hz) oscillation in the presence of *trans*-ACPD (100 μM). Note that there is a rapid transition to the "up" phase characterised by a LTCP-mediated burst of action potentials. In addition, there is a rapid transition back to the "down" phase that can be marked by a clear inflection point (1). Bar in (1) indicates expanded portion (2). Graph showing the normalised rate (frequency / maximum frequency) of action potential firing for the "up" phase shown above (3).

(B) One cycle of the undulating (<1Hz) oscillation in the presence of *trans*-ACPD (100 μM). Note the slowly developing and diminishing action potential firing (1). Bar in (1) indicates expanded portion (2). Graph showing the normalised rate (frequency / maximum frequency) of action potential firing for the "up" phase shown above (3).

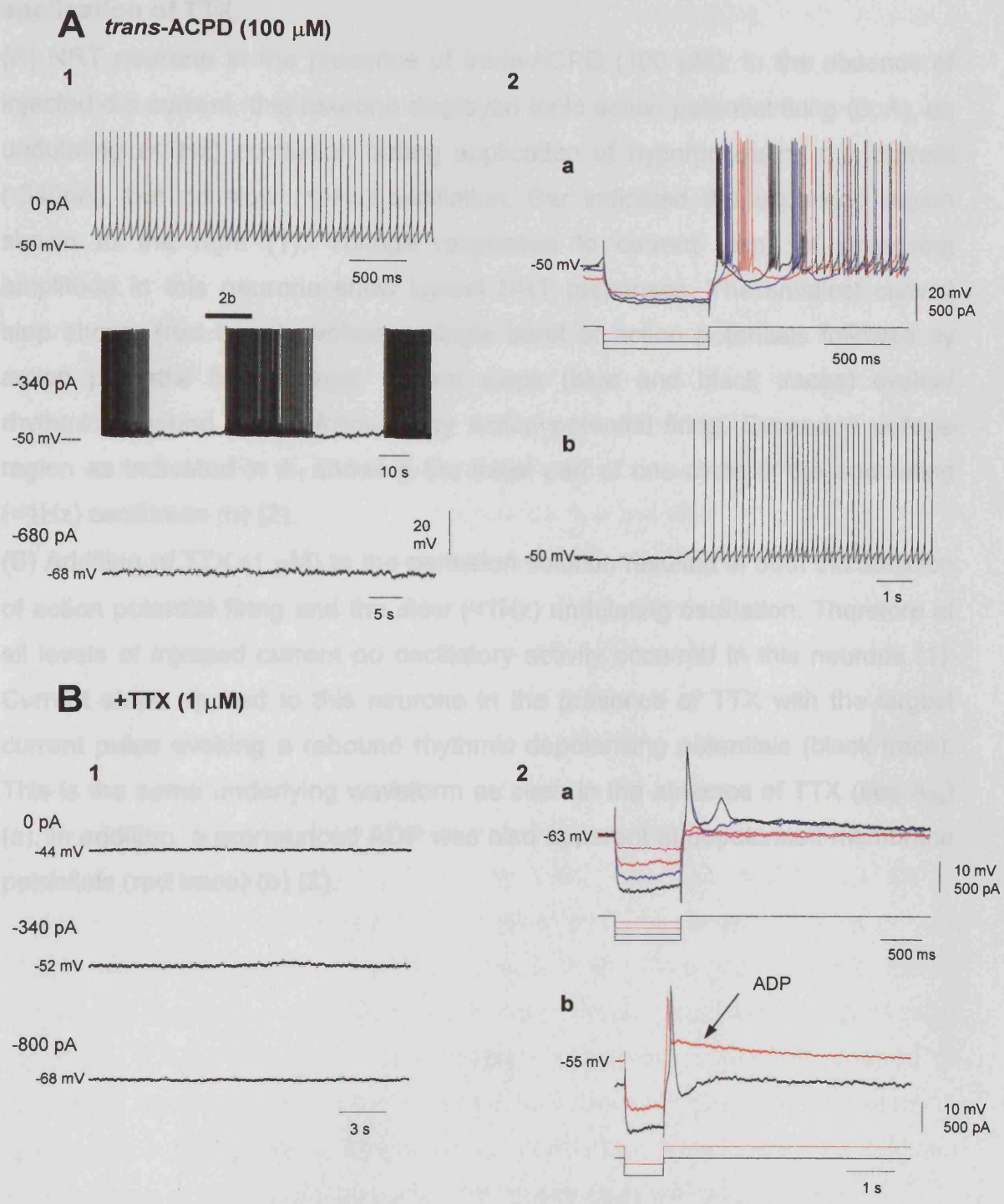

Figure 5.14 The undulating (<1Hz) oscillation is abolished following application of TTX.

Figure 5.14 The undulating (<1Hz) oscillation is abolished following application of TTX.

(A) NRT neurone in the presence of *trans*-ACPD (100 μM). In the absence of injected d.c current, this neurone displayed tonic action potential firing (0pA), an undulating (<1Hz) oscillation during application of hyperpolarising d.c. current (-340pA), but no slow (<1Hz) oscillation. Bar indicated the expanded region shown to the right (1). Voltage responses to current steps of increasing amplitude in this neurone show typical NRT responses. The smallest current step shown (red trace) evokes a single burst of action potentials followed by action potential firing, larger current steps (blue and black traces) evoked rhythmic rebound bursts followed by action potential firing. Expanded voltage region as indicated in A_1 showing the initial part of one cycle of the undulating (<1Hz) oscillation (b) (2).

(B) Addition of TTX (1 μM) to the perfusion solution resulted in both the abolition of action potential firing and the slow (<1Hz) undulating oscillation. Therefore at all levels of injected current no oscillatory activity occurred in this neurone (1). Current steps applied to this neurone in the presence of TTX with the largest current pulse evoking a rebound rhythmic depolarising potentials (black trace). This is the same underlying waveform as seen in the absence of TTX (see A_{2a}) (a). In addition, a pronounced ADP was also apparent at depolarised membrane potentials (red trace) (b) (2).

trans-ACPD as described here always caused a robust depolarisation and induced sustained action potential firing in accordance with previous observations. However, not previously described is the induction of a slow (<1Hz) oscillation in NRT neurones *in vitro* that has identical properties to that observed in NRT neurones *in vivo* (Fig. 5.15) (Steriade et al. 1987; Steriade et al. 1993a; Timofeev and Steriade 1996) including: 1) clearly distinguished "up" and "down" states; 2) a LTCP-mediated burst marking the transition to the "up" phase; 3) an LHP encompassing the "down" state; and 4) the ability to group spindle frequency action potential bursts within the <1Hz frequency. Extracellular recordings of NRT neurones in the presence of *trans*-ACPD indicate both that the slow (<1Hz) oscillation can normally occur and that its generation is dependent on the *trans*-ACPD concentration and therefore the level of neuronal depolarisation as demonstrated by the induction of the slow (<1Hz) oscillation in between quiescence and tonic firing activity as *trans*-ACPD was washed on (Fig. 5.6). The dependence of the generation of the slow (<1Hz) oscillation on activation normally arising from corticothalamic inputs in the intact brain was demonstrated *in vitro* as the *trans*-ACPD effect could be 1) mimicked by the specific Group I agonist DHPG and 2) was abolished by the selective mGluR1a antagonist LY 367385. These observations are consistent with previous demonstration that mGluR activation occurs via corticothalamic inputs to NRT neurones (McCormick and von Krosigk 1992; Lee and McCormick 1997). Additionally, the predominant mGluR input to NRT neurones results in a long-lasting depolarisation (Lee and McCormick 1997; Cox and Sherman 1999), suggesting that as in TC neurones, corticothalamic activation results in tonic activation of NRT neurones. Given the similarity of the slow (<1Hz) oscillation described *in vitro* here to that observed in vivo (Steriade et al. 1993a; Contreras and Steriade 1996), this is likely to be the first *in vitro* demonstration of the slow (<1Hz) sleep oscillation occurring in NRT neurones *in vivo* during sleep.

5.4.2 Grouped bursting activity in NRT neurones.

In a number of cases, both intracellularly and extracellularly, the slow (<1Hz) oscillation grouped bursting activity at frequencies ranging from 1-13Hz. This therefore encompasses δ (1-2Hz) and spindle (7-14Hz) frequency ranges. In most cases, the bursting frequency was lower than that typically described as spindle frequencies although this may be the effect of recording *in vitro* as the

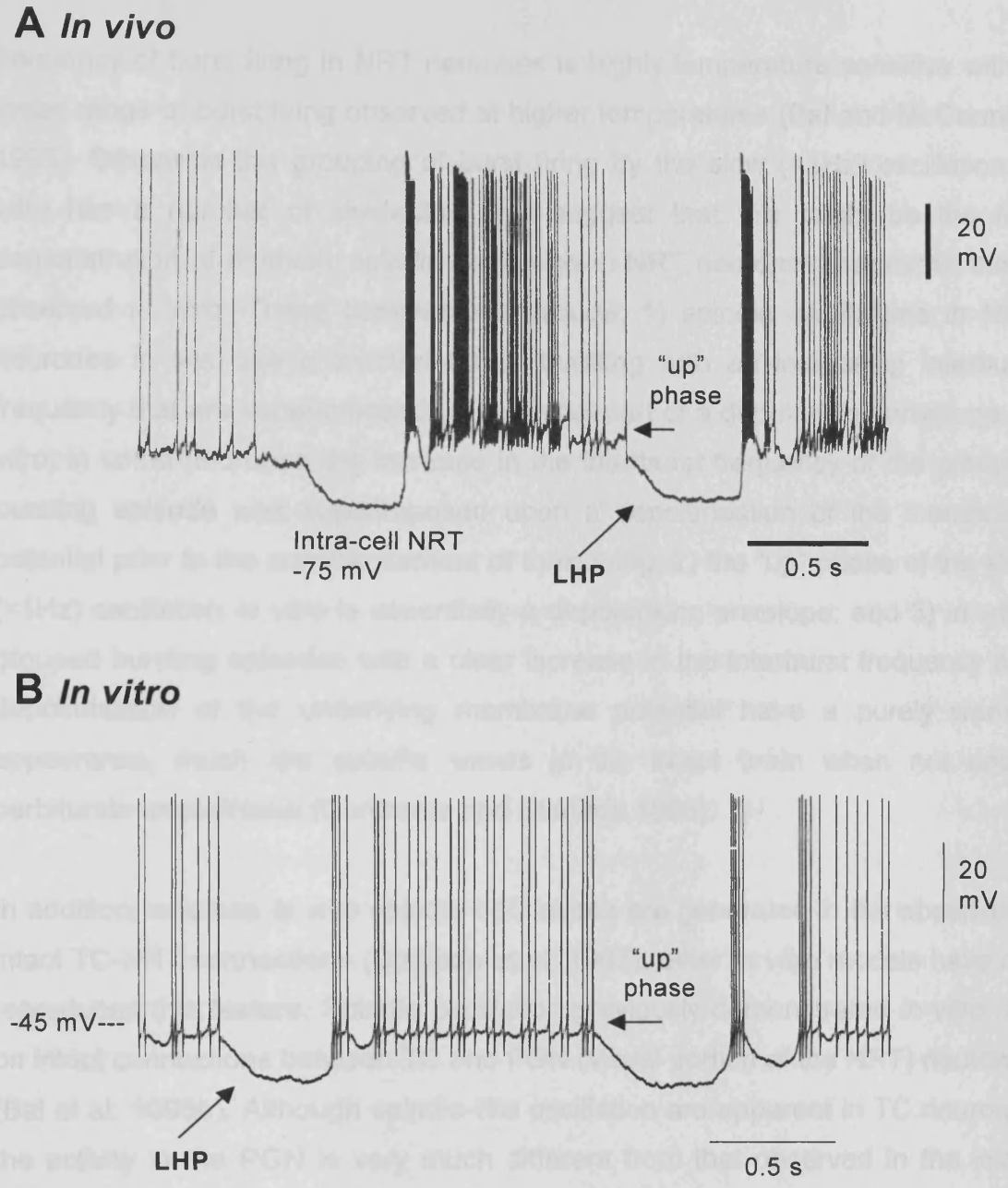

Figure 5.15 Comparison of the slow (<1Hz) oscillation in NRT neurones *in vivo* and *in vitro*.

(A) Example of the slow (<1Hz) oscillation in a NRT neurone *in vivo* (from Contreras 1996).

(B) Example of the slow (<1Hz) oscillation in a NRT neurone *in vitro*.

frequency of burst firing in NRT neurones is highly temperature sensitive with a faster range of burst firing observed at higher temperatures (Bal and McCormick 1993). Otherwise the grouping of burst firing by the slow (<1Hz) oscillation *in vitro* has a number of similarities that suggest that this might be the first demonstration of rhythmic spindle oscillation in NRT neurones that mimic those observed *in vivo*. These observations include: 1) spindle oscillations in NRT neurones *in vivo* are characterised by bursting with an increasing interburst frequency that are superimposed on the initial part of a depolarising envelope. *In vitro*, in some neurones the increase in the interburst frequency of the grouped bursting episode was superimposed upon a depolarisation of the membrane potential prior to the commencement of tonic firing; 2) the "up" phase of the slow (<1Hz) oscillation *in vitro* is essentially a depolarising envelope; and 3) *in vitro*, grouped bursting episodes with a clear increase in the interburst frequency and depolarisation of the underlying membrane potential have a purely waning appearance, much like spindle waves in the intact brain when not under barbiturate anaesthesia (Contreras and Steriade 1996).

In addition, whereas *in vivo* spindle oscillations are generated in the absence of intact TC-NRT connections (Steriade et al. 1987), other *in vitro* models have not reproduced this feature. Spindle oscillation previously demonstrated *in vitro* rely on intact connections between TC and PGN (visual portion of the NRT) neurones (Bal et al. 1995b). Although spindle-like oscillation are apparent in TC neurones the activity in the PGN is very much different from that observed in the intact brain, with the PGN spindle oscillation comprising rhythmic sequences of LTCP-mediated bursting with an underlying progressive hyperpolarisation and followed by a period of silence as the membrane potential slowly repolarises before the next cycle begins (Bal et al. 1995b). In addition, in this *in vitro* model the periodicity of spindle oscillations is abolished by blocking I_h in TC neurones, resulting in a continual bombardment of IPSPs in TC neurones presumably from NRT neurones and thus indicating that the NRT is no longer generating rhythmic activity (Luthi et al. 1998).

5.4.3 Mechanism of the slow (<1Hz) oscillation in NRT neurones.

The slow (<1Hz) oscillation in NRT neurones was generated both in the absence of synaptic inputs and also the underlying slow (<1Hz) oscillation waveform

persisted in the presence of TTX. In the presence of TTX the waveform of the slow (<1Hz) oscillation was remarkably similar in both NRT and TC neurones. As in TC neurones, the transition from the "down" phase of the oscillation was marked by a LTCP, followed by a long-lasting depolarised phase comprising the "up" phase followed by a return to the hyperpolarised "down" phase often marked by a clear inflection point and finally followed by a slowly depolarising phase before the initiation of a subsequent LTCP.

As the slow (<1Hz) oscillation is critically dependent on $I_{Twindow}$ in TC neurones (see Chapters 3 and 4) (Williams et al. 1997a; Hughes et al. 1999) a role for $I_{Twindow}$ for the generation of the slow (<1Hz) oscillation in NRT neurones may be suggested. Only on few occasions were voltage responses indicative of the presence of $I_{Twindow}$ observed in NRT neurones displaying a slow (<1Hz) oscillation (Fig. 5.10A_{1c}). However, application of TTX effectively enhanced these responses and neurones displaying a slow (<1Hz) oscillation in the presence of TTX also displayed bistability-mediated activities, including input amplification and a clear inflection point during hyperpolarising voltage perturbations (Fig. 5.10A_{2c}). Additionally, TTX consistently increased the R_N of NRT neurones suggesting that the persistent Na^+ current (I_{Nap}), the Na^+-activated K^+ current (I_{KNa}) are effective in masking $I_{Twindow}$ mediated activities during evoked voltage responses. Conclusive demonstration of the role of $I_{Twindow}$ through application of Ni^{2+} or use of the dynamic clamp system has yet to be performed.

As previously described, (Bal and McCormick 1993), TTX application was also effective in unmasking a pronounced ADP following the LTCP in NRT neurones irrespective of their ability to display the slow (<1Hz) oscillation. This ADP, that has previously been demonstrated as being generated by I_{CAN}, underlies the tonic tail of action potential firing following evoked LTCPs and is critically dependent on the level of neuronal polarisation (Bal and McCormick 1993). The "up" phase of the slow (<1Hz) oscillation is similar to this evoked LTCP-ADP response in that 1) generation of the slow (<1Hz) oscillation is also dependent on the level of neuronal polarisation; and 2) the "up" phase comprises decelerating tonic firing consistent with the transient tonic tail. This suggests that the LTCP-ADP sequence has a role in determining the manifestation of the slow (<1Hz)

oscillation (as in TC neurones, see Chapter 4) although has yet to be demonstrated.

In most cases the "down" phase of the slow (<1Hz) oscillation comprised a slowly depolarising phase (Fig. 5.3, 5.4, 5.5, 5.8, 5.10, 5.11). In TC neurones this slow repolarisation is attributed to the activation of I_h. (McCormick and Pape 1990; Leresche et al. 1991; Soltesz et al. 1991), see Chapter 4). However, in NRT neurones, I_h is suggested not to have a critical role in the oscillatory activity as rhythmic burst firing persists in the presence of extracellular Cs^+ (Bal and McCormick 1993). A number of observations support the presence of I_h in NRT neurones including: 1) the small but evident slow "sag" during application of negative current steps; 2) the lack of this slow depolarisation in the presence of ZD 7288, which should not abolish the I_{KNa} (Kim and McCormick 1998a); and 3) the cessation of grouped δ frequency burst firing by ZD 7288. Therefore, it may be the case that different mechanisms are responsible for rhythmic bursting activity at different frequencies in NRT neurones. Rhythmic burst firing from δ (1-2Hz) to spindle (7-14Hz) frequencies occurs as a continuum with the frequency increasing as neurones are depolarised (Llinas and Geijo-Barrientos 1988; Bal and McCormick 1993). Therefore there may be an I_T / I_h dependent mechanism generating slower bursting activity at hyperpolarised membrane potentials (as in TC neurones) and the well documented I_T / I_{KCa} dependent mechanism (Llinas and Geijo-Barrientos 1988; Avanzini et al. 1989; Bal and McCormick 1993) generating faster bursting activity at depolarised membrane potentials with the level of neuronal polarisation determining which is the dominant mechanism. This could account for the observation here that ZD 7288 abolished bursts firing at δ frequencies, where as previous observation of the role of I_h only describe results based on faster frequency bursting (Llinas and Geijo-Barrientos 1988; Avanzini et al. 1989; Bal and McCormick 1993). As only δ frequency bursting activity was seen prior to the application of ZD 7288, no assessment of the faster frequency bursting could be made in the presence of ZD 7288. The fact that ZD 7288 also abolished the rhythmicity of the slow (<1Hz) oscillation but left intact the ability to generate the LTCP following appropriate d.c. current injection (Fig. 5.11) suggests that I_h could have a role in the generation of the slow (<1Hz) oscillation.

The role of other K^+ currents should not be neglected here. Following evoked but sustained tonic firing in NRT neurones a two-component long-lasting AHP (5-15 seconds), involving I_{KNa}, is observed at the offset of firing (Kim and McCormick 1998a). The slowly repolarising nature of this response could play a role in the slow depolarisation during the "down" phase of the slow (<1Hz) oscillation. It appears that this long-lasting response develops slowly during an episode of bursts or sustained action potential firing and suggests that it is not responsible for the rapid transition from the "up" state to the "down" state (Kim and McCormick 1998a). The persistence of the slow (<1Hz) oscillation shown here in TTX indicates that Na+ channels are not critically required, although a role for I_{KNa} in prolonging the "down" phase is possible. In light of these observations, the dependence of the properties of the slow (<1Hz) oscillation on the level of injected d.c. current and the similarity of the underlying waveform in the presence of TTX in both NRT and TC neurones, it is very likely that the slow (<1Hz) oscillation in NRT neurones is also critically dependent on the presence of $I_{Twindow}$. Further investigations will be required to definitively answer this question.

5.4.4 The slow (<1Hz) undulating oscillation in NRT neurones.

Although observed in the presence of *trans*-ACPD and having a similar minimum frequency range, the undulating (<1Hz) oscillation had a number of properties that distinguished it from the slow (<1Hz) oscillation (Fig. 5.12 and 5.13), including: 1) the slow (<1Hz) oscillation is characterised by a LTCP marking the transition to the "up" state and a rapid transition back to the "down" state often marked with a clear inflection point. In contrast, the undulating (<1Hz) oscillation is characterised by a slow transition both to the "up" state and back to the "down" state; 2) a much larger membrane potential range between the "up" state and "down" state of the slow (<1Hz) oscillation when compared to the undulating (<1Hz) oscillation; 3) the frequency of the slow (<1Hz) oscillation was a clearly dependent on the level of injected d.c. current and decreased as neurones were depolarised, whereas the frequency of the undulating (<1Hz) oscillation appeared to be far less dependent on injected d.c. current; and 4) the "up" phase of the slow (<1Hz) oscillation was characterised by decelerating action potential firing and that of the undulating slow (<1Hz) oscillation by accelerating and then decelerating action potential firing. These substantial differences and the

observation of both types of <1Hz oscillation were observed in one NRT neurone at different levels of membrane potential, and apparently independently of each other, suggest that the mechanism of generation of the undulating (<1Hz) oscillation differs from the mechanism generating the slow (<1Hz) oscillation. The undulating (<1Hz) oscillation persisted in the presence of blockade of glutamatergic and GABAergic receptors, but was abolished by application of TTX, indicating a dependence on Na^+ channels. A number of different mechanisms could be responsible including: 1) the interaction of I_{Nap} and K^+ currents at fairly depolarised membrane potentials, 2) transient activation of Na^+-dependent K^+ channels; or 3) or the activation of Ca^{2+} dependent K^+ currents caused by Ca^{2+} influx during action potential firing. It is possible that this type of oscillation can arise in *trans*-ACPD due to the reduced I_{KLeak}, which, by increasing R_N, may effectively couple interacting currents. However, perhaps this type of oscillation may only occur on a background of low neuronal activity i.e. lack of synaptic inputs in the membrane potential region where the oscillation is occurring, or if the neurone was recorded in the presence of synaptic blockers (as described here).

CHAPTER 6

SPIKELETS AND DYE-COUPLING IN THE THALAMUS: ELECTROPHYSIOLOGICAL AND MORPHOLOGICAL INDICATORS OF ELECTROTONIC COUPLING

6.1 INTRODUCTION

During the course of intracellular recordings made in TC and NRT neurones, it became apparent that subsets of each neuronal type displayed small, stereotyped depolarising potentials, or spikelets. These spikelets had a very similar appearance to spikelets that are observed in neuronal populations that have been shown to communicate electrotonically and thought to arise through direct interneuronal communication via gap junctions (GJs) (Logan et al. 1996; Galarreta and Hestrin 1999; Galarreta and Hestrin 2001; Landisman et al. 2002).

Spikelets are believed to arise as a result of ionic membrane changes resulting from the generation of action potentials in a coupled neurone transferred via GJs (Logan et al. 1996; Galarreta and Hestrin 2001; Landisman et al. 2002). Action potentials are filtered or attenuated as they pass along the dendrites of the interconnected neurones and hence the spikelet generated in the coupled neurone will take the form of a filtered action potential. As such, spikelets have an all-or-none appearance (as do action potentials) and a faster repolarising phase than conventional postsynaptic potentials since the repolarising phase of the action potential is an active process. In addition, the AHP following each action potential is also transmitted via the GJ and leads to the generation of an often pronounced spikelet AHP (Galarreta and Hestrin 2001; Landisman et al. 2002).

Dye-coupling is also taken as an indication of the presence of GJs allowing direct interneuronal communication (MacVicar and Dudek 1981; Nunez et al. 1990; O'Donnell and Grace 1993; Valiante et al. 1995; Mann-Metzer and Yarom 1999). Although often associated with neuronal populations that are known to communicate electrotonically, dye-coupling is notably absent in GABAergic neuronal populations that have otherwise been demonstrated to communicate electrotonically (Gibson et al. 1999; Galarreta and Hestrin 2001; Landisman et al. 2002). The notable absence of dye-coupling in electrotonically coupled populations of interneurones is thought to be due to the particular properties of Cx36 channels, the Cx subtype is associated with electrotonic coupling in these neuronal populations. In particular, intercellular channels formed by Cx36 have the smallest single channel conductance of any tested connexin and are only slightly permeable to some organic dyes that permeate other connexin channels

easily (Srinivas et al. 1999; Teubner et al. 2000). Therefore with the presently available intracellular dyes it is suggested that dye transfer is restricted by specific connexin type. An additional factor may be the strength of connections made between neurones (Galarreta and Hestrin 2001), presumably with a greater number of GJs at a given site facilitating the transfer of dye to an electrotonically coupled neurone.

Direct interneuronal communication, via electrotonic coupling, between NRT neurones has been demonstrated, although only in brain slices from neonatal rodents (Landisman et al. 2002). As the extent of electrotonic communication / GJs decreases during development (Dermietzel and Spray 1993; Rozental et al. 2000), it is unknown whether or not electrotonic communication is a functional interneuronal form of communication in the adult NRT. In addition, investigations into electrotonic coupling have been carried out predominantly in rodents and assumptions have to be made regarding the applicability of the information derived from these studies to general thalamic mechanisms. So-called fastprepotentials (FPPs) in NRT neurones *in vitro* and *in vivo* and in TC neurones *in vivo* have properties similar to spikelets (Deschenes et al. 1984; Llinas and Geijo-Barrientos 1988; Steriade et al. 1991b; Amzica et al. 1992; Contreras et al. 1993; Timofeev and Steriade 1997). This suggests that thalamic neurones may communicate directly via an electrotonic mechanism in the intact brain. However, as the origin of these FPPs has not been fully elucidated, this remains as yet an unanswered question.

This chapter describes the properties and experimental observations regarding the spikelets and dye-coupling observed in TC and NRT neurones during intracellular recordings. The aims are to characterise the properties or characteristics of spikelets and dye-coupling in these neuronal populations and to determine the origin of spikelets.

6.2 METHODS

6.2.1 Electrophysiology.

Intracellular and extracellular recordings were performed in adult cat thalamic slices as described in Chapter 2. Recordings were made from both TC and PGN

or NRT neurones. All PGN or NRT neurones are hereafter referred to as NRT neurones in this chapter for simplicity.

6.2.2 Data analysis.

Data analysis was performed as described in Chapter 2 except:

6.2.2.1 Spikelet analysis.

Spikelet analysis was performed using Clampfit software (Axon Instruments). Spikelet frequency was calculated using the reciprocal of the preriod between the peak of successive spiekelets (Fig. 6.1A) at a given level of injected d.c. current. Spikelet amplitude, time to peak, spikelet duration and spikelet decay time constant (τ_{decay}: calculated by fitting an exponential curve between maximum and minimum spikelet amplitude (Fig. 6.1B) were measured. The spikelet AHP amplitude and AHP decay time constant (AHP τ_{decay}: calculated by fitting an exponential curve between the maximum and minimum membrane potentials of the spikelet AHP as shown) were also measured (Fig. 6.1C).

6.2.2.2 Burstlet analysis.

The burstlets described here are groups of spikelets with an underlying depolarising potential. Burstlets properties were also analysed using Clampfit software and measured parameters included the burstlet frequency, duration, amplitude and time to peak (Fig. 6.2).

6.2.3 Morphological procedure.

Morphological processing and identification of TC and NRT neurones was performed as described in Chapter 2 except:

6.2.3.1 Identification and analysis of dye-coupled neurones.

The criteria for dye-coupling was the presence of 2 or more closely associated soma in an area where only one cell had been impaled and recorded. 2-4 penetrations were made per thalamic slice in order to avoid multiple penetrations in a given region of the slice (see Chapter 2). Identification was made visually under a light microscope (Labophot-2, Nikon). The injected neurone could at times be identified as the most densely stained neurone and often the site of electrode penetration was apparent. The approximate distance between coupled

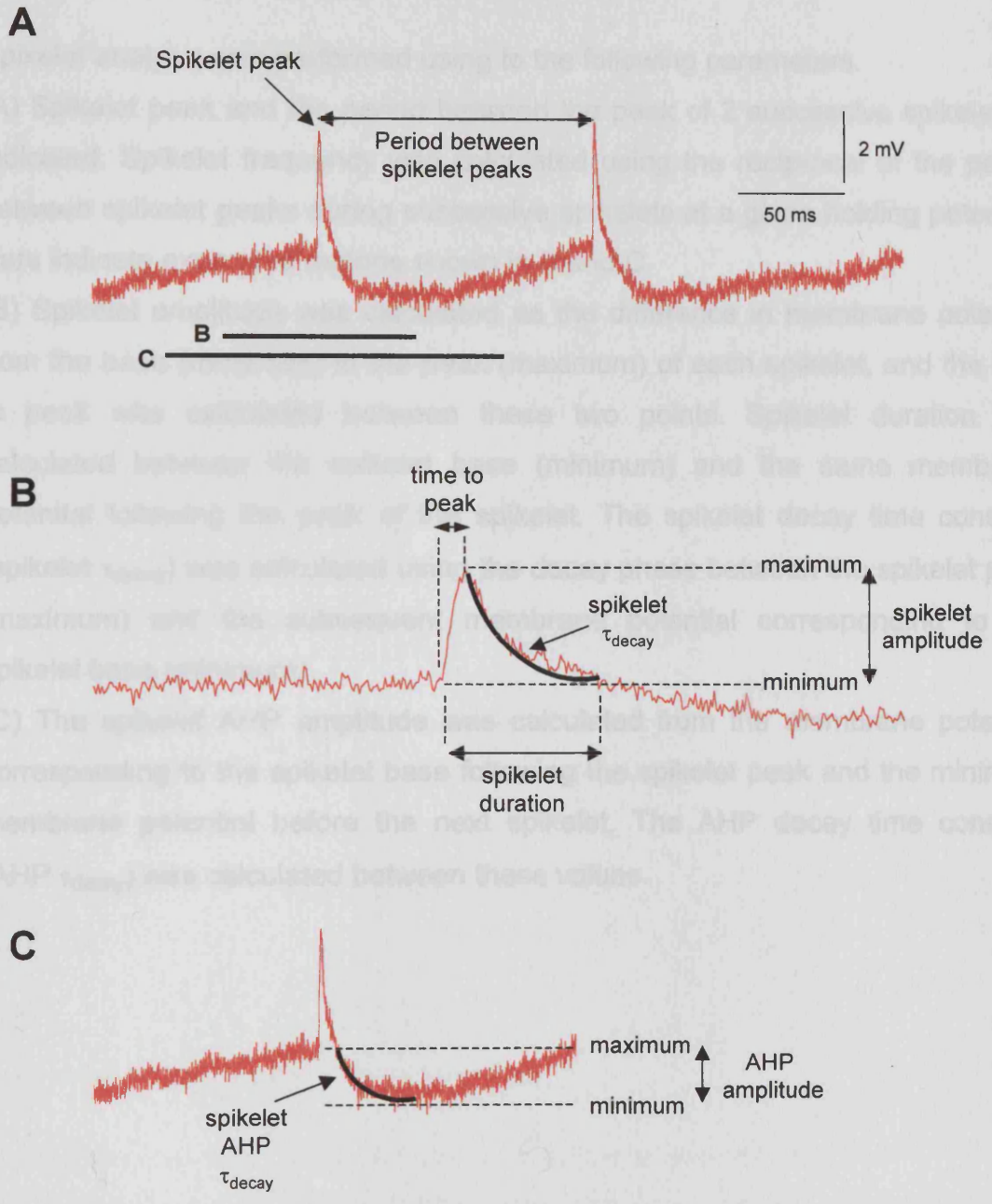

Figure 6.1 Spikelet analysis parameters.

Figure 6.1 Spikelet analysis parameters.

Spikelet analysis was performed using to the following parameters.
(A) Spikelet peak and the period between the peak of 2 successive spikelets is indicated. Spikelet frequency was calculated using the reciprocal of the period between spikelet peaks during successive spikelets at a given holding potential. Bars indicate expanded regions shown in B and C.
(B) Spikelet amplitude was calculated as the difference in membrane potential from the base (minimum) to the peak (maximum) of each spikelet, and the time to peak was calculated between these two points. Spikelet duration was calculated between the spikelet base (minimum) and the same membrane potential following the peak of the spikelet. The spikelet decay time constant (spikelet τ_{decay}) was calculated using the decay phase between the spikelet peak (maximum) and the subsequent membrane potential corresponding to the spikelet base (minimum).
(C) The spikelet AHP amplitude was calculated from the membrane potential corresponding to the spikelet base following the spikelet peak and the minimum membrane potential before the next spikelet. The AHP decay time constant (AHP τ_{decay}) was calculated between these values.

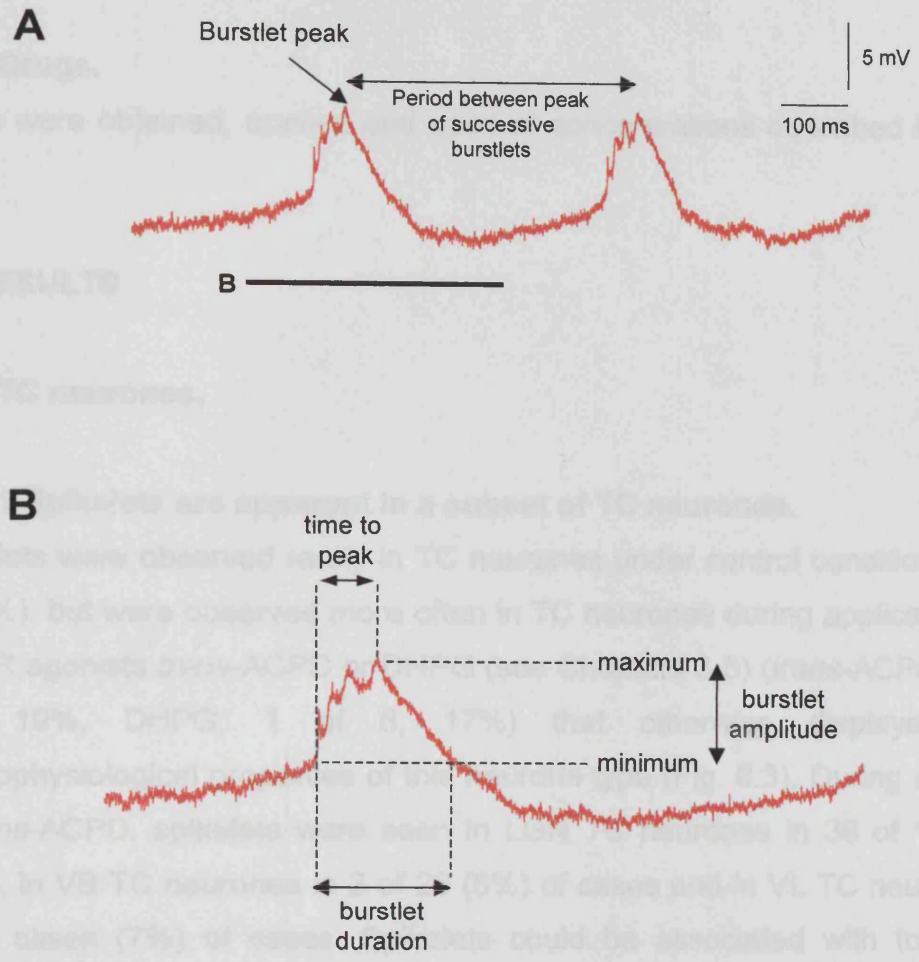

Figure 6.2 Burstlet analysis parameters.

Burstlet analysis was performed using the following parameters.

(A) Burstlet frequency was calculated using the reciprocal of the period between burstlet peaks (measured at the maximum membrane potential observed during each burstlet) of successive burstlets at a given holding potential. Bar indicates the expanded region shown in B.

(B) Burstlet amplitude was calculated as the difference in membrane potential from the base (minimum) to the peak (maximum) of each burstlet and the time to peak was calculated between these two points. Burstlet duration was calculated between the burstlet base (minimum) and the same membrane potential following the peak of the burstlet.

neurones was measured as the distance between the apparent centres of recorded and coupled somas at x100 magnification.

6.2.4 Drugs.

Drugs were obtained, applied and used at concentrations described in Chapter 2.

6.3 RESULTS

6.3.1 TC neurones.

6.3.1.1 Spikelets are apparent in a subset of TC neurones.

Spikelets were observed rarely in TC neurones under control conditions (n=2 of 79, 3%), but were observed more often in TC neurones during application of the mGluR agonists *trans*-ACPD or DHPG (see Chapters 3-5) (*trans*-ACPD: n=39 of 205, 19%, DHPG: 1 of 6, 17%) that otherwise displayed typical electrophysiological properties of this neurone type (Fig. 6.3). During application of *trans*-ACPD, spikelets were seen in LGN TC neurones in 36 of 137 (26%) cases, in VB TC neurones in 2 of 26 (8%) of cases and in VL TC neurones in 1 of 15 cases (7%) of cases. Spikelets could be associated with tonic action potential firing (Fig. 6.3A), the LTCP (Fig. 6.3B) or during depolarised phases of the slow (<1Hz) oscillation (Fig. 6.3C) (see Chapter 3). Spikelets were apparent as stereotypical, short duration (range = 4.3 –17.8 ms, mean = 9.0 ± 0.08 ms, n=60 from 20 neurones) subthreshold depolarising potentials (Fig. 6.3). The presence of spikelets was extremely robust and could remain unaltered for substantially long recording periods (>3 hours). Spikelets were presumably dependent on neuronal depolarisation (brought about by mGluR activation) as they were rarely observed in the absence of *trans*-ACPD (Fig. 6.4A) or DHPG, but could appear following an increase in extracellular [K^+] from 3.25 to 6 mM (n=2 of 10, 20%) (Fig. 6.4B).

6.3.1.2 Spikelets have stereotypical properties in TC neurones.

Spikelets were apparent both during application of a cocktail of synaptic antagonists (CNQX, APV, BMI, CGP 5699A, n=27) and in its absence (n=12). Even though the waveform of spikelets (time to peak: mean = 1.22 ± 0.08 ms,

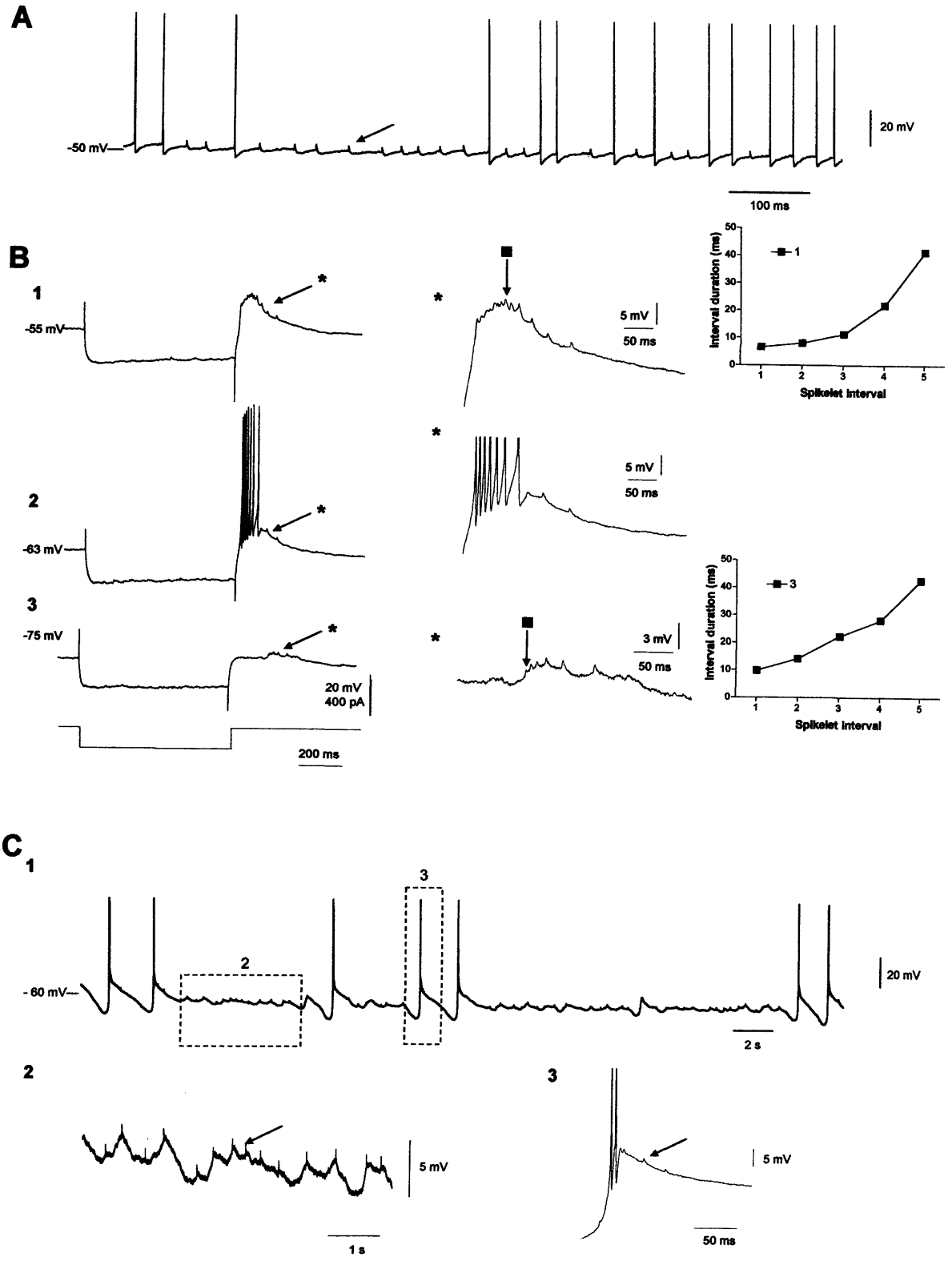

Figure 6.3 Spikelets in TC neurones.

Figure. 6.3 Spikelets in TC neurones.

Spikelets, as indicated by arrows (↙) throughout, are apparent in TC neurones in association with otherwise normal TC activities.

(A) Spikelets are apparent at relatively depolarised membrane potentials and sometimes lead to the generation of action potentials.

(B) TC neurones at increasingly hyperpolarised membrane potentials (1-3) with spikelets apparent on the LTCP-mediated depolarisation (1) and partially masked by the LTCP-mediated burst of action potentials (2). At the most hyperpolarised membrane potential, no rebound LTCP was evoked, however spikelets were still apparent (3). Expanded sections (*) are shown to the right of each trace. In the cases where spikelets are not masked by action potentials, spikelets had a decelerating frequency much like the LTCP-mediated bursts of action potentials, characteristic of TC neurones (graphs in 1 and 3, ■ indicates the 1st spikelet used to construct each graph).

(C) TC neurones showing spikelets during the depolarised phases of the slow (<1Hz) oscillation (1), both on the depolarised plateau phase (although not leading to action potential firing in this case) (2) and also associated with the LTCP-mediated depolarisation (3). Boxed sections are expanded and shown below the main trace.

trans-ACPD (100 μM) was present in all cases.

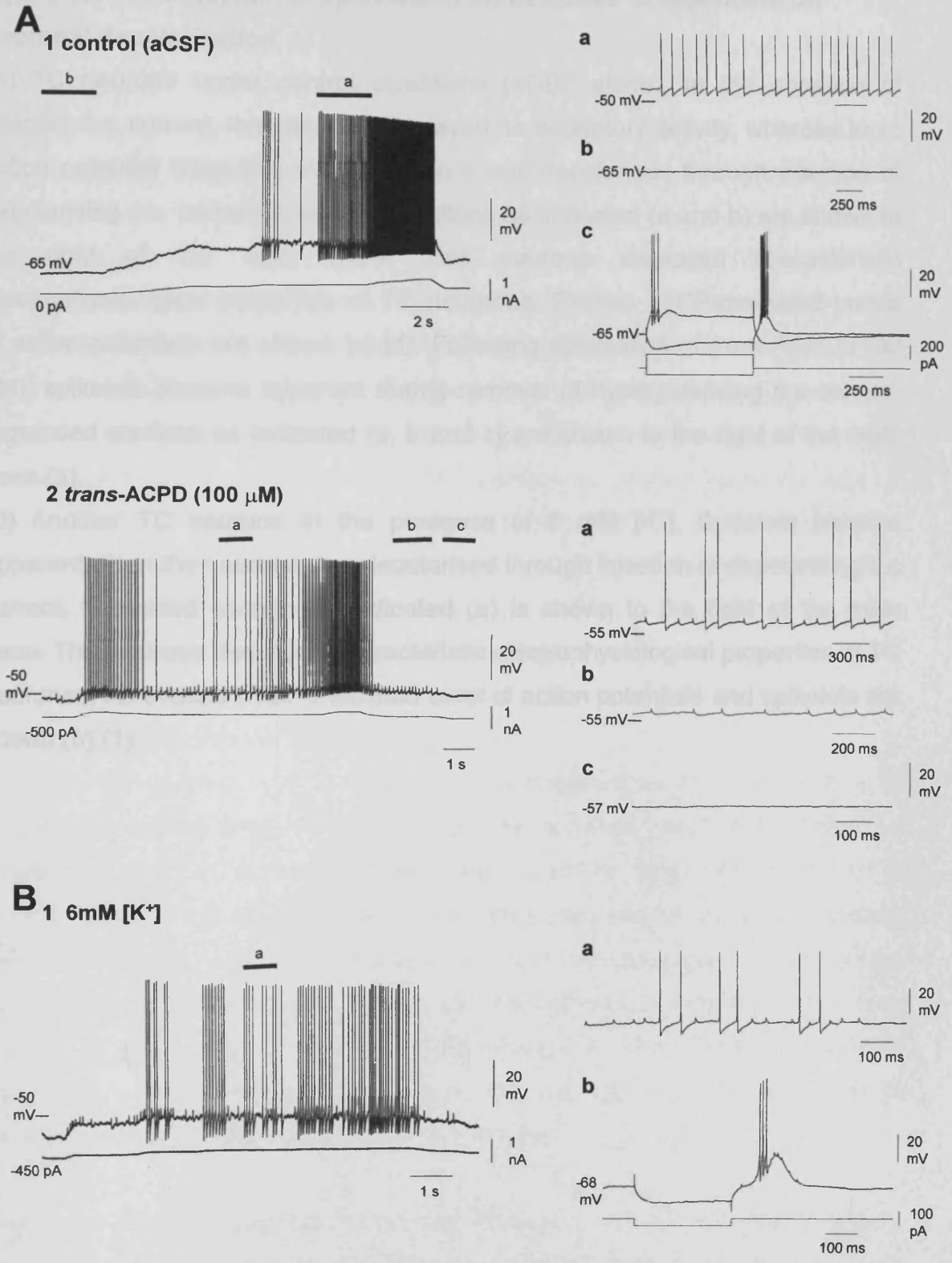

Figure 6.4 The induction of spikelets in TC neurones is dependent on neuronal depolarisation.

Figure 6.4 The induction of spikelets in TC neurones is dependent on neuronal depolarisation.

(A) TC neurone under control conditions (aCSF alone). In the absence of injected d.c. current, this neurone displayed no oscillatory activity, whereas tonic action potential firing was evident when it was depolarised through injection of depolarising d.c. current. Expanded sections as indicated (a and b) are shown to the right of the main trace. This neurone displayed characteristic electrophysiological properties of TC neurones. Evoked LTCP-mediated bursts of action potentials are shown (c) (1). Following application of *trans*-ACPD (100 μM), spikelets became apparent during removal of hyperpolarising d.c current. Expanded sections as indicated (a, b and c) are shown to the right of the main trace (2).

(B) Another TC neurone in the presence of 6 mM [K^+]. Spikelets became apparent when the neurone was depolarised through injection of depolarising d.c current. Expanded section as indicated (a) is shown to the right of the main trace. This neurone displayed characteristic electrophysiological properties of TC neurones. An evoked LTCP-mediated burst of action potentials and spikelets are shown (b) (1).

n=60 form 20 neurones, decay time constant (τ decay): mean = 3.85 ± 0.45 ms, n=60) was similar to that of conventional postsynaptic potentials, they could be distinguished on the basis of the following observations. Although the amplitude of spikelets was variable in different TC neurones (range = 2-7 mV), the amplitude of spikelets in a given neurone did not vary greatly leading to an apparent all-or-none appearance and suggesting that each spikelet represents a discrete event. In addition the presence of a transient AHP not seen with conventional postsynaptic potentials also suggested a different origin. A comparison of the spikelet and action potential waveforms shows that the time to peak and repolarisation was slightly slower for the spikelet than for the action potential (Fig. 6.5). The frequency of spikelets was dependent on neuronal depolarisation, with the frequency of spikelets increasing with injection of depolarising d.c. current (Fig. 6.6) and decreasing (and then usually abolished) with injection of progressively hyperpolarising d.c. current (Fig. 6.4A_2, 6.9A). Notably though, the amplitude and time to peak of spikelets were largely unaffected by membrane polarisation (Fig. 6.6B_2).

6.3.1.3 Spikelets entrain TC firing activities.

In a few TC neurones (n= 7) spikelets were apparent as rhythmic grouped or summated events, that I will hereafter call burstlets, each comprising 2-4 spikelets (Fig. 6.7A). Burstlets occurred within a slower range of frequencies 1.4 – 11.7 Hz, 4.8 ± 0.2 (n=83 in 7 neurones) than observed for spikelets. Burstlets had some similar properties to those of discrete individual spikelets, in that the burstlet frequency was dependent on the level of neuronal depolarisation (see Fig. 6.7B). In addition, there was little change in other burstlet properties examined, with no apparent change in the burstlet amplitude and a slight decrease in the burstlet duration and time to peak (Fig. 6.7B_3).

The dependence of spikelets or burstlet frequency on neuronal depolarisation, with little or no change to the characteristics of each event is particularly reminiscent of firing activities in TC neurones. Both spikelets and action potentials are all or none events (Fig. 6.8A_1) and the frequency of tonic action potential firing, like that of spikelets, is dependent on neuronal depolarisation (see Fig. 6.4A_1 for action potentials and Fig. 6.6B_1 for spikelets). On the other hand, burstlets comprise grouped spikelets, whilst high-threshold (HT) bursts

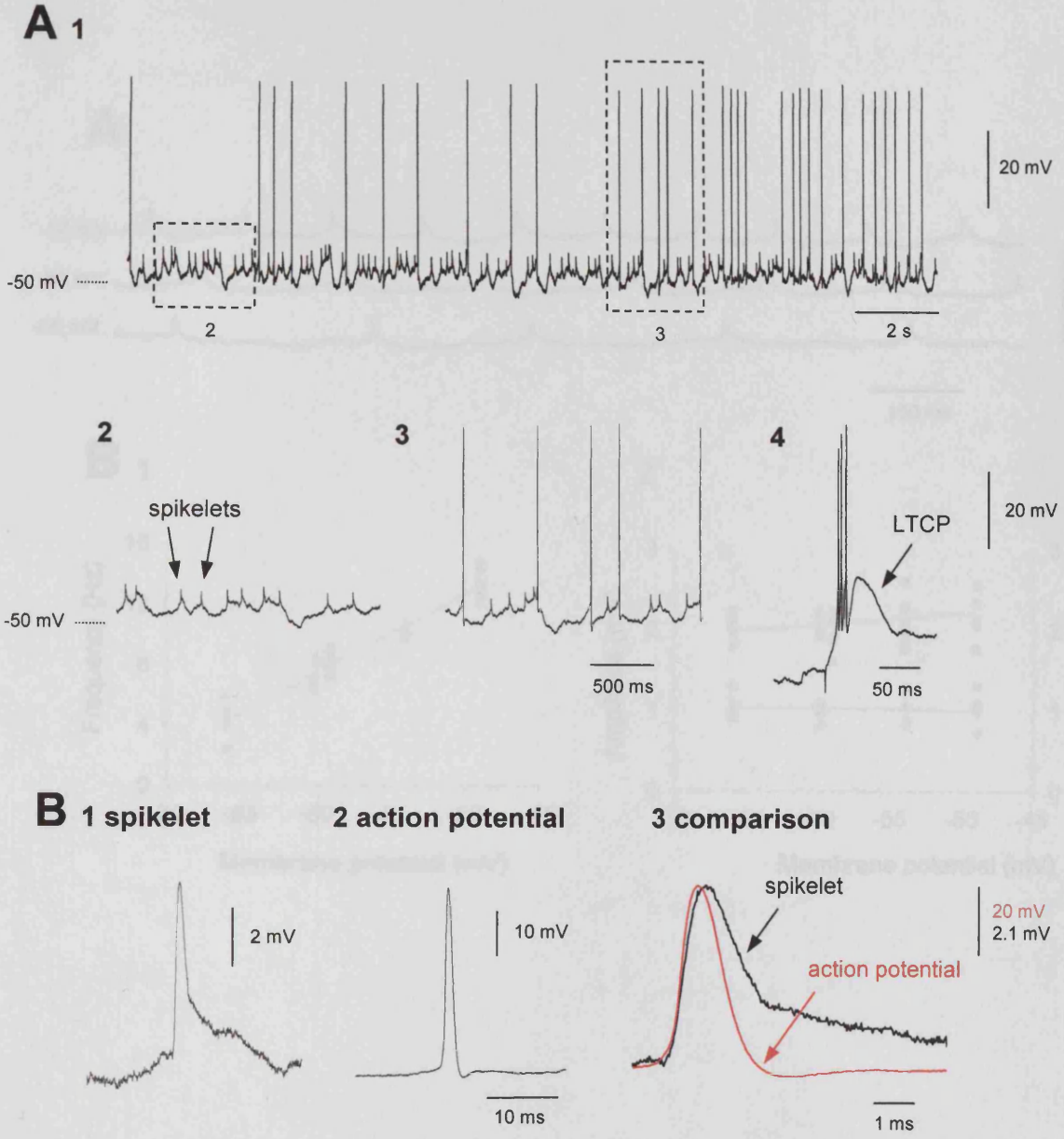

Figure. 6.5 Spikelets in TC neurones have a stereotypical waveform.

(A) TC neurone recorded in the presence of *trans*-ACPD (100 μM) exhibiting spikelets. Expanded sections in 2 and 3 illustrate the stereotypical nature of spikelets. Apart from the presence of spikelets, this cell exhibited properties that are typical of TC neurones, most notably a robust LTCP (3).

(B) Comparison of spikelets (1) and action potentials (2) show a similar waveform. However the overlay of the spikelet and the action potential shows that the spikelet has a slightly longer time to peak and substantially slower decay than the action potential (3).

Published in Hughes et al. 2002a

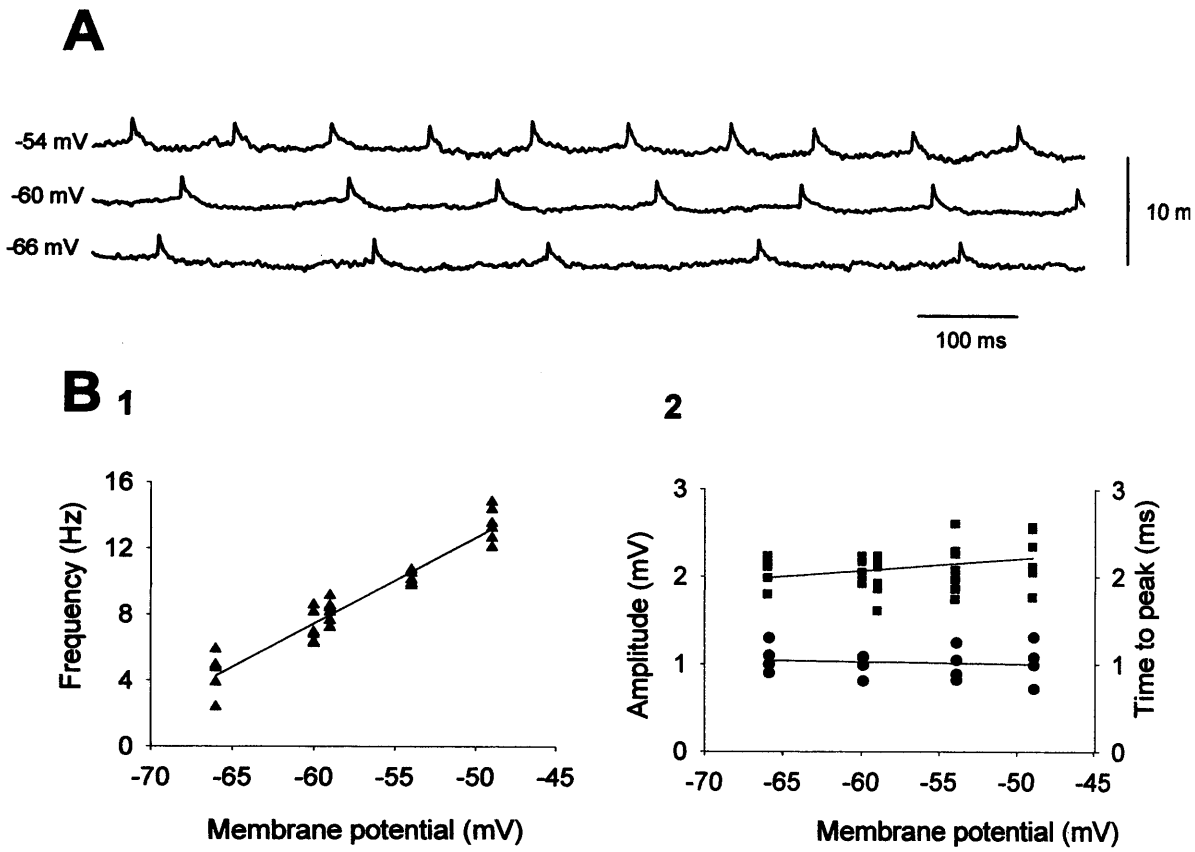

Figure 6.6 Spikelet properties in TC neurones.

(A) The effect of varying membrane potential through the injection of steady d.c. current on the generation of spikelets.

(B) Graph showing the voltage-dependence of the frequency of spikelets (▲) (1). Graphs illustrating the relationship between spikelet amplitude and membrane potential (■), and the relationship between the time to peak of spikelets and membrane potential (•). Lines were generated by performing a linear regression analysis on the data points shown (2).

Published in Hughes et al 2002a

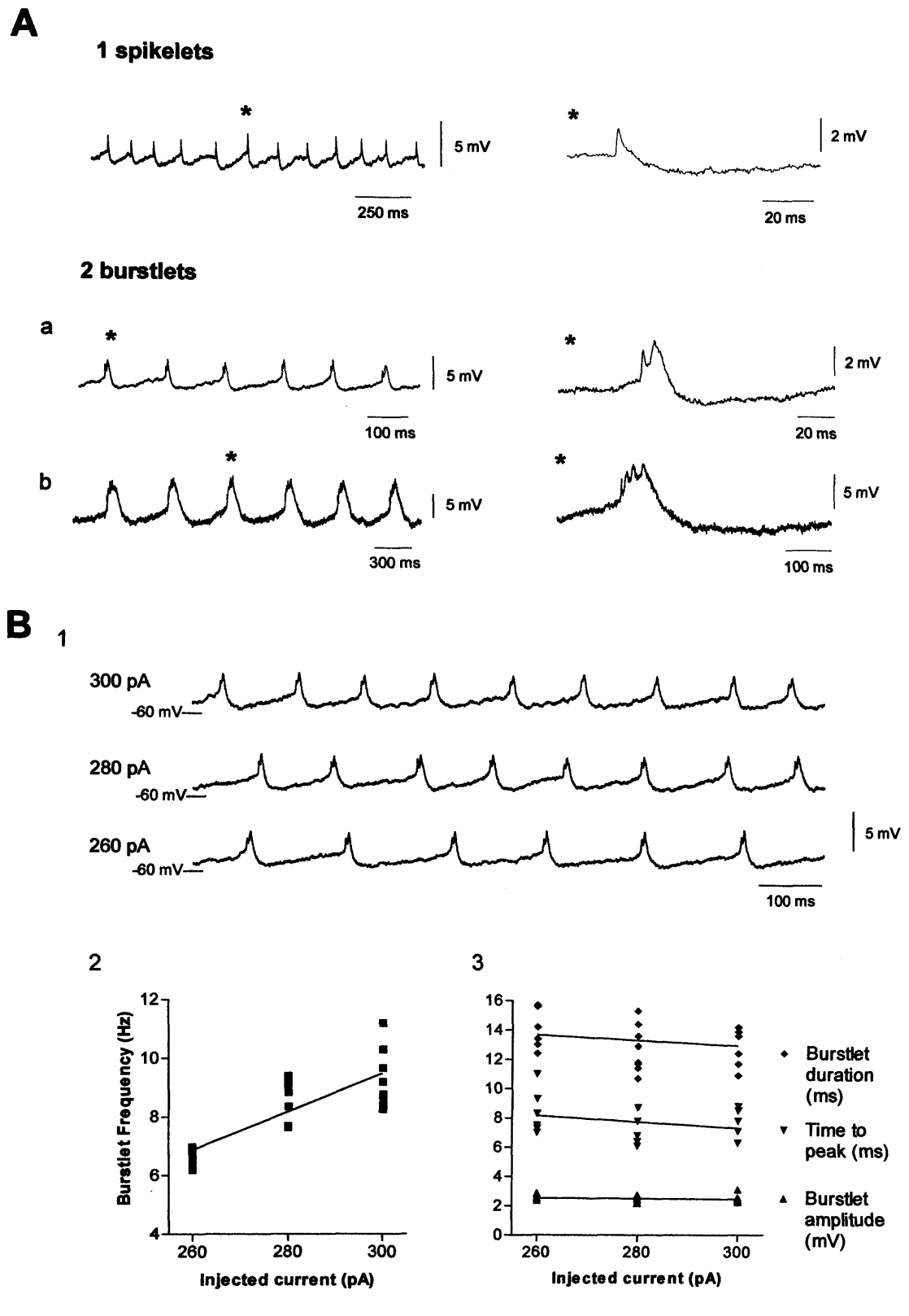

Figure 6.7 Burstlets in TC neurones.

Figure. 6.7 Burstlets in TC neurones.

(A) Spikelets in a TC neurone (1). Two examples of burstlets in different TC neurones (2). Expanded spikelet or burstlet (*) are shown to the right of each trace.

(B) Analysis of burstlet properties at different levels of injected d.c. current. Burstlets shown at different levels of injected d.c. current as indicated (1). Graph showing burstlet frequency (■) at the different levels of injected d.c. current shown in 1 (2). Graph showing the properties of individual burstlets including burstlet duration (♦), burstlet amplitude (▼) and time to peak (▲) at the different levels of injected d.c. current as indicated in 1. Lines were generated by performing a linear regression analysis on the data points shown (3).

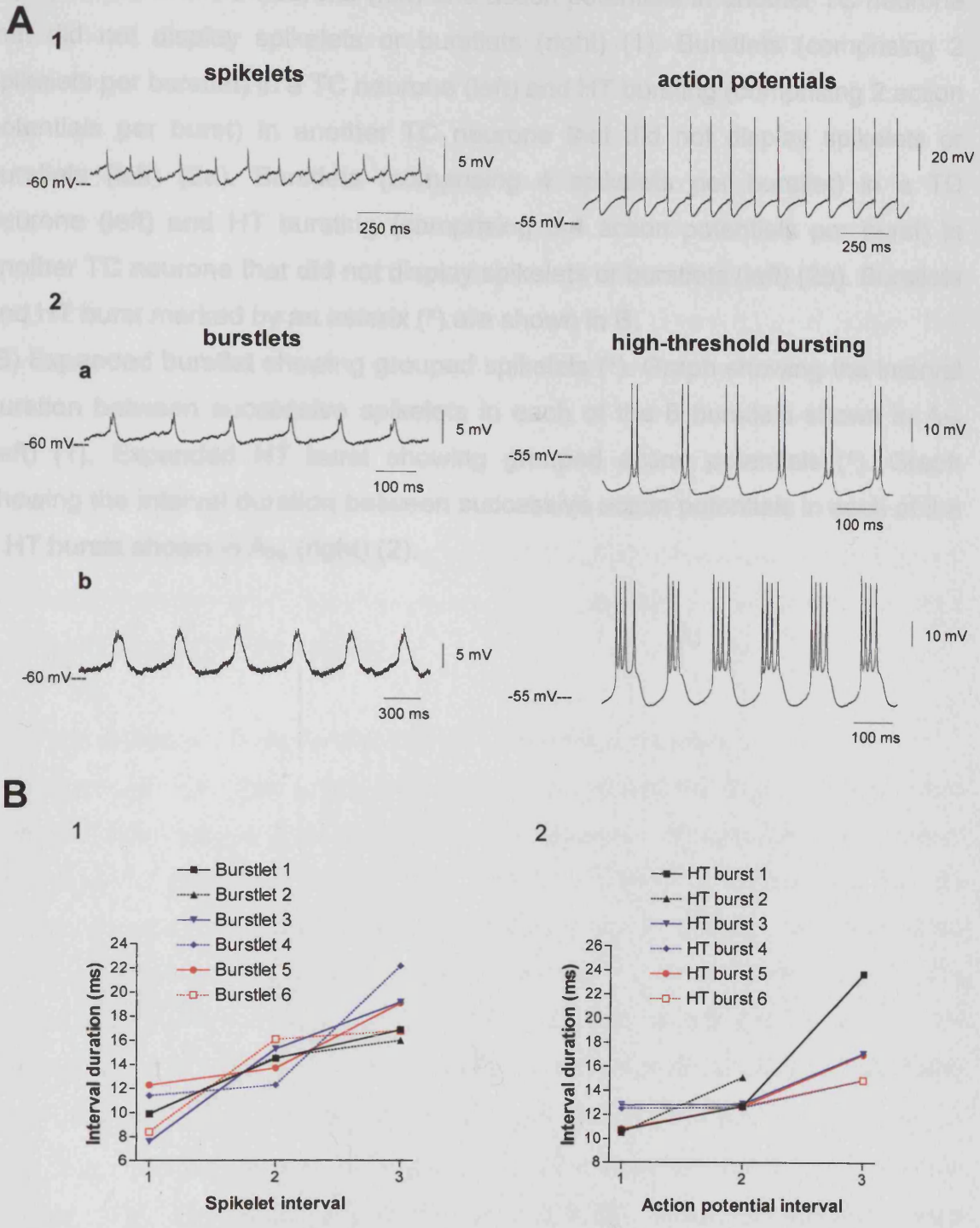

Figure. 6.8 Burstlets and high-threshold (HT) bursting in TC neurones.

Figure. 6.8 Burstlets and high-threshold (HT) bursting in TC neurones.
(A) Spikelets in a TC neurone (left) and action potentials in another TC neurone that did not display spikelets or burstlets (right) (1). Burstlets (comprising 2 spikelets per burstlet) in a TC neurone (left) and HT bursting (comprising 2 action potentials per burst) in another TC neurone that did not display spikelets or burstlets (left) (2a). Burstlets (comprising 4 spikelets per burstlet) in a TC neurone (left) and HT bursting (comprising 3-4 action potentials per burst) in another TC neurone that did not display spikelets or burstlets (left) (2b). Burstlets and HT burst marked by an asterix (*) are shown in B.
(B) Expanded burstlet showing grouped spikelets (*). Graph showing the interval duration between successive spikelets in each of the 6 burstlets shown in A_{2b} (left) (1). Expanded HT burst showing grouped action potentials (*). Graph showing the interval duration between successive action potentials in each of the 6 HT bursts shown in A_{2b} (right) (2).

comprised grouped action potentials (Fig. 6.8A_2). Once again, the frequency of burstlets and HT bursting are dependent on neuronal depolarisation with little change in the other properties of each type of activity at different levels of injected d.c. current (see Fig. 6.7B_1 for burstlets and Fig. 6.9B for HT bursting).

Another interesting observation was that burstlets were predominantly observed in TC neurones that were also able to generate HT bursts (6 of 7 neurones). This led to an apparent observation of two types of TC neurones: those that displayed spikelets and fired conventional action potentials (Type 1) and those that displayed burstlets and were able to generate HT bursts (Type 2). In Type 1 TC neurones (Fig. 6.9A), spikelets could effectively entrain action potentials at ~10-25 Hz, although at other levels of injected d.c. current spikelets were unable to effectively trigger action potentials. In Type 2 TC neurones (Fig. 6.9B), burstlets could effectively entrain HT bursting at ~3-5 Hz. This observation suggests that restricted networks of TC neurones may be responsible for generating rhythmic activities at particular frequencies.

6.3.1.4 Spikelets are dependent of Na^+ channel activation.

Investigations into the origin of spikelets demonstrated that spikelets were routinely observed in the presence of antagonists of synaptic transmission (CNQX, APV, BMI, CGP 5699A) (Fig. 6.9B and 6.10A), confirming that they do not represent conventional postsynaptic potentials. In addition, spikelets were not a manifestation of dendritic Ca^{2+} spikes as they were resistant to the blockade of voltage-dependent Ca^{2+} channels with wither the T-type channel blocker, Ni^{2+} (500 μM) (n=2) (not shown), the L-type channel blocker, nifedipine (1-10 μM) (n=3) (Fig. 6.10B_1), the N/P/Q-type channel blocker ω-cgTx MVIIC (2 μM) (Fig. 6.10B_2) or the non-specific high–voltage activated Ca^{2+} channel blocker Cd^{2+} (250-500 μM) (n=5) (Fig. 6.10B_3). However spikelets were abolished by application of the Na^+ channel blocker TTX (1μM) indicating their dependence on Na^+ channel activation (Fig. 6.10C).

6.3.1.5 Spikelets are associated with dye-coupling in TC neurones.

In TC neurones exhibiting spikelets, injection of Biocytin or Neurobiotin led to the staining of >1 cell in 83% of cases (5 of 6 neurones) (Fig. 6.11). Even when spikelets were not evident, dye-coupling still occurred regularly between TC

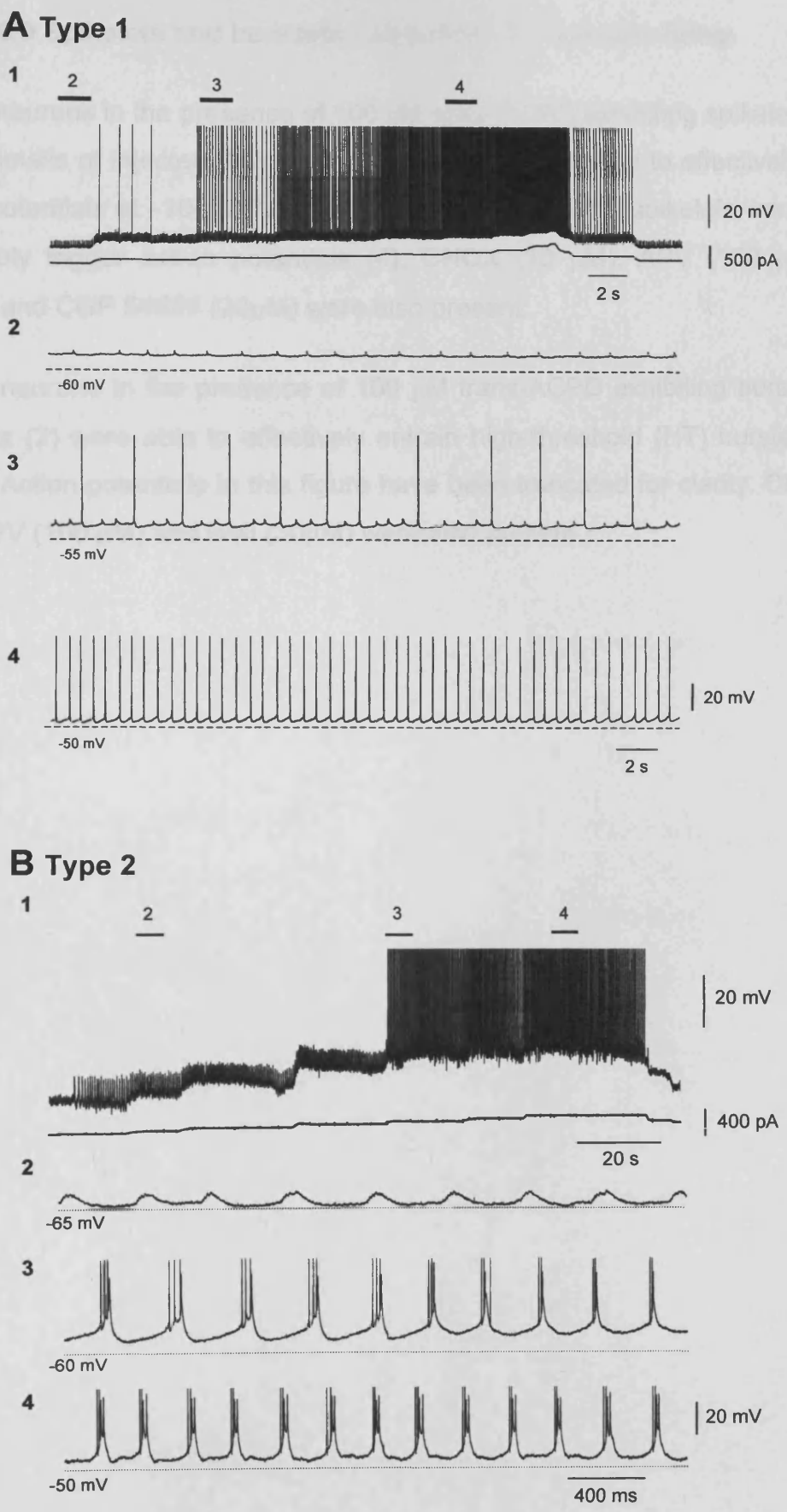

Figure 6.9 Spikelets and burstlets can entrain TC neurone firing.

Figure 6.9 Spikelets and burstlets can entrain TC neurone firing.

(A) TC neurons in the presence of 100 μM trans-ACPD exhibiting spikelets (1). At certain levels of injected d.c. current spikelets (2) were able to effectively entrain action potentials at ~10-25 Hz (3) where as at other levels, spikelets were unable to reliably trigger action potentials (4). CNQX (10 μM), APV (100 μM), BMI (30μM) and CGP 54626 (20μM) were also present.

(B) TC neurone in the presence of 100 μM trans-ACPD exhibiting burstlets (1). Burstlets (2) were able to effectively entrain high-threshold (HT) bursts at ~3-5 Hz (3). Action potentials in this figure have been truncated for clarity. CNQX (10 μM), APV (100 μM) and BMI (30μM) were also present.

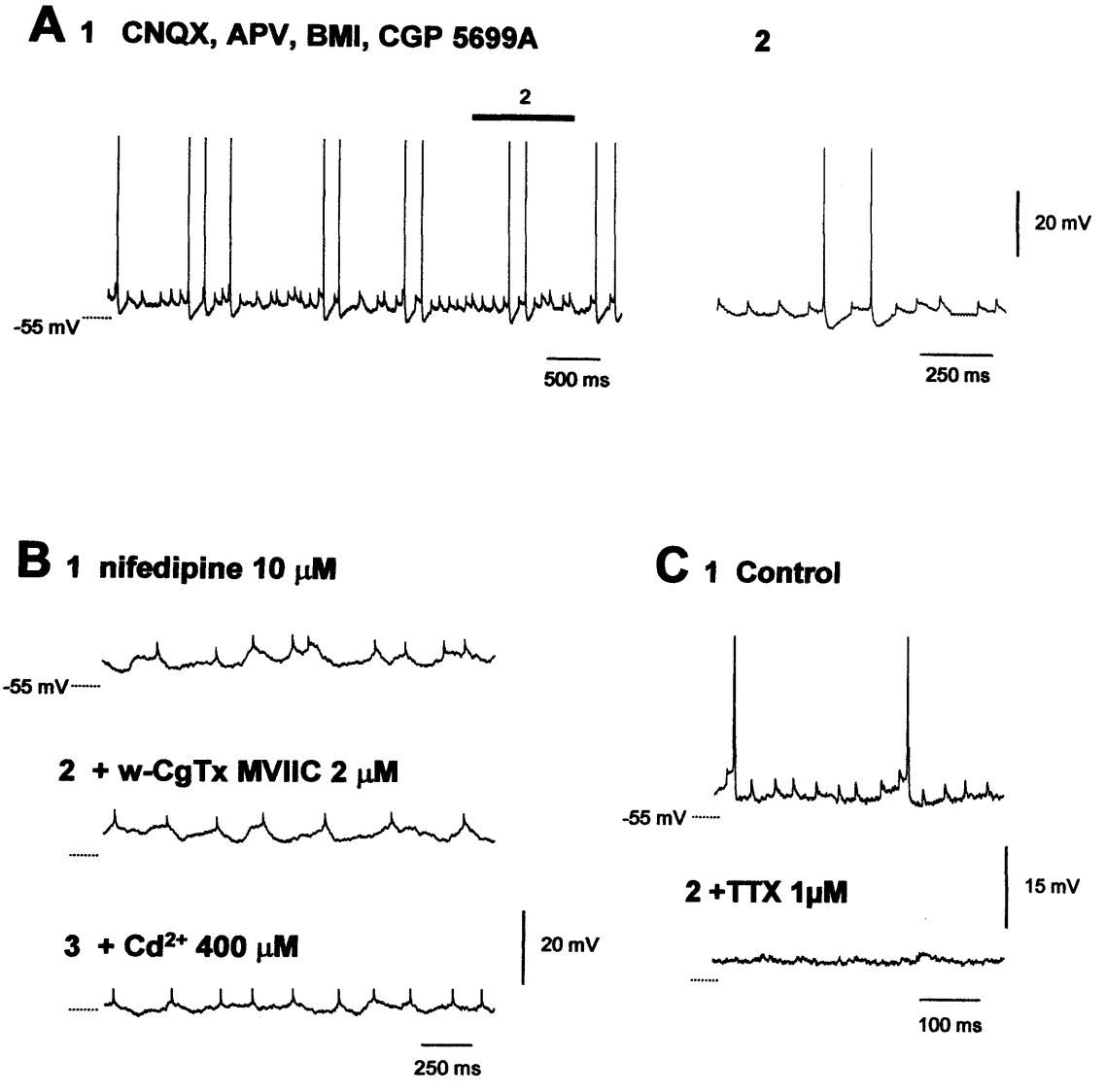

Figure 6.10 Spikelets are dependent on Na^+ channel activation.

Figure 6.10 Spikelets are dependent on Na^+ channel activation.

(A) Recording from a TC neurone in the presence of CNQX (20 μM), APV (100 μM), BMI (30 μM) and CGP 5699A (20μM) showing the presence of rhythmic spikelets that occasionally led to the generation of full-blown action potentials (expanded in 2).

(B) Spikelets in another TC neurone recorded in the presence of the L-type Ca^{2+} channel blocker nifedipine (10 μM) (1). Application of the N/P/Q-type Ca^{2+} channel blocker ω-CgTx MVIIC (2 μM) to this neurone did not affect the generation of spikelets (2). Similarly, subsequent application of Cd^{2+} (400 mM) also did not affect spikelets (3).

(C) TC neurone exhibiting spikelets that sometimes led to the generation of full-blown action potentials (1). Neither action potentials nor spikelets could be observed following the addition of TTX (1 μM) to the recording medium (2). Action potentials in this figure have been truncated for clarity.

Published in Hughes et al. 2002a

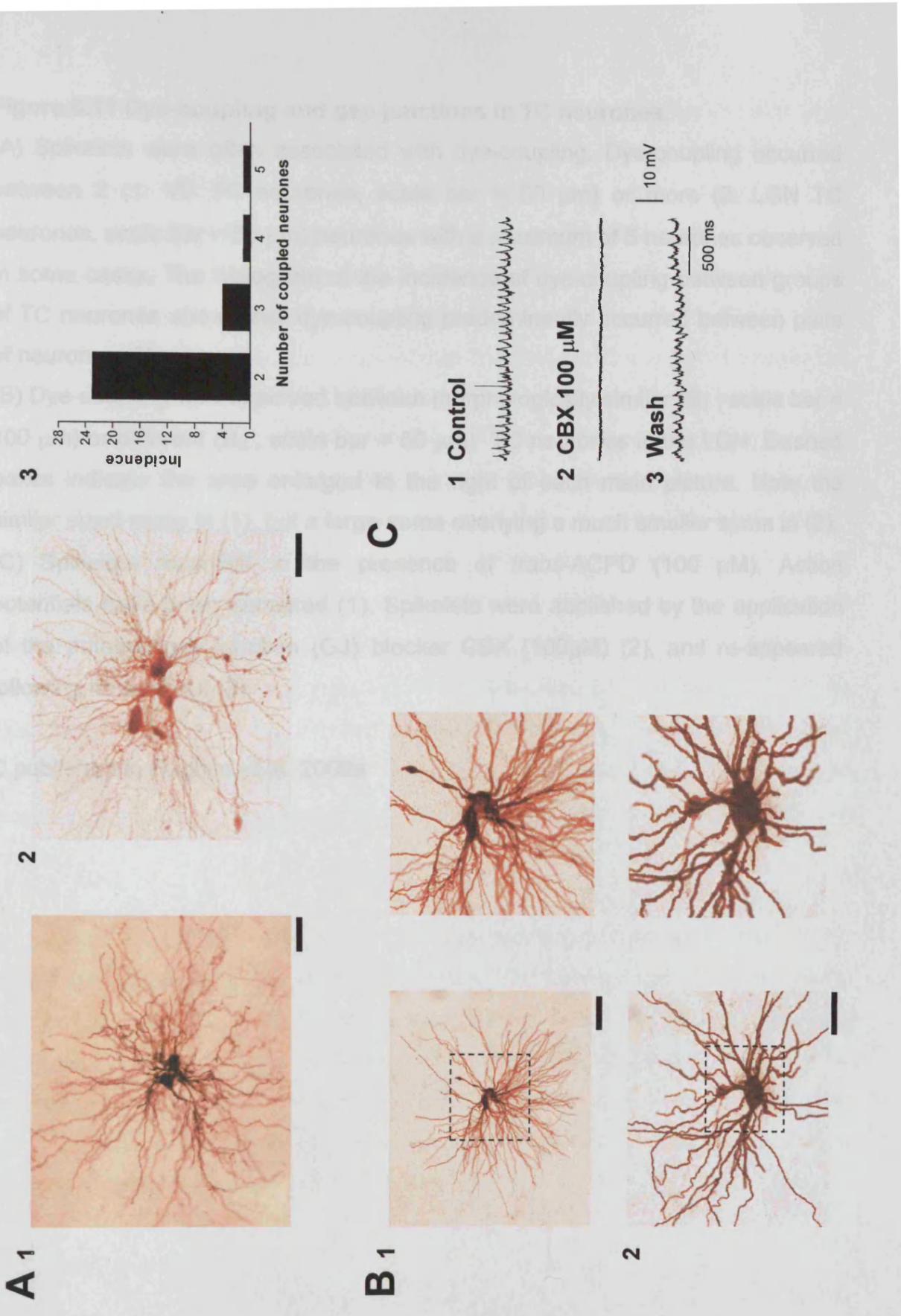

Figure 6.11 Dye-coupling and gap junctions in TC neurones.

Figure 6.11 Dye-coupling and gap junctions in TC neurones.

(A) Spikelets were often associated with dye-coupling. Dye-coupling occurred between 2 (1: VB TC neurones, scale bar = 50 μm) or more (2: LGN TC neurones, scale bar = 50 μm) neurones with a maximum of 5 neurones observed in some cases. The histogram of the incidence of dye-coupling between groups of TC neurones shows that dye-coupling predominantly occurred between pairs of neurones (3).

(B) Dye-coupling was observed between morphologically similar (B_1 , scale bar = 100 μm) or different (B_2 , scale bar = 50 μm) TC neurones in the LGN. Dashed boxes indicate the area enlarged to the right of each main picture. Note the similar sized soma in (1), but a large soma overlying a much smaller soma in (2).

(C) Spikelets recorded in the presence of *trans*-ACPD (100 μM). Action potentials have been truncated (1). Spikelets were abolished by the application of the putative gap junction (GJ) blocker CBX (100μM) (2), and re-appeared following its washout (3).

C published in Hughes et al. 2002a

neurones, with 25 % of cases (30 of 121 neurones) exhibiting dye transfer to at least 1 other neurone (Fig. 6.11A_3). In the LGN, dye coupling (24 of 72, 33%) was observed both between TC neurones with similar (n=17 cases, injected somal diameter: 27.26 ± 1.30, n=17, coupled somal diameter: 24.21 ± 1.2, n=17, P = 0.122) (Fig. 6.11B_1) and distinct (n=7 cases, injected somal diameter: 35.34 ± 2.21, n=7, coupled somal diameter: 18.51 ± 1.6, n=7, P = 0.0013) (Fig. 6.11B_2) morphological features suggesting that dye-coupling can occur between different classes of LGN TC neurones. Additionally, in cases where the lamination of the nucleus was evident, dye-coupling in the LGN was always restricted to pairs or groups of neurones with somas lying within a specific lamina (n=11). Given the morphological similarities of TC neurones in the VB, VL and MGN no distinction could be made between dye-coupled TC neurones in these nuclei: VB: dye coupled: 2 of 10 (20%), injected somal diameter: 21.00 ± 1.00, n=2, coupled diameter: 24.00 ± 0.57, n=3. VL: dye coupled: 2 of 16 (13%), injected somal diameter: 24.50 ± 0.50, n=2, coupled somal diameter: 22.50 ± 3.50, n=2. MGN: dye coupled: 2 of 23 (9%), injected somal diameter: 24.50 ± 1.50, n=2, coupled somal diameter: 26.00 ± 2.00, n=2. The apparent distance between the somas of coupled neurones in all nuclei ranged from 20 – 180 μm, 62.25 ± 5.75 μm (n=38).

In accordance with the convention that dye-coupling occurs as a result of the presence of GJs between cells, the effect of the putative gap junction blocker carbenoxolone (CBX) on spikelets and the incidence of dye-coupling was examined. CBX (100-200 μM) reversibly abolished spikelets (n=4) in TC neurones (Fig. 6.11C) without any apparent effect on R_N. In addition, dye-coupling was never observed in the presence of CBX in TC neurones identified by their electrophysiological characteristics (n= 18).

6.3.2 NRT neurones.

6.3.2.1 Spikelets are apparent in a subset of NRT neurones.

Spikelets were also observed in NRT neurones (Fig. 6.12) in the presence of *trans*-ACPD (n=4 of 37, 11%) or DHPG (n=1 of 6, 17%), that otherwise had normally observed electrophysiological properties for this cell type (Fig. 6.12A_4).

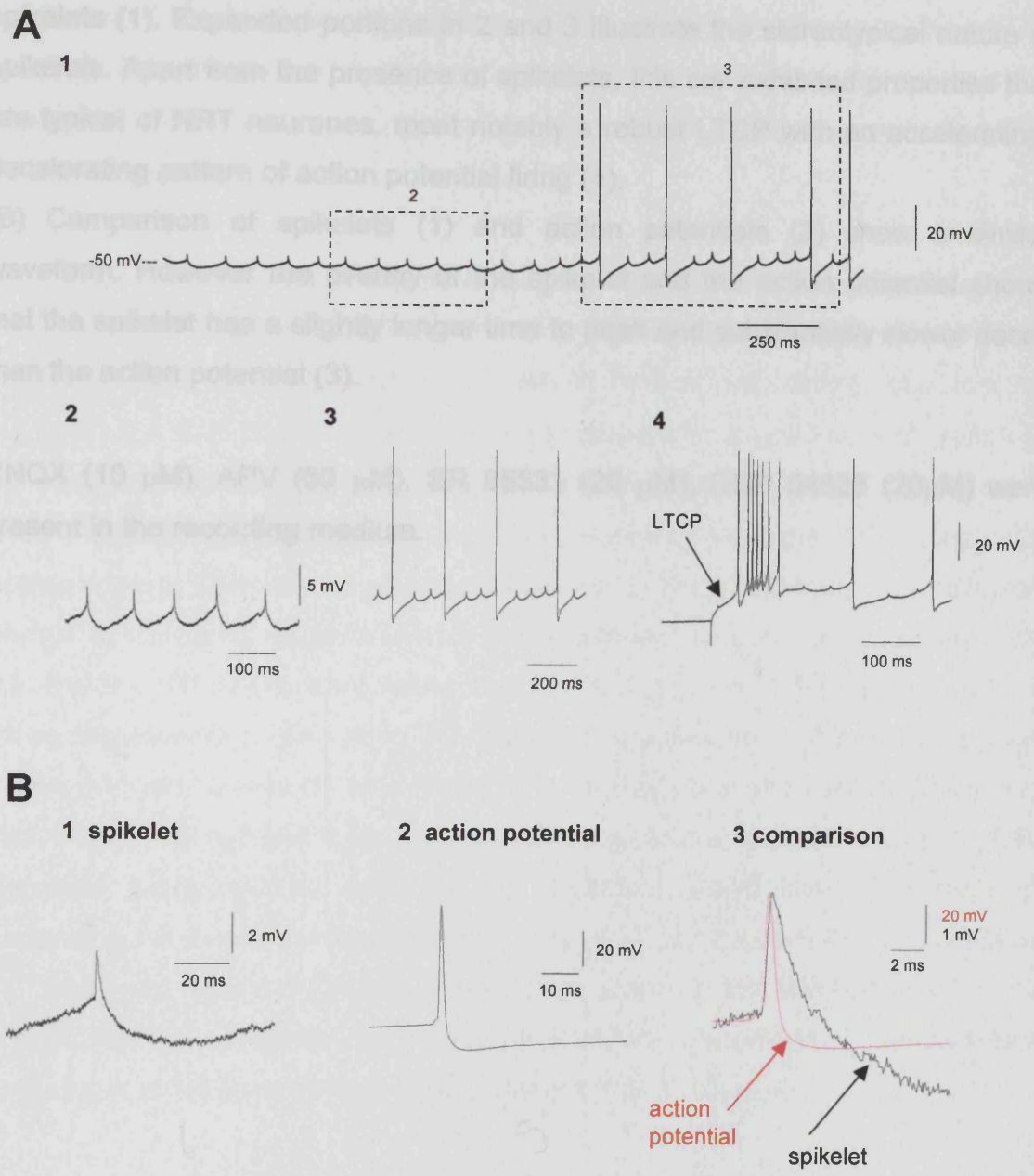

Figure 6.12 Spikelets in NRT neurones have a stereotypical waveform.

Figure 6.12 Spikelets in NRT neurones have a stereotypical waveform.

(A) NRT neurone recorded in the presence of DHPG (100 μM) exhibiting spikelets (1). Expanded portions in 2 and 3 illustrate the stereotypical nature of spikelets. Apart from the presence of spikelets, this cell exhibited properties that are typical of NRT neurones, most notably a robust LTCP with an accelerating-decelerating pattern of action potential firing (4).

(B) Comparison of spikelets (1) and action potentials (2) show a similar waveform. However the overlay of the spikelet and the action potential shows that the spikelet has a slightly longer time to peak and substantially slower decay than the action potential (3).

CNQX (10 μM), APV (50 μM), SR 95531 (20 μM), CGP 54626 (20μM) were present in the recording medium.

Spikelets in NRT neurones were dependent on the presence of *trans*-ACPD or DHPG as they were never observed in aCSF alone and were observed in the presence of the receptor antagonists (APV, CNQX, SR 95531, CGP 54626, n=4). Spikelets were apparent as short duration subthreshold depolarising potentials (2.9 ± 0.2 ms, range = 1.8 – 5.1 ms, n=30 from 5 neurones) (Fig. 6.12).

6.3.2.2 Spikelets have stereotypical properties in NRT neurones.

As in TC neurones, spikelets observed in NRT neurones had a stereotypical waveform (time to peak: 0.70 ± 0.03, n= 30 from 5 cells; decay time constant (τ_{decay}): 1.3 ± 0.15 ms, n=30 from 5 cells) followed by a spikelet AHP. Although the spikelet amplitude differed between NRT neurones (range = 0.56 – 2.8 mV, n=30 from 5 cells), it was always consistent within a given neurone leading to the appearance of spikelets as all-or-none events. In NRT neurones, spikelets were always apparent as discrete events and never as burstlets. In accordance with this finding, HT bursts were never seen in NRT neurones during the course of these experiments. Again as in TC neurones, a comparison of the spikelets and action potential waveform was made. The time to peak and repolarisation were slower for the spikelet than for the action potential waveform (Fig. 6.12B). Spikelets were always apparent as rhythmic events with the frequency depending on neuronal depolarisation (Fig. 6.12, 6.13 and 6.14). Again, as for TC neurones, spikelet frequency was dependent on the level of injected d.c. current, but the amplitude and time to peak of NRT spikelets was very consistent regardless of the level of injected d.c. current (Fig. $6.13_{1 \text{ and } 2}$).

6.3.2.3 Spikelets entrain action potential firing in NRT neurones.

In NRT neurones, rhythmic spikelets could entrain action potential firing at 24.9 – 39.8Hz, mean = 30.9 ± 0.9Hz, (n=30 from 3 neurones) (Fig. 6.14A and B_3). The value of injected d.c. current required to polarise the neurone to a level where spikelets entrained action potential firing was variable in different neurones (range: -430pA to +250pA). In a given neurone, at more hyperpolarised ranges of injected d.c. current than required to observe action potential entrainment, spikelets could not reliably evoke action potentials (Fig. 6.14A and B_2), or spikelets were observed alone (Fig. 6.14A and B_1).

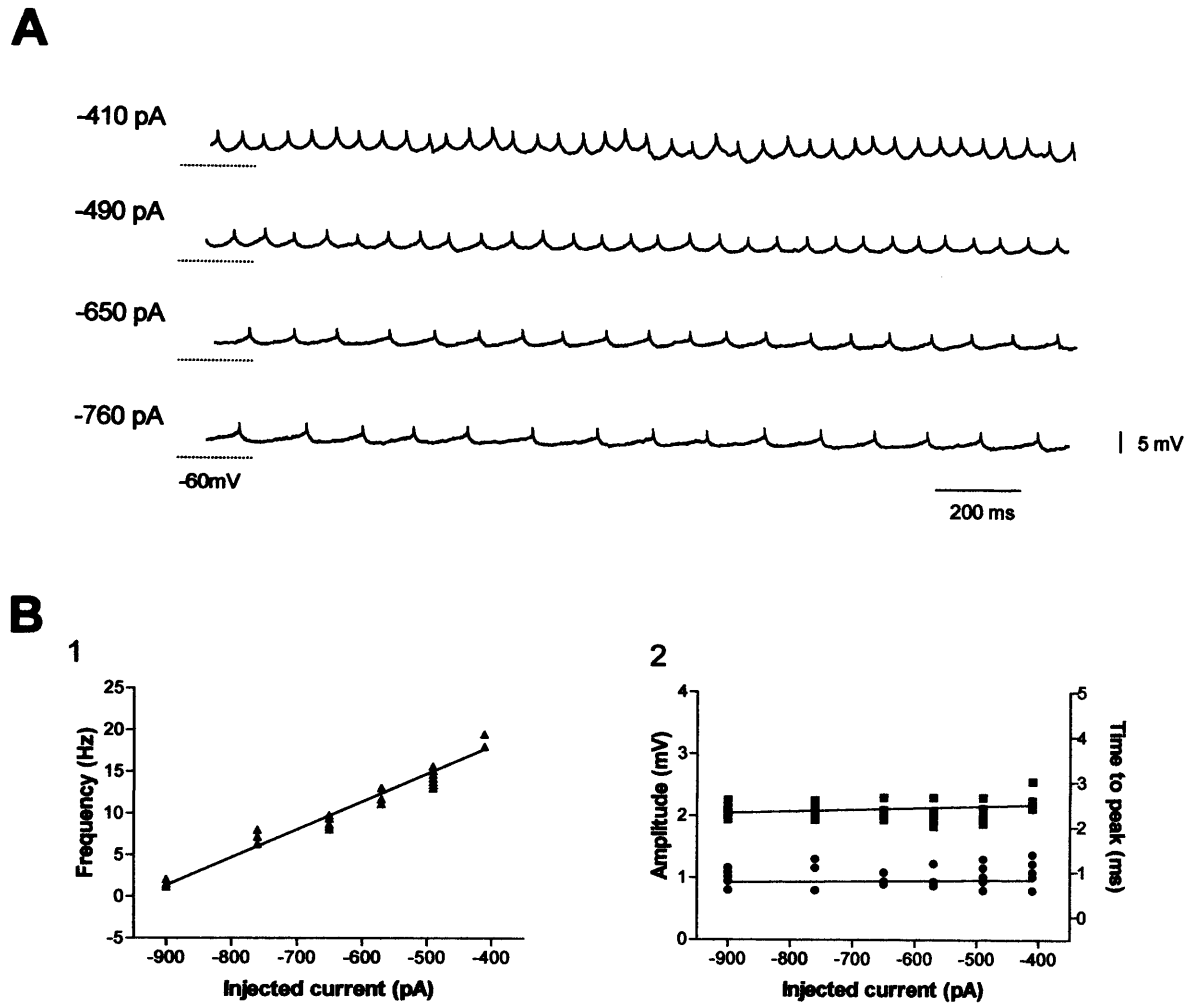

Figure 6.13 Spikelet properties in NRT neurones.

(A) The effect of varying membrane potential through the injection of steady d.c. current on the generation of spikelets.

(B) Graph showing the voltage-dependence of the frequency of spikelets (▲)(1). Graphs illustrating the relationship between spikelet amplitude and injected d.c. current (■), and the relationship between the time to peak of spikelets and injected d.c. current (●). Lines were generated by performing a linear regression analysis on the data points shown (2).

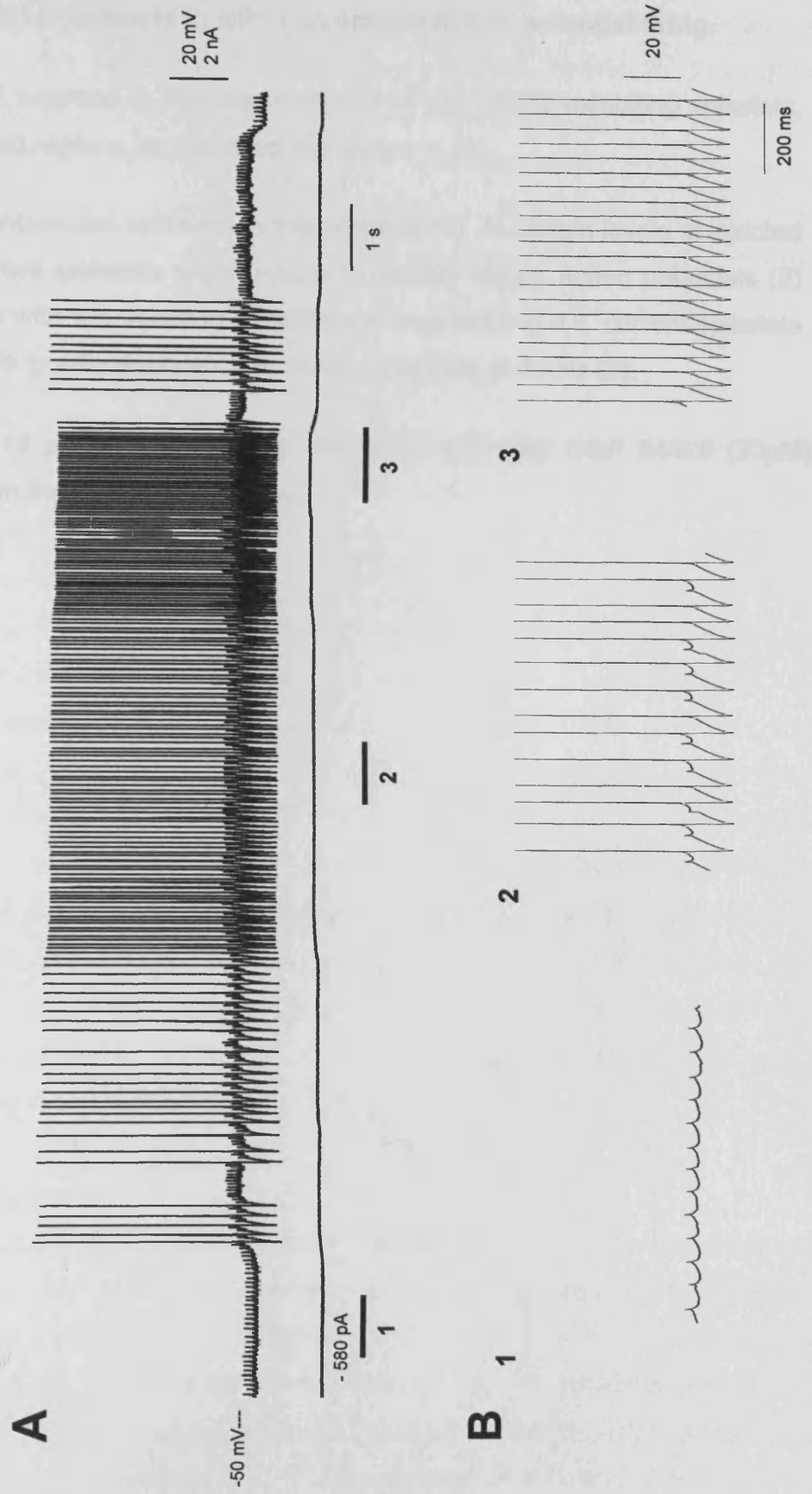

Figure 6.14 Spikelets in NRT neurones can entrain action potential firing.

Figure 6.14 Spikelets in NRT can entrain action potential firing.

(A) NRT neurone in the presence of 100 μM DHPG exhibiting spikelets. Expanded regions as indicated are shown in (B).

(B). Spontaneous spikelets in this neurone (1). At certain levels of injected d.c. current spikelets were unable to reliably trigger action potentials (2) whereas with the injection of additional depolarizing d.c. current spikelets were able to effectively entrain action potentials at 40 Hz (3).

CNQX (10 μM), APV (50 μM), SR 95531 (20 μM), CGP 54626 (20μM) were present in the recording medium.

6.3.2.4 Spikelets are not associated with dye-coupling in NRT neurones.

Although Biocytin or Neurobiotin was routinely added to the intracellular electrode solution, in no cases was dye-coupling seen in NRT neurones (n=30) under any experimental conditions. This is consistent with previous observations in NRT neurones and in other populations of GABAergic neurones that have been conclusively demonstrated to be electrotonically coupled (Galarreta and Hestrin 1999; Galarreta and Hestrin 2001; Landisman et al. 2002).

6.3.3 Comparison of spikelets in TC and NRT neurones.

In order to compare spikelets in TC and NRT neurones a full analysis of spikelets properties (as described in section 6.2) were performed on rhythmic sequences of spikelets occurring at ~10Hz in a number of TC (n=3) and NRT (n=3) neurones. The overlaid traces (Fig. 6.15B) highlight some of the differences that were observed between spikelets within the two neuronal populations, and are also summarised in Table 6.1. Firstly, the amplitude of spikelets in TC neurones encompassed a higher range of values than those seen in NRT neurones. Due to the overlapping range of values included in this part of the analysis there was no significant difference between these values (Table 6.1). The time to peak, spikelet duration and spikelet τ_{decay} were generally larger for TC than NRT neurones, and for each of these parameters a statistically significant difference was found between the two neuronal types (Table 6.1). The spikelet AHP and AHPτ_{decay} were generally smaller for TC spikelets than for NRT spikelets. Again for each of these parameters a statistically significant difference was found between the two neuronal types (Table 6.1).

6.4 DISCUSSION

The novel findings described in this chapter are 1) the presence of spikelets in a subset of TC neurones in adult thalamic slices maintained *in vitro*, 2) the presence of burstlets in a subset of TC neurones in adult thalamic slices maintained *in vitro,* 3) the demonstration that TC spikelets are not synaptic potentials, but are dependent on Na^+ channel activation, 4) the presence of dye-coupling in TC neurones and 5) the presence of spikelets in NRT neurones in adult thalamic slices maintained in vitro.

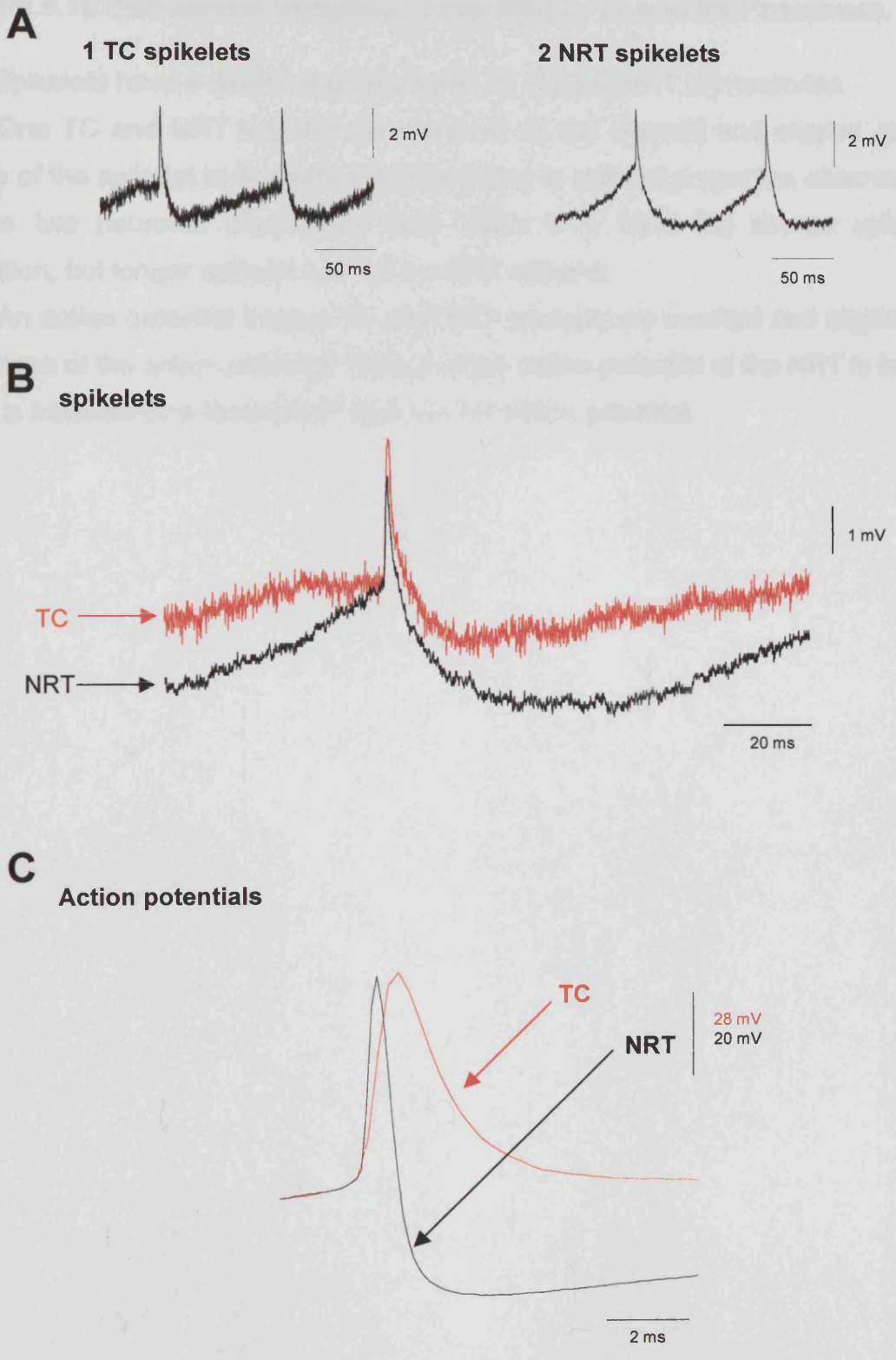

Figure 6.15 Comparison of spikelet properties in TC and NRT neurones.

Figure 6.15 Comparison of spikelet properties in TC and NRT neurones.

(A) Spikelets have a similar appearance in TC (1) and NRT (2) neurones.
(B) One TC and NRT spikelet (as shown in A) are overlaid and aligned at the base of the spikelet to illustrate the differences in spikelet properties observed in these two neuronal populations (see Table 6.1). Note the shorter spikelet duration, but longer spikelet AHP of the NRT spikelet.
(C) An action potential from a TC and NRT neurone are overlaid and aligned at the base of the action potential. Note that the action potential of the NRT is faster and is followed by a larger AHP than the TC action potential.

	Spikelet amplitude (mV)	Time to peak (ms)	Spikelet duration (ms)	Spikelet τ_{decay} (ms)	AHP amplitude (mV)	AHP τ_{decay} (ms)
TC	2.51± 0.11 (1.87-3.62) n=18	1.34± 0.12 (0.74-3.17) n=18	7.22± 0.74 (3.17-15.12) n=18	3.04± 0.47 (1.36-6.89) n=18	1.63± 0.17 (0.99-2.44) n=18	5.47± 0.71 (2.49-10.84) n=18
NRT	1.90± 0.20 (0.56-2.68) n=18	0.78± 0.03 (0.55-1.04) n=18	3.18± 0.22 (1.83-4.76) n=18	1.30± 0.15 (0.57-1.87) n=18	2.13± 0.16 (0.99-3.18) n=18	7.25± 0.69 (3.67-11.20) n=18
P value	*P* = 0.22	*P* < 0.0001 **	*P* < 0.0001 **	*P* = 0.005 *	*P* = 0.024 *	*P* = 0.048 *

Table 6.1 Comparison of spikelet properties in TC and NRT neurones.

An analysis of spikelet properties was performed for sequences of spikelets occurring at 10 Hz in TC (n=3) and NRT (n=3). Values in the table are mean ± SEM and followed by the range in parentheses and then the total number of spikelets analysed. (*P<0.05, **P<0.0001).

6.4.1 Origin of spikelets in TC neurones.

The novel findings in this chapter strongly suggest that spikelets are generated as a result of electrotonic coupling in TC neurones and possibly through a mechanism involving GJs. This conclusion is supported by the following observations: 1) spikelets were most commonly observed during application of Group I mGluR agonists or elevation of the external [K^+]. Such conditions depolarise TC neurones (see Chapters 3 and 4) (McCormick and von Krosigk 1992; von Krosigk et al. 1999; Turner and Salt 2000) and generally increase the excitability of the thalamic slice. In this way spontaneous action potential firing could give rise to the spontaneously occurring spikelets observed in TC neurones under these conditions; 2) the presence of spikelets during pharmacological blockade of glutamatergic and GABAergic receptors indicates that they are not generated by conventional excitatory postsynaptic potentials; 3) the all or none nature of spikelets, irrespective of the membrane potential, is also in contrast to the properties of conventional post synaptic potentials where the amplitude, but not the frequency, is dependent on the membrane potential of the postsynaptic neurone; 4) the dependence of spikelets on Na^+ channel activation therefore suggests their dependence on action potential generation as failure of presynaptic transmitter release can be excluded (as spikelets are not dependent of synaptic transmission) and the time course of the spikelet waveform excludes their generation by a persistent Na^+ current (Parri and Crunelli 1998); 5) the spikelets waveform is distinctive in that it has a fast rise time and repolarising phase and is followed by a spikelet AHP. This waveform is very similar to that of action potentials (Fig. 6.5) except that the time to peak and the repolarising phase are slower; and 6) the amplitude of the spikelet AHP could be of a comparable size to the spikelet itself (Table 6.1) which would arise if generated by an action potential that has been transmitted along the neuronal dendrite thereby preserving the slower part of the waveform more faithfully. i.e. the AHP, rather than the much faster action potential itself.

The presence of burstlets is an additional feature not previously reported *in vitro* in TC neurones. Spikelets and burstlets appear to be related in the same ways as action potentials and HT bursting (see Chapter 3 and 4) in TC neurones. That is: 1) burstlets are groups of spikelets with an underlying depolarising potential and HT bursts are a groups of action potentials riding on a depolarising potential,

2) spikelets and action potentials are all or none events, as are burstlets and HT bursts; and 3) the frequency of spikelets and action potential firing is dependent on neuronal depolarisation as is the frequency of both burstlet and HT bursting in TC neurones. These similarities suggest that HT bursts might be transmitted to coupled neurones and manifested as burstlets. The more faithful transmission of the underlying depolarisation is in keeping with the characteristics of signals transmitted via electrotonic junctions and hence burstlets have a pronounced depolarisation underlying much smaller spikelets. Further to this, no cases of burstlets were seen in NRT neurones and no examples of HT bursts were observed in NRT neurones.

Comparison of the properties of spikelets in TC and NRT neurones also supports the idea that spikelets are generated by action potential that are transmitted via GJs. The spontaneous spikelets described here in adult NRT neurones have a very similar appearance to spikelets observed during paired recordings of electrotonically coupled NRT neurones (Landisman et al. 2002) in that: 1) NRT spikelets were present following synaptic receptor antagonism; 2) had an all-or-none waveform; 3) were dependent on neuronal depolarisation; and 4) showed a distinctive spikelets AHP, suggesting they are a manifestation of electrotonic communication. The similarity between the spikelets observed in neonatal (Landisman et al. 2002) and adult NRT neurones suggests that electrotonic coupling persists in the adult animal. In addition the fact that TC and NRT spikelets had very similar properties suggests that TC spikelets also occurred as a result of electrotonic coupling and therefore that electrotonic communication may also be present between TC neurones in the adult.

The drawback of single intracellular recordings is that one can only speculate as to the network of neurones that might be electrotonically coupled. Previous observations of spikelets or spikelet-like potentials (FPPs) in NRT neurones *in vivo* and *in vitro* suggest a dendritic origin (Mulle et al. 1986; Llinas and Geijo-Barrientos 1988; Contreras et al. 1993; Landisman et al. 2002). It would seem very likely that the origin of spikelets in NRT neurones is from other NRT neurones and possibly via dendritic connections as: 1) direct electrotonic communication has been shown between NRT neurones (Landisman et al. 2002); 2) the NRT contains a homogeneous population (Houser et al. 1980); 3)

NRT neurones are known to make dendrodendritic appositions (Deschenes et al. 1985) thus potentially providing a substrate for electrotonic communication, whereas other inputs to NRT neurones are via conventional synaptic terminals (see section 1.3.3); and 4) Cx36 has been localised predominantly with dendrites of NRT neurones and not with pre- or postsynaptic regions (Liu and Jones 2003). In thalamic relay nuclei, this situation is somewhat complicated. The dendrites of TC neurones in thalamic relay nuclei are described as forming close appositions or filamentous contacts that resemble GJs in the cat (Peters and Palay 1966; Kodota and Kodota 1979) and rats (Lieberman and Spacek 1997), these may provide a substrates for such direct interneuronal connections between TC neurones. Although spikelets are not generated by dendritic HVA Ca^{2+} currents as shown here by their lack of sensitivity to the various HVA Ca^{2+} channels blockers, their dendritic origin is not excluded, and in addition spikelet-like FPPs observed in TC neurones *in vivo* have been suggested to have a dendritic origin (Contreras et al. 1993). However, the specialised dendritic appendages of interneurones present in cat thalamic relay nuclei terminate on the dendrites of TC neurones within and outside the triadic arrangement (Jones and Powell 1969; Famiglietti and Peters 1972; Wilson 1989). Despite this though, electrotonic coupling may exist within the TC population, in keeping with observations in other neuronal networks, where electrotonic coupling predominantly exists between alike neuronal subtypes (MacVicar and Dudek 1981; Galarreta and Hestrin 1999; Galarreta and Hestrin 2001; Landisman et al. 2002) but also see (Venance et al. 2000). The fact that occasionally spikelets were apparent with a decelerating pattern that is reminiscent of LTCP-mediated burst firing in TC neurones (Fig. 6.3) also suggests that in these cases coupling exits amongst TC neurones.

Further support arises from the pattern of dye-coupling observed following impalement of single TC neurones, where only groups of TC neurones were dye-coupled. If neuronal damage due to microelectrode impalement had resulted in the apparent dye-coupling, then the pattern observed would have included both TC and interneurones, not exclusively TC neurones as was observed. However, given the nature of the overlapping dendritic fields (Fig. 6.11) it was not possible to ascertain any points of connection between the dye-coupled neurones so the nature of direct interneuronal communication These conclusions do not exclude

the possibility that interneurones in thalamic relay nuclei may also communicate via electrotonic mechanisms as observed in other networks of GABAergic neurones (Galarreta and Hestrin 1999; Venance et al. 2000; Galarreta and Hestrin 2001; Landisman et al. 2002).

The question of why spikelets in TC neurones have not been previously observed might be due to the preparation of the tissue. During the preparation of the thalamic slices used for experiments described in this thesis, the cyclooxygenase (COX) inhibitor indomethacin and anti-oxidant ascorbic acid were present in the tissue slicing solution. The use of the COX inhibitor will prevent the synthesis of prostaglandins (Rang et al. 2003) that mediate the inflammatory responses in the tissue and therefore help to prevent cellular depolarisation and toxicity leading to permanent neuronal damage. In accordance with this, the addition of COX and ascorbic acid has been shown to aid preservation of the electrophysiological and morphological characteristics of tissue slices (Pakhotin et al. 1997; Pakhotin et al. 1999; Rice 1999). The reason why others have previously observed spikelets in neonatal NRT neurones without the use of these compounds (Landisman et al. 2002) may be due to the fact that the NRT is a thin nucleus and surrounds the thalamus and will be quickly infiltrated with solution once the brain is removed from the skull. The underlying thalamus may not be so quickly preserved especially in larger species. Cx proteins are known to be sensitive to intracellular pH (Rozental et al. 2001) and thus intracellular acidification due to metabolic stress during the slice preparation procedure may play a role on closing or damaging GJs during this phase. In accordance with this, Cx43 has been shown to be internalised, thus presumably preventing intercellular communication, following exposure to ischemic conditions (Nagy and Li 2000). This may be a common mechanism applicable to many of the different subtypes of Cx proteins. Therefore, perhaps the addition of the COX inhibitor and anti-oxidants aids tissue preservation such that GJs are not disrupted during the tissue preparation procedure, in addition to aiding the preservation of electrophysiological and morphological characteristics (Pakhotin et al. 1997; Pakhotin et al. 1999; Rice 1999).

6.4.2 Gap junctions as a substrate for electrotonic coupling.

Support for the role of GJs in the generation of spikelets was provided by the reversible abolition of spikelets by CBX and also by the presence of dye-coupling. CBX is a putative GJ blocker (Ross et al. 2000; Gladwell and Jefferys 2001; Rozental et al. 2001), and did not appear to have any obvious effect on other electrophysiological properties of TC neurones. In addition, when TC neurones were recorded in the presence of CBX, no dye-coupling was observed and TC neurones displayed normal electrophysiological activities. It appears therefore that CBX in this case might be one of the more useful pharmacological agents that can be used to investigate GJ functions. Many of the pharmacological agents that are known to block or disrupt GJs conductance are also known to have other cellular effects that may simply be damaging neurones, activating other receptors or activating via other membrane proteins rather than actually blocking the GJs themselves (Rekling et al. 2000; Rozental et al. 2001; Rouach et al. 2003). The reversible effect of CBX on spikelets and the lack of other effects on the activity of recorded TC neurones support the notion that CBX was acting on GJs here.

As a technique for demonstrating the existence of GJ communication, dye-coupling is somewhat controversial as impaling multiple neurones with a single microelectrode may occur (Alger et al. 1983). In addition, slice preparation (Gutnick et al. 1985) and the use of different intracellularly injected dyes (Hatton and Yang 1994) may have an impact on the extent of observed dye-coupling. As dye-coupling is only one of the methods used in this investigation in order to establish the origin of spikelets in TC neurones and all TC neurones used for analysis displayed normal electrophysiological characteristics (Jahnsen and Llinas 1984b; Jahnsen and Llinas 1984a; Crunelli et al. 1986; Crunelli et al. 1987b; Pape and McCormick 1989), it seems to be a fairly reliable technique if care is taken. Care was taken to ensure that multiple penetrations were not made in a given areas of the thalamic slice and in addition, the specificity of dye-coupling within LGN lamina and to restricted neuronal populations again suggest that the dye-coupling observed in TC neurones was not artefactual. Previous studies have failed to demonstrate the existence of dye-coupling in TC neurones, although LY, the highest molecular weight intracellular dye commonly used, was only injected into a limited number of cat TC neurones *in vivo* (Deschenes et al. 1984).

The presence of dye-coupling in TC but not NRT neurones may suggest a different Cx subunit composition of GJs in different populations of thalamic neurones. To date, neuronal populations that are associated with Cx36 do not show dye-coupling and these are mostly inhibitory interneuronal networks (Galarreta and Hestrin 2001; Landisman et al. 2002). This may be a particular feature of this Cx subtype and as Cx36 expression is reportedly low or absent in TC neurones (Condorelli et al. 2000; Parenti et al. 2000; Liu and Jones 2003) then other Cx subtypes that may be present and involved in electrotonic coupling between TC neurones (Micevych and Abelson 1991).

6.4.3 Physiological role for electrotonic coupling in the thalamus.

The data presented here strongly suggests that electrotonic coupling is a functional form of intercellular communication in the adult thalamus. Given that spikelets are effective in giving rise to action potentials in TC and NRT neurones, therefore this is in line with the role of electrotonic coupling in generating synchronised rhythmic activity within neuronal networks (Dermietzel and Spray 1993; Logan et al. 1996; Draguhn et al. 1998; Simon and Goodenough 1998; Galarreta and Hestrin 1999; Beierlein et al. 2000; Galarreta and Hestrin 2001).

The presence of both spikelets and burstlets in TC neurones, suggests multiple roles for electrotonic coupling in thalamic relay nuclei. In TC neurones it was apparent that there were 2 different networks of interconnected TC neurones: Type 1 in which spikelets evoked and entrained action potentials and Type 2 in which burstlets evoked and entrained HT bursting. There was also a differential frequency preference between entrainment of these different networks. HT bursts appeared to be entrained around 3-10 Hz, where as action potential firing was entrained at 10 – 25 Hz. This could predispose different networks of TC neurones to generate different frequencies of synchronised activity.

CHAPTER 7

GENERAL DISCUSSION

7.1 MAJOR FINDINGS OF THIS THESIS

The data described in Chapters 3-6 of this thesis provides a significant contribution to the understanding of the mechanisms of oscillatory activity in TC and NRT neurones. In Chapter 3, the induction of a slow (<1Hz) oscillation in TC neurones was achieved through both corticothalamic stimulation of mGluR receptors and by tonic activation of mGluR receptors through pharmacological manipulations. In Chapter 4, the mechanism of this slow (<1Hz) oscillation was fully described and shown to be due to intrinsic ionic conductances in TC neurones following the reduction of I_{KLeak} induced by mGluR activation. The slow (<1Hz) oscillation was critically dependent on $I_{Twindow}$ and enhanced and stabilised by a hitherto undescribed current in TC neurones, I_{CAN}. The similarity of the properties of the slow (<1Hz) oscillation in TC neurones described in Chapter 3 and 4 and those of the slow (<1Hz) oscillation in TC neurones *in vivo* (Steriade et al. 1993a; Timofeev and Steriade 1996) strongly indicate that this is the cellular correlate or *in vitro* manifestation of the slow (<1Hz) oscillation occurring *in vivo* during sleep. The results in Chapter 3 and 4 also expand the role of I_T, but more specifically $I_{Twindow}$, in TC neurones by demonstrating the dependence of the slow (<1Hz) oscillation *in vitro* on the expression of $I_{Twindow}$.

Results detailed in Chapter 5 showed that two different types of <1Hz oscillatory activity with different characteristics were induced in NRT neurones following activation of mGluR receptors. The first, a slow (<1Hz) oscillation has the same characteristic properties as the slow (<1Hz) oscillation observed *in vivo* during sleep (Steriade et al. 1993a; Steriade et al. 1996), leading to the suggestion that this may be the cellular correlate or *in vitro* manifestation of the slow (<1Hz) oscillation in NRT neurones observed in the intact brain during sleep. The second, I have called an undulating (<1Hz) oscillation due to the slowly developing and diminishing wave-like underlying depolarisation of the membrane potential that characterises this type of oscillatory behaviour. These different types of <1Hz oscillatory activity in NRT neurones had sufficiently different characteristics to suggest that they may be generated by different cellular mechanisms.

Finally, Chapter 6 describes the presence and properties of small depolarising potentials, spikelets, in TC and NRT neurones and details investigations into the

origin of the spikelets in TC neurones. The results lead to the conclusion that these spikelets are a manifestation of electrotonic coupling between thalamic neurones and demonstrates that electrotonic coupling may be a hitherto unrealised mechanism of intercellular communication in the adult thalamus.

7.2 THE ROLE OF BISABILITY-MEDIATED ACTIVITIES IN TC NEURONES DURING THE SLOW (<1Hz) SLEEP RHYTHM.

The findings described in Chapter 3 and 4, demonstrate that both corticothalamic stimulation and pharmacological manipulation that tonically activate mGluR1a receptors on TC neurones can induce a slow (<1Hz) oscillation. This is in keeping with the localisation of mGluR1a receptors on the distal dendrites of TC neurones (Godwin et al. 1996). The dense projections of corticothalamic neurones to the thalamus (Hamos et al. 1985; Montero and Singer 1985) and the long-lasting depolarising response of mGluR activation (McCormick and von Krosigk 1992), suggests that tonic mGluR activation could be maintained in the intact brain. In that case, tonic mGluR1a activation could increase the responsiveness of TC neurones through a reduction in g_{Leak} and thus increase the electrotonic compactness. This will then provide a background on which incoming faster synaptic events could be more effective in evoking a response in TC neurones. A reduction of g_{Leak} is a mechanism common to other neurotransmitters in the thalamus (McCormick 1992). The ability of other thalamic neurotransmitters or neuromodulators in unmasking bistability-mediated behaviours in thalamic neurones is unknown. Likewise, the interaction of other thalamic neurotransmitters with the mGluR-induced reduction of g_{Leak} in the modulation of slow (<1Hz) oscillatory activity in TC neurones is also unknown.

In accordance with previous observations (McCormick and von Krosigk 1992; von Krosigk et al. 1999; Turner and Salt 2000), mGluR activation was effective in depolarising TC neurones, and additionally, but not previously described, was effective in inducting a slow (<1Hz) oscillation in a subset of TC neurones within each thalamic relay nucleus examined. Although, the manifestation of the slow (<1Hz) oscillation was variable, most prominently in LGN TC neurones (see section 3.3.2.2), the basic underlying waveform always comprised rhythmic transitions from a hyperpolarised "down" state to a depolarised "up" state. The

similarity of the underlying basic waveform in all TC neurones displaying the slow (<1Hz) oscillation indicates that induction of this slow (<1Hz) oscillation is most likely a feature of all TC neurones where g_{Leak} is sufficiently reduced. This is in keeping with the demonstration that all TC neurones posses the ionic conductances necessary to generate bistability-mediated activities (Hughes et al. 1999).

Data in Chapters 3 and 4 demonstrate the very similar properties of the slow (<1Hz) sleep oscillation *in vitro* and *in vivo*. The compelling similarity of these observations *in vitro* and *in vivo*, suggest that the slow (<1Hz) oscillation in the thalamus is not simply a reflection of the slow (<1Hz) oscillation in the cortex, but can be generated in TC neurones through a bistability-mediated mechanism as a result of tonic mGluR activation derived from the cortex. These observations therefore suggest that the slow (<1Hz) oscillation in TC neurones may have a greater role than hitherto realised in the organisation of the slow (<1Hz) oscillation in the cortex. As TC neurones become hyperpolarised as the cortical and brainstem drive is reduced during deepening sleep, the ability of TC neurones to generate large hyperpolarising potentials (LHP) that reliably evoke bursts of action potentials will provide a strong and reliable drive to the cortex to aid organisation of cortical activity. This organisational role is in combination with the already described role of the slow (<1Hz) oscillation in the thalamus in aiding maintenance of the global synchronisation of the slow (<1Hz) rhythm in the corticothalamic loop by virtue of its reciprocal projections back to the cortex (Steriade et al. 1993a; Steriade et al. 1993d).

The slow (<1Hz) oscillation in TC neurones will also presumably serve to synchronise global thalamic activity though reciprocal projections with the overlying NRT. Activation of NRT neurones, due to firing of TC neurones, will send an inhibitory drive back to TC neurones (see section 1.3). This inhibitory drive may help to hyperpolarise TC neurones in the presence of cortical drive and so move the membrane potential to a range where the LHP could be initiated. Therefore this reciprocal inhibitory projection from the NRT may also assist in the development and organisation of the slow (<1Hz) sleep oscillation in the thalamus and cortex as sleep deepens.

Bistability-mediated activity may also provide a mechanism by which neurones more reliably generate burst responses, thus providing a strong and reliable drive to the cortex. Burst firing in TC neurones during the awake state has be been suggested to have a role in stimulus detection an attentive processes (Guido and Weyand 1995; Guido and Sherman 1998; Reinagel et al. 1999; Swadlow and Gusev 2001). The ability of the LHP to generate a burst response in TC neurones from a depolarised membrane potential is in contrast to the classical view that only two modes of TC firing exist: tonic firing at depolarised membrane potential and bursting at hyperpolarised membrane potentials (see section 1.5). Therefore by virtue of the LHP, burst responses can be reliably triggered from more depolarised membrane potentials as typically observed during the awake state.

In conclusion, this is a clear demonstration that $I_{Twindow}$-mediated bistability is an integral part of the electroresponsiveness of TC neurones and may contribute to a variety of manifestations of TC activity during different behavioural states in the intact brain.

7.3 <1Hz OSCILLATORY ACTIVITY IN NRT NEURONES

7.3.1 The role of bistability-mediated activities in NRT neurones during the slow (<1Hz) sleep rhythm.

The experiments described in Chapter 5 indicted that <1Hz oscillatory activity can arise through activation of mGluR receptors and, in particular, that bistability-mediated behaviours may be generated, through unmasking of $I_{Twindow}$, in NRT neurones. Although a window component for I_T is predicted in NRT neurones (Chemin et al. 2002; Perez-Reyes 2003), this appears to be the first indication that $I_{Twindow}$ may be functionally significant in NRT neurones.

The similarity of the slow (<1Hz) oscillation in NRT neurones *in vitro* and *in vivo*, may indicate, that this demonstration of the slow (<1Hz) oscillation in NRT neurones is the cellular correlate of the slow (<1Hz) sleep oscillation in NRT neurones *in vivo* (Steriade et al. 1993a). The ability of the slow (<1Hz) oscillation to group spindle frequency bursts *in vitro* further supports this idea and provides evidence that spindle oscillations *in vivo* can be generated in individual NRT

neurones when g_{Leak} is sufficiently reduced. The interaction of NRT neurones that can generate spindle oscillations may provide the mechanisms by which the synchronisation of spindle waves in the thalamus in the absence of cortical inputs in generated (Steriade et al. 1987). As yet the significance of sleep spindles in the EEG, other than as a useful tool for determining sleep stages (Cooper 1994) has yet to be defined. Whether or not spindle frequency activity of the NRT during sleep has a functional role in information processing in the brain or signalling the state of alertness during this behavioural state, or is simply a manifestation of the intrinsic properties of NRT neurones under favourable conditions that allow its expression, will be difficult to determined given that this neuronal population is so densely connected to TC and cortical neurones within the corticothalamic system.

7.3.2 Different mechanisms of bursting activity in NRT neurones.

It has previously been suggested that different mechanism generate bursting activity in NRT neurones dependent on the level of neuronal depolarisation (Llinas and Geijo-Barrientos 1988). The data described in Chapter 5, leads to the suggestion that this may be the case and that different mechanisms can lead to the generation of intrinsically generated rhythmic bursting activities within different frequency ranges. TC neurones provide a clear demonstration that two different types of bursting activity can be present, with LTCP burst firing occurring at hyperpolarised membrane potentials and high-threshold (HT) bursting occurring when neurones are more depolarised (see Fig. 3.2). Based on the observation described in Chapter 5, I have suggested that I_h may have a functional role in NRT neurones and further suggest that the interaction of I_T and I_h may be responsible for the generation of δ (1-2Hz) frequency bursting as in TC neurones (McCormick and Pape 1990; Leresche et al. 1991; Soltesz et al. 1991). This suggestion is in contrast to previous indications that I_h has no role in generating rhythmic activity in NRT neurones (Bal and McCormick 1993). Therefore, it may be entirely possible that the I_T / I_{Kca} mechanism that underlies spindle (7-14Hz) frequency bursts and an I_T / I_h mechanism generating δ (1-2Hz) frequency bursts can co-exist by predominating at different levels of neuronal depolarisation.

7.4 A ROLE FOR ELECTROTONIC COUPLING IN THE THALAMUS

The data detailed in Chapter 6 provides strong evidence that the spikelets observed in TC and NRT neurones are the manifestation of electrotonic coupling within these neuronal populations.

A direct demonstration of electrotonic coupling in NRT neurones has been performed in neonatal thalamic slices (Landisman et al. 2002). The properties of the spikelets in NRT neurones described in Chapter 6 are in keeping with those observed previously (Landisman et al. 2002). The importance of the observation here is that electrotonic coupling persists in adult NRT neurones and may therefore play a role in determining the output of the NRT. Cx36 expression is high in the NRT (Condorelli et al. 2000; Parenti et al. 2000; Liu and Jones 2003) and has be localised predominantly to dendritic locations on NRT neurones (Liu and Jones 2003). The observation that GJs in NRT neurones are located at dendritic sites is in keeping with the appearance of spikelets above a certain level of depolarisation of the recorded neurone, suggesting that the dendrites need to be depolarised in order to transmit spikelets to the soma, or that GJ opening occurs above a certain threshold level of neuronal depolarisation (see section 7.4.4). Additionally, the lack of dye-coupling in NRT neurones, despite the intracellular dyes Biocytin or Neurobiotin routinely being present in the electrode solution, is in keeping with the observations that dye-coupling does not occur in NRT neurones (Landisman et al. 2002) or other GABAergic neuronal populations that are electrotonically coupled (Galarreta and Hestrin 1999; Venance et al. 2000; Galarreta and Hestrin 2001).

A comparison of spikelets observed in TC and NRT neurones found that they have virtually identical properties. This is compelling evidence that they are generated by the same mechanism and indicates that spikelets in TC neurones are an electrophysiological manifestation of electrotonic coupling that persists during development and is present in adult cat TC neurones. The Cx subtype that may be involved in the formation of GJs between TC neurones is a question of speculation. Cx36 mRNA, the Cx subtype that is suggested to be predominantly associated with GJs between neurones (Rash et al. 2000), is expressed at low levels in thalamic relay nuclei (Parenti et al. 2000) and therefore is a candidate for thalamic GJs. Other Cx subtypes, however, have also been localised to the thalamus (Micevych and Abelson 1991).

As TC neurones are the output neurones of the thalamus, the role of electrotonic coupling amongst TC neurones may be significant in therefore determining cortical activity. This observation may be pertinent to the fact that synchronised action potential firing and or burst firing in thalamic relay nuclei is seen during different behavioural states. For example, synchronised, output from neighbouring TC neurones in the LGN have been shown to be more effective in driving the output to single cortical neurones than their individual effects (Alonso et al. 1996). Although the origin of the synchronous firing in LGN TC neurones derives from simultaneous stimulation from retinal inputs, electrotonic coupling may play a role in ensuring that interconnected neuronal networks of TC neurones, depolarised by the retinal input, do generate a synchronised input to the cortex, thereby selectively strengthening the cortical response to retinal stimulation. The data presented in Chapter 6 is in keeping with this idea, where spikelets can only reliably entrain action potential firing when neurones are sufficiently depolarised. The ability of spikelets to entrain action potential firing within a specific frequency range may also indicate a role for electrotonic coupling in detecting stimuli eliciting neuronal activity a specific frequencies or coincidence detection. Observation of FPPs in TC neurones *in vivo* (Deschenes et al. 1984; Steriade et al. 1991b), with very similar properties to the spikelets seen in TC neurones as described in Chapter 6, have been acssociated with the generation of synchronised fast (20-40Hz) oscillations in the thalamus and cortex (Steriade et al. 1991b; Timofeev and Steriade 1997).

Another interesting feature of the EEG is the existence of the posterior alpha rhythm in the occipital cortex and the mu rhythm of the somatosensory cortex during periods of quiet wakefulness (Cavonius and Estevez-Uscanga 1974; Bouyer et al. 1982; Bouyer et al. 1983; Chatila et al. 1993; Cooper 1994; Rougeul-Buser and Buser 1997; Goldman et al. 2002). Both rhythms occur in the 10-15Hz frequency range, are distinguished from the 7-14Hz sleep spindles originating in the NRT (Timofeev and Steriade 1996) due to their appearance during quiet immobility / drowsiness prior to the onset of sleep (Cavonius and Estevez-Uscanga 1974; Cooper 1994; Goldman et al. 2002). It has been proposed that these 10-15Hz EEG rhythms during quiet wakefulness originate from or are determined by the thalamus as localised regions of the LGN and VP

nuclei have been shown to be highly synchronised with the posterior alpha rhythm of the occipital cortex and the mu rhythm of the somatosensory cortex, respectively (Bouyer et al. 1982; Bouyer et al. 1983; Chatila et al. 1993; Rougeul-Buser and Buser 1997). The restricted projection sites of TC neurones within the LGN or VP nuclei (Steriade et al. 1997) and restricted sites of these 10-15Hz EEG rhythms during quite wakefulness supports this notion along with the observation that in the VP the rhythmic thalamic cells were identified as TC neurones (Bouyer et al. 1982). Whether or not these thalamic rely nuclei can act as pacemakers for these particular EEG rhythms has yet to be conclusively demonstrated. As rhythmic activity within the 10-15Hz frequency range could not be elicited in the VP through tactile or deep somatic stimulation (normal methods used to evoke responses in the VP), the idea that a subset of TC neurones within the VP that are distinct from the classical role of TC neurones as relay cells has been suggested (Bouyer et al. 1982; Rougeul-Buser and Buser 1997). This theory certainly is in accordance with the appearance of the EEG mu rhythm during periods of quite drowsiness whereas stimulation or movement will abolish the mu rhythm and induce an EEG rhythm that is characteristic of the alert state (Bouyer et al. 1983). The same feature is seen with the EEG posterior alpha rhythm, with development of the rhythm during quiet immobility, but visual stimulation or eye movements resulting in a desynchronised EEG rhythm characterising alertness (Cavonius and Estevez-Uscanga 1974; Chatila et al. 1993; Cooper 1994). It is of note here that a subset of TC neurones within the LGN *in vitro* are capable of generating rhythmic bursting responses (HT bursts) within the 10-15Hz frequency range and that burstlets could also entrain HT bursts within this frequency (see Fig. 6.9) (Hughes et al. 2004). These observations certainly indicate that the LGN is capable of generating synchronous rhythmic activity within the 10-15Hz frequency range and therefore may indeed provide a cellular thalamic mechanism that could act as a pacemaker for the EEG posterior alpha rhythm (Hughes et al. 2004). As the observations described in Chapter 6 suggest that burstlets are also a manifestation of electrotonic coupling in the thalamus, then the synchronisation of HT bursts in TC neurones via electrotonic coupling may indeed be a important mechanism in determining synchronised rhythmic cortical activity.

7.5 SUGGESTIONS FOR FURTHER WORK

7.5.1 Other neurotransmitter-mediated induction of the slow (<1Hz) oscillation.

The data presented in this thesis show that the reduction of g_{Leak} in thalamic neurones is an effective way of inducing bistability-mediated activities. The fact that other thalamic neurotransmitters, Ach and NA in particular, are effective in decreasing g_{Leak} of TC neurones suggests that they may also be able to induce bistability-mediated activities. This is a simplified suggestion as effects on neuronal activity induced by these neurotransmitters have also been shown to be mediated though an enhancement of I_h. However, it is a question of significant interest that warrants further investigation.

7.5.2 Interaction of TC and NRT neurones during the slow (<1Hz) oscillation.

The results detailed in Chapters 3-5 describe the generation of a slow (<1Hz) oscillation in both TC and NRT neurones when they are essentially devoid of interaction with each other. Given that the slow (<1Hz) oscillation in TC and NRT neurone is closely synchronised during sleep, the interaction of the slow (<1Hz) oscillation in TC and NRT neurones *in vitro* is of interest. Investigation of their interaction in thalamic slices may yield further information regarding the significance of the thalamic slow (<1Hz) oscillation. The ability to generate synchronised slow (<1Hz) oscillatory activity in thalamic relay nuclei, presumably utilising reciprocal interconnections with the NRT would support the role of the slow (<1Hz) oscillation in the organisation of the slow (<1Hz) oscillation in the cortex.

7.5.3 Demonstration of non-negligible $I_{Twindow}$ in NRT neurones.

The results detailed in Chapter 5 strongly indicate that $I_{Twindow}$ underlies the slow (<1Hz) oscillation in NRT neurones though a bistability-mediated interaction with g_{Leak} (see section 5.4.3) (Williams et al. 1997a; Hughes et al. 1999). The existence of $I_{Twindow}$ is predicted in NRT neurones, but functional existence and the role of this current have yet to be demonstrated. The use of the dynamic clamp technique has been utilised to investigate the role of $I_{Twindow}$ in bistability-mediated activities in TC neurones (Hughes et al. 1999). This technique could be

employed to also demonstrate both the existence and role of $I_{Twindow}$ in NRT neurones.

7.5.4 Full elucidation of the slow (<1Hz) oscillation in NRT neurones.

The experiments detailed in Chapter 5 show that following mGluR activation, the slow (<1Hz) oscillation in NRT neurone is generated though a mechanism involving the intrinsic conductances of the neurone. As the appearance and properties of the underlying waveform of the slow (<1Hz) oscillation in NRT neurones and TC neurones *in vitro* is virtually identical (see section 5.4.1), it is very likely that they occur by the same mechanism. The dependence of the slow (<1Hz) oscillation on $I_{Twindow}$ should be confirmed. In addition, the mGluR-mediated effect is presumed to be predominantly through a reduction of g_{Leak} (Lee and McCormick 1997), as NRT neurones were depolarised and the input resistance was increased. The role of g_{Leak} in the induction of the slow (<1Hz) oscillation in NRT neurones should also be confirmed.

7.5.5 Contribution of I_h to oscillatory activity in NRT neurones.

A number of observation described in Chapter 5 suggest that I_h may have a functional role in determining the oscillatory activity of NRT neurones. A number of experiments utilising the pharmacological I_h blocker, ZD 7288, and the use of the dynamic clamp system to re-introduce this current (Hughes et al. 1998) could be used to investigate it's expression, properties and role in NRT neurones or otherwise confirm that it has no contribution to oscillatory activity in NRT neurones (Bal and McCormick 1993).

7.5.6 Prevalence and mechanism of the undulating (<1Hz) oscillation in NRT neurones.

As the undulating (<1Hz) oscillation was seen in NRT neurones was seen on a background of reduced fast glutamatergic and fast and slow GABAergic inputs, its generation under more physiological conditions is uncertain. Extracellular recording in the NRT could indicate if this is a common type of oscillatory activity and under what conditions it can is present. In addition, elucidation of the mechanism of this type of <1Hz oscillatory activity could indicate how it may make a contribution to other activities of NRT neurones.

7.5.7 Direct demonstration of electrotonic coupling between TC neurones.

Chapter 6 details a significant amount of indirect experimental evidence that indicates that electrotonic communication is a functional method of intercellular coupling in the adult thalamus. A direct demonstration of electrotonic coupling by utilising a method paired electrophysiological recordings of TC neurones is required to confirm this unequivocally.

7.5.8 Physiological role of electrotonic coupling between thalamic neurones.

Synchronised neuronal firing is a feature of thalamic neurones during different behavioural states (Chatila et al. 1993; Alonso et al. 1996; Rougeul-Buser and Buser 1997). Electrotonic coupling is associated with synchronising neuronal activity in neurones. Therefore, the ability of electrotonic coupling to generate rhythmic activity in the thalamus is of great interest as the thalamus provides a strong excitatory influence to the cortex and may have a role in determining rhythmic activity in the cortex. The role that electrotonic coupling between thalamic neurones play and the extant of this influence may be found by specifically investigating rhythmic synchronous activities occurring naturally *in vivo*.

CHAPTER 8

REFERENCES

8.1 BIBLIOGRAPHY

Achermann, P. and A. A. Borbely (1997). Low-frequency (< 1 Hz) oscillations in the human sleep electroencephalogram. Neuroscience 81(1): 213-22.

Agmon, A. and B. W. Connors (1991). Thalamocortical responses of mouse somatosensory (barrel) cortex in vitro. Neuroscience 41(2-3): 365-79.

Ahlsen, G., K. Grant and S. Lindstrom (1982). Monosynaptic excitation of principle cells in the lateral geniculate nucleus by corticofugan fibers. Brain Research 234: 454-8.

Alger, B. E., M. McCarren and R. S. Fisher (1983). On the possibility of simultaneously recording from two cells with a single microelectrode in the hippocampal slice. Brain Research 270(1): 137-41.

Alonso, J. M., W. M. Usrey and R. C. Reid (1996). Precisely correlated firing in cells of the lateral geniculate nucleus. Nature 383(6603): 815-9.

Amzica, F., A. Nunez and M. Steriade (1992). Delta frequency (1-4 Hz) oscillations of perigeniculate thalamic neurons and their modulation by light. Neuroscience 51(2): 285-94.

Amzica, F. and M. Steriade (1995a). Disconnection of intracortical synaptic linkages disrupts synchronization of a slow oscillation. Journal of Neuroscience 15(6): 4658-77.

Amzica, F. and M. Steriade (1995b). Short- and long-range neuronal synchronization of the slow (< 1 Hz) cortical oscillation. Journal of Neurophysiology 73(1): 20-38.

Amzica, F. and M. Steriade (1997). The K-complex: its slow (<1-Hz) rhythmicity and relation to delta waves. Neurology 49(4): 952-9.

Amzica, F. and M. Steriade (1998a). Cellular substrates and laminar profile of sleep K-complex. Neuroscience 82(3): 671-86.

Amzica, F. and M. Steriade (1998b). Electrophysiological correlates of sleep delta waves. Electroencephalography and Clinical Neurophysiology 107(2): 69-83.

Avanzini, G., M. de Curtis, F. Panzica and R. Spreafico (1989). Intrinsic properties of nucleus reticularis thalami neurones of the rat studied in vitro. Journal of Physiology (London) 416: 111-22.

Bal, T. and D. A. McCormick (1993). Mechanisms of oscillatory activity in guinea-pig nucleus reticularis thalami in vitro: a mammalian pacemaker. Journal of Physiology (London) 468: 669-91.

Bal, T. and D. A. McCormick (1996). What stops synchronized thalamocortical oscillations? Neuron 17(2): 297-308.

Bal, T., M. von Krosigk and D. A. McCormick (1995a). Role of the ferret perigeniculate nucleus in the generation of synchronized oscillations in vitro. Journal of Physiology (London) 483(Pt 3): 665-85.

Bal, T., M. von Krosigk and D. A. McCormick (1995b). Synaptic and membrane mechanisms underlying synchronized oscillations in the ferret lateral geniculate nucleus in vitro. Journal of Physiology (London) 483(Pt 3): 641-63.

Barbaresi, P., R. Spreafico, C. Frassoni and A. Rustioni (1986). GABAergic neurons are present in the dorsal column nuclei but not in the ventroposterior complex of rats. Brain Research 382(2): 305-26.

Bartos, M., I. Vida, M. Frotscher, J. R. Geiger and P. Jonas (2001). Rapid signaling at inhibitory synapses in a dentate gyrus interneuron network. Journal of Neuroscience 21(8): 2687-98.

Bazhenov, M., I. Timofeev, M. Steriade and T. J. Sejnowski (1999). Self-sustained rhythmic activity in the thalamic reticular nucleus mediated by depolarizing GABAA receptor potentials. Nature Neuroscience 2(2): 168-74.

Beierlein, M., J. R. Gibson and B. W. Connors (2000). A network of electrically coupled interneurons drives synchronized inhibition in neocortex. Nature Neuroscience 3(9): 904-10.

Bennett, M. V. L. (1996). Gap junctions as electrical synapses. Gap Junctions in the nervous system. D. C. Spray and R. Dermietzel. Austin, RG Landes Company.

Bickford, M. E., A. E. Gunluk, W. Guido and S. M. Sherman (1993). Evidence that cholinergic axons from the parabrachial region of the brainstem are the exclusive source of nitric oxide in the lateral geniculate nucleus of the cat. Journal of Comparative Neurology 334(3): 410-30.

Bloomfield, S. A., J. E. Hamos and S. M. Sherman (1987). Passive cable properties and morphological correlates of neurones in the lateral geniculate nucleus of the cat. Journal of Physiology (London) 383: 653-92.

Bloomfield, S. A. and S. M. Sherman (1988). Postsynaptic potentials recorded in neurons of the cat's lateral geniculate nucleus following electrical stimulation of the optic chiasm. Journal of Neurophysiology 60(6): 1924-45.

Bouyer, J. J., A. Rougeul and P. Buser (1982). Somatosensory rhythms in the awake cat: a single unit exploration of their thalamic concomitant in the nucleus ventralis posterior and vicinity. Archives Italiennes de Biologie 120(1-3): 95-110.

Bouyer, J. J., C. Tilquin and A. Rougeul (1983). Thalamic rhythms in cat during quiet wakefulness and immobility. Electroencephalography and Clinical Neurophysiology 55(2): 180-7.

Brunton, J. and S. Charpak (1998). mu-Opioid peptides inhibit thalamic neurons. Journal of Neuroscience 18(5): 1671-8.

Budde, T., R. Mager and H. C. Pape (1992). Different Types of Potassium Outward Current in Relay Neurons Acutely Isolated from the Rat Lateral Geniculate Nucleus. European Journal of Neuroscience 4(8): 708-22.

Budde, T., T. Munsch and H. C. Pape (1998). Distribution of L-type calcium channels in rat thalamic neurones. European Journal of Neuroscience 10(2): 586-97.

Cavonius, C. R. and O. Estevez-Uscanga (1974). Local suppression of alpha activity by pattern in half the visual field. Nature 251(5474): 412-414.

Chatila, M. C., A. Milleret, A. Rougeul and P. Buser (1993). Alpha rhythm in the cat thalamus. Comptes Rendud de L'Academie des Sciences. Serie III 316(1): 51-8.

Chemin, J., A. Monteil, E. Perez-Reyes, E. Bourinet, J. Nargeot and P. Lory (2002). Specific contribution of human T-type calcium channel isotypes (alpha(1G), alpha(1H) and alpha(1I)) to neuronal excitability. Journal of Physiology (London) 540(Pt 1): 3-14.

Chen, Q. X. (1991). Intracellular Ca2+ suppressed a transient potassium current in hippocampal neurones. Journal of Neuroscience 11(2): 337-43.

Chuang, S.-C., R. Bianchi and R. K. S. Wong (2000). Group 1 mGluR activation turns on a voltage-gated inwad curent in hippocampal pyramidal cells. Journal of Neurophysiology 83: 2844-53.

Condorelli, D. F., N. Belluardo, A. Trovato-Salinaro and G. Mudo (2000). Expression of Cx36 in mammalian neurons. Brain Research Brain Research Reviews 32(1): 72-85.

Connors, B. W., M. J. Gutnick and D. A. Prince (1982). Electrophysiological properties of neocortical neurons in vitro. Journal of Neurophysiology 48(6): 1302-20.

Contreras, D., R. Curro Dossi and M. Steriade (1992). Bursting and tonic discharges in two classes of reticular thalamic neurons. Journal of Neurophysiology 68(3): 973-7.

Contreras, D., R. Curro Dossi and M. Steriade (1993). Electrophysiological properties of cat reticular thalamic neurones in vivo. Journal of Physiology (London) 470: 273-94.

Contreras, D., A. Destexhe, T. J. Sejnowski and M. Steriade (1996). Control of spatiotemporal coherence of a thalamic oscillation by corticothalamic feedback. Science 274(5288): 771-4.

Contreras, D., A. Destexhe, T. J. Sejnowski and M. Steriade (1997). Spatiotemporal patterns of spindle oscillations in cortex and thalamus. Journal of Neuroscience 17(3): 1179-96.

Contreras, D. and M. Steriade (1995). Cellular basis of EEG slow rhythms: a study of dynamic corticothalamic relationships. Journal of Neuroscience 15(1 Pt 2): 604-22.

Contreras, D. and M. Steriade (1996). Spindle oscillation in cats: the role of corticothalamic feedback in a thalamically generated rhythm. Journal of Physiology (London) 490(Pt 1): 159-79.

Contreras, D. and M. Steriade (1997). Synchronization of low-frequency rhythms in corticothalamic networks. Neuroscience 76(1): 11-24.

Cooper, R. (1994). Normal sleep. Sleep. R. Cooper. London, Chapman & Hall.

Coulter, D. A., J. R. Huguenard and D. A. Prince (1989). Calcium currents in rat thalamocortical relay neurones: kinetic properties of the transient, low-threshold current. Journal of Physiology (London) 414: 587-604.

Cox, C. L., J. R. Huguenard and D. A. Prince (1995). Cholecystokinin depolarizes rat thalamic reticular neurons by suppressing a K+ conductance. Journal of Neurophysiology 74(3): 990-1000.

Cox, C. L. and S. M. Sherman (1999). Glutamate inhibits thalamic reticular neurons. Journal of Neuroscience 19(15): 6694-9.

Cox, C. L., Q. Zhou and S. M. Sherman (1998). Glutamate locally activates dendritic outputs of thalamic interneurons. Nature 394(6692): 478-82.

Crabtree, J. W., G. L. Collingridge and J. T. Isaac (1998). A new intrathalamic pathway linking modality-related nuclei in the dorsal thalamus. Nature Neuroscience 1(5): 389-94.

Crunelli, V., M. Haby, D. Jassik-Gerschenfeld, N. Leresche and M. Pirchio (1988). Cl- - and K+-dependent inhibitory postsynaptic potentials evoked by interneurones of the rat lateral geniculate nucleus. Journal of Physiology (London) 399: 153-76.

Crunelli, V., N. Leresche, J. W. Hynd, N. M. Patel and J. G. Parnavelas (1987a). An in vitro slice preparation of the cat lateral geniculate nucleus. Journal of Neuroscience Methods 20(3): 211-9.

Crunelli, V., N. Leresche and J. G. Parnavelas (1986). X- and Y-cells identified in the cat lateral geniculate nucleus in vitro. Brain Research 380(2): 371-4.

Crunelli, V., N. Leresche and J. G. Parnavelas (1987b). Membrane properties of morphologically identified X and Y cells in the lateral geniculate nucleus of the cat in vitro. Journal of Physiology (London) 390: 243-56.

Crunelli, V., S. Lightowler and C. E. Pollard (1989). A T-type Ca2+ current underlies low-threshold Ca2+ potentials in cells of the cat and rat lateral geniculate nucleus. Journal of Physiology (London) 413: 543-61.

Cucchiaro, J. B., D. J. Uhlrich and S. M. Sherman (1991). Electron-microscopic analysis of synaptic input from the perigeniculate nucleus to the A-laminae of the lateral geniculate nucleus in cats. Journal of Comparative Neurology 310(3): 316-36.

Curro Dossi, R., D. Pare and M. Steriade (1992). Various types of inhibitory postsynaptic potentials in anterior thalamic cells are differentially altered by stimulation of laterodorsal tegmental cholinergic nucleus. Neuroscience 47(2): 279-89.

De Biasi, S., A. Amadeo, R. Spreafico and A. Rustioni (1994). Enrichment of glutamate immunoreactivity in lemniscal terminals in the ventropostero lateral thalamic nucleus of the rat: an immunogold and WGA-HRP study. The Anatomical Record 240(1): 131-40.

De Biasi, S., C. Frassoni and R. Spreafico (1988). The intrinsic organization of the ventroposterolateral nucleus and related reticular thalamic nucleus of the rat: a double-labeling ultrastructural investigation with gamma-aminobutyric acid immunogold staining and lectin-conjugated horseradish peroxidase. Somatosensory Research 5(3): 187-203.

De Biasi, S. and A. Rustioni (1990). Ultrastructural immunocytochemical localization of excitatory amino acids in the somatosensory system. Journal of Histochemistry and Cytochemistry 38(12): 1745-54.

De Curtis, M., R. Spreafico and G. Avanzini (1989). Excitatory amino acids mediate responses elicited in vitro by stimulation of cortical afferents to reticularis thalami neurones in the rat. Neuroscience 33: 275-283.

Deans, M. R., J. R. Gibson, C. Sellitto, B. W. Connor and D. L. Paul (2001). Synchronous activity of inhibitory networks in neocortex requires electrical synapses containing connexin 36. Neuron 31(3): 377-85.

Debarbieux, F., J. Brunton and S. Charpak (1998). Effect of bicuculline on thalamic activity: a direct blockade of IAHP in reticularis neurons. Journal of Neurophysiology 79(6): 2911-8.

Dermietzel, R. and D. C. Spray (1993). Gap junctions in the brain: where, what type, how many and why? Trends in Neurosciences 16(5): 186-92.

Deschenes, M. and B. Hu (1990). Electrophysiology and Pharmacology of the Corticothalamic Input to Lateral Thalamic Nuclei: an Intracellular Study in the Cat. European Journal of Neuroscience 2(2): 140-52.

Deschenes, M., A. Madariaga-Domich and M. Steriade (1985). Dendrodendritic synapses in the cat reticularis thalami nucleus: a structural basis for thalamic spindle synchronization. Brain Research 334(1): 165-8.

Deschenes, M., M. Paradis, J. P. Roy and M. Steriade (1984). Electrophysiology of neurons of lateral thalamic nuclei in cat: resting properties and burst discharges. Journal of Neurophysiology 51(6): 1196-219.

Destexhe, A., D. Contreras, M. Steriade, T. J. Sejnowski and J. R. Huguenard (1996). In vivo, in vitro, and computational analysis of dendritic calcium currents in thalamic reticular neurons. Journal of Neuroscience 16(1): 169-85.

Domich, L., G. Oakson and M. Steriade (1986). Thalamic burst patterns in the naturally sleeping cat: a comparison between cortically projecting and reticularis neurones. Journal of Physiology (London) 379: 429-49.

Draguhn, A., R. D. Traub, D. Schmitz and J. G. Jefferys (1998). Electrical coupling underlies high-frequency oscillations in the hippocampus in vitro. Nature 394(6689): 189-92.

Eaton, S. A. and T. E. Salt (1996). Role of N-methyl-D-aspartate and metabotropic glutamate receptors in corticothalamic excitatory postsynaptic potentials in vivo. Neuroscience 73(1): 1-5.

Ellinor, P. T., J. F. Zhang, A. D. Randall, M. Zhou, T. L. Schwarz, R. W. Tsien and W. A. Horne (1993). Functional expression of a rapidly inactivating neuronal calcium channel. Nature 363(6428): 455-8.

Erisir, A., S. C. Van Horn and S. M. Sherman (1998). Distribution of synapses in the lateral geniculate nucleus of the cat: differences between laminae A and A1 and between relay cells and interneurons. Journal of Comparative Neurology 390(2): 247-55.

Famiglietti, E. V., Jr. and A. Peters (1972). The synaptic glomerulus and the intrinsic neuron in the dorsal lateral geniculate nucleus of the cat. Journal of Comparative Neurology 144(3): 285-334.

Fitzpatrick, D., G. R. Penny and D. E. Schmechel (1984). Glutamic acid decarboxylase-immunoreactive neurons and terminals in the lateral geniculate nucleus of the cat. Journal of Neuroscience 4(7): 1809-29.

Friedlander, M. J., C. S. Lin, L. R. Stanford and S. M. Sherman (1981). Morphology of functionally identified neurones in the lateral geniculate nucleus of the cat. Journal of Neurophysiology 46(6): 80-129.

Frigyesi, T. L. (1972). Intracellular recordings from neurons in dorsolateral thalamic reticular nucleus during capsular, basal ganglia and midline thalamic stimulation. Brain Research 48: 157-72.

Gabbott, P. L., J. Somogyi, M. G. Stewart and J. Hamori (1986). A quantitative investigation of the neuronal composition of the rat dorsal lateral geniculate nucleus using GABA-immunocytochemistry. Neuroscience 19(1): 101-11.

Galarreta, M. and S. Hestrin (1999). A network of fast-spiking cells in the neocortex connected by electrical synapses. Nature 402(6757): 72-5.

Galarreta, M. and S. Hestrin (2001). Electrical synapses between GABA-releasing interneurons. Nature Reviews Neuroscience 2(6): 425-33.

Gibson, J. R., M. Beierlein and B. W. Connors (1999). Two networks of electrically coupled inhibitory neurons in neocortex. Nature 402(6757): 75-9.

Gil, Z. and Y. Amitai (1996). Adult thalamocortical transmission involves both NMDA and non-NMDA receptors. Journal of Neurophysiology 76(4): 2547-54.

Gil, Z., B. W. Connors and Y. Amitai (1997). Differential regulation of neocortical synapses by neuromodulators and activity. Neuron 19(3): 679-86.

Gladwell, S. J. and J. G. Jefferys (2001). Second messenger modulation of electrotonic coupling between region CA3 pyramidal cell axons in the rat hippocampus. Neuroscience Letters 300(1): 1-4.

Glenn, L. L. and M. Steriade (1982). Discharge rate and excitability of cortically projecting intralaminar thalamic neurons during waking and sleep states. Journal of Neuroscience 2(10): 1387-404.

Godwin, D. W., S. C. Van Horn, A. Eriir, M. Sesma, C. Romano and S. M. Sherman (1996). Ultrastructural localization suggests that retinal and cortical inputs access different metabotropic glutamate receptors in the lateral geniculate nucleus. Journal of Neuroscience 16(24): 8181-92.

Gokcebay, N., S. Cooper, R. L. Williams, M. Hirshkowitz and C. A. Moore (1994). Function of sleep. Sleep. R. Cooper. London, Chapman & Hall.

Goldman, R. I., J. M. Stern, J. J. Engle and M. S. Cohen (2002). Simultaneous EEG and fMRI of the alpha rhythm. Neuroreport 13(8): 2487-92.

Golshani, P., X. B. Liu and E. G. Jones (2001). Differences in quantal amplitude reflect GluR4-subunit number at corticothalamic synapses on two populations of thalamic neurons. Proceedings of the National Acadamy of Sciences USA 98(7): 4172-7.

Guido, W., S. M. Lu and S. M. Sherman (1992). Relative contributions of burst and tonic responses to the receptive field properties of lateral geniculate neurons in the cat. Journal of Neurophysiology 68(6): 2199-211.

Guido, W. and S. M. Sherman (1998). Response latencies of cells in the cat's lateral geniculate nucleus are less variable during burst than tonic firing. Visual Neuroscience 15(2): 231-7.

Guido, W. and T. Weyand (1995). Burst responses in thalamic relay cells of the awake behaving cat. Journal of Neurophysiology 74(4): 1782-6.

Guillery, R. W. (1966). A study of Golgi preparations from the dorsal lateral geniculate nucleus of the adult cat. Journal of Comparative Neurology 128(1): 21-50.

Gutierrez, C., C. L. Cox, J. Rinzel and S. M. Sherman (2001). Dynamics of low-threshold spike activation in relay neurons of the cat lateral geniculate nucleus. Journal of Neuroscience 21(3): 1022-32.

Gutnick, M. J., R. Lobel-Yaakov and G. Rimon (1985). Incidence of neuronal dye-coupling in neocortical slices depends on the plane of section. Neuroscience 15(3): 659-66.

Guyon, A. and N. Leresche (1995). Modulation by different GABAB receptor types of voltage-activated calcium currents in rat thalamocortical neurones. Journal of Physiology (London) 485(Pt 1): 29-42.

Hallanger, A. E., A. I. Levey, H. J. Lee, D. B. Rye and B. H. Wainer (1987). The origins of cholinergic and other subcortical afferents to the thalamus in the rat. Journal of Comparative Neurology 262(1): 105-124.

Hamos, J. E., S. C. Van Horn, D. Raczkowski and S. M. Sherman (1987). Synaptic circuits involving an individual retinogeniculate axon in the cat. Journal of Comparative Neurology 259(2): 165-92.

Hamos, J. E., S. C. Van Horn, D. Raczkowski, D. J. Uhlrich and S. M. Sherman (1985). Synaptic connectivity of a local circuit neurone in lateral geniculate nucleus of the cat. Nature 317(6038): 618-21.

Hatton, G. I. and Q. Z. Yang (1994). Incidence of neuronal coupling in supraoptic nuclei of virgin and lactating rats: estimation by neurobiotin and lucifer yellow. Brain Research 650(1): 63-9.

Hernandez-Cruz, A. and H. C. Pape (1989). Identification of two calcium currents in acutely dissociated neurons from the rat lateral geniculate nucleus. Journal of Neurophysiology 61(6): 1270-83.

Hillyard, D. R., V. D. Monje, I. M. Mintz, B. P. Bean, L. Nadasdi, J. Ramachandran, G. Miljanich, A. Azimi-Zoonooz, J. M. McIntosh, L. J. Cruz and et al. (1992). A new Conus peptide ligand for mammalian presynaptic Ca2+ channels. Neuron 9(1): 69-77.

Horikawa, K. and W. E. Armstrong (1988). A versatile means of intracellular labeling: injection of biocytin and its detection with avidin conjugates. Journal of Neuroscience Methods 25(1): 1-11.

Houser, C. R., J. E. Vaughn, R. P. Barber and E. Roberts (1980). GABA neurons are the major cell type of the nucleus reticularis thalami. Brain Research 200(2): 341-54.

Hughes, S. W., K. L. Blethyn, D. W. Cope and V. Crunelli (2002a). Properties and origin of spikelets in thalamocortical neurones in vitro. Neuroscience 110(3): 395-401.

Hughes, S. W., D. W. Cope, K. Blethyn and V. Crunelli (2002b). Cellular mechanisms of the slow (<1 Hz) oscillation in thalamocortical neurons in vitro. Neuron 33(6): 947-58.

Hughes, S. W., D. W. Cope and V. Crunelli (1998). Dynamic clamp study of Ih modulation of burst firing and delta oscillations in thalamocortical neurons in vitro. Neuroscience 87(3): 541-50.

Hughes, S. W., D. W. Cope, T. I. Toth, S. R. Williams and V. Crunelli (1999). All thalamocortical neurones possess a T-type Ca2+ 'window' current that enables the expression of bistability-mediated activities. Journal of Physiology (London) 517(Pt 3): 805-15.

Hughes, S. W., M. Lorincz, D. W. Cope, K. L. Blethyn, K. A. Kekesi, H. R. Parri, G. Juhasz and V. Crunelli (2004). Synchronized oscillations at alpha and theta frequencies in the lateral geniculate nucleus. Neuron 42(2): 253-68.

Huguenard, J. R., D. A. Coulter and D. A. Prince (1991). A fast transient potassium current in thalamic relay neurons: kinetics of activation and inactivation. Journal of Neurophysiology 66(4): 1304-15.

Huguenard, J. R. and D. A. McCormick (1992). Simulation of the currents involved in rhythmic oscillations in thalamic relay neurons. Journal of Neurophysiology 68(4): 1373-83.

Huguenard, J. R. and D. A. Prince (1991). Slow inactivation of a TEA-sensitive K current in acutely isolated rat thalamic relay neurons. Journal of Neurophysiology 66(4): 1316-28.

Huguenard, J. R. and D. A. Prince (1992). A novel T-type current underlies prolonged Ca(2+)-dependent burst firing in GABAergic neurons of rat thalamic reticular nucleus. Journal of Neuroscience 12(10): 3804-17.

Huguenard, J. R. and D. A. Prince (1994). Clonazepam suppresses GABAB-mediated inhibition in thalamic relay neurons through effects in nucleus reticularis. Journal of Neurophysiology 71(6): 2576-81.

Ide, L. S. (1982). The fine structure of the perigeniculate nucleus in the cat. Journal of Comparative Neurology 210(4): 317-34.

Jahnsen, H. and R. Llinas (1984a). Electrophysiological properties of guinea-pig thalamic neurones: an in vitro study. Journal of Physiology (London) 349: 205-26.

Jahnsen, H. and R. Llinas (1984b). Ionic basis for the electro-responsiveness and oscillatory properties of guinea-pig thalamic neurones in vitro. Journal of Physiology (London) 349: 227-47.

Jahnsen, H. and R. Llinas (1984c). Voltage-dependent burst-to-tonic switching of thalamic cell activity: an in vitro study. Archives Italiennes de Biologie 122(1): 73-82.

Jefferys, J. G. (1995). Nonsynaptic modulation of neuronal activity in the brain: electric currents and extracellular ions. Physiological Reviews 75(4): 689-723.

Jones, E. G. (1975). Some aspects of the organization of the thalamic reticular complex. Journal of Comparative Neurology 162(3): 285-308.

Jones, E. G. (1985). The thalamus. New York, Plenum.

Jones, E. G. and T. P. Powell (1969). Electron microscopy of synaptic glomeruli in the thalamic relay nuclei of the cat. Proceedings of the Royal Society of London, Series B, Biological Sciences 172(27): 153-71.

Kammermeier, P. J. and S. W. Jones (1997). High-voltage-activated calcium currents in neurons acutely isolated from the ventrobasal nucleus of the rat thalamus. Journal of Neurophysiology 77(1): 465-75.

Kandel, E. R., J. H. Schwartz and J. T. M. (1991). Principles of Neural Science, Appleton and Lang.

Kim, U. and D. A. McCormick (1998a). Functional and ionic properties of a slow afterhyperpolarization in ferret perigeniculate neurons in vitro. Journal of Neurophysiology 80(3): 1222-35.

Kim, U. and D. A. McCormick (1998b). The functional influence of burst and tonic firing mode on synaptic interactions in the thalamus. Journal of Neuroscience 18(22): 9500-16.

Kita, H. and W. Armstrong (1991). A biotin-containing compound N-(2-aminoethyl)biotinamide for intracellular labeling and neuronal tracing studies: comparison with biocytin. Journal of Neuroscience Methods 37(2): 141-50.

Kodota, T. and K. Kodota (1979). Filamentous contactscontaining subjuctional dense and tubular smooth endoplasmic reticulum in cat lateral geniculate nuclei. Brain Research 177(1): 49-59.

Kultas-Ilinsky, K. and I. A. Ilinsky (1988). GABAergic systems of the motor thalamus: neurones, synapses and receptors. Cellular Thalamic mechanisms. M. Bentivoglio and R. Spreafico. Amsterdam, Elsivier.

Landisman, C. E., M. A. Long, M. Beierlein, M. R. Deans, D. L. Paul and B. W. Connors (2002). Electrical synapses in the thalamic reticular nucleus. Journal of Neuroscience 22(3): 1002-9.

Lee, K. H. and D. A. McCormick (1997). Modulation of spindle oscillations by acetylcholine, cholecystokinin and 1S,3R-ACPD in the ferret lateral geniculate and perigeniculate nuclei in vitro. Neuroscience 77(2): 335-50.

Leger, L., K. Sakai, D. salvert, M. Touret and M. Jouvet (1975). Delineation of dorsal lateral geniculate afferents from the cat brainstem as visualised by the horsradish peroxidase technique. Brain Research 93(3): 490-6.

Leresche, N., E. Asprodini, Z. Emri, D. W. Cope and V. Crunelli (2000). Somatostatin inhibits GABAergic transmission in the sensory thalamus via presynaptic receptors. Neuroscience 98(3): 513-22.

Leresche, N., D. Jassik-Gerschenfeld, M. Haby, I. Soltesz and V. Crunelli (1990). Pacemaker-like and other types of spontaneous membrane potential oscillations of thalamocortical cells. Neuroscience Letters 113(1): 72-7.

Leresche, N., S. Lightowler, I. Soltesz, D. Jassik-Gerschenfeld and V. Crunelli (1991). Low-frequency oscillatory activities intrinsic to rat and cat thalamocortical cells. Journal of Physiology (London) 441: 155-74.

Lieberman, A. R. (1973). Neurons with presynaptic perikarya and presynaptic dendrites in the rat lateral geniculate nucleus. Brain Research 59: 35-59.

Lieberman, A. R. and J. Spacek (1997). Filamentous contacts: the ultrastructure and three-dimensional organization of specialized non-synaptic interneuronal appositions in thalamic relay nuclei. Cell and Tissue Research 288(1): 43-57.

Liu, X. B., C. N. Honda and E. G. Jones (1995a). Distribution of four types of synapse on physiologically identified relay neurons in the ventral posterior thalamic nucleus of the cat. Journal of Comparative Neurology 352(1): 69-91.

Liu, X. B. and E. G. Jones (1999). Predominance of corticothalamic synaptic inputs to thalamic reticular nucleus neurons in the rat. Journal of Comparative Neurology 414(1): 67-79.

Liu, X.-B. and G. J. Jones (2003). Fine struntural localisation of Connexin-36 immunoreactivity in mouse cerebral cortex and thalamus. Journal of Comparative Neurology 466: 457-67.

Liu, X. B., R. A. Warren and E. G. Jones (1995b). Synaptic distribution of afferents from reticular nucleus in ventroposterior nucleus of cat thalamus. Journal of Comparative Neurology 352(2): 187-202.

Llinas, R. and E. Geijo-Barrientos (1988). In vitro studies of mammalian thalamic and reticularis thalami neurones. Cellular thalamic mechanisms. M. Bentivoglio and R. Spreafico. Amsterdam, Elsevier.

Logan, S. D., A. E. Pickering, I. C. Gibson, M. F. Nolan and D. Spanswick (1996). Electrotonic coupling between rat sympathetic preganglionic neurones in vitro. Journal of Physiology (London) 495(Pt 2): 491-502.

Lubke, J. (1993). Morphology of neurons in the thalamic reticular nucleus (TRN) of mammals as revealed by intracellular injections into fixed brain slices. Journal of Comparative Neurology 329(4): 458-71.

Luthi, A., T. Bal and D. A. McCormick (1998). Periodicity of thalamic spindle waves is abolished by ZD7288,a blocker of Ih. Journal of Neurophysiology 79(6): 3284-9.

Lüthi, A. and D. A. McCormick (1998). Periodicity of thalamic synchronized oscillations: the role of Ca2+- mediated upregulation of Ih. Neuron 20(3): 553-63.

MacVicar, B. A. and F. E. Dudek (1981). Electrotonic coupling between pyramidal cells: a direct demonstration in rat hippocampal slices. Science 213(4509): 782-5.

Majorossy, K. and A. Kiss (1976). Types of interneurons and their participation in the neuronal network of the medial geniculate body. Experimental Brain Research 26(1): 19-37.

Mann-Metzer, P. and Y. Yarom (1999). Electrotonic coupling interacts with intrinsic properties to generate synchronized activity in cerebellar networks of inhibitory interneurons. Journal of Neuroscience 19(9): 3298-306.

Maquet, P. (2001). The role of sleep in learning and memory. Science 294: 1048-1052.

McCarley, R. W., O. Benoit and G. Barrionuevo (1983). Lateral geniculate nucleus unitary discharge in sleep and waking: state- and rate-specific aspects. Journal of Neurophysiology 50(4): 798-818.

McCormick, D. A. (1991a). Cellular mechanims underlying cholinergic and noradrenergic modulation of neuronal firing mode in the cat and guinea pig dorsal lateral geniculate nucleus. Journal of Neurophysiology 66: 278-89.

McCormick, D. A. (1991b). Functional properties of a slowly inactivating potassium current in guinea pig dorsal lateral geniculate relay neurons. Journal of Neurophysiology 66(4): 1176-89.

McCormick, D. A. (1992). Neurotransmitter actions in the thalamus and cerebral cortex. Journal of Clinical Neurophysiology 9(2): 212-23.

McCormick, D. A. and J. R. Huguenard (1992). A model of the electrophysiological properties of thalamocortical relay neurons. Journal of Neurophysiology 68(4): 1384-400.

McCormick, D. A. and H. C. Pape (1988). Acetylcholine inhibits identified interneurons in the cat lateral geniculate nucleus. Nature 334(6179): 246-8.

McCormick, D. A. and H. C. Pape (1990). Properties of a hyperpolarization-activated cation current and its role in rhythmic oscillation in thalamic relay neurones. Journal of Physiology (London) 431: 291-318.

McCormick, D. A. and M. von Krosigk (1992). Corticothalamic activation modulates thalamic firing through glutamate "metabotropic" receptors. Proceedings of the National Acadamy of Sciences USA 89(7): 2774-8.

McCormick, D. A. and Z. Wang (1991). Serotonin and noradrenaline excite GABAergic neurones of the guinea-pig and cat nucleus reticularis thalami. Journal of Physiology (London) 442: 235-55.

Micevych, P. E. and L. Abelson (1991). Distribution of mRNAs coding for liver and heart gap junction proteins in the rat central nervous system. Journal of Comparative Neurology 305(1): 96-118.

Montero, V. M. (1989). Ultrastructural identification of synaptic terminals from cortical axons and from collateral axons of geniculo-cortical relay cells in the perigeniculate nucleus of the cat. Experimental Brain Research 75(1): 65-72.

Montero, V. M. (1990). Quantitative immunogold analysis reveals high glutamate levels in synaptic terminals of retino-geniculate, cortico-geniculate, and geniculo-cortical axons in the cat. Visual Neuroscience 4(5): 437-43.

Montero, V. M. (1991). A quantitative study of synaptic contacts on interneurons and relay cells of the cat lateral geniculate nucleus. Experimental Brain Research 86(2): 257-70.

Montero, V. M. and G. L. Scott (1981). Synaptic terminals in the dorsal lateral geniculate nucleus from neurons of the thalamic reticular nucleus: a light and electron microscope autoradiographic study. Neuroscience 6(12): 2561-77.

Montero, V. M. and W. Singer (1985). Ultrastructural identification of somata and neural processes immunoreactive to antibodies against glutamic acid decarboxylase (GAD) in the dorsal lateral geniculate nucleus of the cat. Expreimental Brain Research 59(1): 151-65.

Morest, D. K. (1965). The laminar structure of the medial geniculate body of the cat. Journal of Anatomy (London) 99(1): 143-160.

Morison, R. S. and D. L. Bassett (1945). Electrical activity of the thalamus and basal gaglia in decorticate cats. Journal of Physiology (London) 8: 309-314.

Morris, B. J. (1989). Neuronal localisation of neuropeptide Y gene expression n rat brain. Journal of Comparative Neurology 290: 358-368.

Morrison, J. H. and S. L. Foote (1986). Noradrenergic and serotoninergic innervation of cortical, thalamic, and tectal visual structures in Old and New World monkeys. Journal of Comparative Neurology 243(1): 117-38.

Mulle, C., A. Madariaga and M. Deschenes (1986). Morphology and electrophysiological properties of reticularis thalami neurons in cat: in vivo study of a thalamic pacemaker. Journal of Neuroscience 6(8): 2134-45.

Mulle, C., M. Steriade and M. Deschenes (1985). Absence of spindle oscillations in the cat anterior thalamic nuclei. Brain Research 334(1): 169-71.

Nagy, J. I. and W. E. Li (2000). A brain slice model for in vitro analyses of astrocytic gap junction and connexin43 regulation: actions of ischemia, glutamate and elevated potassium. European Journal of Neuroscience 12(12): 4567-72.

Nowycky, M. C., A. P. Fox and R. W. Tsien (1985). Three types of neuronal calcium channel with different calcium agonist sensitivity. Nature 316(6027): 440-3.

Nunez, A., R. Curro Dossi, D. Contreras and M. Steriade (1992). Intracellular evidence for incompatibility between spindle and delta oscillations in thalamocortical neurons of cat. Neuroscience 48(1): 75-85.

Nunez, A., E. Garcia-Austt and W. Bunto (1990). In vivo electrophysiological analysis of Lucifer yellow-coupled Hippocampal pyramids. Experimental Neurology 108: 76-82.

O'Donnell, P. and A. A. Grace (1993). Dopaminergic modulation of dye coupling between neurones in the core and the shell regions of the nucleus accumbens. Journal of Neuroscience 13(8): 3456-71.

Ohara, P. T., G. Chazal and H. J. Ralston, 3rd (1989). Ultrastructural analysis of GABA-immunoreactive elements in the monkey thalamic ventrobasal complex. Journal of Comparative Neurology 283(4): 541-58.

Ohara, P. T. and A. R. Lieberman (1985). The thalamic reticular nucleus of the adult rat: experimental anatomical studies. Journal of Neurocytology 14(3): 365-411.

Ohara, P. T., A. J. Sefton and A. R. Lieberman (1980). Mode of termination of afferents from the thalamic reticular nucleus in the dorsal lateral geniculate nucleus of the rat. Brain Research 197(2): 503-6.

Pakhotin, P. I., I. D. Pakhotina and A. A. Andreev (1997). Functional stability of hippocampal slices after treatment with cyclooxygenase inhibitors. Neuroreport 8(7): 1755-9.

Pakhotin, P. I., L. L. Pavlik, I. D. Pakhotina and A. A. Andreev (1999). Long-term morphofunctional survival of guinea pig hippocampal slices after brief treatment with cyclooxygenase inhibitors. Neuroscience and Behavioural Physiology 29(5): 595-8.

Panula, P., U. Pirvola, A. S. and M. S. Airaksinen (1989). Histamine-immunoreactive nerve fibres in the rat brain. Neuroscience 28: 585-610.

Pape, H. C. (1992). Adenosine promotes burst activity in guinea-pig geniculocortical neurones through two different ionic mechanisms. Journal of Physiology (London) 447: 729-53.

Pape, H. C., T. Budde, R. Mager and Z. F. Kisvarday (1994). Prevention of Ca(2+)-mediated action potentials in GABAergic local circuit neurones of rat thalamus by a transient K+ current. Journal of Physiology (London) 478(Pt 3): 403-22.

Pape, H. C. and R. Mager (1992). Nitric oxide controls oscillatory activity in thalamocortical neurons. Neuron 9(3): 441-8.

Pape, H. C. and D. A. McCormick (1989). Noradrenaline and serotonin selectively modulate thalamic burst firing by enhancing a hyperpolarization-activated cation current. Nature 340(6236): 715-8.

Pape, H. C. and D. A. McCormick (1995). Electrophysiological and pharmacological properties of interneurons in the cat dorsal lateral geniculate nucleus. Neuroscience 68(4): 1105-25.

Pare, D., Y. Smith, A. Parent and M. Steriade (1988). Projections of brainstem core cholinergic and non-cholinergic neurons of cat to intralaminar and reticular thalamic nuclei. Neuroscience 25(1): 69-86.

Parent, A., D. Pare, Y. Smith and M. Steriade (1988). Basal forebrain cholinergic and noncholinergic projections to the thalamus and brainstem in cats and monkeys. Journal of Comparative Neurology 277(2): 281-301.

Parenti, R., M. Gulisano, A. Zappala and F. Cicirata (2000). Expression of connexin36 mRNA in adult rodent brain. Neuroreport 11(7): 1497-502.

Parri, H. R. and V. Crunelli (1998). Sodium current in rat and cat thalamocortical neurons: role of a non- inactivating component in tonic and burst firing. Journal of Neuroscience 18(3): 854-67.

Partridge, L. D. and D. Swandulla (1988). Calcium-activated non-specific cation channels. Trends in Neurosciences 11(2): 69-72.

Pedroarena, C. and R. Llinas (1997). Dendritic calcium conductances generate high-frequency oscillation in thalamocortical neurons. Proceedings of the National Acadamy of Sciences USA 94(2): 724-8.

Penny, G. R., D. Fitzpatrick, D. E. Schmechel and I. T. Diamond (1983). Glutamic acid decarboxylase-immunoreactive neurons and horseradish peroxidase-labeled projection neurons in the ventral posterior nucleus of the cat and Galago senegalensis. Journal of Neuroscience 3(9): 1868-87.

Perez-Reyes, E. (2003). Molecular physiology of low-voltage-activated t-type calcium channels. Physiological Reviews 83(1): 117-61.

Peters, A. and S. L. Palay (1966). The morphology of lamina Aand A1of the dorsal nucleus of the lateral geniculate body of the cat. Journal of Anatomy 100(3): 451-486.

Pin, J. P. and R. Duvoisin (1995). The metabotropic glutamate receptors: structure and functions. Neuropharmacology 34(1): 1-26.

Pinault, D., J. Bourassa and M. Deschenes (1995a). The axonal arborization of single thalamic reticular neurons in the somatosensory thalamus of the rat. European Journal of Neuroscience 7(1): 31-40.

Pinault, D., J. Bourassa and M. Deschenes (1995b). Thalamic reticular input to the rat visual thalamus: a single fiber study using biocytin as an anterograde tracer. Brain Research 670(1): 147-52.

Pinault, D., Y. Smith and M. Deschenes (1997). Dendrodendritic and axoaxonic synapses in the thalamic reticular nucleus of the adult rat. Journal of Neuroscience 17(9): 3215-33.

Prinz, A. A., L. F. Abbott and E. Marder (2004). The dynamic clamp comes of age. Trends Neurosci 27(4): 218-24.

Qian-Quan, S., G. Akk, J. R. Huguenard and D. A. Prince (2001). Differential regulation of GABA release and neuronal excitability mediated by neuropeptide Y_1 and Y_2 receptors in rat thalamic neurones. Journal of Physiology (London) 531(Pt 1): 81-94.

Qian-Quan, S., S. C. Barbon, D. A. Prince and J. R. Huguenard (2003). Target-specific Neuropeptide Y-ergic synaptic inhibition and its network consequences within the mammalian thalamus. Journal of Neuroscience 23(29): 9639-49.

Qian-Quan, S., J. R. Huguenard and D. A. Price (2002). Somatostatin inhibits thalamic network oscillations in Vitro: Actions on the GABAergic neurones of the reticular nucleus. Journal of Neuroscience 22(1): 5374-86.

Ralston, H. J. I., P. T. Ohara, D. D. Ralston and G. Chazal (1988). The neuronal and synaptic organization of the cat and primate somatosensory thalamus. Cellular Thalamic mechanisms. M. Bentivoglio and R. Spreafico. Amsterdam, Elsiver.

Ramcharan, E. J., J. W. Gnadt and S. M. Sherman (2000). Burst and tonic firing in thalamic cells of unanesthetized, behaving monkeys. Visual Neuroscience 17(1): 55-62.

Randall, A. and R. W. Tsien (1995). Pharmacological dissection of multiple types of Ca2+ channel currents in rat cerebellar granule neurons. Journal of Neuroscience 15(4): 2995-3012.

Rang, H. P., M. M. Dale and J. M. Ritter (2003). Pharmacology. Edinburgh, Churchill Livingstone.

Rash, J. E., W. A. Staines, T. Yasumura, D. Patel, C. S. Furman, G. L. Stelmack and J. I. Nagy (2000). Immunogold evidence that neuronal gap junctions in adult rat brain and spinal cord contain connexin-36 but not connexin-32 or connexin-43. Proceedings of the National Acadamy of Sciences USA 97(13): 7573-8.

Rash, J. E., T. Yasumura, F. E. Dudek and J. I. Nagy (2001). Cell-specific expression of connexins and evidence of restricted gap junctional coupling between glial cells and between neurons. Journal of Neuroscience 21(6): 1983-2000.

Reinagel, P., D. Godwin, S. M. Sherman and C. Koch (1999). Encoding of visual information by LGN bursts. Journal of Neurophysiology 81(5): 2558-69.

Rekling, J. C., X. M. Shao and J. L. Feldmam (2000). Electrical coupling and excitatory synaptic transmission between rhythmogenic respiratory neurones in the preBotzinger complex. Journal of Neuroscience 20(23): RC113.

Rice, M. E. (1999). Use of ascorbate in the preparation and maintenance of brain slices. Methods 18(2): 144-9.

Robson, J. A. (1984). Reconstructions of corticogeniculate axons in the cat. Journal of Comparative Neurology 225: 89-103.

Ross, F. M., R. Gwyn, D. Spanswick and S. N. Davies (2000). Carbenoxolone depresses spontaneous epileptiform activity in the CA1 region of the rat hippocampus. Neuroscience 100(4): 789-796.

Roth, T., T. Roehrs, J. A. Costa e Silva and M. A. Chase (1999). Public health and insomnia. Sleep 22(3): S417-420.

Rouach, N., E. Avignone, W. Meme, A. Koulakoff, L. Venance, F. Blomstrand and C. Giaume (2002). Gap junctions and connexin expression in the normal and pathological central nervous system. Biology of the Cell 94(7-8): 457-75.

Rouach, N., M. Segal, A. Koulakoff, C. Giaume and E. Avigone (2003). Carbenoxolone blockade of neuronal activity in culture is not mediated by an action on gap junctions. Journal of Physiology 533(Pt 3): 729-45.

Rougeul-Buser, A. and P. Buser (1997). Rhythms in the alpha band in cats and their behavioural correlates. International Journal of Psychophysiology 26(1-3): 191-203.

Rozental, R., C. Giaume and D. C. Spray (2000). Gap junctions in the nervous system. Brain Research Brain Research Reviews 32(1): 11-5.

Rozental, R., M. Srinivas and D. C. Spray (2001). How to close a gap junction channel. Efficacies and potencies of uncoupling agents. Methods in Molecular Biology 154: 447-76.

Salt, T. E. (1986). Mediation of thalamic sensory input by both NMDA receptors and non-NMDA receptors. Nature 322(6076): 263-5.

Salt, T. E. (1987). Excitatory amino acid receptors and synaptic transmission in the rat ventrobasal thalamus. Journal of Physiology (London) 391: 499-510.

Salt, T. E. and S. A. Eaton (1996). Functions of ionotropic and metabotropic glutamate receptors in sensory transmission in the mammalian thalamus. Progress in Neurobiology 48(1): 55-72.

Salt, T. E., C. L. Meier, N. Seno, T. Krucker and P. L. Herrling (1995). Thalamocortical and corticocortical excitatory postsynaptic potentials mediated by excitatory amino acid receptors in the cat motor cortex in vivo. Neuroscience 64(2): 433-42.

Salt, T. E. and J. P. Turner (1998). Modulation of sensory inhibition in the ventrobasal thalamus via activation of group II metabotropic glutamate receptors by 2R,4R-aminopyrrolidine-2,4-dicarboxylate. Experimental Brain Research 121(2): 181-5.

Salt, T. E., J. P. Turner and A. E. Kingston (1999). Evaluation of agonists and antagonists acting at Group I metabotropic glutamate receptors in the thalamus in vivo. Neuropharmacology 38(10): 1505-10.

Sanchez-Vives, M. V., T. Bal and D. A. McCormick (1997). Inhibitory interactions between perigeniculate GABAergic neurons. Journal of Neuroscience 17(22): 8894-908.

Sanchez-Vives, M. V. and D. A. McCormick (1997). Functional properties of perigeniculate inhibition of dorsal lateral geniculate nucleus thalamocortical neurons in vitro. Journal of Neuroscience 17(22): 8880-93.

Sanchez-Vives, M. V. and D. A. McCormick (2000). Cellular and network mechanisms of rhythmic recurrent activity in neocortex. Nature Neuroscience 3(10): 1027-34.

Sato, F., Y. Nakamura and Y. Shinoda (1997). Serial electron microscopic reconstruction of axon terminals on physiologically identified thalamocortical neurons in the cat ventral lateral nucleus. Journal of Comparative Neurology 388(4): 613-31.

Sawyer, S. F., J. M. Tepper and P. M. Groves (1994). Cerebellar-responsive neurons in the thalamic ventroanterior-ventrolateral complex of rats: light and electron microscopy. Neuroscience 63(3): 725-45.

Scharfman, H. E., S. M. Lu, W. Guido, P. R. Adams and S. M. Sherman (1990). N-methyl-D-aspartate receptors contribute to excitatory postsynaptic potentials of cat lateral geniculate neurons recorded in thalamic slices. Proceedings of the National Acadamy of Sciences USA 87(12): 4548-52.

Semba, K. (2000). Multiple output pathways of the basal forebrain: organisation, chemical heterogeneity, and roles in vigilance. Behavioural Brain Research 115: 117-141.

Sharp, A. A., M. B. O'Neil, L. F. Abbott and E. Marder (1993). The dynamic clamp: artificial conductances in biological neurons. Trends Neurosci 16(10): 389-94.

Sherman, S. M. and M. J. Friedlander (1988). Identification of X versus Y properties for interneurons in the A-laminae of the cat's lateral geniculate nucleus. Experimental Brain Research 73(2): 384-92.

Sherman, S. M. and R. W. Guillery (1996). Functional organisation of thalamocortical relays. Journal of Neurophysiology 76(3): 1367-95.

Shu, Y. and D. A. McCormick (2002). Inhibitory interactions between ferret thalamic reticular neurons. Journal of Neurophysiology 87(5): 2571-6.

Sillito, A. M., P. C. Murphy and T. E. Salt (1990a). The contribution of the non-N-methyl-D-aspartate group of excitatory amino acid receptors to retinogeniculate transmission in the cat. Neuroscience 34(2): 273-80.

Sillito, A. M., P. C. Murphy, T. E. Salt and C. I. Moody (1990b). Dependence of retinogeniculate transmission in cat on NMDA receptors. Journal of Neurophysiology 63(2): 347-55.

Simon, A. M. and D. A. Goodenough (1998). Diverse functions of vertebrate gap junctions. Trends in Cell Biology 8(12): 477-83.

Smith, Y., D. Pare, M. Deschenes, A. Parent and M. Steriade (1988). Cholinergic and non-cholinergic projections from the upper brainstem core to the visual thalamus in the cat. Experimental Brain Research 70(1): 166-80.

Soltesz, I. and V. Crunelli (1992). A role for low-frequency, rhythmic synaptic potentials in the synchronization of cat thalamocortical cells. Journal of Physiology (London) 457: 257-76.

Soltesz, I., S. Lightowler, N. Leresche and V. Crunelli (1989a). On the properties and origin of the GABAB inhibitory postsynaptic potential recorded in morphologically identified projection cells of the cat dorsal lateral geniculate nucleus. Neuroscience 33(1): 23-33.

Soltesz, I., S. Lightowler, N. Leresche and V. Crunelli (1989b). Optic tract stimulation evokes GABAA but not GABAB IPSPs in the rat ventral lateral geniculate nucleus. Brain Research 479(1): 49-55.

Soltesz, I., S. Lightowler, N. Leresche, D. Jassik-Gerschenfeld, C. E. Pollard and V. Crunelli (1991). Two inward currents and the transformation of low-frequency oscillations of rat and cat thalamocortical cells. Journal of Physiology (London) 441: 175-97.

Spacek, J. and A. R. Lieberman (1974). Ultrastructure and three-dimensional organization of synaptic glomeruli in rat somatosensory thalamus. Journal of Anatomy (London) 117(Pt 3): 487-516.

Spreafico, R., M. de Curtis, C. Frassoni and G. Avanzini (1988). Electrophysiological characteristics of morphologically identified reticular thalamic neurons from rat slices. Neuroscience 27(2): 629-38.

Spreafico, R., D. E. Schmechel, L. C. Ellis, Jr. and A. Rustioni (1983). Cortical relay neurons and interneurons in the N. ventralis posterolateralis of cats: a horseradish peroxidase, electron-microscopic, Golgi and immunocytochemical study. Neuroscience 9(3): 491-509.

Srinivas, M., R. Rozental, T. Kojima, R. Dermietzel, M. Mehler, D. F. Condorelli, J. A. Kessler and D. C. Spray (1999). Functional properties of channels formed by the neuronal gap junction protein connexin36. J Neurosci 19(22): 9848-55.

Stanford, L. R., M. J. Friedlander and S. M. Sherman (1981). Morphology of functionally identified W-cells in the C-lamina of the cat lateral geniculate nucleus. Journal of Neuroscience 1(6): 578-584.

Stanford, L. R., M. J. Friedlander and S. M. Sherman (1983). Morphological and physiological properties of geniculate W-cells of the cat: a comparison with X- and Y-cells. Journal of Neurophysiology 50(3): 582-608.

Steriade, M. (1993). Cholinergic blockage of network- and intrinsically generated slow oscillations promotes waking and REM sleep activity patterns in thalamic and cortical neurons. Progress in Brain Research 98: 345-55.

Steriade, M., D. Contreras and F. Amzica (1994). Synchronized sleep oscillations and their paroxysmal developments. Trends in Neurosciences 17(5): 199-208.

Steriade, M., D. Contreras, F. Amzica and I. Timofeev (1996). Synchronization of fast (30-40 Hz) spontaneous oscillations in intrathalamic and thalamocortical networks. Journal of Neuroscience 16(8): 2788-808.

Steriade, M., D. Contreras, R. Curro Dossi and A. Nunez (1993a). The slow (< 1 Hz) oscillation in reticular thalamic and thalamocortical neurons: scenario of sleep rhythm generation in interacting thalamic and neocortical networks. Journal of Neuroscience 13(8): 3284-99.

Steriade, M., S. Datta, D. Pare, G. Oakson and R. C. Curro Dossi (1990). Neuronal activities in brain-stem cholinergic nuclei related to tonic activation processes in thalamocortical systems. Journal of Neuroscience 10(8): 2541-59.

Steriade, M., M. Deschenes, L. Domich and C. Mulle (1985). Abolition of spindle oscillations in thalamic neurons disconnected from nucleus reticularis thalami. Journal of Neurophysiology 54(6): 1473-97.

Steriade, M., L. Domich and G. Oakson (1986). Reticularis thalami neurons revisited: activity changes during shifts in states of vigilance. Journal of Neuroscience 6(1): 68-81.

Steriade, M., L. Domich, G. Oakson and M. Deschenes (1987). The deafferented reticular thalamic nucleus generates spindle rhythmicity. Journal of Neurophysiology 57(1): 260-73.

Steriade, M., R. C. Dossi and A. Nunez (1991a). Network modulation of a slow intrinsic oscillation of cat thalamocortical neurons implicated in sleep delta waves: cortically induced synchronization and brainstem cholinergic suppression. Journal of Neuroscience 11(10): 3200-17.

Steriade, M., R. C. Dossi, D. Pare and G. Oakson (1991b). Fast oscillations (20-40 Hz) in thalamocortical systems and their potentiation by mesopontine cholinergic nuclei in the cat. Proceedings of the National Acadamy of Scienecs USA 88(10): 4396-400.

Steriade, M. and L. L. Glenn (1982). Neocortical and caudate projections of intralaminar thalamic neurons and their synaptic excitation from midbrain reticular core. Journal of Neurophysiology 48(2): 352-71.

Steriade, M., E. G. Jones and D. A. McCormick (1997). THALAMUS. Oxford, Elsevier Science.

Steriade, M., D. A. McCormick and T. J. Sejnowski (1993b). Thalamocortical oscillations in the sleeping and aroused brain. Science 262(5134): 679-85.

Steriade, M., A. Nunez and F. Amzica (1993c). Intracellular analysis of relations between the slow (< 1 Hz) neocortical oscillation and other sleep rhythms of the electroencephalogram. Journal of Neuroscience 13(8): 3266-83.

Steriade, M., A. Nunez and F. Amzica (1993d). A novel slow (< 1 Hz) oscillation of neocortical neurons in vivo: depolarizing and hyperpolarizing components. Journal of Neuroscience 13(8): 3252-65.

Steriade, M., G. Oakson and N. Ropert (1982). Firing rates and patterns of midbrain reticular neurons during steady and transitional states of the sleep-waking cycle. Experimental Brain Research 46(1): 37-51.

Steriade, M., D. Pare, A. Parent and Y. Smith (1988). Projections of cholinergic and non-cholinergic neurons of the brainstem core to relay and associational thalamic nuclei in the cat and macaque monkey. Neuroscience 25(1): 47-67.

Steriade, M., I. Timofeev and F. Grenier (2001). Natural waking and sleep states: a view from inside neocortical neurons. Journal of Neurophysiology 85(5): 1969-85.

Steriade, M., I. Timofeev, F. Grenier and N. Durmuller (1998). Role of thalamic and cortical neurons in augmenting responses and self- sustained activity: dual intracellular recordings in vivo. Journal of Neuroscience 18(16): 6425-43.

Steriade, M. and P. Wyzinski (1972). Cortically elicited activities in thalamic reticularis neurons. Brain Research 42(2): 514-20.

Sun, Q. Q., J. R. Huguenard and D. A. Prince (2001). Neuropeptide Y receptors differentially modulate G-protein-activated inwardly rectifying K+ channels and high-voltage-activated Ca2+ channels in rat thalamic neurons. Journal of Physiology (London) 531(Pt 1): 67-79.

Swadlow, H. A. and A. G. Gusev (2001). The impact of 'bursting' thalamic impulses at a neocortical synapse. Nature Neuroscience 4(4): 402-8.

Talley, E. M., L. L. Cribbs, J. H. Lee, A. Daud, E. Perez-Reyes and D. A. Bayliss (1999). Differential distribution of three members of a gene family encoding low voltage-activated (T-type) calcium channels. Journal of Neuroscience 19(6): 1895-911.

Tamas, G., E. H. Buhl, A. Lorincz and P. Somogyi (2000). Proximally targeted GABAergic synapses and gap junctions synchronize cortical interneurons. Nature Neuroscience 3(4): 366-71.

Tennigkeit, F., D. W. Schwarz and E. Puil (1999). Effects of metabotropic glutamate receptor activation in auditory thalamus. Journal of Neurophysiology 82(2): 718-29.

Teubner, B., J. Degen, G. Sohl, M. Guldenagel, F. F. Bukauskas, E. B. Trexler, V. K. Verselis, C. I. De Zeeuw, C. G. Lee, C. A. Kozak, E. Petrasch-Parwez, R. Dermietzel and K. Willecke (2000). Functional expression of the murine connexin 36 gene coding for a neuron-specific gap junctional protein. J Membr Biol 176(3): 249-62.

Teubner, B., B. Odermatt, M. Guldenagel, G. Sohl, J. Degen, F. Bukauskas, J. Kronengold, V. K. Verselis, Y. T. Jung, C. A. Kozak, K. Schilling and K. Willecke (2001). Functional expression of the new gap junction gene connexin47 transcribed in mouse brain and spinal cord neurons. Journal of Neuroscience 21(4): 1117-26.

Timofeev, I., D. Contreras and M. Steriade (1996). Synaptic responsiveness of cortical and thalamic neurones during various phases of slow sleep oscillation in cat. Journal of Physiology (London) 494(Pt 1): 265-78.

Timofeev, I., F. Grenier and M. Steriade (2001). Disfacilitation and active inhibition in the neocortex during the natural sleep-wake cycle: an intracellular study. Proceedings of the National Acadamy of Sciences USA 98(4): 1924-9.

Timofeev, I. and M. Steriade (1996). Low-frequency rhythms in the thalamus of intact-cortex and decorticated cats. Journal of Neurophysiology 76(6): 4152-68.

Timofeev, I. and M. Steriade (1997). Fast (mainly 30-100 Hz) oscillations in the cat cerebellothalamic pathway and their synchronization with cortical potentials. Journal of Physiology (London) 504(Pt 1): 153-68.

Tokimasa, T. (1985). Intracellular Ca2+-ions inactivate K+-current in bullfrog sympathetic neurons. Brain Research 337(2): 386-91.

Toth, T. and V. Crunelli (1992). Computer simulation of the pacemaker oscillations of thalamocortical cells. Neuroreport 3(1): 65-8.

Toth, T. I., S. W. Hughes and V. Crunelli (1998). Analysis and biophysical interpretation of bistable behaviour in thalamocortical neurons. Neuroscience 87(2): 519-23.

Turner, J. P., C. M. Anderson, S. R. Williams and V. Crunelli (1997). Morphology and membrane properties of neurones in the cat ventrobasal thalamus in vitro. Journal of Physiology (London) 505(Pt 3): 707-26.

Turner, J. P., N. Leresche, A. Guyon, I. Soltesz and V. Crunelli (1994). Sensory input and burst firing output of rat and cat thalamocortical cells: the role of NMDA and non-NMDA receptors. Journal of Physiology (London) 480(Pt 2): 281-95.

Turner, J. P. and T. E. Salt (1998). Characterization of sensory and corticothalamic excitatory inputs to rat thalamocortical neurones in vitro. Journal of Physiology (London) 510(Pt 3): 829-43.

Turner, J. P. and T. E. Salt (1999). Group III metabotropic glutamate receptors control corticothalamic synaptic transmission in the rat thalamus in vitro. Journal of Physiology (London) 519(Pt 2): 481-91.

Turner, J. P. and T. E. Salt (2000). Synaptic activation of the group I metabotropic glutamate receptor mGlu1 on the thalamocortical neurons of the rat dorsal lateral geniculate nucleus in vitro. Neuroscience 100(3): 493-505.

Uhlrich, D. J., J. B. Cucchiaro, A. L. Humphrey and S. M. Sherman (1991). Morphology and axonal projection patterns of individual neurons in the cat perigeniculate nucleus. Journal of Neurophysiology 65(6): 1528-41.

Uhlrich, D. J., K. A. Manning and T. P. Pienkowski (1993). The histaminergic innervation of the lateral geniculate complex in the cat. Visual Neuroscience 10: 225-35.

Ulrich, D. and J. R. Huguenard (1996). GABAB receptor-mediated responses in GABAergic projection neurones of rat nucleus reticularis thalami in vitro. Journal of Physiology (London) 493(Pt 3): 845-54.

Usrey, W. M., J. B. Reppas and R. C. Reid (1999). Specificity and strength of retinogeniculate connections. Journal of Neurophysiology 82(6): 3527-40.

Valiante, T. A., J. L. Perez Velazquez, S. S. Jahromi and P. L. Carlen (1995). Coupling potentials in CA1 neurons during calcium-free-induced field burst activity. Journal of Neuroscience 15(10): 6946-56.

Venance, L., A. Rozov, M. Blatow, N. Burnashev, D. Feldmeyer and H. Monyer (2000). Connexin expression in electrically coupled postnatal rat brain neurons. Proceedings of the National Acadamy of Sciences USA 97(18): 10260-5.

von Krosigk, M., T. Bal and D. A. McCormick (1993). Cellular mechanisms of a synchronized oscillation in the thalamus. Science 261(5119): 361-4.

von Krosigk, M., J. E. Monckton, P. B. Reiner and D. A. McCormick (1999). Dynamic properties of corticothalamic excitatory postsynaptic potentials and thalamic reticular inhibitory postsynaptic potentials in thalamocortical neurons of the guinea-pig dorsal lateral geniculate nucleus. Neuroscience 91(1): 7-20.

Wang, S., M. E. Bickford, S. C. Van Horn, A. Erisir, D. W. Godwin and S. M. Sherman (2001). Synaptic targets of thalamic reticular nucleus terminals in the visual thalamus of the cat. Journal of Comparative Neurology 440(4): 321-41.

Waszak, M. (1974). Firing pattern of neurons in the rostral and ventral part of nucleus reticularis thalami during EEG spindles. Experimental Neurology 43(1): 38-58.

Weber, A. J., R. E. Kalil and M. Behan (1989). Synaptic connections between corticogeniculate axons and interneurons in the dorsal lateral geniculate nucleus of the cat. Journal of Comparative Neurology 289(1): 156-64.

Weyand, T. G., M. Boudreaux and W. Guido (2001). Burst and tonic response modes in thalamic neurons during sleep and wakefulness. Journal of Neurophysiology 85(3): 1107-18.

Wilkinson, J. L. (1992). Neuroanatomy for medical students, Butterworth-Heinemann.

Williams, S. R. and G. J. Stuart (2000). Action potential backpropagation and somato-dendritic distribution of ion channels in thalamocortical neurons. Journal of Neuroscience 20(4): 1307-17.

Williams, S. R., T. I. Toth, J. P. Turner, S. W. Hughes and V. Crunelli (1997a). The 'window' component of the low threshold Ca2+ current produces input signal amplification and bistability in cat and rat thalamocortical neurones. Journal of Physiology (London) 505(Pt 3): 689-705.

Williams, S. R., J. P. Turner, C. M. Anderson and V. Crunelli (1996). Electrophysiological and morphological properties of interneurones in the rat dorsal lateral geniculate nucleus in vitro. Journal of Physiology (London) 490(Pt 1): 129-47.

Williams, S. R., J. P. Turner, S. W. Hughes and V. Crunelli (1997b). On the nature of anomalous rectification in thalamocortical neurones of the cat ventrobasal thalamus in vitro. Journal of Physiology (London) 505(Pt 3): 727-47.

Williamson, A. M., P. T. Ohara and H. J. Ralston, 3rd (1993). Electron microscopic evidence that cortical terminals make direct contact onto cells of the thalamic reticular nucleus in the monkey. Brain Research 631(1): 175-9.

Wilson, J. R. (1989). Synaptic organization of individual neurons in the macaque lateral geniculate nucleus. Journal of Neuroscience 9(8): 2931-53.

Wilson, J. R., M. J. Friedlander and S. M. Sherman (1984). Fine structural morphology of identified X- and Y-cells in the cat's lateral geniculate nucleus. Proceedings of the Royal Society of London, Series B, Biological Sciences 221(1225): 411-36.

Winer, J. A. (1985). The medial geniculate body of the cat. Advances in Anatomy, Embryology and Cell Biology 86: 1-97.

Winfield, D. A. (1980). The synaptic organization of glomeruli in the magnocellular and parvocellular laminae of the lateral geniculate nucleus in the monkey. Brain Research 198(1): 55-62.

Yen, C. T., M. Conley, S. H. Hendry and E. G. Jones (1985a). The morphology of physiologically identified GABAergic neurons in the somatic sensory part of the thalamic reticular nucleus in the cat. Journal of Neuroscience 5(8): 2254-68.

Yen, C. T., M. Conley and E. G. Jones (1985b). Morphological and functional types of neurons in cat ventral posterior thalamic nucleus. Journal of Neuroscience 5(5): 1316-38.

Zhan, X. J., C. L. Cox and S. M. Sherman (2000). Dendritic depolarization efficiently attenuates low-threshold calcium spikes in thalamic relay cells. Journal of Neuroscience 20(10): 3909-14.

Zhang, J. F., A. D. Randall, P. T. Ellinor, W. A. Horne, W. A. Sather, T. Tanabe, T. L. Schwarz and R. W. Tsien (1993). Distinctive pharmacology and kinetics of cloned neuronal Ca2+ channels and their possible counterparts in mammalian CNS neurons. Neuropharmacology 32(11): 1075-88.

Zhu, J. J., D. J. Uhlrich and W. W. Lytton (1999). Burst firing in identified rat geniculate interneurons. Neuroscience 91(4): 1445-60.

8.2 PUBLICATIONS

8.2.1 Papers: published, submitted or pending publication.

Hughes SW, Blethyn KL, Cope DW, Crunelli V. Properties and origin of spikelets in thalamocortical neurones *in vitro*. Neuroscience 2002. 110:395-401.

Hughes SW, Cope DW, Blethyn KL, Crunelli V. Cellular mechanisms of the slow (<1Hz) oscillation in thalamocortical neurones *in vitro*. Neuron 2002. 33:947-58.

Crunelli V, Blethyn KL, Cope DW, Hughes SW, Parri HR, Turner JP, Toth TI, Williams SR. Novel neuronal and astrocytic mechanisms in thalamocortical loop dynamics. Philosophical Transactions of the Royal Society of London, Series B, Biological Sciences 2002. 357:1675-93.

Hughes SW, Blethyn KL, Cope DW, Crunelli V. Neuronal basis of alpha (α) and theta (θ) rhythms in the lateral geniculate nucleus. Neuron. Accepted for publication.

Blethyn KL, Hughes SW, Crunelli V. Properties and origin of an intrinsic slow (<1Hz) oscillation in thalamic reticular neurones *in vitro*. Manuscript in preparation.

Blethyn KL, Hughes SW, Crunelli V, Nucleus-Specific properties of the slow (<1Hz) oscillation in thalamocortical neurones *in vitro*. Manuscript in preparation.

8.2.2 Abstracts.

Blethyn KL, Hughes SW, Cope DW, Crunelli V. The role of ionic conductances underlying a slow (<1Hz) oscillation in neurones of the thalamic reticular nucleus *in vitro*. 2003. Society for Neuroscience Abstracts P699.3.

Blethyn KL, Hughes SW, Cope DW, Crunelli V. Nucleus-specific properties of the slow (<1Hz) oscillation in thalamic neurones *in vitro*. 2002. Society for Neuroscience Abstracts P532.4.

Hughes SW, Blethyn KL, Cope DW, Crunelli V. Pharmacology and Nucleus-specific properties of the slow (<1Hz) oscillation in thalamic neurones *in vitro*. 2002. FENS Abstracts P244.

Blethyn KL, Hughes SW, Cope DW, Crunelli V. Synchronised alpha and theta oscillations in the isolated lateral geniculate nucleus. 2001. Society for Neuroscience Abstracts P395.5.

Crunelli V, Cope DW, Blethyn KL, Watson A, Hughes SW. Involvement of distinct calcium channels in the generation of alpha/theta oscillation in thalamocortical neurones. 2000. Society for Neuroscience Abstracts P547.17

Hughes SW, Cope DW, Blethyn KL, Crunelli V. Facilitation of fast (5-50Hz) and slow (0.1-1Hz) oscillations in thalamocortical neurones by activation of group 1 metabotropic glutamate receptors. 2000. Proceeding of the British Pharmacological society. BJP,131, 45P